Volume 68A
Number 5
Sept.-Oct. 1964

Physics and Chemistry

U.S. DEPARTMENT OF COMMERCE

SECTION A

JOURNAL OF RESEARCH

NATIONAL BUREAU OF STANDARDS

Journal of Research

of the

National Bureau of Standards

A. Physics and Chemistry

Sept.–Oct. • 1964

VOLUME • 68A

NUMBER • 5

Editor: C. W. Beckett

Associate Editors: D. D. Wagman
I. M. Richardson

Publication dates:
Feb. 1, Apr. 1, June 1, Aug. 1, Oct. 1, Dec. 1, 1964

JOURNAL OF RESEARCH

The National Bureau of Standards Journal of Research reports research and development in the fields of activity shown at right. Also included from time to time are survey articles on topics closely related to the Bureau's scientific and technical program.

The Journal is published in four separate sections as follows:

A. Physics and Chemistry

Contains papers of interest primarily to scientists working in these fields. Issued six times a year. Annual subscription: domestic, $4.00; foreign, $4.75. Single copy, 70c.

B. Mathematics and Mathematical Physics

Presents studies and compilations designed mainly for the mathematician and the theoretical physicist. Issued quarterly. Annual subscription: domestic, $2.25; foreign, $2.75. Single copy, 75c.

C. Engineering and Instrumentation

Reports research and development results of interest chiefly to the engineer and the applied scientist. Issued quarterly. Annual subscription: domestic, $2.25; foreign, $2.75. Single copy, 75c.

D. Radio Science (formerly Radio Propagation)

Published in cooperation with U.S. National Committee of URSI. Presents papers in radio propagation, communications, and radio science generally. Issued monthly. Annual subscription: domestic, $9.00; foreign, $11.50. Single copy $1.00.

The National Bureau of Standards is a principal focal point in the Federal Government for assuring maximum application of the physical and engineering sciences to the advancement of technology in industry and commerce. Its responsibilities include development and maintenance of the national standards of measurement, and the provision of means for making measurements consistent with those standards; determination of physical constants and properties of materials; development of methods for testing materials, mechanisms, and structures, and making such tests as may be necessary, particularly for government agencies; cooperation in the establishment of standard practices for incorporation in codes and specifications; advisory service to government agencies on scientific and technical problems; invention and development of devices to serve special needs of the Government; assistance to industry, business and consumers in the development and acceptance of commercial standards and simplified trade practice recommendations; administration of programs in cooperation with United States business groups and standards organizations for the development of international standards of practice; and maintenance of a clearinghouse for the collection and dissemination of scientific, technical, and engineering information.

Institute for Basic Standards. Electricity. Metrology. Heat. Radiation Physics. Mechanics. Applied Mathematics. Atomic Physics. Physical Chemistry. Laboratory Astrophysics.* Radio Standards Laboratory: Radio Standards Physics; Radio Standards Engineering.** Office of Standard Reference Data.

Institute for Materials Research. Analytical Chemistry. Polymers. Metallurgy. Inorganic Materials. Reactor Radiations. Cryogenics.** Office of Standard Reference Materials.

Central Radio Propagation Laboratory.** Ionosphere Research and Propagation. Troposphere and Space Communications. Radio Systems. Upper Atmosphere and Space Physics.

Institute for Applied Technology. Textiles and Apparel Technology Center. Building Research. Industrial Equipment. Information Technology. Performance Test Development. Instrumentation. Transport Systems. Office of Technical Services. Office of Weights and Measures. Office of Engineering Standards. Office of Industrial Services.

*NBS Group, Joint Institute for Laboratory Astrophysics at the University of Colorado.
**Located at Boulder, Colo.

U.S. DEPARTMENT OF COMMERCE
Luther H. Hodges, Secretary

NATIONAL BUREAU OF STANDARDS
A. V. Astin, Director

Order all publications from the Superintendent of Documents
U.S. Government Printing Office, Washington, D.C., 20402

Use of funds for printing this publication approved by the Director of the Bureau of the Budget (June 19, 1961).

JOURNAL OF RESEARCH of the National Bureau of Standards—A. Physics and Chemistry
Vol. 68A, No. 5, September–October 1964

Relaxation Modes of Trapped Crystal Point Defects: the Three-Neighbor Shells Model in NaCl

A. D. Franklin,* A. Shorb, and J. B. Wachtman, Jr.

(May 11, 1964)

The results of a relaxation-mode analysis are presented for two cases of trapped-defect relaxation in the NaCl structure, in which both defects occupy the same type of site (e.g., impurity divalent ion and trapped vacancy), or in which they occupy the two different types of sites (vacancy pair). The relaxation analysis is presented in the form of a set of basis vectors in occupation-probability space and a set of secular equations. Solutions to the equations provide the relaxation rates and also the coefficients in the linear combinations of the basis vectors which constitute the relaxation modes.

Calculations of the relaxation rates and contributions to the polarizability of the various modes for a three-shell model with jump frequencies chosen to represent the relaxation of an impurity-ion vacancy pair in NaCl(Mn) have confirmed the results of Lozovskii. Even though the third shell makes a significant and even large contribution to the process, one mode dominates and the relaxation as seen in a-c measurements would take place with essentially a single relaxation time. The d-c techniques of Dreyfus are sensitive enough to detect more than one of these relaxations at low temperatures, but the slowest of these will always be the dominant one. Any relaxation slower than the major one must be ascribed to some other mechanism.

1. Introduction

Point defects in crystals give rise to mechanical and elastic relaxation in a variety of ways. In particular, because of their interaction with each other, pairs of them can become mutually trapped, forming centers which can contribute to the response to applied mechanical or electrical stresses. If one defect is considered as the trap, then the trapped defect can occupy various lattice sites in the neighborhood of the trap. These accessible sites may be restricted to those in the nearest neighbor shell to the trap because of very strong interaction, or they may include sites in shells further away from the trap. Under the influence of the applied stress, some of the accessible sites become preferred over others that are equivalent in the stress free crystal, and the redistribution of the trapped defects according to the new scheme constitutes the relaxation process.

The rate equations governing this redistribution process constitute an eigenvalue problem, for which group representation theory combined with a knowledge of the symmetry around the trap provide a powerful tool for solution [1–3]. [1] The results of this treatment are expressed in terms of relaxation modes, which represent certain distributions of the trapped defects among the accessible sites. Each of these distributions relaxes as a unit with the same exponential time function, exhibiting a single relaxation time, governing the occupation probability of all the sites.

Haven and van Santen [1, 2] applied the group theory technique to the case of cation vacancies trapped near divalent cation impurities in the NaCl structure, with only the nearest neighbor sites included. Wachtman [3] showed that the relaxation modes of the undriven

*Temporarily attached to United Kingdom Atomic Energy Research Establishment, Harwell, Berks, England.

[1] Figures in brackets indicate the literature references at the end of this paper.

situation were also solutions for the driven case in the limit of small applied stresses, and applied the technique to the relaxation of oxygen vacancies trapped at divalent cation impurities (Ca ions) in ThO_2, again restricting the vacancies to nearest neighbor sites. Bhagavantam and Pantulu [4] have summarized this approach for the case of nearest neighbor sites and have emphasized the similarity of the symmetry arguments to those arising in the treatment of infrared and Raman spectra. Franklin [5] showed that the technique could be extended to the case in which additional shells, further out than the nearest-neighbor shell, were accessible, and gave solutions for the case of cation vacancies trapped at divalent cation impurities in the NaCl structure, including two shells of accessible sites.

In considering the dielectric and mechanical behavior of these centers, the more distant shells of sites must, at least in principle, be included. It is expected that, at least beyond the first two shells, the binding energy of the sites will decrease with distance from the center, and the probability of occupation will fall off in the more distant sites. However, there are more sites available in the more distant shells. In the dielectric case, also, the more distant sites will make a larger contribution through their larger dipole moments, so that even a relatively small occupation probability could be important. The influence of the more distant shells is expected to be important when the differences in binding energies of the shells are not too large, and when the temperatures are high.

The experimental data are best defined in the case of dielectric relaxation in the alkali halides containing divalent impurities [6–10]. When care is taken to avoid precipitation of the divalent impurity, the frequency spectrum of the relaxation ascribable to these centers can be described as a typical Debye peak, with but a single relaxation time. Lidiard [11] has shown that this is to be expected if the first two shells of neighbors are included in the calculation, and reasonable values assigned to the probabilities for jumps of the vacancy between and within shells. Recently, Dreyfus [12], using a d-c technique of considerably greater time resolution than found in the usual a-c methods, was able to separate two distinct relaxations for which he could account using Lidiard's treatment, and another, slower, relaxation which he has tentatively ascribed to the third and more distant shells.

Lozovskii [13] has made a relaxation mode analysis for this dielectric relaxation including three shells of sites, but considering two rather special cases. For binding energies of the various shells, he chose (1) purely Coulombic values arising from the electrostatic interaction between point charges in a dielectric medium, and (2) the same value for all shells. He calculated both the relaxation times relative to the jump time in the first shell and the relative contributions to the polarizability from each mode. His results indicate that there should be four active modes, but that one will predominate, so that a close approximation to a Debye peak should result even when the third shell is included. Furthermore, the dominant relaxation in both cases was the slowest one. Dreyfus "fast" and "very fast" polarizations can be ascribed to the dominant mode and a superposition of the other three; but since the dominant mode should be the slowest, Lozovskii's result suggests that Dreyfus' "slow" polarization should not be ascribed to the outer shells.

In part 1 of the present paper, we extend the mode analysis to the third shell of neighbors for two cases in the NaCl structure. The Matched Point Defect Pair, in which the trap and the moving defect are both on lattice sites of one kind, as for a cation (anion) vacancy trapped near a cation (anion) impurity; and the Unmatched Point Defect Pair, in which the trap is on one kind of site and the moving defect is on the other, as in a vacancy pair, where either vacancy can be considered as the trapped and the other as the moving defect. This analysis includes all possible relaxation modes under all possible stresses, and includes a discussion of the determination of which modes are excited by a given applied stress. In part 2, we present calculations similar to those of Lozovskii for the relaxation times and polarizabilities for the dielectric relaxation of the three-shell model of a Matched Pair. These calculations have been made with a set of binding energies chosen to provide as realistic as possible a description of the situation in NaCl (Mn), and the results are compared to the available data.

2. Relaxation Modes of Pairs of Point Defects in the NaCl Structure

2.1. Matched Defect Pair (Impurity Ion—Vacancy)

This calculation is a straightforward extension of that reported previously [5] for the two-shell model. The modes for the three-shell model will be linear combinations of the previous ones together with new contributions from the third shell. Because of the complexity of the situation, with 42 sites available to the moving defect, it is preferable to report the modes in tabular form rather than graphically as done before. A 42-fold vector space is defined by the occupation probabilities of the accessible sites. Any distribution is then expressed as a vector $\vec{p}$ in this space. The rate equations are expressible in matrix form, involving a matrix **C** whose elements are c_{ij}, the negative probabilities per unit time that the moving defect will jump from the ith site to the jth site, and c_{ii}, the sum of all jump probabilities out of the ith site. The solutions to the rate equations are then expressible as sums of the eigenvectors of the matrix **C**,

$$\vec{p}=\left[\vec{u}_1+\sum_{i=2}^{N} f_i\vec{u}_i\right]\left(\sum_K u_{1k}\right)^{-1}, \text{ where } f_i=f_{i0}\exp\left[-\lambda_i t\right].$$

In this equation, the $\vec{u}_i$ are the normalized eigenvectors of **C**, $\vec{u}_1$ is the eigenvector for which the eigenvalue (jump rate) is zero and which represents the equilibrium distribution, and the u_{1k} are the components of $\vec{u}_1$. N is the total number of accessible sites, the λ_i are the eigenvalues (jump rates, or reciprocal relaxation times), and the f_{i0} are determined by the initial distribution.

In the irreducible representation technique, the eigenvectors $\vec{u}_i$ are expressed in terms of a set of normalized basis vectors $\vec{v}_{ij}$. To each irreducible representation of the point group of the relaxing center in the vector space of site occupation probabilities corresponds a subspace, spanned by one set of these basis vectors, and from which an equal number of eigenvectors can be constructed. If a transformation matrix is constructed of all of these vectors as columns, it can then be used to transform the matrix **C** to reduced form. The problem has then been reduced to a set of secular equations, one for each irreducible representation whose solutions provide the eigenvalues and the coefficients in the linear combinations of the rectors $\vec{v}_{ij}$ that form the eigenvectors $\vec{u}_i$.

In table 2.1 below, we list the 42 basis vectors used for this problem. The first column numbers the 42 sites in the first three shells of neighbors, and the second column identifies their lattice position with respect to the impurity atom, relative to the cation-anion separation. In the succeeding columns are listed the vectors used as basis vectors, arranged by irreducible representations, which are identified at the top of the columns. As it stands, this table is also the transformation matrix, except that for convenience of presentation, the basis vectors have not been normalized. The irreducible representations are identified in the notation of Eyring, Walter, and Kimball [14].

The secular equations corresponding to each irreducible representation are presented next. It is understood that in solving these secular equations, the normalized basis vectors must be used. The w_{ij} are the probabilities per unit time that the vacancy in a site in the ith shell will jump into a neighboring one in the jth shell. Only jumps from a site to one of its 12 nearest neighbors are allowed. For the interchange of the impurity ion and a vacancy on a first shell site, w_i is used. Analytical solutions for the eigenvalues and for the coefficients in the linear combinations of the basis vectors to form the eigenvectors have not been obtained for the E_g, T_{1u} and the T_{2g} representations.

A_{1g}:

$$\begin{pmatrix} A & -2\sqrt{2}w_{21} & -2\sqrt{2}w_{31} \\ -2\sqrt{2}w_{12} & B & -2w_{32} \\ -2\sqrt{2}w_{13} & -2w_{23} & C \end{pmatrix}\vec{u}=\lambda\vec{u}$$

TABLE 2.1. *Basis vectors (unnormalized) for the matched point defect pair in the NaCl structure*

Site	*xyz*	A_{1g}	A_{2u}	E_g					E_u		T_{1g}			T_{1u}											T_{2g}									T_{2u}					
		1	2	3	4	5	6	7	8	9	10	11	12	13	14	15	16	17	18	19	20	21	22	23	24	25	26	27	28	29	30	31	32	33	34	35	36	37	38	39	40	41	42
1	$\bar{1}\bar{1}0$	1				−2			0								−1			−1					0			1			0			0			0			1		
2	$0\bar{1}1$	1				1			−1								0			−1					1			0			−1			0			−1			1		
3	$1\bar{1}0$	1				−2			0								1			−1					0			−1			0			0			1			−1		
4	$0\bar{1}\bar{1}$	1				1			−1								0			−1					−1			1			0			−1			1			0		
5	$\bar{1}01$	1				1			1								−1			0					1			0			0			1			1			0		
6	101	1				1			1								1			0					−1			0			0			−1			−1			0		
7	$10\bar{1}$	1				1			1								1			0					−1			0			0			−1			−1			0		
8	$\bar{1}0\bar{1}$	1				1			1								−1			0					1			0			0			1			0			−1		
9	$\bar{1}10$	1				−2			0								−1			1					0			−1			0			0			−1			1		
10	011	1				1			−1								0			1					1			0			−1			0			1			−1		
11	110	1				−2			0								1			1					0			−1			0			1			0			1		
12	$01\bar{1}$	1				1			−1								0			1					−1			0														
13	$\bar{2}00$		1				−1			1								−1			0					0																	
14	002		1				2			0								0			0					1																	
15	200		1				−1			1								1			0					0																	
16	$00\bar{2}$		1				2			0								0			0					−1																	
17	$0\bar{2}0$		1				−1			−1								0			−1					0																	
18	020		1				−1			−1								0			1					0																	
19	$\bar{2}\bar{1}1$			1	1			−1			1	−1	1	1	−1	0			−1	0			0	−1		0	1		0	1		−1	0		0	−1		1		0		1
20	$\bar{1}\bar{1}2$			1	1			2			0	2	0	0	1	1			0	−1			0	−1		1	0		1	0		0	−1		0	−1		−1		−1		0
21	$\bar{1}21$			1	1			−1			−1	−1	−1	−1	0	−1			0	−1			−1	0		0	1		0	1		0	−1		−1	0		0	−1		−1		
22	$\bar{2}11$			1	−1			−1			1	1	−1	−1	−1	0			−1	0			0	1		0	1		0	−1		1	0		0	−1		1		0		−1
23	$\bar{1}21$			1	−1			−1			−1	1	1	1	0	1			0	−1			1	0		0	1		0	1		0	1		0	1		0		1		1
24	$\bar{1}12$			1	−1			2			0	−2	0	0	1	−1			0	−1			0	1		1	0		−1	0		0	−1		0	−1		0		1		
25	121			1	1			−1			−1	−1	−1	−1	0	1			0	1			1	0		0	1		0	1		0	1		1	0		−1		1		0
26	211			1	1			−1			1	−1	1	1	1	0			1	0			0	1		0	1		0	1		1	0		0	1		1		0		−1
27	112			1	1			2			0	2	0	0	−1	−1			0	1			1	0		1	0		1	0		0	1		0	1		0		1		1
28	$1\bar{2}1$			1	−1			−1			−1	1	1	1	0	−1			0	1			−1	0		0	1		0	−1		0	−1		1	0		−1		1		0
29	$2\bar{1}1$			1	−1			−1			1	1	−1	−1	1	0			1	0			0	−1		0	1		−1	0		0	−1		0	1		0		−1		−1
30	$1\bar{1}2$			1	−1			2			0	−2	0	0	−1	1			0	1			0	−1		1	0		−1	0		0	−1		0	1		0		−1		
31	$\bar{1}2\bar{1}$			1	−1			−1			−1	1	1	−1	0	1			0	−1			−1	0		0	−1		0	1		0	1		1	0		1		0		0
32	$\bar{1}\bar{1}2$			1	−1			2			0	−2	0	0	−1	−1			0	−1			0	−1		0	−1		1	0		0	1		0	1		−1		0		−1
33	$2\bar{1}\bar{1}$			1	−1			−1			1	1	−1	1	1	0			−1	0			0	1		0	−1		0	−1		1	0		0	1		0		−1		1
34	$\bar{2}1\bar{1}$			1	1			−1			1	−1	1	−1	1	0			−1	0			0	1		−1	0		−1	0		0	−1		0	1		0		1		0
35	$\bar{1}\bar{1}2$			1	1			2			0	2	0	0	−1	1			0	−1			1	0		0	−1		0	−1		0	−1		1	0		−1		0		
36	$\bar{1}21$			1	1			−1			−1	−1	−1	1	0	−1			0	1			0	−1		0	1		0	−1		0	−1		1	0		1		−1		1
37	$2\bar{1}\bar{1}$			1	−1			−1			1	1	−1	1	−1	0			1	0			0	1		0	−1		0	1		−1	0		0	−1		−1		0		1
38	$\bar{1}\bar{1}2$			1	−1			2			0	−2	0	0	1	1			0	1			0	1		0	−1		0	1		0	−1		−1	0		1		1		0
39	$\bar{1}21$			1	−1			−1			−1	1	1	−1	0	−1			0	1			1	0		0	−1		0	1		0	−1		−1	0		1		0		
40	$2\bar{1}\bar{1}$			1	1			−1			1	−1	1	−1	−1	0			1	0			0	−1		0	−1		0	−1		1	0		0	−1		−1		0		−1
41	$\bar{1}\bar{1}2$			1	1			2			0	2	0	0	1	−1			0	1			−1	0		0	−1		0	−1		0	1		−1	0		1		1		0
42	$\bar{1}21$			1	1			−1			−1	−1	−1	1	0	1			0	1			−1	0		0	−1		0	1		0	−1		−1	0		1		−1		
Vector No.		1	2	3	4	5	6	7	8	9	10	11	12	13	14	15	16	17	18	19	20	21	22	23	24	25	26	27	28	29	30	31	32	33	34	35	36	37	38	39	40	41	42

where

$$A=2w_{12}+4w_{13}$$

$$B=4w_{21}+4w_{23}$$

$$C=2w_{31}+w_{32}.$$

Solutions for λ are

$$\lambda=0,\ 1/2\{(A+B+C)\pm[(B-C+2w_{12}-4w_{13})^2+16(w_{13}-w_{23})(2w_{12}-w_{32})]^{1/2}\}$$

$$\vec{u}=a\vec{v}_1+b\vec{v}_2+c\vec{v}_3.$$

(The vectors $\vec{v}_1$, etc., are given in table 2.1.)

. . . . . .

A_{2u}:

$$\lambda=C$$

$$\vec{u}=\vec{v}_4$$

. . . . . .

E_g:

$$\begin{bmatrix} D & -\sqrt{2}w_{21} & -\sqrt{2}w_{31} \\ -\sqrt{2}w_{12} & B & -2w_{32} \\ -\sqrt{2}w_{13} & -2w_{23} & E \end{bmatrix}\vec{u}=\lambda\vec{u}$$

where

$$D=2w_{12}+4w_{13}+6w_{11}$$

$$E=2w_{31}+w_{32}+3w_{33}$$

$$\vec{u}=a\vec{v}_5+b\vec{v}_6+c\vec{v}_7$$

or

$$=a\vec{v}_8+b\vec{v}_9+c\vec{v}_{10}$$

. . . . . .

E_u:

$$\lambda=2w_{31}+w_{32}+3w_{33}$$

$$\vec{u}=\vec{v}_{11} \text{ or } \vec{v}_{12}$$

. . . . . .

T_{1g}:

$$\lambda=2w_{31}+w_{32}+3w_{33}$$

$$\vec{u}=\vec{v}_{13},\ \vec{v}_{14},\text{ or } \vec{v}_{15}$$

. . . . . .

T_{1u}:

$$\begin{bmatrix} K & -2w_{21} & -2w_{31} & -\sqrt{2}w_{31} \\ -2w_{12} & B & -2w_{32} & 0 \\ -2w_{13} & -2w_{23} & G & -\sqrt{2}w_{33} \\ -\sqrt{2}w_{13} & 0 & -\sqrt{2}w_{33} & H \end{bmatrix}\vec{u}=\lambda\vec{u}$$

where

$$K=2w_{12}+4w_{13}+2w_{11}+2w_{1}$$

$$\vec{u}=a\vec{v}_{16}+b\vec{v}_{17}+c\vec{v}_{18}+d\vec{v}_{19}$$

or

$$=a\vec{v}_{20}+b\vec{v}_{21}+c\vec{v}_{22}+d\vec{v}_{23}$$

or

$$=a\vec{v}_{24}+b\vec{v}_{25}+c\vec{v}_{26}+d\vec{v}_{27}$$

. . . . . .

T_{2g}:

$$\begin{pmatrix} F & 0 & -2w_{31} \\ 0 & G & -\sqrt{2}w_{33} \\ -2w_{13} & -\sqrt{2}w_{33} & H \end{pmatrix} \vec{u}=\lambda\vec{u}$$

where

$$F=2w_{12}+4w_{13}+4w_{11}$$

$$G=2w_{31}+w_{32}+2w_{33}$$

$$H=2w_{31}+w_{32}+w_{33}$$

$$\vec{u}=a\vec{v}_{28}+b\vec{v}_{29}+c\vec{v}_{30}$$

or

$$=a\vec{v}_{31}+b\vec{v}_{32}+c\vec{v}_{33}$$

or

$$=a\vec{v}_{34}+b\vec{v}_{35}+c\vec{v}_{36}$$

. . . . . .

T_{2u}:

$$\begin{pmatrix} J & -\sqrt{2}w_{31} \\ -\sqrt{2}w_{13} & E \end{pmatrix} \vec{u}=\lambda\vec{u}$$

where

$$J=2w_{12}+4w_{13}+6w_{11}+2w_{t}.$$

Solutions for λ are: $\lambda=1/2\{(J+E)\pm[(J-E)^2+8w_{13}w_{31}]^{1/2}\}$

$$\vec{u}=a\vec{v}_{37}+b\vec{v}_{38}$$

or

$$=a\vec{v}_{39}+b\vec{v}_{40}$$

or

$$=a\vec{v}_{41}+b\vec{v}_{42}$$

. . . . . .

2.2. Unmatched Point Defect Pair (Vacancy Pair)

The method of calculation is similar to that for the matched point defect pair. Each configuration can be changed into another accessible one by jump of either the cation or the anion defect. Hence, the jump probabilities always occur as the sum of that for the cation and that for the anion defect, and in the notation used here, only these sums will be used. It should also be noted that there are two different types of jumps from a site in the third shell to another in the same shell, distinguished by the path taken. For example, the sites in the third shell are designated by (2,1,0) and its permutations, including negative signs. A jump can only be made to another site in this shell for which the x,y,z differ by ± 1. If the zero stays fixed, there is only one such jump, and the defect remains in a (100) plane as it moves. During the jump, it is screened from the other defect by an ion of opposite sign, in the same (100) plane. The other two possible jumps are with the two remaining fixed, for which the path is

not screened. Presumably, the activation energies for these two jumps will not be the same, and so they will have different jump probabilities. These will be designated by w'_{33} for the screened and w''_{33} for the unscreened jump. With these changes, the notation as used for the previous example will be used to designate the jump probabilities.

The basis vectors are given in table 2.2, again using the cation-anion separation lattice parameter as the repeat distance in designating the sites. The secular equations are given below from which the eigenvalues and coefficients in the linear combinations of basis vectors constituting the eigenvectors can be derived as before.

A_{1g}:

$$\begin{pmatrix} A' & -2\sqrt{3}w_{21} & -2w_{31} \\ -2\sqrt{3}w_{12} & B' & -2\sqrt{3}w_{32} \\ -2w_{13} & -2\sqrt{3}w_{23} & C' \end{pmatrix} \vec{u} = \lambda \vec{u}$$

where

$$A' = 4w_{12} + 4w_{13}$$

$$B' = 3w_{21} + 6w_{23}$$

$$C' = w_{31} + 2w_{32}.$$

Solutions for λ are

$$\lambda = 0,\ 1/2\{(A' + B' + C') \pm [(B' - C' + 4w_{12} - 4w_{13})^2 + 16(2w_{13} - 3w_{23})(2w_{12} - w_{32})]^{1/2}\}$$

$$\vec{u} = a\vec{v}_1 + b\vec{v}_2 + c\vec{v}_3.$$

(The vectors $\vec{v}_1$, etc., are given in table 2.2.)

. . . . . .

A_{2g}:

$$\lambda = w_{31} + 2w_{32} + 2w'_{33} + 4w''_{33}$$

$$\vec{u} = \vec{v}_4$$

. . . . . .

A_{2u}:

$$\lambda = 3w_{21} + 6w_{23}$$

$$\vec{u} = \vec{v}_5$$

. . . . . .

E_g:

$$\begin{pmatrix} D' & -\sqrt{3}w_{31} & -w_{31} \\ -\sqrt{3}w_{13} & E' & -\sqrt{3}w''_{33} \\ -w_{13} & -\sqrt{3}w''_{33} & E'' \end{pmatrix} \vec{u} = \lambda \vec{u}$$

where

$$D' = 4w_{12} + 4w_{13} + 6w_{11}$$

$$E' = w_{31} + 2w_{32} + 2w'_{33} + w''_{33}$$

$$E'' = w_{31} + 2w_{32} + 3w''_{33}$$

$$\vec{u} = a\vec{v}_6 + b\vec{v}_7 + c\vec{v}_8$$

$$= a\vec{v}_9 + b\vec{v}_{10} + c\vec{v}_{11}$$

. . . . . .

TABLE 2.2. *Basis vectors (unnormalized) for the unmatched point defect pair in the NaCl structure*

Site	xyz	A_{1g}		A_{2g}	A_{2u}	E_g						T_{1g}			T_{1u}										T_{2g}						T_{2u}					
1	100	1				−1			1						1				0				0														
2	100	1				−1			1						−1				0				0														
3	010	1				1			−1						0				1				0														
4	0$\bar{1}$0	1				1			−1						0				−1				0														
5	001	1				2			0						0				0				1														
6	00$\bar{1}$	1				2			0						0				0				−1														
7	111		1		1													1				1				1			1							
8	1$\bar{1}$1		1		−1											1		−1				−1				1			1							
9	11$\bar{1}$		1		1											−1		−1				1				1			−1							
10	1$\bar{1}\bar{1}$		1		−1											1		1				−1				1			−1							
11	$\bar{1}$11		1		1											−1		1				−1				−1			1							
12	$\bar{1}$1$\bar{1}$		1		−1											1		−1				−1				−1			1							
13	$\bar{1}\bar{1}$1		1		1											−1		−1				1				−1			−1							
14	111		1		−1											−1		1				1				−1			−1							
15	210			1	1		0	2		−2	0	1	0	0		−1	2			2	1			0	0		1		0		0	0	0	1	2	−2	1
16	1$\bar{2}$0			1	−1		0	2		−2	0	1	0	0		2	1			1	−2			0	0		−1		0		0	0	0	2	−1	2	−1
17	2$\bar{1}$0			1	1		0	2		−2	0	1	0	0		1	−2			−2	−1			0	0		1		0		0	0	0	−1	2	−1	−2
18	120			1	−1		0	2		−2	0	1	0	0		−2	−1			−1	2			0	0		−1		0		0	0	0	2	−1	−1	−2
19	12$\bar{0}$			1	−1		0	2		−2	0	−1	0	0		2	1			−1	2			0	0		1		0		0	0	0	1	2	2	−1
20	2$\bar{1}$0			1	1		0	2		−2	0	−1	0	0		−1	2			−2	−1			0	0		−1		0		0	0	0	−2	1	1	2
21	1$\bar{2}$0			1	−1		0	2		−2	0	−1	0	0		−2	−1			1	−2			0	0		1		0		0	0	0	−1	−2	−2	1
22	210			1	1		0	2		−2	0	−1	0	0		1	−2			2	1			0	0		−1		0		0	0	0	−1	0	0	1
23	021			1	1			1	−1		1	0	1	0			0	0			−1	2			2	1		0		1		0	−2	1	0	0	2	−1
24	01$\bar{2}$			1	−1			−1	−1		−1	0	1	0			0	0			2	1			1	−2		0		−1		0	1	2	0	0	−1	−2
25	0$\bar{2}$1			1	1			1	−1		1	0	1	0			0	0			1	−2			−2	−1		0		1		0	2	−1	0	0	−2	1
26	0$\bar{1}$2			1	−1			−1	−1		−1	0	1	0			0	0			−2	−1			−1	2		0		−1		0	−1	−2	0	0	2	−1
27	012			1	−1			−1	−1		−1	0	−1	0			0	0			2	1			−1	2		0		−1		0	−1	−2	0	0	2	1
28	02$\bar{1}$			1	1			1	−1		1	0	−1	0			0	0			−2	−1			−2	1		0		1		0	2	1	0	0	−2	1
29	0$\bar{1}\bar{2}$			1	−1			−1	−1		−1	0	−1	0			0	0			1	−2			2	1		0		−1		0	−2	1	0	0	−1	−2
30	021			1	1			1	−1		1	0	−1	0			0	0			1	−2			−2	1		0		−1		0	−2	1	0	0	−1	−2
31	102			1	1		−1		−1		1	−1	0	0	1			2	1			0	0			−1	2		0		0		1	1	2	−2	1	0	0
32	20$\bar{1}$			1	−1		−1		−1		1	−1	0	0	1			1	−2			0	0			2	1		0		0		−1	2	−1	1	2	0	0
33	10$\bar{2}$			1	1		−1		−1		1	−1	0	0	1			−2	−1			0	0			1	−2		0		0		1	−1	−2	2	−1	0	0
34	20$\bar{1}$			1	−1		−1		−1		1	−1	0	0	1			−1	2			0	0			−2	−1		0		0		−1	−2	1	−2	1	0	0
35	201			1	−1		−1		1		−1	−1	0	0	−1			−1	2			0	0			2	1		0		0		1	2	−1	−1	−2	0	0
36	10$\bar{2}$			1	1		−1		−1		−1	1	0	0	−1			−2	1			0	0			−1	2		0		0		−1	1	2	2	−1	0	0
37	20$\bar{1}$			1	−1		−1		1		−1	1	0	0	−1			1	−2			0	0			1	−2		0		0		1	−2	−2	1	0	0	0
38	10$\bar{2}$			1	1		−1		−1		1	−1	0	0	−1			2	1			0	0			1	−2		0		0		1	−1	−2	−2	1	0	0
Vector No.		1	2	3	4	5	6	7	8	9	10	11	12	13	14	15	16	17	18	19	20	21	22	23	24	25	26	27	28	29	30	31	32	33	34	35	36	37	38

T_{1g}:

$$\lambda = w_{31} + 2w_{32} + 2w'_{33} + 2w''_{33}$$

$$\vec{u} = \vec{v}_{12},\ \vec{v}_{13},\ \text{or}\ \vec{v}_{14}$$

. . . . . .

T_{1u}:

$$\begin{pmatrix} K' & -2w_{21} & 2w_{31}/\sqrt{5} & -4w_{31}/\sqrt{5} \\ -2w_{12} & B' & -2w_{32}/\sqrt{5} & -6w_{32}/\sqrt{5} \\ 2w_{13}/\sqrt{5} & -2w_{23}/\sqrt{5} & L' & -(4w''_{33}-3w'_{33})/5 \\ -4w_{13}/\sqrt{5} & -6w_{23}/\sqrt{5} & -(4w''_{33}-3w'_{33})/5 & L'' \end{pmatrix} \vec{u} = \lambda \vec{u}$$

where

$$K' = 4w_{12} + 4w_{13} + 4w_{11}$$

$$L' = w_{31} + 2w_{32} + (9/5)w'_{33} + (8/5)w''_{33}$$

$$L'' = w_{31} + 2w_{32} + (1/5)w'_{33} + (2/5)w''_{33}$$

$$\vec{u} = a\vec{v}_{15} + b\vec{v}_{16} + c\vec{v}_{17} + d\vec{v}_{18}$$

or

$$= a\vec{v}_{19} + b\vec{v}_{20} + c\vec{v}_{21} + d\vec{v}_{22}$$

or

$$= a\vec{v}_{23} + b\vec{v}_{24} + c\vec{v}_{25} + d\vec{v}_{26}$$

. . . . . .

T_{2g}:

$$\begin{pmatrix} B' & -2w_{32} \\ -2w_{23} & G' \end{pmatrix} \vec{u} = \lambda \vec{u}$$

where

$$G' = w_{31} + 2w_{32} + 2w''_{33}.$$

Solutions for λ are $\lambda = 1/2\{(B'+G') \pm [(B'-G')^2 + 16w_{23}w_{32}]^{1/2}\}$

$$\vec{u} = a\vec{v}_{27} + b\vec{v}_{28}$$

$$= a\vec{v}_{29} + b\vec{v}_{30}$$

or

$$= a\vec{v}_{31} + b\vec{v}_{32}$$

. . . . . .

T_{2u}:

$$\begin{pmatrix} J' & (4w''_{33}-3w''_{33})/5 \\ (4w''_{33}-3w'_{33})/5 & J'' \end{pmatrix} \vec{u} = \lambda \vec{u}$$

where

$$J' = w_{31} + 2w_{32} + (1/5)w'_{33} + (12/5)w''_{33}$$

$$J'' = w_{31} + 2w_{32} + (9/5)w'_{33} + (18/)w''_{33}.$$

Solutions for λ are $\lambda = (w_{31} + 2w_{32} + w'_{33} + 3w''_{33}) \pm [w'^2_{33} + w''^2_{33}]^{1/2}$

$$\vec{u} = a\vec{v}_{33} + b\vec{v}_{34}$$

or

$$= a\vec{v}_{35} + b\vec{v}_{36}$$

or

$$= a\vec{v}_{37} + b\vec{v}_{38}$$

. . . . . .

2.3. Excitation of the Modes by Applied Stresses

While the analysis above reveals the modes by which a relaxation process can take place it does not provide any way of deciding which modes will be excited by a given applied stress. This question can, however, be answered in the following way. Consider the system under a constant stress of the specified sort. The influence of the stress will be to lower the symmetry of the crystal to that common to the applied stress and the undisturbed crystal (Curie's law [15]). Thus, from a knowledge of the symmetry of the applied stress and the undisturbed point group of the defect center under consideration, the point group under stress can be determined. It will be a subgroup of the unstressed point group. In the presence of the stress, the system will adopt the equilibrium configuration appropriate to the new point group, and represented by the new A_{1g} mode, for which the relaxation rate is zero. When the stress is removed, the system will begin to relax, but now with the modes appropriate to the undisturbed point group. Hence, the problem of deciding which modes will be excited is the problem of expressing the equilibrium mode under the stressed point group in terms of the unstressed modes.

The irreducible representations of the unstressed group each correspond to a subspace of the total vector space, such that these subspaces are mutually orthogonal. Under the stressed group, the equilibrium mode corresponds to a single vector, which must of necessity be a linear combination of mutually orthogonal components drawn from the appropriate subspaces identified with the irreducible representations of the unstressed group. Since each of these components, in turn, can be expressed as a linear combination of the basis vectors of the corresponding unstressed irreducible representation, then the stressed equilibrium mode must be expressible as a linear combination of the unstressed modes whose corresponding irreducible representations have as a component the stressed irreducible representation A_{1g}. Hence, the problem is to examine the irreducible representations of the unstressed group and determine which of these has as a component the stressed A_{1g} irreducible representation.

This determination is readily done with the character table. Since the irreducible representations of a group are also representations, although not necessarily irreducible, of its subgroups, the character table of the irreducible representations of the full group can be consulted, and the examination restricted to the entries under the elements of the subgroup. For a given irreducible representation of the full group, these constitute the characters of that representation of the subgroup, and by inspection and comparison to the character table for the subgroup, the components among the irreducible representations of the subgroup determined. In this way, all of the irreducible representations of the full group can be found that have as a component the A_{1g} representation of the subgroup. The corresponding relaxation modes of the unstressed system are those that will be excited by the stress that produced the subgroup.

As an example, consider the case of the matched point defect pair in NaCl, and let the stress be an electric field applied along one cube axis. The unstressed group is the full cubic group, m3m in the international notation; while under the field, this is reduced to 4mm. Inspection of the character tables reveals that the unstressed irreducible representations which have the A_1 irreducible representation of the stressed subgroup as a component are the A_{1g}, the E_g, and the T_{1u}. On the other hand, a simple tension or compression along a cube axis reduces the point group to 4/mmm, and results in excitation of the A_{1g} and the E_g. This result can be interpreted as follows. The A_{1g} mode will always be excited in principle, because a stress will never shift the distribution completely away from the equilibrium distribution, and there must be a term to describe what is left. The E_g mode represents the departure from equilibrium that provides the symmetric extension or contraction along the cube axis produced by the tension or compression. Under the axial electric field, this mode is also excited and corresponds to the electrostriction.

There is a rather simple way of determining the number of independent relaxation times to expect for the excited modes that parallels the above development. Under the applied stress, in the new point group, the sites will have been further subdivided into independent and noninteracting subspaces, analogous to the various shells of neighbors of the unstressed crystal.

The A_{1g} mode in the stressed point group will be the sum of vectors, one from each subspace, each formed simply by assigning unity to each site in the subspace. These vectors are the mutually orthogonal components making up the new equilibrium as discussed above. The number of distinct relaxation times observable in principle under the applied stress will be just the number of these independent subspaces produced with the proviso that one of these relaxation times will be infinite, corresponding to the equilibrium mode, and the others finite.

This treatment can, of course, be generalized. A listing of all subgroups reached by the application of any homogeneous second rank tensor stress to any crystal was given by Wachtman and Peiser [16]. In table 2.3, we complete this tabulation by listing all subgroups reached by the application of a vector stress, such as an electric field. Koptsik [17] has tabulated the subgroups reached by various types of influence, but his tables apparently do not apply to the present case. The subgroups which can be reached by application of an electric field have previously been listed by Vlokh and Zheludev, [18] but the meaning of their table for the cubic groups is hard to interpret, at least in the English translation. Table 2.3 also gives some additional information. The subgroups are classified as to whether they are normal subgroups (sometimes termed self-conjugate or invariant subgroups) of the starting point group. This classification shows that the cryptosymmetry theory of Niggli [19] and Wittke [20] apparently cannot be applied directly to the treatment of relaxation modes. In Niggli's theory, each atom is considered to have some additional property, such as magnetic moment, and the symmetry group possessed by the crystal when this additional property is taken into account must be a subgroup of the group obtained when this additional property is ignored. One might attempt to take the probability of occupation by a vacancy as the additional property and discuss relaxation modes in terms of cryptosymmetry. However, in Niggli's theory, only normal subgroups are permitted, and table 2.3 shows that many of the subgroups which can be reached by the action of an electric field are not normal subgroups. It thus appears that some modification or extension of the concept of cryptosymmetry would be required if it were applied to relaxation modes.

TABLE 2.3

Original point group	Vector field: Subgroups										Total number of symmetry subgroups other than original group	Number of subgroups other than original group reached by application of vector	Number of subgroups other than original group reached by application of symmetric tensor of second rank
	(C_{6v})	(C_6)	(C_{3v})	(C_3)	(C_{4v})	(C_4)	(C_{2v})	(C_s)	(C_2)	(C_1)			
	6mm	6	3m	3	4mm	4	mm2	m	2	1			
m3m (O_h)			x−		x−		x−	x−		x	24	5	5
43m (T_d)			x−				x−	x−		x	10	4	7
432 (O)				x−		x−			x−	x	8	4	5
m3 (T_h)				x−			x−	x−		x	11	4	4
23 (T)				x−					x−	x	4	3	4
6/mmm(D_{6h})	x						x−	x		x	19	4	3
6m2 (D_{3h})			x				x−	x		x	8	4	4
6mm (C_{6v})	0							x−		x	7	2	3
622 (D_6)		x							x	x	6	3	3
6/m (C_{6h})		x						x		x	9	3	2
6 (C_{3h})*				x				x		x	3	3	2
6 (C_6)*		0								x	3	1	2
3m (D_{3d})			x					x−	x−	x	9	4	2
3m (C_{3v})			0					x−		x	3	2	2
32 (D_3)				x					x−	x	3	3	2
3 (C_{3i})*				x						x	3	2	1
3 (C_3)*				0						x	1	1	1
4/mmm (D_{4h})					x		x	x		x	14	4	3
42m (D_{2d})							x	x−	x	x	6	4	5
4mm (C_{4v})					0			x−		x	5	2	4
422 (D_4)						x			x	x	4	3	3
4/m (C_{4h})						x		x		x	7	3	2
4 (S_4)*									x	x	2	2	2
4 (C_4)*						0				x	2	1	2
mmm(D_{2h})*							x	x		x	7	3	2
mm2(C_{2v})*							0	x		x	3	2	3
222 (D_2)*									x	x	2	2	2
2/m (C_{2h})*								x	x	x	4	3	1
m (C_s)*								0		x	1	1	1
2 (C_2)*									0	x	1	1	1
1 (C_i)*										x	1	1	0
1 (C_1)*										0	0	0	0

x Subgroup other than original point group.
0 Original point group is a permissible subgroup of itself under vector field.
x− Indicates nonnormal subgroup.
* Cyclic parent, all subgroups normal.

Table 2.3 also shows that some groups can occur as their own subgroups under the action of electric field while others cannot. This distinguishes between cases in which it is possible to apply a suitably oriented electric field which will excite no relaxation mode (except, of course, the trivial mode) and other cases in which any field no matter what its orientation will excite a nontrivial mode. It should be noted that if a purely arbitrary direction of the stress axis be chosen, it can always be arranged that no symmetry elements exist in common with the unstressed point group and the stress, so that the symmetry is reduced to the identity operation 1, and all modes are excited. The application of a homogeneous tensor stress to a centrosymmetric crystal can reach $\bar{1}$, so that any centrosymmetric mode can be excited. These results have their parallel in the expansion of the thermodynamic potential of a crystal in terms of elastic, dielectric, piezoelectric, electrostrictive, etc., coefficients, including higher order terms.

The ability of a suitably oriented electric field to excite all relaxation modes does not conflict with the classification of modes by Haven and van Santen [1, 2] into electrically active, mechanically active, etc., provided that their classification is taken to mean the modes which are most strongly excited by the appropriate influence with the understanding that other modes may be less strongly excited. One can understand how this occurs by considering the effect of an electric field upon an electrically active mode and upon a mechanically active mode. The effect of a static electric field is to shift the energy levels of the sites. These energy shifts, E_j, affect the occupation probabilities exponentially through their appearance in Boltzmann factors; each exponential can be expanded in a power series and only the first few terms kept if the energy shift is small compared to kT. The zeroth order terms are each multiplied by the shift in occupation probability for the corresponding site and then summed to give the change in potential energy. For an electrically active mode (one with a dipole moment) the sum will not be zero, and the mode will be excited to first order in the field; for a mechanically active mode, the sum must be exactly zero because the mode is centrosymmetric so that the mode will not be excited to first order in the field. However, the second order terms from the power series will all be of the same sign and when multiplied by a centrosymmetric pattern of occupation probability and summed, these will give a nonzero result so that a mechanical mode can be excited in second order by an electric field. This line of argument leads to the following rule for the excitation of relaxation modes in terms of their lowest order nonzero moments: Modes having a dipole moment can be excited in the first order by electric field; those with a quadrupole moment can be excited in the first order by mechanical stress or in the second order by electric field; those having an octapole moment can be excited in the third order by electric field; those having a 16-pole moment can be excited in the second order by mechanical stress and in the fourth order by electric field.

Chang [22] has recently tabulated the mechanical modes (in the above sense) for paired point defects in a number of structures with m3m point group symmetry.

3. Dielectric Relaxation in NaCl Containing Divalent Impurity Ions

In order to assess as realistically as possible the influence of the third shell on the dielectric behavior of a real system, we have calculated the dielectric relaxation times and polarizabilities using jump frequencies estimated to correspond to a vacancy trapped near a Mn^{++} ion in NaCl, and employing the results of the present paper. The jump frequencies were chosen as follows. It was assumed that the jump frequency from the ith to the jth site could be given by $w_{11} \exp [(E_j - E_t)/2kT]$, where the E_j are the binding energies of the various sites, and the w_{11} is the jump frequency in the first shell. Furthermore, following Haven [21], w_{33} was taken to be $\frac{1}{3}\, w_{11}$ and w_t was neglected. For the binding energies, the value of 0.41 eV given by Watkins [23] for the first shell was used, and the value of 0.38, derived from his determination of 0.034 eV as the difference in binding energies between the first and second shells, was chosen for the latter. Coulombic energies were plotted for the first nine shells, and a

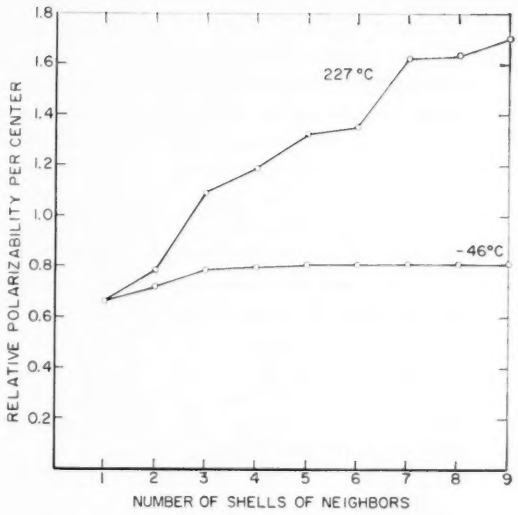

FIGURE 1. *Relative polarizabilities for the matched point defect pair, in units of* $(ea)^2/kT$ *where* e *is the charge on each defect and* a *is the nearest neighbor distance, for models allowing from 1 to 9 shells of neighbors.*

smooth curve drawn through Watkins two values and joining the Coulombic curve at and above the fifth shell. Temperatures of −46° and 227° C were chosen to match the experimental ranges of Dreyfus [12] and Watkins [23] respectively.

With these values for the binding energies, an estimation of the polarizability per center could be made for models allowing access to various numbers of shells of neighbors. The relative polarizabilities per center, in units of $(ea)^2/kT$ where e is the charge per defect and a is the distance between nearest neighors, are shown in figure 1 for the two temperatures. At −46 °C, little error is made in stopping at the third shell, but at 227 °C, the magnitude of the polarizability is at least three times that estimated from a single shell of neighbors. The influence of outer shells certainly cannot be neglected, at least at the higher temperatures.

The contribution of each of the electrically active modes to the total polarizability is given in table 3.1. The outstanding feature is the dominance of the slowest mode. This contributes 96 percent of the total polarizability at both −46 °C and 227 °C, and leads to the conclusion that a Debye peak would result from an a-c study of the dielectric relaxation with an apparent single relaxation time, even if the influence of the third shell were included.

In the present calculation, the third shell contributed 46 percent of the polarizability at 227 °C, and 10 percent at −46 °C. It appears that the dominance of one mode in the polarizability may be a general feature of these models, regardless of the number of shells included.

The effect of temperature upon the relaxation can be seen from the figures in table 3.1.

TABLE 3.1. *Dielectric relaxation of 3-shell model*

	Relaxation rate		Contribution to polarizability	
Mode	−46 °C	227 °C	−46 °C	227 °C
1	2.38 w_{11}	2.07 w_{11}	96.0%	96.5%
2	11.14 w_{11}	6.31 w_{11}	2.7	0.5
3	14.21 w_{11}	8.10 w_{11}	1.2	1.2
4	15.54 w_{11}	10.05 w_{11}	0.1	2.8

4. Summary

The results of a relaxation mode analysis are presented for two cases of trapped-defect elaxation in the NaCl structure, in which both defects occupy the same type of site (e.g.,

impurity divalent ion and trapped vacancy), or in which they occupy the two different types of sites (vacancy pair). The relaxation analysis is presented in the form of a set of basis vectors in occupation-probability space and a set of secular equations. Solutions to the equations provide the relaxation rates and also the coefficients in the linear combinations of the basis vectors which constitute the relaxation modes.

The modes excited by the application of a given stress can be deduced from the subgroup of the full symmetry group of the crystal reached by action of the stress. Under this subgroup, some of the group representations that were irreducible under the full group become reducible. Some of them contain the A_{1g} irreducible representation of the subgroup as a component. The corresponding modes are then the ones that are excited by the stress.

Calculations of the relaxation rates and contributions to the polarizability of the various modes for a three-shell model with jump frequencies chosen to represent the relaxation of an impurity-ion vacancy pair in NaCl (Mn) have confirmed the results of Lozovskii [13]. Even though the third shell makes a significant and even large contribution to the process, one mode dominates and the relaxation as seen in a-c measurements would take place with essentially a single relaxation time. The d-c techniques of Dreyfus [12] are sensitive enough to detect more than one of these relaxations at low temperatures, but the slowest of these will always be the dominant one. Any relaxation slower than the major one must be ascribed to some other mechanism.

The authors thank H. S. Peiser for help with table 2.3.

5. References

[1] Y. Haven and J. H. van Santen, J. Chem. Phys. **22,** 1146 (1954).
[2] Y. Haven and J. H. van Santen, Nuovo Cimento **7,** 605 (1958).
[3] J. B. Wachtman, Jr., Phys. Rev. **131,** 517 (1963).
[4] S. Bhagavantam and P. V. Pantulu, Point Defects and Relaxation Phenomena in Crystals, Proc. Indian Academy of Sciences **58,** 183–196 (1963).
[5] A. D. Franklin, J. Res. NBS **67A,** 291 (1963).
[6] A. B. Lidiard in Handbuch der Physik **20,** 246 (1957) (Ed. S. Flugge; Springer—Verlag, Berlin).
[7] J. S. Dryden and R. J. Meakins, Disc. Far. Soc. **23,** 39 (1957).
[8] G. D. Watkins, Phys. Rev. **113,** 91 (1959).
[9] J. S. Cook and J. S. Dryden, Australian J. Phys. **13,** 260 (1960).
[10] G. Jacobs, L. G. Vandewiele, and A. Hamerlinck, J. Chem. Phys. **36,** 2946 (1962).
[11] A. B. Lidiard, Defects in Crystalline Solids—Report of 1954 Bristol Conference (The Physical Society, London 1955), p. 283.
[12] R. W. Dreyfus, Phys. Rev. **121,** 1675 (1961).
[13] V. N. Lozovskii, Izv. Akad. Nauk S. S. S. R. **24,** 161 (1960).
[14] H. Eyring, J. Walter, and G. E. Kimball, Quantum Chemistry (John Wiley & Sons, New York, N.Y., 1944).
[15] P. Curie, J. de Phys. **3,** 393 (1894).
[16] J. B. Wachtman, Jr., and H. S. Peiser, Appl. Phys. Ltrs. **1,** 20 (1962).
[17] V. A. Koptsik, Polymorphic Phase Transitions and Symmetry, Soviet Physics-Crystallography **5,** 889–898 (1961). Translated from Kristallografiya **5,** 932–943 (1961).
[18] O. G. Vlokh and I. S. Zheludev, Changes in the Optical Parameters of Crystals Caused by Electric Fields, Soviet Physics—Crystallography **5,** 368–380 (1961). Translated from Kristallografiya **5,** 390–402 (1961).
[19] A. Niggli, Zur Systematik und gruppentheoretischen Ableitung der Symmetrie, Antisymmetrie—und Entartungssymmetriegruppen. Z. Kristallogr. **111,**, 283–300 (1959).
[20] Oscar Wittke, The Colour-symmetry Groups and Cryptosymmetry Groups Associated with the 32 Crystallographic Point Groups, Z. Kristallogr. **117,** 153–165 (1962).
[21] Y. Haven, Defects in Crystalline Solids—Report of 1954 Bristol Conference (The Physical Society, London 1955), p. 261.
[22] Roger Chang, Mechanical Relaxation Associated with Paired Point Defects in Cubic Lattices of O_h Point Group Symmetry. Submitted to J. Phys. Chem. Solids.
[23] G. D. Watkins, Phys. Rev. **113,** 79 (1959).

(Paper 68A5-290)

JOURNAL OF RESEARCH of the National Bureau of Standards—A. Physics and Chemistry
Vol. 68A, No. 5, September–October 1964

Viscosity of a Standard Soda-Lime-Silica Glass

Albert Napolitano and Earl G. Hawkins

(May 11, 1964)

The viscosity of a soda-lime-silica glass has been measured at the National Bureau of Standards and seven other laboratories. Determinations were made in the range of 10^2 to 10^{15} poises. The rotating cylinder was used at the higher temperatures (800 to 1450 °C) and the fiber elongation method at the lower temperatures (520 to 658 °C). The results have been critically evaluated and the glass has been issued as Standard Sample No. 710. This glass is available from the National Bureau of Standards.

1. Introduction

As a part of a program of establishing standard samples of glasses, the National Bureau of Standards has obtained a large quantity of soda-lime-silica glass of uniform composition. The viscosity of this glass has been measured at the National Bureau of Standards and at seven other laboratories.[1] The results have been analyzed and tabulated in a "Certificate of Viscosity Values" and the glass (with certificate) has been issued as Standard Sample No. 710.

The soda-lime-silica glass was selected as the first of a series of standard glasses because it is relatively stable both in storage and at the temperatures at which viscosity measurements are made. Also it is of a composition close to that of commercial glasses that are made in the largest quantities.

A lead-silicate glass which is representative of another important commercial group of glasses has been selected as a second standard glass. This will soon be issued as a viscosity standard (No. 711). As a continuation of this program on standard glasses, other physical properties will be measured on these two glasses as well as on other glasses to be issued as standards.

2. Sample

Over the course of a number of years there have been several attempts by individual laboratories and by cooperative efforts among several laboratories to produce lots of glass that could be used for standards of viscosity and other physical properties. In spite of painstaking measurements of properties, these attempts were not completely successful and it has been generally concluded that the major reason has been that the lots of glass from which samples were taken were not sufficiently uniform for the purpose. With this background, every effort was made at the start of this work to obtain a quantity of glass that was as uniform as possible and to verify the uniformity before attempting to make viscosity measurements.

A contract was placed with a glass producer to furnish 900 kg of soda-lime-silica glass in equipment which is used for the continuous production of optical glass of instrument quality. It was specified that the entire lot was to be produced in one continuous operation, without changes in the batch composition. It was further specified that the index of refraction of the entire lot should be uniform within ± 0.0001 after all samples had been given a uniform heat treatment. The supplier was able to comply with these stringent requirements except that no glass was supplied for three brief periods during the operation when the glass was apparently either off index or was discarded for other reasons.

The glass was made in the form of bars having a cross section of about 5 cm by 7.5 cm. This was cut in lengths of 60 to 100 cm. The bars were marked with the hour of manufacture to show the sequence of production.

When the glass was received the homogeneity was checked by measuring the index of refraction on specimens taken from about every 10 kg of glass. This corresponded to an average of two to three index samples for every hour of the production run. Samples were measured both in the condition as received and after they all had been given the same heat treatment. The results of these index measurements are shown in figure 1. Only one value is plotted for each hour for clarity. Index of refraction (N_D-line) measurements were made on a Grauer-type refractometer which is accurate to approximately ± 0.00002 [1].[2]

Uniformity of index is not an absolute check on uniformity of composition, since it is possible for glasses of widely different chemical composition to have the same index of refraction. However, considering the conditions under which this glass was made, that is, in a continuous operation with no deliberate changes in batch composition, it would require a most unusual set of circumstances to permit a significant change in composition that

[1] List of participating laboratories which made viscosity and other property measurements on Standard Sample No. 710:
Armstrong Cork Co., Lancaster, Pa.
Bausch & Lomb, Inc., Rochester, N.Y.
Brockway Glass Co., Inc., Brockway, Pa.
Corning Glass Works, Corning, N.Y.
Emhart Manufacturing Co., Hartford, Conn.
General Electric Co., Cleveland, Ohio
Hazel-Atlas Glass Co., Plainfield, Ill.
Kimble Glass Div., Owens-Illinois, Vineland, N.J.
National Bureau of Standards, Washington, D.C. (Lab. A).
Owens-Corning Fiberglas Corp., Granville, Ohio
Owens-Illinois, Toledo, Ohio
University of Rochester, Rochester, N.Y.

[2] Figures in brackets indicate the literature references at the end of this paper.

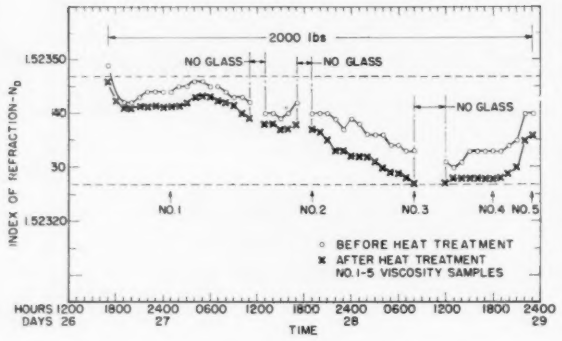

FIGURE 1. *Index variation of Standard Glass No. 710.*

would not be reflected by changes in index of refraction. The most likely causes of composition changes in the glass produced in a continuous type of melting operation would be changes in volatilization losses, refractory solution, or inadvertent changes in batch composition during the more than two days required to make the lot of glass.

The chemical composition of the glass as calculated from batch composition was as follows:

SiO_2	70.5 percent
Na_2O	8.7
K_2O	7.7
CaO	11.6
Sb_2O_3	1.1
SO_3	0.2
R_2O_3	0.2 (Fe_2O_3—0.02%)

Chemical analyses[3] were made by four of the participating laboratories and their results indicate that the glass composition conforms closely to that given above. No attempt was made to analyze a large number of samples from the melt since it was believed that the chemical methods would not be sufficiently sensitive to reflect the small differences in composition that could be detected by measurements of index of refraction. In this composition range a change of approximately 0.06 percent in Na_2O will change the index by 0.0001 [2].

As a further check on uniformity, measurements of viscosity were made on five samples taken from different positions in the lot of glass (fig. 1, Nos. 1, 2, 3, 4, and 5). Three of the samples, Nos. 2, 3, and 5, were selected in regions where index of refraction showed the greatest rate of change. It will be seen later (table 4) that the uniformity of these samples was within specified limits. The details of these measurements are given in the section of this paper on Results.

3. Apparatus and Method of Measurement

The apparatus and methods used at the National Bureau of Standards for measuring viscosity are described in detail, those used by the cooperating laboratories are covered by brief descriptions or literature references.[4]

3.1. High-Temperature Viscometer

In the range of 10^2 to 10^6 poises the rotating concentric cylinder method was used to measure the viscosity. This method has been used by many earlier investigators in their studies on glass. The geometry of the apparatus was similar to that of Bockris and Lowe [3], Lillie [4], and Robinson and Peterson [5] except for a modification of method of measuring the torque on the spindle.

The platinum-wound resistance furnace, figure 2 consists of one main coil and two auxiliary coils. The main heating coil (inner core) was wound on a 7.6 cm (3 in.) i.d. alundum core 35.6 cm (14 in.) long with 80 percent Pt–20 percent Rh resistance wire 0.081 cm (0.032 in.) diam and six turns per 2.54 cm (1 in.). The outer heating coils (outer core) were wound at each end of an alundum core 9.5 cm (3¾ in.) i.d. and 35.6 cm (14 in.) long. Each coil consisted of 18 to 20 turns. There were separate controls for each winding.

The crucible was made of 1-mm-thick platinum and was 5 cm diam and 10 cm high. The bob was 1.25 cm diam, 3.75 cm long with 45° tapered ends, and was suspended by a hollow platinum spindle 0.635 cm diam and 29.5 cm long. The bore of the spindle, 0.3175 cm diam, extended into the center of the bob to accommodate a thermocouple for measuring the temperature of the glass before and after viscosity measurements.

The crucible was mounted and centered on a mullite pedestal which extended out through the bottom of the furnace and was attached to a turntable which was an integral part of the driving mechanism. The 25.0 cm pedestal was hollow and accommodated another thermocouple to read temperatures directly below the bottom of the crucible. A commercial insulation "Fiberfrax" which was used to pack the opening around the pedestal, offered no resistance to the rotation or vertical movement.

The complete driving mechanism was mounted on an elevator table which had 25.0 cm vertical travel. The drive consisted of an 1800-rpm, ⅛-hp synchronous motor connected to interchangeable gear reducers which gave a range of crucible speeds from 0.030288 rpm to 1.3493 rpm.

The short (15-sec) term period of frequency stability of the power line had a mean error from 60 c/s of 0.1 percent and a maximum error from 60 c/s of 0.2 percent. For a long (30-min) term period the frequency stability had a mean error from 60 c/s of 0.038 percent and a maximum error from 60 c/s of 0.077 percent. This gave very good speed control on the outer crucible during viscosity measurements.

An electromagnetic torque balance [3] based on the principle of a large moving coil galvanometer was used to measure the torque by a null detection method.

[3] This glass is not intended as a standard for chemical analysis.

[4] The authors have gone into considerable detail on the design and construction of their apparatus because of the numerous inquiries they have received asking about this particular experimental setup.

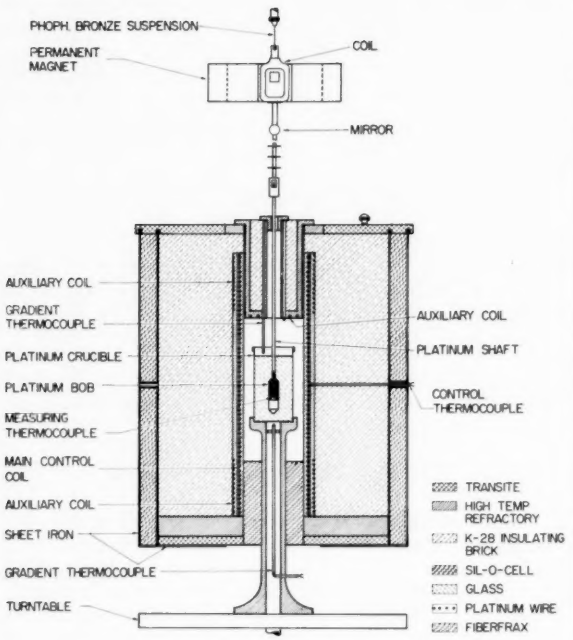

FIGURE 2. *High-temperature viscosity furnace.*

The galvanometer was made up of a permanent magnet Alnico II (sintered) with a 1650 gauss gap field strength and a coil which was an integral part of the suspension apparatus. The C-type magnet had a gap 4.76 cm wide, 4.76 cm high, and 3.81 cm deep. It was mounted on movable plates so that the magnet could be adjusted in any horizontal direction. The coil consisted of a rectangular aluminum frame with about 500 m of No. 34 insulated copper wire wound around it. The resistance of the coil was 425 Ω. In series with the coil were several resistors adjustable from 20,000 Ω to 300,000 Ω, fixed resistors 1 MΩ to 10 MΩ and four standard fixed resistors 10 Ω, 25 Ω, 100 Ω, and 1000 Ω. Current in the coil was adjusted to set up a coupling force which was opposite to that set up by the rotating crucible. The balance was observed through a telescope on a 1-m-radius scale set 1 m distant from a reflecting mirror on the axis of the suspension shaft just below the coil. The amount of current through the coil was found by measuring the voltage across a standard resistor with a Type K potentiometer. Polarity in the circuit could be reversed to accommodate reversal of crucible rotation.

The coil of the suspension apparatus was connected to an adjustable head. The suspensions were 5 cm long and made of phosphor-bronze wire ranging in diameter from 0.020 cm to 0.0635 cm, and were easily interchangeable to obtain sensitivity needed. The coil was connected to the platinum spindle by a brass rod which had a series of fins on it to radiate heat and a chuck to hold the platinum spindle of the bob.

The apparatus was calibrated at 25 °C and 40 °C with NBS Standard oils. These oils ranged in viscosity from 1 P to 500 P. Temperatures were measured with a calibrated copper-constatan thermocouple in the same way that they would be measured at higher temperatures with Pt–PtRh thermocouples. Since molten glasses cover such a wide range of viscosities the calibration was checked at higher viscosities (10^2 to 10^5 P) with "abitol."[5]

Calibration was carried out at a given level of liquid (oil) in the crucible and the bob immersed to 12 mm of the bottom of the crucible. These conditions of liquid level and depth of immersion were maintained at elevated temperatures, using molten glass, by adjusting the position of the crucible to allow for expansion of glass and the furnace components with increase in temperature. This amounted to lowering the crucible about 0.5 mm for every 100° C increase in temperature of measurement. The calibration was also corrected for the volume expansion of the platinum bob when used at the higher temperatures. This correction ranged from 2.5 to 4.5 percent depending on the temperature of measurement.

In making measurements at high temperatures, readings were taken on three thermocouples: one above the surface of the glass, one just below the crucible, and one inside the inner cylinder or bob. Once the two thermocouples above and below the glass read within 1 °C, a reading was taken of the one inside the bob; torque measurements were made at various angular velocities in both directions, and then another reading of the thermocouples was taken. The leads to the thermocouples inside the bob and below the crucible were disconnected when the torque measurements were taken. The average of the two temperature readings, before and after, was taken as the viscosity temperature of measurement.

The current I required to counterbalance or zero the torque producing the deflection angle of the inner bob (in the rotating viscometer) is directly proportional to the viscosity η of the test liquid and the angular velocity ω of the outer rotating crucible, i.e.,

$$I = C\omega\eta \tag{1}$$

where C=constant of proportionality depending on the geometry of the apparatus.

Comparing the current I_2 of an unknown liquid with that of a "standard" or liquid of known viscosity, I_1, [6] one has

$$\frac{I_2}{I_1} = \frac{\eta_2\omega_2}{\eta_1\omega_1}$$

or

$$\eta_2 = \eta_1 \frac{I_2\omega_1}{I_1\omega_2} \tag{2}$$

[5] A sample (Lot AZK108) was obtained from Hercules Powder Co., Wilmington, Del., for experimental use only. This was measured, using a calibrated Hoeppler viscometer, at 30, 40, and 50 °C.

where the subscripts 1 and 2 stand for the known and unknown liquids, respectively.

3.2. Low-Temperature Viscosity

Measurements of low-temperature viscosity were made by the fiber elongation method. This method has been developed by many investigators such as Lillie [4], Robinson and Peterson [5], Poole [7], Norton [8], and Boow and Turner [9]. The derivation of the equation used for determining the viscosity by this method is given by Lewis, Squires, and Broughton [10].

$$\eta = \frac{Fl}{3A\frac{dl}{dt}} \tag{3}$$

or as used in these calculations

$$\eta = \frac{60Flf}{3A\frac{dl}{dt}}$$

where:

F=extending force (dyn)
l=fiber length (cm)
A=fiber cross-section area (cm^2)
f=multiplying factor of optical lever
$\frac{1}{f}\frac{dl}{dt}$=elongation rate (cm/min)

The tube furnace used in these measurements was 50.8 cm (20 in.) high and 15.2 cm (6 in.) diam, figure 3. It was heated by three separately controlled windings of 80 percent Pt–20 percent Rh resistance wire wound on a 4.1 cm (1–5/8 in.) i.d. alundum core. The inner silver core 25.4 cm (10 in.) long and 3.81 cm (1 1/2 in.) diam had an inside bore 0.635 cm (1/4 in.) diam to accommodate the fiber and also two off-center holes at the top and bottom to the midpoint of the core for thermocouples. The fiber was suspended by means of stainless steel rods and Inconel chucks.

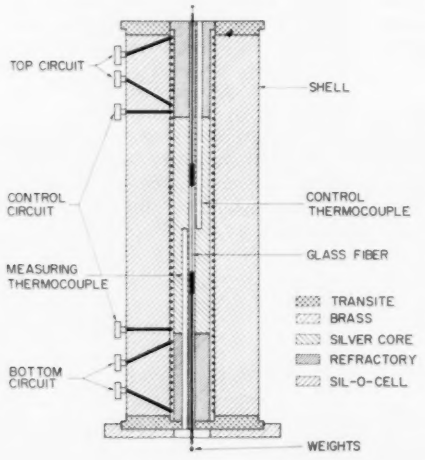

FIGURE 3. *Low-temperature viscosity furnace.*

The fibers used in these measurements were 0.5 to 1 mm in diameter, 10 cm long, and of uniform diameter throughout their length. All fibers were well-annealed and those that were used for determinations below the annealing temperature were "stabilized" for lengthy periods. Weights ranging from 5 to 1000 g, depending on the temperature of test, were used to apply tension to the fibers. An optical lever with a multiplying factor of 50 was used to observe the elongation rates using a telescope equipped with a vertical scale.

3.3. Participating Laboratories

The methods used by the participating laboratories are given by literature reference and very brief notes in table 1. Calibration methods used by each participating laboratory (except Laboratory A) are not discussed here because it is assumed that each laboratory followed procedures given in their literature references. These methods are essentially the same as Lillie [4] and Robinson and Peterson [5]. In the case of Laboratories C and F, a Brookfield RVT viscometer was used to make torque measurements.

TABLE 1. *Methods used by participating laboratories*

Lab.	High temperature	Low temperature
A*	Rotating cylinder [3, 4]	Fiber elongation [5, 9]
B*	Rotating cylinder [4]	Fiber elongation [7]
C	Rotating cylinder [4] The inner cylinder was rotated and torque measurements made with a Brookfield RVT Viscometer Sillimanite crucibles used.	Fiber elongation [7]
D*	Rotating cylinder [4]	Beam bending [12]
E*	Rotating cylinder [5] Method of measuring deflection consisted of a disk graduated in 360° mounted directly on the spindle shaft.	
F*	Rotating cylinder [14]	
G	Rotating cylinder [4, 5] Furnace heated by eight globars placed symmetrically between a furnace lining and a vertical refractory core	
H	Rotating cylinder [4]	

*Laboratories A, B, D, E, F, I, and J determined softening point following ASTM Procedure [11].
Laboratories A, D, E, I, and J determined annealing and strain point following ASTM Procedure [13].

4. Results

4.1. Viscosity Measurements Made at NBS (Laboratory A)

The lower temperature limit used in the analysis of the viscosity data was the annealing region

(actually some 15 °C above the the annealing temperature, 546 °C). Measurements taken below this temperature showed that the measured viscosity was dependent on the thermal history of the glass. This was first observed by Lillie [15] and subsequently by Otto [16].

The effect of thermal history on the fibers used in this study can be seem from table 2 and figure 5. Viscosity measurements were made on fibers that received two different heat treatments. One group of fibers was measured at the test temperature in the state they were drawn, i.e., high "fictive temperature" [17]. The other group of fibers was heat-treated at the annealing temperature (546 °C) for 1 hr and then measured at the test temperature.

TABLE 2. *Low-temperature viscosity of fibers of different thermal histories*

Stabilized fibers			Annealed fibers		
Temp.	log η	Holding time [1]	Temp.	Log η	Holding time [2]
°C		hr	°C		hr
519.2	15.048	265	519.5	14.604	4
538.4	13.804	100	529.6	14.072	2
548.9	13.385	65	538.7	13.729	1
556.6	12.968	18	549.5	13.201	1
			558.3	12.854	1
560.2	12.751	16			
565.7	12.480	16	564.7	12.485	1
569.4	12.311	8	574.6	12.064	1
571.6	12.203	2	585.2	11.645	1
575.8	12.000	1			
580.4	11.804	½			
590.0	11.425				
600.1	11.066				
609.8	10.712				
618.7	10.436				
626.5	10.144				
628.4	10.067				
633.9	9.918				
639.6	9.734				

[1] Time held at indicated temperature before measurements of viscosity were made.
[2] Time needed for furnace to reach thermal equilibrium at test temperature.

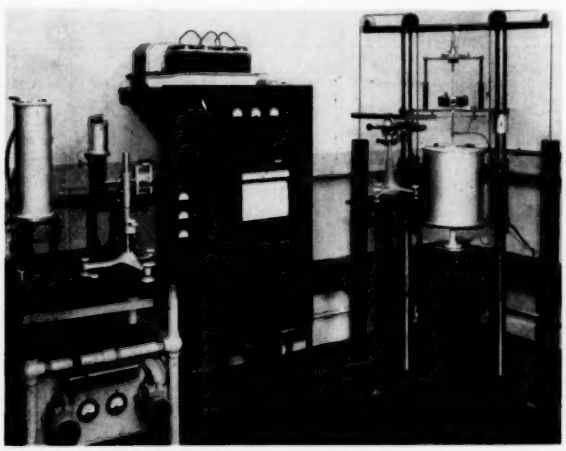

FIGURE 4. *Laboratory setups of viscosity apparatus.*

At approximately 560 °C and above, figure 5, all thermal history of the glass is erased in a very short time and the measured viscosity reflects the equilibrium state of the glass at the temperature of measurement. Measurements made at 560 °C after holding for 16 hr or 1 hr on fibers with two different thermal histories gave the same result.

The results of viscosity measurements on five samples selected from the lot of glass as indicated in figure 1 are given in table 3. All of these measurements were made by laboratory A (NBS).

In order to derive a viscosity curve for each of the five glasses, the data points from both the low temperature fiber elongation method and the high temperature rotating cylinder method were combined and fitted to the Fulcher equation [18] by a least squares calculation. This equation [6] has the form:

$$\log_{10} \eta = A + \frac{B}{T - T_0} \tag{4}$$

[6] The fit of viscosity-temperature data for glasses to the Fulcher equation has been shown by previous investigators to be exceptionally good. For ease of manipulation, interpolation, and examining data for nonsystematic errors it has proven to be very useful. The use of data points from both the low temperature fiber elongation method and the high temperature rotating cylinder method are compatible within experimental error. Data to be published from this laboratory will show that, in the range 10^6 to 10^{10} P, the continuity of the two methods can be substantiated.

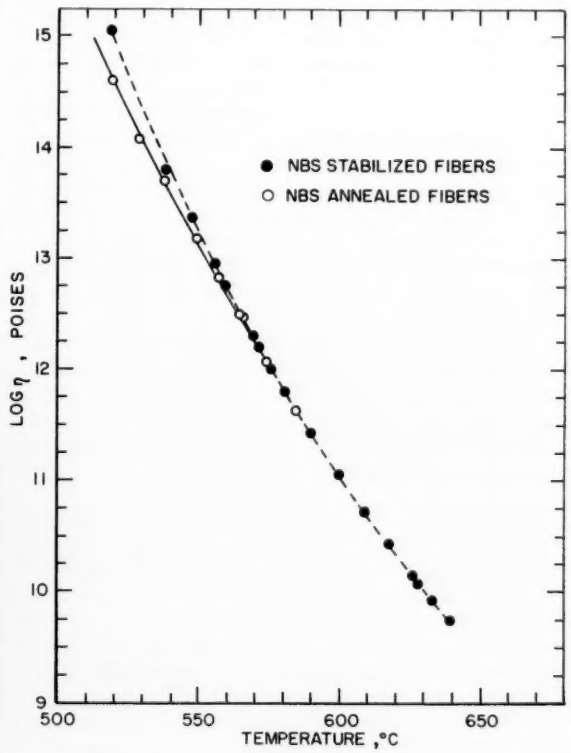

FIGURE 5. *Viscosity of glass after different heat treatments.*

TABLE 3. *Viscosities of five samples*

Sample No. 1		Sample No. 2		Sample No. 3		Sample No. 4		Sample No. 5		Test method
Temp	Log η_{obs}	Temp	Log η_{obs}	Temp	Log η_{obs}	Temp	Log η_{obs}	Temp	Log η_{obs}	
°C		°C		°C		°C		°C		
560.2	12.751	565.7	12.480	574.6	12.064	575.8	12.000	580.4	11.804	Fiber elongation.
600.1	11.066	590.0	11.425	585.2	11.645	609.8	10.712	618.7	10.436	
639.6	9.734	626.5	10.144	628.4	10.067			633.9	9.918	
855.1	5.561	905.1	4.999	900.3	5.045	904.7	5.030	903.0	4.999	Rotating cylinder.
881.4	5.255	1025.3	3.950	945.7	4.601	963.4	4.441	954.4	4.557	
901.4	5.032	1124.6	3.295	1019.1	4.015	996.5	4.163	963.5	4.411	
907.4	4.997	1198.5	2.923	1054.6	3.751	1103.1	3.437	1054.8	3.739	
946.8	4.598	1248.0	2.690	1103.5	3.428	1123.0	3.316	1104.5	3.430	
1000.4	4.136	1315.6	2.416	1200.6	2.912	1214.8	2.853	1149.9	3.164	
1102.9	3.433	1411.1	2.082	1212.0	2.853	1315.7	2.437	1194.3	2.947	
1112.4	3.373			1298.4	2.475	1414.5	2.074	1250.4	2.681	
1202.5	2.899			1402.4	2.111			1250.8	2.684	
1306.1	2.435							1338.5	2.311	
1306.7	2.445							1399.8	2.105	
1412.3	2.060							1402.7	2.082	

where T = temperature in °C
η = viscosity in poises
and A, B, and T_0 are constants.

The values of the parameters and of temperatures for specified viscosities calculated therefrom for each of the five samples are given respectively in tables 4 and 5. In table 5 it is noted that the temperatures for the five samples at certain viscosity values are reproducible to well within 1 °C. Due to this reproducibility temperatures throughout this paper are given to the nearest 0.1 °C for Laboratory A as well as for the participating laboratories. Even though all precautions were taken to eliminate temperature gradients in this work it is conceivable that they are still significant in these measurements. The data points from these five samples were also combined and treated as one sample to give one curve to represent the viscosity for the entire lot of glass. The constants for this equation are given on the bottom line of table 4.

Table 6 gives the viscosity values along with their standard deviation (from the Fulcher equation) for each of the five glasses for T=1300 °C and T=600 °C. The values from the Fulcher equation using the combined data points from all five glasses are also shown in table 6.

TABLE 4. *Fulcher equation constants (five samples)*

Sample No.	A	B	T_0
1	−1.655	4266	264.5
2	−1.596	4204	267.4
3	−1.593	4202	267.6
4	−1.579	4195	267.6
5	−1.649	4258	265.1
Combined 1–5	−1.626	4239	265.7

TABLE 5. *Comparison of temperatures corresponding to specified viscosities calculated from the Fulcher equation parameters for each sample*

log η	Temperature, °C					
	Sample No. 1	Sample No. 2	Sample No. 3	Sample No. 4	Sample No. 5	Combined No. 1–5
2.1	1400.5	1404.9	1405.3	1407.8	1400.8	1403.3
2.5	1291.1	1293.8	1294.1	1296.0	1291.3	1293.0
3.0	1180.8	1182.2	1182.4	1183.7	1181.0	1182.0
3.5	1092.0	1092.4	1092.6	1093.5	1092.0	1092.6
4.0	1018.8	1018.7	1018.8	1019.5	1018.8	1019.1
4.5	957.5	957.1	957.2	957.6	957.5	957.6
5.0	905.5	904.8	904.9	905.2	905.5	905.4
5.5	860.7	859.9	859.9	860.2	860.7	860.5
6.0	821.7	820.9	820.9	821.1	821.8	821.5
7.0	757.3	756.5	756.5	756.6	757.4	757.1
8.0	706.3	705.5	705.6	705.5	706.4	706.0
9.0	664.8	664.2	664.2	664.1	664.9	664.6
10.0	630.5	630.0	630.0	629.9	630.6	630.3
11.0	601.6	601.2	601.2	601.1	601.8	601.4
12.0	576.9	576.6	576.7	576.5	577.1	576.8

TABLE 6. *Comparison of values of log η and standard deviations calculated for two specified temperatures from the data of the participating laboratories*

Lab.	T=1300 °C	σ	Lab.	T=600 °C	σ
A—No. 1	2.465	0.005	A—No. 1	11.060	0.016
No. 2	2.475	.002	No. 2	11.044	.022
No. 3	2.476	.005	No. 3	11.048	.020
No. 4	2.484	.009	No. 4	11.041	.032
No. 5	2.465	.010	No. 5	11.065	.041
Comb. 1–5	2.472	.010	Comb. 1–5	11.054	.029
B	2.469	.004	B	11.071	.048
C	2.467	.003	C	11.075	.001
D	2.468	.005			
E	2.464	.002			
F	2.541	.003			
G	2.514	.005			
H	2.534	.009			
Comb. A–H	2.487	.027	Comb. A–H	11.060	.040
Comb. A–E	2.471	.003	Comb. A–E	11.057	.033

The following two conclusions are clear from table 6:

(1) For both temperatures (1300 and 600 °C) the values of viscosity for each individual sample may be said to agree with the corresponding values from the combined equation (based on all five samples) using plus or minus one standard deviation from the individual sample and from the combined equation as the test of agreement. Thus, the combined

equation represents to within its uncertainty [19] the viscosity of any of the five constituent samples, and also, it is assumed, of any other sample from this lot. It is recalled, figure 1, that these samples were chosen in the least favorable case for uniformity.

(2) The uncertainty of the viscosity as given by the standard deviation is a function of temperature, the precision at the higher temperature being better by a factor of about three. This is due to the well established fact that the rotating cylinder method is more precise than the methods which are used at low temperatures. This was the reason for the choice of the representative temperatures 1300 and 600 °C.

4.2. Viscosity Measurements Made at Participating Laboratories

One sample from the lot of glass was sent to each of 10 cooperating laboratories to determine high- and low-temperature viscosity for comparison with each other and with Laboratory A. In addition they were asked to determine the softening, annealing, and strain points using standard ASTM procedures [11, 13]. These results were also compared with similar determinations made in Laboratory A.

The results of the viscosity measurements from all of these laboratories are listed in table 7. It is seen from table 7 that only two laboratories made both high- and low-temperature viscosity measurements.

The data points submitted by each laboratory were fitted to the Fulcher equation by the standard least square technique in the same manner as that used for Laboratory A. The values of the constants so obtained for A, B, and T_0, for all laboratories (including Laboratory A) are shown in table 8 in the range of temperatures in which viscosity measurements were actually made. A comparison of the data from each laboratory is shown in table 9. Temperatures at specified values of log viscosity were calculated using those constants derived from each laboratory's data.

The data points from the seven participating laboratories shown in table 7 and those from the five samples of Laboratory A were combined and fitted to the Fulcher equation. This gave:

$$\log \eta = -1.568 + \frac{4181}{T\ °C - 268.9}.$$

TABLE 7. *Experimental results of participating laboratories*

Lab. B		Lab. C		Lab. D		Lab. E		Lab. F		Lab. G		Lab. H		Test method
Temp	Log η_{obs}	Temp	Log η_{obs}	Temp	Log η_{obs}	Temp	Log η_{obs}	Temp	Log η_{obs}	Temp	Log η_{obs}	Temp	Log η_{obs}	
°C		°C		°C		°C		°C		°C		°C		
[a] 534.9	13.976													Fiber elongation.
551.7	13.159													
560.2	12.720													
582.2	11.761													
612.8	10.615													
662.2	9.159	[b] 584.5	11.680											
1014.4	4.035	1098.5	3.478	803.8	6.217	802.0	6.339	1025.6	4.000	790.0	6.400	840.0	5.775	Rotating cylinder.
1042.2	3.827	1158.0	3.131	844.4	5.659	852.0	5.650	1063.9	3.750	886.0	5.220	848.0	5.670	
1093.3	3.491	1183.7	3.000	878.6	5.257	900.0	5.077	1103.3	3.500	983.0	4.270	928.0	4.787	
1153.3	3.151	1216.0	2.835	930.8	4.719	950.0	4.587	1147.8	3.250	1088.0	3.540	1077.0	3.623	
1204.4	2.890	1282.5	2.539	960.3	4.449	1001.0	4.170	1196.1	3.000	1290.0	2.560	1095.0	3.518	
1256.6	2.656			998.1	4.132	1048.0	3.792	1248.9	2.750	1335.0	2.380	1145.0	3.219	
1309.4	2.436			1040.4	3.828	1101.0	3.436	1309.4	2.500			1251.0	2.715	
				1080.6	3.562	1151.0	3.158	1378.9	2.250			1304.0	2.525	
				1117.1	3.342	1199.0	2.909	1456.1	2.000			1313.0	2.487	
				1157.2	3.121	1249.0	2.682							
				1192.1	2.949	1288.0	2.513							
				1230.2	2.764									
				1272.0	2.584									
				1308.9	2.435									
				1353.1	2.266									

[a] Lab. B—Holding times were respectively reading downward 119 hr, 195 hr, 39 hr, 15 min, 10 min, and 5 min.
[b] Lab. C—Holding time not given.

TABLE 8. *Fulcher equation constants from the data submitted by each participating laboratory*

Laboratory	Range	A	B	T_0
	°C			
A[1]	560–1400	−1.626	4,239	265.7
B	560–1300	−1.655	4,271	264.4
C	580–1300	−1.761	4,413	256.2
D	800–1350	−1.584	4,186	266.9
E	800–1300	−1.586	4,124	281.8
F	1025–1450	−1.727	4,580	226.8
G	790–1340	−1.473	4,112	268.7
H	840–1310	−1.211	3,711	309.0
Gen. eq [2]	560–1450	−1.626	4,236	266.0

[1] Data from samples 1–5 combined.
[2] Data from Laboratories A–E combined—see text.

Following the same procedure as was done for the five samples from Laboratory A, the values of log η along with their standard deviation for $T=1300$ °C and $T=600$ °C were calculated and are shown in table 6. The values using the combined data of Laboratories A through H are also shown in table 6.

It can be seen from table 6 that the values of viscosity at 1300 °C, plus or minus their standard deviation, for Laboratories F, G, and H fall outside the viscosity value, plus or minus its standard deviation, from the combined data points of Laboratories A through H. If the data points from only Labora-

TABLE 9.—*Comparison of temperatures for specified viscosities calculated from appropriate Fulcher equation parameters (see table 8)*

Log viscosity	Temperature, °C								
	Laboratories								Value from combined equation
	A [1]	B	C	D	E	F	G	H	
P									
2.00						1455.7			1434.3
2.10	1403.3					1423.6			1402.9
2.25	1359.3			1358.7		1378.5			1358.9
2.50	1293.0	1292.4	1297.3	1291.9	1291.0	1310.4	1303.7	1308.9	1292.7
2.75	1234.3	1234.1	1236.4	1232.8	1232.8	1249.9	1242.4	1245.8	1234.0
3.00	1182.0	1182.0	1182.4	1180.1	1181.0	1195.7	1188.0	1190.2	1181.7
3.50	1092.6	1093.0	1090.7	1090.3	1092.6	1103.1	1095.6	1096.6	1092.4
4.00	1019.1	1019.7	1016.0	1016.5	1020.0	1026.6	1020.0	1021.1	1019.0
4.50	957.6	958.4	953.8	954.9	959.4		957.1	958.7	957.5
5.00	905.4	906.2	901.3	902.6	907.9		904.0	906.4	905.3
5.50	860.5	861.4	856.4	857.8	863.7		858.4	861.9	860.5
6.00	821.5	822.4	817.5	818.8	825.4		819.0	823.6	821.5
6.50	787.3	788.2	783.5	784.7	791.8				787.3
7.00	757.1	757.9	753.6						757.1
8.00	706.0	706.8	703.2						706.1
9.00	664.6	665.3	662.5						664.7
10.00	630.3	630.9	628.9						630.4
11.00	601.4	601.9	600.7						601.5
12.00	576.8	577.2	576.7						576.9

[1] Results from Lab. A are the combined results from five samples.

tories A through E are combined and fitted to the Fulcher equation, one obtains:

$$\log \eta = -1.626 + \frac{4{,}236}{T\ °\text{C} - 266}.$$

The values of viscosity at 1300 and 600 °C along with their standard deviations from this equation are also given in table 6. In the last column of table 9 the temperatures at specified values of viscosity are given for the combined data from Laboratories A through E.

In figure 6, the calculated viscosities, represented by a horizontal line at zero ordinate, are based on the Fulcher equation computed from the data of Laboratories A through E. The differences in the observed and calculated viscosities of each laboratory's data using this equation are plotted in figure 6 to show the scatter in these measurements. Closer inspection of figure 6 and table 9 shows that part of the data points submitted by Laboratories G and H (below 1100 °C) also fits this second equation. The scatter between laboratories is mostly confined, or nearly so, between the arbitrary limits ±10 percent viscosity in poises used by H. R. Lillie [7] in his analysis of similar measurements. Also shown in figure 6 are the ±5 °C limits which at 1400 °C represents a ±0.015 log viscosity (±3.5 percent viscosity) and at 600 °C represents about ±0.2 log viscosity (±50 percent viscosity). About 90 percent of the observed points of the participating laboratories fall between these two limits.

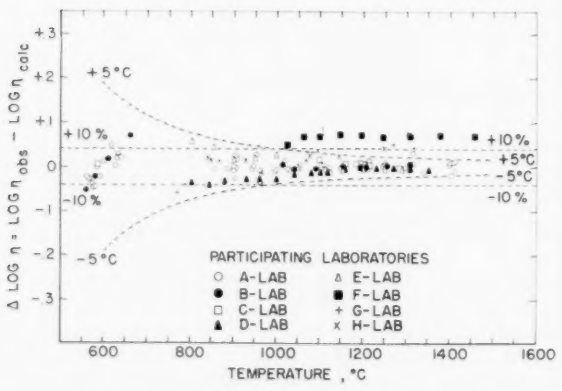

FIGURE 6. *Differences in observed and calculated viscosities of participating laboratories on Standard Glass No. 710.*

The observed values of log viscosity of each laboratory were plotted against the function of temperature $4236/T$–266 (derived from the combined data points of Laboratories A through E) and are shown in figure 7. Most of the experimental points submitted by the participating laboratories are seen to fall on a straight line having a slope of unity [2]. The portion of the curve within the dashed rectangle has been expanded and plotted on the right. This range (log 2 to log 4) is the one in which most viscosity measurements are made since these temperatures are most critical in the melting, fining, and forming of glass.

At the beginning of this program only three participating laboratories (A, B, and C) made viscosity measurements by the fiber elongation method. These results (down to 560 °C) were included in the calculations of the constants for the final equation. Since then, Laboratory C has sent in one more determination and Laboratory D has made numerous determinations, covering the range 530 to 700 °C,

[7] H. R. Lillie, Report No. R-163, April 15, 1954, American Ceramic Society Glass Division Standard Glasses, "Test Results from Several Laboratories." Corning Glass Works, Corning, N.Y.

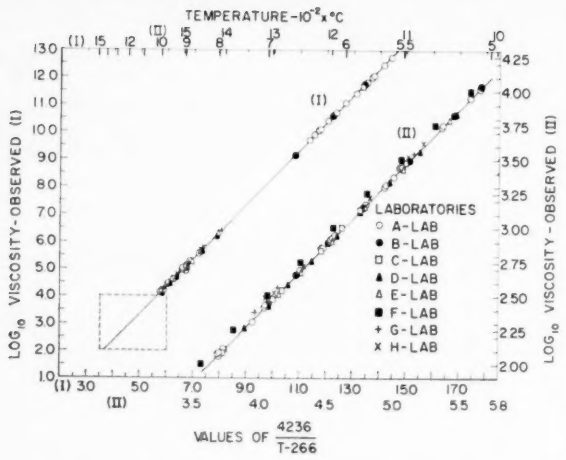

FIGURE 7. *Observed values of log viscosity plotted against the function of temperature* $\frac{4236}{T\ °C-266}$.

by a beam bending test. These additional determinations (see below) agree very well with the measurements made by Laboratories A, B, and C and would not significantly affect the constants of the final equation if calculated over again.

Laboratory C: (Fiber elongation method)

$\log \eta = 12.97$ at 556.3 °C (No holding time given)

Laboratory D:[8] (Beam-bending method)

$\log \eta = 14.367$ at 530.0 °C (No holding time given)
$= 13.834$ at 538.0 °C (Do.)
$= 13.577$ at 546.0 °C (Do.)
$= 13.130$ at 553.0 °C (Do.)

4.3. Softening, Annealing, and Strain Points

These empirical points were determined by five participating laboratories with an additional two laboratories determining only the softening point. The definition of these points and method of determining them are given in the ASTM Standards [11, 13]. The results are shown in table 10.

TABLE 10. *Softening, annealing, and strain points of standard glass No. 710 by participating laboratories*

	Temperature, °C							
	Laboratories							
	A	B	D	E	F	I	J	Avg
Softening pt	727	723	721	721	723	725	727	724
Annealing pt	546	.....	544	546	.....	545	547	546
Strain pt	503	.....	501	504	.....	505	508	504

[8] Other low-temperature viscosity measurements on this glass have been published in a paper by H. E. Hagy [12].

5. Summary

(1) The National Bureau of Standards has established a viscosity standard for glass, No. 710 (Soda-Lime-Silica).[9]

(2) Viscosity measurements have been made on this glass by eight participating laboratories between 520 and 1450 °C, using the rotating cylinder and fiber elongation methods.

(3) A viscosity-temperature curve was determined from these measurements by fitting the data points to the Fulcher equation by the method of least squares.

(4) The softening, annealing, and strain points of this glass have been determined by seven of the participating laboratories.

The authors acknowledge the interest taken by C. H. Hahner in initiating and directing this program and F. W. Glaze (retired) for his assistance in the calibration work and preliminary calculations. The authors also express their sincerest thanks to all the participating laboratories for their cooperation in making viscosity measurements on this glass.

6. References

[1] An improved refractometer, NBS Tech. News Bull. **37,** 135 (1953); **38,** 63 (1954).

[2] Proceedings of the Society of Glass Technology. Report by the Physical Properties Committee of the Society of Glass Technology, XI, pp. 58–104 (1956).

[3] J. O'M. Bockris and D.C. Lowe, An electromagnetic viscometer for molten silicates at temperatures up to 1800 °C, J. Sci. Instr. **30,** 403 (1953).

[4] a. H. R. Lillie, High-temperature viscosities of soda-silica glasses, J. Am. Ceram. Soc. **22,** No. 11, 367 (1939).

b. H. R. Lillie, Measurement of absolute viscosity by use of concentric cylinders, J. Am. Ceram. Soc. **12,** No. 8, 505 (1929).

c. H. R. Lillie, Viscosity measurements in glass, J. Am. Ceram. Soc. **12,** No. 8, 516 (1929).

d. H. R. Lillie, Viscosity of glass between strain point and melting temperature, J. Am. Ceram. Soc. **14,** No. 7, 502 (1931).

[5] H. A. Robinson and C. A. Peterson, Viscosity of recent container glass, J. Am. Ceram. Soc. **27,** No. 5, 129 (1944).

[6] E. Hatschek, The viscosity of liquids, p. 31, G. Bell & Sons, Ltd., London, 1928.

[7] J. P. Poole, Improved apparatus for measuring viscosity of glasses in annealing range of temperature, J. Am. Ceram. Soc. **32,** No. 7, 215 (1949).

[8] F. H. Norton, Measuring viscosity of glass, Glass Ind. **16,** No. 5, 143 (1935).

[9] J. Boow and W. E. S. Turner, Viscosity and Working Characteristics of Glasses; I. Viscosity of Some Commercial Glasses at Temperatures Between 500 °C–1400 °C, J. Soc. Glass Tech. **26,** No. 117, 215 (1942).

[10] W. K. Lewis, L. Squire and G. Broughton, Industrial Chemistry of Colloidal and Amorphous Materials, p. 24 Macmillan Co., New York, 1942.

[11] ASTM Standards, 1961; "Softening Point of Glass" ASTM Designation: C338–57, pp. 695–698.

[9] At present, 1 kg (about 2 lb) samples of Standard Glass No. 710 (Soda-Lime-Silica) are available from the National Bureau of Standards. These samples are rectangular-shaped bars (5×7.5×10 cm) and may be purchased for $40.00.

[12] H. E. Hagy, Experimental evaluation of beam-bending method of determining glass viscosities in the range 10^8 to 10^{15} poises, J. Am. Ceram. Soc. **46,** No. 2, 93 (1963).
[13] ASTM Standards, 1961, Annealing Point and Strain Point of Glass ASTM Designation C336–54T, pp. 645–650.
[14] R. L. Tiede, Improved apparatus for rapid measurement of viscosity of glass at high temperatures, J. Am. Ceram. Soc. **42,** No. 11, 537 (1959).
[15] H. R. Lillie, Viscosity-Time-Temperature Relations in Glass at Annealing Temperatures, J. Am. Ceram. Soc. **16,** No. 12, 619 (1933).
[16] W. H. Otto, Compaction Effects in Glass Fibers, J. Am. Ceram. Soc. **44,** No. 2, 68 (1961).
[17] A. Q. Tool, Viscosity and the extraordinary heat effects in glass, J. Res. NBS **37,** 73–90 (1946) RP1730; Ceram. Abstr. **30,** 7 (1947).
[18] G. S. Fulcher, Analysis of Recent Measurements of Viscosity of Glasses, J. Am. Ceram. Soc. **8,** No. 6, 339 (1925).
[19] B. P. Dudding, Errors in the Measurements of Viscosity of Glass, Proc. Third Intern. Congr. on Glass, pp. 296–317, Associazione Nazionale Degli Industriali Del Vetro, Rome (1954).

(Paper 68A5–291)

JOURNAL OF RESEARCH of the National Bureau of Standards—A. Physics and Chemistry
Vol. 68A, No. 5, September–October 1964

Hydrothermal Preparation of a Gehlenite Hydrate

Elmer T. Carlson

(May 11, 1964)

Hydrothermal treatment of synthetic gehlenite ($2CaO{\cdot}Al_2O_3{\cdot}SiO_2$) or of various mixtures of oxides, hydrates, etc., approximating the composition of gehlenite, at 260 to 650° C, produced a hitherto unreported compound having the composition $2CaO{\cdot}Al_2O_3{\cdot}SiO_2{\cdot}H_2O$. Other phases, usually hydrogarnet, were always present in small amounts. A natural gehlenite containing Fe_2O_3 and MgO was partly converted to the same hydrate at 450° C. The compound $2CaO{\cdot}Al_2O_3{\cdot}SiO_2{\cdot}8H_2O$ was converted to a hydrogarnet at 250 °C, but formed $2CaO{\cdot}Al_2O_3{\cdot}SiO_2{\cdot}H_2O$ at 350 °C. The new compound has a body-centered cubic structure, with $a_0=8.83$ Å. The index of refraction is 1.628. An x-ray diffraction pattern is given, and some similarities between $CaO{\cdot}Al_2O_3{\cdot}SiO_2{\cdot}H_2O$ and the ternary compound $4CaO{\cdot}3Al_2O_3{\cdot}3H_2O$ are pointed out.

1. Introduction

The mineral gehlenite is of relatively uncommon occurrence in nature, but is a common constituent of air-cooled blast-furnace slags and is present in some high-alumina cements [1].[1] The ideal formula is $2CaO{\cdot}Al_2O_3{\cdot}SiO_2$, but other oxides, particularly MgO and Fe_2O_3, may be present in solid solution, forming a group of minerals known as melilites. From a practical standpoint, gehlenite usually has been considered a useless constituent of cements and slags, since it reacts very slowly with water and does not have cementitious properties [1]. There is evidence, however, that glasses having the oxide composition of gehlenite are more reactive with water than is the crystalline mineral. It has been shown by Locher [2] that vitreous slags in the gehlenite area of the system $CaO{-}Al_2O_3{-}SiO_2$ develop cementitious properties when activated with lime, cement, or anhydrite.

The cementitious properties of such slags have been attributed, at least in part [2], to the so-called gehlenite hydrate, $2CaO{\cdot}Al_2O_3{\cdot}SiO_2{\cdot}8H_2O$, crystallizing as hexagonal plates. This compound was first prepared by Strätling, whose work was reported by Büssem [3] at the Symposium on the Chemistry of Cements (Stockholm, 1938). It has since been prepared by several investigators, including the author, from various starting materials, at temperatures ranging from 1 to 50 °C. Early attempts to prepare it from gehlenite were unsuccessful. The application of hydrothermal treatment to speed up the hydration resulted in formation of a hydrogarnet [4]. Crystallographic studies [5, 6] indicate that there is no close structural relationship between gehlenite (crystallizing in the tetragonal system [1]) and the so-called gehlenite hydrate.

During the course of some hydrothermal studies in the system $CaO{-}Al_2O_3{-}SiO_2{-}H_2O$, the author observed a series of unidentified x-ray diffraction lines in the powder patterns of several preparations. The present paper gives the results of experimental work leading to the conclusion that the new pattern is produced by a hitherto unreported "gehlenite hydrate," having the composition $2CaO{\cdot}Al_2O_3{\cdot}SiO_2{\cdot}H_2O$ and crystallizing in the cubic system.

2. Materials and Procedures

The primary starting materials were reagent grade silicic acid, aluminum hydroxide, and calcium carbonate (low alkali). Glasses of various compositions were prepared by heating the mixed raw materials, in the desired proportions, in an electric furnace. Several preparations were heated below the fusion temperature; these are referred to below as "sinters." Synthetic gehlenite was prepared in this manner by heating the properly proportioned materials at about 1460 °C. The product appeared to be about 95 percent gehlenite by microscopic examination. The compound $2CaO{\cdot}Al_2O_3{\cdot}SiO_2{\cdot}8H_2O$ was prepared in two ways: (1) by prolonged treatment of a mixture of calcium hydroxide and a lime-alumina-silica glass, in correct proportions, with water at room temperature; (2) by precipitation from a suspension of silicic acid in calcium aluminate solution, also at room temperature.

A sample of natural gehlenite originally from Tyrol was used for a few experiments. The rock was first crushed, treated with hydrochloric acid to remove most of a calcite intergrowth, washed, dried, and pulverized before use. The x-ray diffraction pattern was in close agreement with that obtained from the synthetic gehlenite, except that the natural material showed additional weak lines due to calcite. Chemical analysis, however, revealed 1.8 percent of Fe_2O_3 and 3.7 percent of MgO, indicating that the mineral departed significantly from the ideal gehlenite composition.

With a few exceptions, the hydrothermal reactions were effected in 18-ml stainless-steel pressure vessels (Morey bombs), the reactants being held in small platinum crucibles. Pressure was estimated from the temperature and the amount of water present.

[1] Figures in brackets indicate the literature references at the end of this paper.

TABLE 1. *Hydrothermal experiments on gehlenite and related compositions*

Expt. No.	Oxide ratio $CaO:Al_2O_3:SiO_2$	Starting material	Temperature	Pressure [a]	Duration	Relative amount of isometric phase [b] present	Other phases present [b c]
			°C	atm	Days		
1	2:1:1	Sinter	182	10	37	nd	hg(s); boh(m)
2	2:1:1	do	260	45	37	m	boh(s); hg(s)
3	2:1:1	Synth. gehlenite	332	125	20	vs	geh(m); hg(w); boh(?)
4	2:1:1	Sinter	350	160	16	vs	hg(w)
5	2:1:1	Synth. gehlenite	405	300	16	vs	geh(s)
6	2:1:1	Sinter	446	400	16	vs	hg(vw)
7	2:1:1	Synth. gehlenite	650	2040	3	vs	geh(vw)
8	2:1:1	do	750	2040	3	nd	geh(vs)
9	2:1:1	Natural gehlenite	348	160	11	nd	hg(s)
10	2:1:1	do	402	290	7	?	hg(vs)
11	2:1:1	do	450	400	11	m	hg(w)
12	2:1:1	$2CaO·Al_2O_3·SiO_2·8H_2O$	150	5	34	nd	C_2ASH_8(vs); hg(m)
13	2:1:1	do	250	40	34	nd	hg(s); boh(s)
14	2:1:1	do	350	160	31	vs	hg(vw)
15	2:1:1	Mixed oxides	346	150	36	vs	hg(w)
16	2:1:1	do	450	420	35	vs	hg(w)
17	1.26:1:1	Glass	382	235	21	s	hg(vs); boh(s)
18	1.5:1:1	Sinter	350	160	135	m	hg(s); boh(w)
19	2.5:1:1	do	406	300	14	vs	$Ca(OH)_2$(s)
20	3:1:1	Glass+$Ca(OH)_2$	355	170	18	vs	$Ca(OH)_2$(s)
21	3:1:0.4	Glass	365	190	14	vs	$Ca(OH)_2$(vs); $C_4A_3H_3$(s)
22	3:1:1.2	do	371	210	18	s	hg(m); $Ca(OH)_2$(w)
23	3:1:2	Glass(devitrified)	350	160	52	m	hg(s)
24	3:1:2	do	448	420	15	m	hg(w)
25	3:1:2	do	570	1020	¼	m	hg(s)
26	3:1:2	Dehyd. kaolin+$Ca(OH)_2$	445	400	7	m	hg(s); $Ca(OH)_2$(w)
27	2:1:0.5	Sinter+$Ca(OH)_2$	358	180	28	s	$C_4A_3H_3$(s); $Ca(OH)_2$(w)
28	1.5:1:0.5	Sinter	350	160	27	vs	$C_4A_3H_3$(m); boh(w)
29	2.5:1.5:1	do	400	280	14	vs	$C_4A_3H_3$(m)
30	4:2.5:1	do	376	220	20	vs	$C_4A_3H_3$(w)

[a] Estimated from temperature and degree of filling, except for Nos. 7, 8, and 25.
[b] Relative amounts of phases estimated from intensities of strongest x-ray lines. The symbols commonly used for relative intensities are here used to indicate estimated amounts of phases present. vs=very strong; s=strong; m=medium; w=weak; vw=very weak; ?=too weak for positive identification; nd=not detected.
[c] boh=boehmite; geh=gehlenite; hg=hydrogarnet; $C_4A_3H_3=4CaO·3Al_2O_3·3H_2O$; $C_2ASH_8=2CaO·Al_2O_3·SiO_2·8H_2O$.

Temperature was controlled to about ±2 °C. For hydrothermal treatment at temperatures above 500 °C, a Tuttle cold-seal apparatus was used. X-ray diffraction diagrams of the powdered preparations were obtained on a diffractometer, using CuKα radiation.

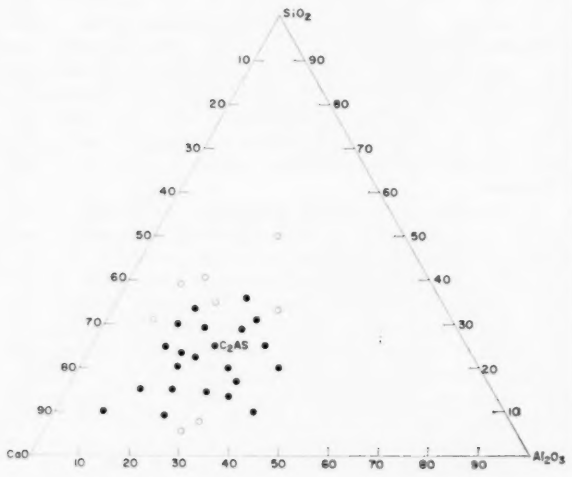

FIGURE 1. *Compositions of compounds and mixtures given hydrothermal treatment, shown in relation to the anhydrous system* $CaO–Al_2O_3–SiO_2$. (*Plotted on molar basis*)

Filled circles: new phase ($2CaO·Al_2O_3·SiO_2·H_2O$) observed in product
Open circles: new phase not observed in product.

3. Results

The new isometric phase has been observed in more than 50 preparations obtained by hydrothermal treatment of various materials and mixtures, both hydrous and anhydrous, having compositions near the gehlenite region of the system $CaO-Al_2O_3-SiO_2$. The location of the various compositions with reference to the ternary diagram is shown in figure 1. Table 1 gives data pertaining to a number of these preparations, selected to show the effects of temperature, composition, and the nature of the starting materials. Experiments 1 to 16 comprise a series in which the molar proportions $CaO:Al_2O_3:SiO_2$, were held at 2:1:1. Two types of synthetic anhydrous starting materials were used. The one referred to as "sinter" had been heated at about 1040 °C, which is far below the temperature at which complete reaction can be expected. The "synthetic gehlenite," in contrast, had been heated at 1460 °C, and was estimated to be about 95 percent gehlenite. On hydrothermal treatment, both types yielded the same hydration products, but the material which had been heated only to 1040 °C reacted more rapidly with water than did the well-crystallized gehlenite. Formation of the new isometric phase occurred in the temperature range 260 to 650 °C, but in no case was a pure product obtained. Small amounts of hydrogarnet were detected in most of the reaction products. Variation in the x-ray line positions indicated an increase in the silica content of the hydrogarnet phase with increasing temperature, in agreement with results published previously [7].

The synthetic gehlenite was largely converted to the isometric hydrate by hydrothermal treatment at 650 °C, but not at 750 °C. At the latter temperature the irregular gehlenite particles were transformed to well formed crystals, but the x-ray pattern indicated no alteration in structure.

The sample of natural gehlenite was partly converted to the isometric hydrate at 450 °C, but not at 348 °C, only the hydrogarnet phase being formed at the latter temperature. The difference in behavior between the natural and the synthetic materials may reasonably be attributed to the presence of other components in the natural mineral, as disclosed by analysis.

Experiments 12 to 14, in which the hexagonal gehlenite hydrate was treated hydrothermally for about a month, are of interest for two reasons. First, the low temperature hydrate underwent little or no alteration at 150 °C. A moderate amount of hydrogarnet was observed in the product, but the same phase was present in the starting material. Second, the low temperature hydrate was decomposed to hydrogarnet and boehmite at 250 °C, indicating that it is not converted to the high temperature hydrate directly by loss of water. The new isometric phase was formed at 350 °C.

Mixtures of the hydrated oxides (experiments 15 and 16) also produced the new phase along with small amounts of hydrogarnet.

The rest of the experiments listed in table 1 cover a range of oxide proportions other than 2:1:1. In Nos. 17 and 18, with the proportion of CaO reduced, the new phase was accompanied by larger amounts of hydrogarnet and a considerable quantity of boehmite. In Nos. 19 and 20 the excess lime appeared as $Ca(OH)_2$. In the remainder of the experiments listed, the proportions of all three solid components were varied. Here the phase relationships naturally became rather complex. No attempt was made to define phase boundries, as the primary purpose here was to ascertain what proportions of oxides gave the best yield of the new phase. It is evident that the 2:1:1 composition satisfied this condition better than any other investigated.

The last three experiments listed were designed to explore the area between the compositions represented by the oxide proportions $2CaO:Al_2O_3:SiO_2$ and $4CaO:3Al_2O_3$, which is of interest because of certain similarities between the new phase and the ternary compound $4CaO{\cdot}3Al_2O_3{\cdot}3H_2O$. The X-ray patterns indicated that both phases were present in the products, with no detectable shift in position of the lines, and hence no evidence of solid solution.

The new isometric phase occurred typically as octahedral crystals, usually with rounded edges. Cubo-octahedra were also observed, and in some preparations some of the crystals were elongated into prisms. The index of refraction was found to be 1.628 ± 0.003.

The water content of five of the more nearly homogeneous preparations was determined from the loss on ignition. The results, in terms of moles of H_2O per mole of $2CaO{\cdot}Al_2O_3{\cdot}SiO_2$, ranged from 1.00 to 1.19, averaging 1.08. Preparations judged to be the most nearly homogeneous had the lowest water contents. Most of the water was driven off between 550 and 750 °C.

The X-ray diffraction pattern of one of the powdered preparations is given in table 2. The pattern indicated a body-centered cubic structure, with $a_0=8.83$Å. A pattern of a new preparation of $4CaO{\cdot}3Al_2O_3{\cdot}3H_2O$ is also given in the table to show the similarities between the strongest lines of the two. Tungsten was used as internal standard in both cases. The pattern of $4CaO{\cdot}3Al_2O_3{\cdot}3H_2O$ is

TABLE 2. *Interplanar spacings of* $2CaO{\cdot}Al_2O_3{\cdot}SiO_2{\cdot}H_2O$ *and* $4CaO{\cdot}3Al_2O_3{\cdot}3H_2O$

$2CaO{\cdot}Al_2O_3{\cdot}SiO_2{\cdot}H_2O$			$4CaO{\cdot}3Al_2O_3{\cdot}3H_2O$	
hkl	*d*	*I*	*d*	*I*
	Å		Å	
200	4.42	7		
211	3.607	93	3.61	100
			3.50	9
			3.274	81
			3.207	3
220	3.122	9	3.109	5
			3.029	28
			2.849	51
310	2.793	100	2.797	66
			2.741	4
			2.614	11
222	2.549	32	2.545	22
			2.419	21
			2.386	5
			2.354	8
321	2.360	29	2.290	26
400	2.208	15	2.225	35
			2.182	4
			2.169	17
			2.137	10
411	2.081	42	2.088	37
			2.071	17
			2.066	5
			2.053	5
			2.019	2
			1.986	3
420	1.974	8	1.970	8
			1.931	4
			1.914	8
332	1.882	4	1.838	5
			1.823	4
422	1.801	12	1.801	6
			1.776	4
510	1.730	13	1.738	6
			1.726	3
			1.681	5
			1.668	3
			1.643	4
			1.619	5
521	1.611	10	1.601	20
			1.597	9
			1.572	44
440	1.559	38	1.552	30
			1.540	7
530	1.513	21	1.511	11
			1.486	5
600	1.470	7	1.470	5
			1.466	6
611	1.431	13	1.429	3
			1.416	3
			1.396	2
			1.375	2
541	1.362	4	1.367	5
622	1.330	7	1.331	3
			1.308	2
			1.289	14
710	1.248	4	1.224	3
			1.219	3
721	1.201	3	1.185	5
642	1.179	3	1.170	6
			1.167	4
730	1.158	11	1.158	3
			1.116	8
800	1.103	3	1.113	3
			1.085	2
			1.083	2
			1.081	2

$a_0=8.83$ Å.

in fair agreement with the one published by Majumdar and Roy [8], the chief difference being that the spacings given in table 2 are consistently slightly greater.

4. Discussion

Even the most nearly homogeneous preparations of the new compound contained significant amounts of at least one other phase, most frequently hydrogarnet. This fact makes it impossible to state with certainty that the proposed formula, $2CaO{\cdot}Al_2O_3{\cdot}SiO_2{\cdot}H_2O$ actually is correct. The amount of hydrogarnet present was estimated to be 10 percent or less in a few cases. Because of the nearness of the oxide ratios in the two phases, the error introduced in the calculated composition resulting from the presence of 10 percent of hydrogarnet is relatively slight. In consideration of this fact, the ignition loss values lead to the conclusion that the new phase has the formula $2CaO{\cdot}Al_2O_3{\cdot}SiO_2{\cdot}H_2O$. Thus it may be considered a hydrate of gehlenite.

The relative ease of preparation of this gehlenite hydrate raises the question as to why it was not discovered earlier. A reexamination of the x-ray patterns obtained in a previous investigation [7] showed that the isometric phase was unquestionably present in many of the preparations. Unfortunately, it had been mistaken for the ternary compound, $4CaO{\cdot}3Al_2O_3{\cdot}3H_2O$, with which it usually was associated. The x-ray patterns (see table 2) are somewhat similar. Many of the strongest lines are practically coincident, while others are shifted only slightly. It should be noted, also, that diffraction diagrams of different preparations of $4CaO{\cdot}3Al_2O_3{\cdot}3H_2O$ may vary widely unless great care is taken to avoid orientation effects when mounts are prepared. This fact tended to obscure the significance of the differences that should have been recognized as arising from the presence of another compound. The patterns given in table 2 were obtained on mounts of powders prepared in such a way as to minimize orientation effects; hence the differences between the two patterns are more obvious. Optically, the two phases are also similar, the isometric phase having $n=1.628$, while the 4:3:3 compound is very slightly birefringent, with n (average)$=$ 1.627. Even in crystal habit there is some similarity, in that the cubic phase was observed in some cases to form prisms like those typical of the aluminate.

Owing to these similarities, it was thought that there might be a structural relationship between the two phases. Experiments 27 to 30 (table 1) were intended to permit formation of an intermediate solid solution, but no evidence of such formation was observed.

(Paper 68A5–292)

To the extent that the isometric phase was mistakenly identified as $4CaO{\cdot}3Al_2O_3{\cdot}3H_2O$, the data given and the conclusions drawn in the earlier work cited above [7] need to be modified. [2]

The hydrothermal synthesis of gehlenite at temperatures as low as 450 °C has been reported recently [9], but no mention was made of a hydrate. The experimental conditions were somewhat different from those of the present work, in that calcium carbonate was used as one of the starting materials, with lime present as a receptor for the carbon dioxide evolved. Nevertheless, from the data given above, it would be expected that the isometric gehlenite hydrate, rather than gehlenite itself, would be formed at 450 °C. The reasons for the apparent conflict in results probably cannot be clarified without additional information regarding experimental details in the work cited.

The existence of the high temperature gehlenite hydrate needs to be taken into account in any future study of phase relations in the system $CaO{\cdot}Al_2O_3{\cdot}SiO_2{\cdot}H_2O$ at elevated temperatures.

The author wishes to express his thanks to H. E. Swanson and coworkers for the x-ray diffraction diagrams, and to C. R. Robbins for experimental runs in the cold-seal apparatus; also to P. Desautels, of the National Museum, who supplied the specimen of natural gehlenite.

[2] The correction applies to the following experiments reported in the paper cited [7]: in table 4, Nos. 6 and 17; in table 6, Nos. 16, 24, and 26; in figure 2, the point at the right end of the curve. In each case the phase reported as $4CaO{\cdot}3Al_2O_3{\cdot}3H_2O$ ($C_4A_3H_3$) actually was the isometric phase, $2CaO{\cdot}Al_2O_3{\cdot}SiO_2{\cdot}H_2O$.

5. References

[1] F. M. Lea, The chemistry of cement and concrete (Revised Edition of Lea and Desch), (Edward Arnold, London, 1956).

[2] F. W. Locher, Hydraulic properties and hydration of glasses of the system $CaO–Al_2O_3–SiO_2$, Proc. Fourth International Symposium on the Chemistry of Cement, NBS Monograph 43, pp. 267–276 (1962).

[3] W. Büssem, X-rays and cement chemistry, Proc. Symposium on the Chemistry of Cements, Stockholm, 1938. (See p. 163).

[4] H. zur Strassen and W. Strätling, The reaction between burned kaolin and lime in aqueous solution. II. The reaction products in relation to the system lime-silica-alumina-water. Z. anorg. allgem. Chem. **245,** 267–278 (1940).

[5] N. Fratini and T. Turriziani, Contribution to the knowledge of a hydrated calcium silicoaluminate (Strätling's Compound), (in Italian), Ric. Sci. **24,** 1654–57 (1954).

[6] C. H. Schmitt, discussion of "Hydration of calcium aluminates and ferrites", by F. E. Jones, Proc. Fourth International Symposium on the Chemistry of Cement (Washington, 1960) p. 244.

[7] E. T. Carlson, Hydrogarnet formation in the system lime-alumina-silica-water, J. Res. NBS **56,** 327–335 (1956).

[8] A. J. Majumdar and R. Roy, The system $CaO–Al_2O_3–H_2O$, J. Am. Ceram. Soc. **39,** 434–442 (1956).

[9] M. Christophe-Michel-Lévy, Hydrothermal synthesis of gehlenite, $Ca_2Al_2SiO_7$, (in French), Compt. rend. **255,** 2781–2 (1962).

JOURNAL OF RESEARCH of the National Bureau of Standards—A. Physics and Chemistry
Vol. 68A, No. 5, September–October 1964

Action of Water on Calcium Aluminoferrites

Elmer T. Carlson

(April 30, 1964)

The action of water on seven preparations of the calcium aluminoferrite solid solution series, ranging in composition from $6CaO \cdot 2Al_2O_3 \cdot Fe_2O_3$ to $2CaO \cdot Fe_2O_3$, was studied (a) by leaching the powdered preparations with water, (b) by stirring in a large volume of water at different temperatures from 10 to 100 °C, and (c) by paste hydration at 1, 25, and 45 °C.

The initial reaction occurring immediately on contact between the aluminoferrite and water is one of incongruent solution. The Al_2O_3, most of the CaO, and a trace of Fe_2O_3 pass into solution, and a residue of Fe_2O_3, possibly hydrated and amorphous, remains. If the suspension is sufficiently concentrated to give a supersaturated solution, a hydrated precipitate will form. At room temperature the major precipitated phase is $2CaO \cdot Al_2O_3 \cdot 8H_2O$, or a limited solid solution of the same. At 70 °C a solid solution of $3CaO \cdot Al_2O_3 \cdot 6H_2O$, in which about one-tenth of the Al_2O_3 is replaced by Fe_2O_3, is precipitated. The rate of reaction increases with temperature and with the proportion of alumina in the aluminoferrite.

Hydration in paste form progresses in a different manner. The hydrogarnet phase produced varies in composition with the parent aluminoferrite, but is always somewhat poorer in Fe_2O_3. The hexagonal plate phase, $4CaO \cdot (Al_2O_3,Fe_2O_3) \cdot nH_2O$ is produced from the aluminoferrites high in Fe_2O_3, especially at the lower temperatures. Another platy phase, $2CaO \cdot Al_2O_3 \cdot 8H_2O$ (or its limited solid solution) is formed from preparations highest in Al_2O_3, also at lower temperatures. Intermediate members give chiefly the hydrogarnet phase even at 25 °C.

1. Introduction

The compound $4CaO \cdot Al_2O_3 \cdot Fe_2O_3$ was first reported in 1928 by Hansen, Brownmiller, and Bogue [1][1], who also demonstrated the existence of a solid solution series extending from $2CaO \cdot Fe_2O_3$ to $4CaO \cdot Al_2O_3 \cdot Fe_2O_3$ (C_2F to C_4AF) [2]. Subsequent research in this area of the system $CaO-Al_2O_3-Fe_2O_3$ has shown that the series extends beyond C_4AF toward a hypothetical C_2A, reaching at least as far as C_6A_2F and probably a little farther. The investigations in this field were summarized by Nurse [2] for the Fourth International Symposium on the Chemistry of Cement (1960). More recently the crystal structure has been investigated by Smith [3], who gives the generalized formula for the series as $Ca_5(Fe_{1-p}Al_p)_5O_{20}$ ($O \leq p \leq 0.69$). The ternary solid solution is of importance because of its presence in portland cement clinker. The Al_2O_3:Fe_2O_3 ratio in the clinker varies with that in the raw mix, but it has been shown [4] that the relationship is not simple. For many clinkers the composition approximates C_4AF, although, according to Smith [3], the C_4AF composition is not a distinct compound. The solid solution often is referred to as the ferrite phase, and is sometimes designated Fss.

The authors who first described C_4AF [1] also reported on its hydraulic properties. In the ensuing years, several other investigations of the hydration of the ferrite phase have been made, yet the subject has by no means been as fully covered as has the hydration of the other major constituents of portland cement.

The individual hydrated compounds usually may be studied more readily on preparations synthesized by precipitation methods rather than by direct hydration of the anhydrous aluminoferrites. By such methods it has been established that there are two series of hydrated calcium aluminoferrite solid solutions, one crystallizing in the cubic system, the other in the form of hexagonal plates. The former series was described by Flint, McMurdie, and Wells in their paper on the garnet-hydrogarnet series [5]. For convenience it may be designated the C_3AH_6—C_3FH_6 series, though it is not yet firmly established that the ferrite end member can be formed in the absence of silica. The hexagonal series, C_4AH_n—C_4FH_n, has been studied extensively by Malquori and Cirilli [6], who also investigated the cubic series. Several other investigators have reported studies of these hydrates. Their work was summarized in 1960 by Jones [7] in a review paper prepared for the Fourth International Symposium on the Chemistry of Cement.

In the two solid solution series described, Fe_2O_3 appears to behave very much as does Al_2O_3. One might therefore expect to find hydrated ferrites analogous to the less basic aluminates, C_2AH_8 and CAH_{10}. The existence of such compounds has indeed been suggested, but there appears to be no definite evidence for them at present [7].

Members of the two known series of solid solutions have been prepared by hydration of C_4AF [5, 6, 7], the hexagonal plate phase being favored by lower

[1] Figures in brackets indicate the literature references at the end of this paper.
[2] The abbreviated formulas commonly adopted by cement chemists (C=CaO, $A=Al_2O_3$, $F=Fe_2O_3$, $S=SiO_2$, $H=H_2O$) will be used in this paper interchangeably with the conventional formulas.

temperatures, the cubic by higher. Both hydrates are richer in CaO than the anhydrous compound and, unless additional CaO is supplied, part of the Al_2O_3 or Fe_2O_3, or both, will be left over after formation of the hydrate. From numerous investigations of the calcium aluminates, excess Al_2O_3 would be expected to form an amorphous hydrated gel, gradually converting to gibbsite. The composition of the excess Fe_2O_3 appears to be still in question. It may be present as hematite or a crystalline hydrate of Fe_2O_3, a ferric hydroxide gel, or a combination of these [7].

In the series C_4AH_n—C_4FH_n, the value of n is not entirely certain. In C_4AH_n, it has been shown recently that $n=19$ for crystals in contact with the aqueous solution, but falls to 13 with only moderate drying [8]. For C_4FH_n, the value of 14 for n has been suggested [7]. with information lacking as to a higher hydrate. No attempt is made herein to settle this point.

The paste hydration of C_4AF at room temperature has been investigated recently by Chatterji and Jeffery [9] by means of electron-optical and x-ray diffraction techniques. It was shown that the initial hydration product contained the hexagonal compounds, C_4AH_n and C_2AH_n, with the cubic C_3AH_6 appearing after 14 days. Substitution of Fe for Al in the C_4AH_n was indicated by enlargement of the unit cell parameter, a. Similar substitution in C_3AH_6 was observed only in the presence of added lime.

Although there is considerable knowledge of the hydration of C_4AF, relatively little has been done in comparing other members of the aluminoferrite series. It is known in a general way that the reactivity with water is less rapid as the iron content is increased. Midgley, Rosaman, and Fletcher [10] have presented data for the relative rates of solution of C_6AF_2, C_4AF, and C_6A_2F in ammoniacal ammonium citrate solution; the rate increases markedly in the order given. No comparable data for reactivity with pure water have been noted. A study of the reactions of the aluminoferrites with a large excess of water is needed to provide a better understanding of the more practical problems of their reactions in paste form and of their interaction with other cement compounds. The present paper describes research which deals mainly with reactions of the aluminoferrites in excess water, and with one series of paste-type reaction mixtures.

2. Materials and Procedures

A series of sintered preparations covering the range from $6CaO{\cdot}2Al_2O_3{\cdot}Fe_2O_3$ to $2CaO{\cdot}Fe_2O_3$ (C_6A_2F to C_2F) were made in approximately 100-gram lots. The raw materials, reagent grade calcium carbonate (low alkali), aluminum hydroxide (gibbsite), and ferric oxide, were mixed dry, passed through a No. 48 sieve, and again mixed dry for two hours in bottles on a rotating wheel. The mixtures were then heated in open platinum dishes in an electric furnace at 1320 °C for two to three hours, cooled, ground, and reheated in the same manner. Each preparation was ground to pass a No. 200 sieve and was then separated into two fractions with a No. 325 sieve. All the sinters except that of C_6A_2F were friable and easy to grind. The C_6A_2F preparation was partially fused.

The preparations were analyzed for Al_2O_3, Fe_2O_3, and CaO in accordance with Federal Test Method Standard No. 158a [11]. Ferrous iron was determined by dichromate titration of a sample dissolved in hydrochloric acid in an atmosphere of carbon dioxide. Free CaO was determined by the glycerol-alcohol-ammonium acetate method. The results of the analyses are given in table 1. X-ray diffraction patterns of the powdered sinters, obtained on an x-ray diffractometer with Cu Kα radiation, were in good agreement with published patterns. The surface area of the fractions passing the No. 325 sieve was determined by the air permeability method [12]. The values are given in the last column of table 1. The fractions retained on the No. 325 sieve were not measured for surface area, being outside the working range of the apparatus.

TABLE 1. *Chemical composition and specific surface of aluminoferrite preparations*

Lot designation	Nominal composition [a]	CaO	Al_2O_3	Fe_2O_3	FeO	Free CaO	Specific surface of fine fraction
		%	%	%	%	%	cm^2/g
Fss–1	C_6A_2F	48.2	28.8	23.3	------	<0.01	1800
Fss–2	$C_6A_{1.75}F_{1.25}$	47.1	24.4	28.5	------	<.01	1200
Fss–3	$C_6A_{1.5}F_{1.5}$ (=C_4AF)	46.3	21.0	32.8	------	.02	1180
Fss–4	$C_6A_{1.25}F_{1.75}$	45.2	17.3	37.5	------	.28	890
Fss–5	C_6AF_2	44.3	13.5	42.1	0.03	.01	830
Fss–6	$C_6A_{0.5}F_{2.5}$	42.6	6.4	51.0	.07	.04	640
C_2F–1	C_2F	41.1	0.0	59.1	.07	<.01	630

[a] C=CaO; A=Al_2O_3; F=Fe_2O_3.

For the experiments described under section 3.1, as well as for certain exploratory tests, a series of preparations made earlier were used. They were comparable to lots Fss–1, –3, and –5 in composition, but were ground only to pass a No. 100 sieve.

Distilled water for the solution experiments was boiled before use to expel carbon dioxide. For the experiments described under section 3.2, 1 g of the sample was added to 1 liter of water in a flask and continuously stirred for several hours. The flask was immersed in a water bath maintaining constant temperature to about ± 0.2 °C at 25 °C, and 0.8 °C at 45 °C. At intervals, portions of the suspension were removed by suction, filtered through a fritted glass crucible in a closed system, and analyzed. Preliminary experiments showed that sorption of calcium hydroxide by the fritted glass, though detectable, was too slight to be significant in the present work.

3. Experimental Results

3.1. Leaching Experiments

The first series of experiments was designed to permit analysis of the solution after very brief

contact between the solid and the water, without regard to close control of either time or temperature. The water was poured over a bed of the powdered sample in a fritted glass crucible fitted to a suction flask, and the filtrate was analyzed. In preliminary tests, the bed of powder was first given an alcohol wash to eliminate fine particles that might go through the filter as such. Evaporation of the alcohol left residues of the order of only 0.1 mg; hence the alcohol wash was omitted thereafter.

The water was added from a pipet, except for the boiling water which was simply poured on. The approximate duration of the leaching period was recorded. The time varied considerably, partly because of variability among crucibles, partly because they became clogged to varying degrees. In some cases the rate was controlled by the delivery speed of the pipet; in others the crucible was slower, and the water accumulated to a depth of 5 mm or more above the bed. A few parallel experiments indicated that a longer leaching period allowed more material to dissolve but did not affect the ratio of the components in solution. This result was further checked by making successive leachings through the same bed with 50-ml portions of water. The first two filtrates were of about the same concentration, the third and fourth progressively more dilute, but the ratio of CaO to Al_2O_3 was approximately constant.

In a separate test it was found that the very first drops passing through the bed of solid on the filter were alkaline to phenolphthalein, showing that there was no "induction period" of appreciable duration.

The filtrates were analyzed for CaO and Al_2O_3 by conventional gravimetric methods. At first, qualitative tests for Fe_2O_3 were made by the thiocyanate method, but the results were always negative, and the test was subsequently omitted.

Results of a series of experiments of this type are given in table 2. Among other things, variation of the temperature of the leaching water was investigated. The temperatures indicated refer to the water at the start of leaching. Since the ambient temperature was about 25° C, the actual temperature varied in that direction during the run. Blank tests showed that the water at 1 °C warmed to about 5 °C, while that at 50 and 100 cooled to about 45 and 85 °C, respectively, before the end of the leaching period. For the present purpose, this variation in temperature was of no concern.

From the results obtained, the following conclusions may be drawn. (1) the amount of iron going into solution is too slight to detect by the method used. (2) The ratio of CaO to Al_2O_3 is lower in the solution than in the solid in all cases, and the difference increases as the CaO:Al_2O_3 ratio in the solid increases. (3) The CaO:Al_2O_3 ratio of the solution shows no consistent trend with temperature. The relatively large spread in values for the C_6AF_2 group may be ascribed to experimental errors, as the concentrations here were rather low. (4) The rate of reaction increases with temperature, as expected.

TABLE 2. *Results of some leaching experiments on three calcium aluminoferrites*

Expt. No.	Composition of solid [a]	Weight of solid	Volume of H_2O	Temperature [b]	Leaching time	Al_2O_3 in solution	CaO in solution	CaO / Al_2O_3 (molar)
		g	*ml*	*°C*	*sec*	*g/liter*	*g/liter*	
1	C_6A_2F	0.50	100	1	125	0.053	0.081	2.8
2	C_6A_2F	1.00	100	25	160	.182	.267	2.7
3	C_6A_2F	0.25	100	50	36	.080	.116	2.6
4	C_6A_2F	.25	100	100	45	.123	.172	2.5
5	C_4AF	1.00	100	1	130	.016	.028	3.2
6	C_4AF	1.00	100	25	120	.078	.141	3.4
7	C_4AF	1.00	100	50	90	.126	.229	3.3
8	C_4AF	1.00	100	100	45	.211	.390	3.4
9	C_6AF_2	1.00	100	1	80	.008	.017	3.9
10	C_6AF_2	1.00	100	25	160	.038	.073	3.5
11	C_6AF_2	1.00	100	50	38	.048	.107	4.0
12	C_6AF_2	1.00	100	100	40	.098	.236	4.4

[a] C = CaO; A = Al_2O_3; F = Fe_2O_3.
[b] Temperature of water at start of leaching. The temperature in the funnel moved progressively toward ambient temperature (about 25 °C) during the leaching.

Although the leaching process took from 36 to 160 sec, it is clear that the first drops coming through had been in contact with the solid for a much shorter period, probably of the order of 0.1 sec. Any Fe_2O_3 that dissolved and remained in solution as long as 0.1 sec would be expected to appear in detectable amount in the filtrate. However, none was found. From this it appears that the reaction after the first 0.1 sec of contact, approximately, is not essentially different from that occurring after several minutes. It was necessary to establish that point before proceeding to the next type of experiment, which was capable of closer control but could not yield reliable data for periods shorter than about 2 min.

3.2. Solution Experiments With Sampling at Several Intervals

The general procedure used was described in section 2, above. The fine fractions of preparations Fss–1 to Fss–6 (see table 1) were used in amounts of 1 g/liter of water. This proportion was chosen in the belief that the maximum concentration attained would be low enough to avoid precipitation of a calcium aluminate hydrate. However, there was some evidence of precipitation in one or two cases before the tests were terminated. As in the work described in the previous section, some of the earlier filtrates were tested qualitatively for iron. None was detected, and the test for iron was discontinued.

Table 3 gives the data obtained in a typical run. The figures in the fourth column show that the ratio of CaO to Al_2O_3 in solution does not change significantly with time. Also, they are in good agreement with the corresponding values in table 2. As the ratio of CaO to Al_2O_3 in the solid was 3:1, and that in the solution somewhat lower, it is clear that some CaO remained in the residue with the Fe_2O_3. Analy. sis of a portion of the residue also showed some Al_2O_3. The data here give no indication as to whether the residual Al_2O_3 represents unaltered an-

hydrous material or a reaction product. However, in similar experiments using a smaller original quantity of solid, or continued for a longer period, the residual Al_2O_3 was reduced to zero. It is assumed, therefore, that the Al_2O_3 that was not found in solution was present in unreacted grains of anhydrous solid. On this basis, the weight fraction that had reacted was calculated (last column).

TABLE 3. *Data relative to the reaction between* $6CaO \cdot 2Al_2O_3 \cdot Fe_2O_3$ *and water*

(Preparation Fss–1; 1.00g; 1 liter H_2O; temperature 24.3 ±0.2 °C)

Time [a]	Al_2O_3 in solution	CaO in solution	CaO:Al_2O_3 (molar)	Weight fraction reacted [b]
	g/liter	*g/liter*		
2 min	0.073	0.114	2.8	0.25
5 min	.138	.192	2.5	.48
11 min	.160	.225	2.6	.55
20 min	.181	.250	2.5	.62
60 min	.204	.300	2.7	.70
3 hr	.227	.345	2.8	.78
7 hr	.247	.386	2.8	.85
23 hr	.254	.392	2.8	.88

[a] Interval between addition of powder to water and start of removal of sample of solution through filter. Filtration required 1-2 minutes. Average period of contact for the sample may therefore be as much as 1 min longer than indicated in column 1.

[b] Based on Al_2O_3 in solution in relation to total Al_2O_3 present. (See text for discussion.)

The ratio of CaO attached to the Fe_2O_3 in the residue was calculated from the CaO:Al_2O_3 ratio in table 3, with the same assumption regarding residual Al_2O_3; it amounted to 0.7 mole CaO per mole Fe_2O_3.

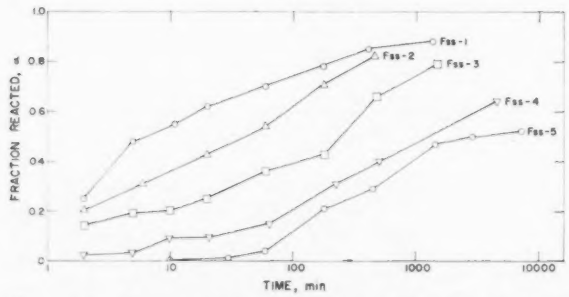

FIGURE 1. *Progress of reaction between calcium aluminoferrite preparations and water as a function of time of stirring.*

1 gram per liter; 25 °C.

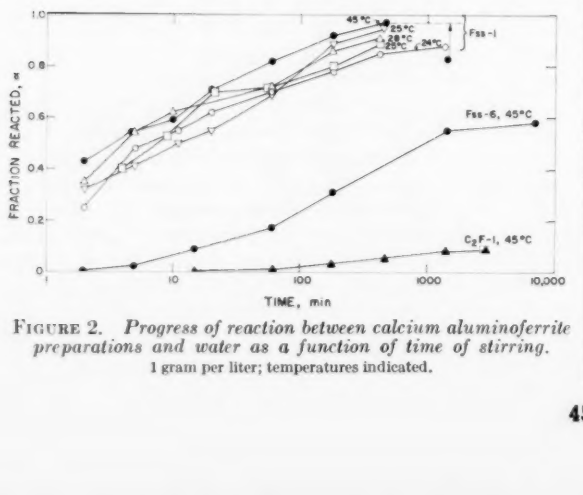

FIGURE 2. *Progress of reaction between calcium aluminoferrite preparations and water as a function of time of stirring.*

1 gram per liter; temperatures indicated.

The data in the first and last columns of table 3 are plotted in figure 1 (upper curve) to give a clearer picture of the course of the reaction. The ordinate is the weight fraction of solid that has reacted (α), computed on the basis of the Al_2O_3 in solution. The other curves in figure 1 are derived from experiments with preparations Fss–2 to Fss–5. The decrease in reactivity with increase in Fe_2O_3:Al_2O_3 ratio is apparent, though it should be borne in mind that part of the observed difference must be attributed to the differences in specific surface (table 1). Preparation Fss–6 reacted so slowly at 25 °C that it was decided to raise the temperature to 45 °C. The results are plotted in figure 2, second curve from bottom. The end member of the series, C_2F, reacted still more slowly (see bottom curve). Since this preparation contained no Al_2O_3, the progress of the reaction was estimated from the CaO in solution.

The upper group of curves in figure 2 represents five separate runs with preparation Fss–1, including the one already shown in figure 1. The purpose here is twofold, to give some idea of the reproducibility and to show the effect of temperature. From the random nature of the deviations from smooth curves, it may be assumed that these deviations reflect irregularities in the procedure (stirring speed or rate of filtering) or errors in analysis. It is apparent that the increase in temperature from 25 to 45 °C has a relatively small effect on the progress of the reaction of the aluminoferrite with water, though the difference is appreciable at the earliest sampling interval. The apparent drop in α between 8 and 24 hours (last 2 points, top curve) should be noted. This resulted from precipitation of Al_2O_3 (and CaO) from the supersaturated solution. The precipitate had a molar CaO:Al_2O_3 ratio of 2.2:1, calculated from the decrease in concentration.

The ratio of CaO to Al_2O_3 in the filtrate showed no consistent change with the progress of the reaction, though there were random deviations from the average. Table 4 gives the average CaO:Al_2O_3 ratios in the filtrate for each of the experiments included in figures 1 and 2. The ratio of CaO to Fe_2O_3 in the residue, calculated as described previously, is also given in table 4.

TABLE 4. *Ratio of* CaO *to* Al_2O_3 *in solution and of* CaO *to* Fe_2O_3 *in the residue for several solution experiments with calcium aluminoferrites*

Expt. No.	Sample No.	Temperature	CaO:Al_2O_3 (molar) in original solid (from analysis)	Fe_2O_3:Al_2O_3 (molar) in original solid (from analysis)	CaO:Al_2O_3 (molar) in solution (average values)	CaO:Fe_2O_3 (molar) in residue, calculated from CaO:Al_2O_3 values
		° C				
1	Fss–1	24.3 ±0.2	2.99	0.50	2.7	0.6
2	Fss–1	24.6 ±0.1	2.99	.50	2.6	.8
3	Fss–1	24.8 ±0.4	2.99	.50	2.7	.6
4	Fss–1	28.4 ±0.4	2.99	.50	2.6	.8
5	Fss–1	45.4 ±0.3	2.99	.50	2.7	.6
6	Fss–2	24.7 ±0.1	3.45	.75	2.9	.7
7	Fss–3	24.8 ±0.1	4.02	1.00	3.6	.4
8	Fss–4	24.9 ±0.1	4.76	1.38	4.3	.3
9	Fss–5	24.9 ±0.2	5.96	1.99	5.0	.5
10	Fss–6	45.4 ±0.4	12.16	5.11	8.6	.7

The $CaO:Fe_2O_3$ ratio in the residue does not show any consistent trend with the composition of the aluminoferrite. There are random variations which may be attributed to uncertainties involved in the method of calculation. At this point the data do not indicate whether the CaO is combined with Fe_2O_3 or adsorbed.

3.3. Effect of Temperature

The foregoing series of experiments showed that the nature of the reaction between the calcium aluminoferrites and a large amount of water is essentially the same after several hours or days as it is at the very beginning. For most of the subsequent studies, therefore, the prolonged reaction period was replaced by a shorter procedure in which the reaction mixture was filtered for analysis only once, after 60 min. The temperature was varied in 5 steps from 10 °C to boiling, but the less reactive preparations were not tested at the lower temperatures. Except for the experiments at 10 °C, a magnetic stirrer with heater was substituted for the apparatus described previously. The initial ratio of solid to water was kept constant at 1 g/liter except for the experiments at the boiling point, for which it was lowered to 0.75 g/liter in an attempt to avoid precipitation of calcium aluminates from solution. In spite of this, a slight precipitate was observed to form on the flask walls in several instances.

TABLE 5. *Solutions obtained from reaction of calcium aluminoferrites (fine fraction) with large amounts of water for 60 minutes*

Expt. No.	Prepn. No.	Wt. of solid	Vol. of H_2O	Temp.[a]	Al_2O_3 in filtrate	CaO in filtrate	CaO: Al_2O_3 Ratio (molar)
		g	*ml*	*°C*	*g/liter*	*g/liter*	
1	Fss-1	0.50	500	10	0.197	0.292	2.7
2	Fss-1	.20	200	25	.202	.304	2.7
3	Fss-1	.20	200	45	.233	.368	2.9
4	Fss-1	.20	200	70	.248	.382	2.8
[b]5	Fss-1	.15	200	100	.164	.259	2.9
6	Fss-2	.35	350	10	.102	.170	3.0
7	Fss-2	.20	200	25	.124	.216	3.2
8	Fss-2	.20	200	45	.190	.323	3.1
9	Fss-2	.20	200	70	.222	.387	3.2
[b]10	Fss-2	.15	200	100	.124	.236	3.5
11	Fss-3	.50	500	10	.054	.102	3.4
12	Fss-3	.20	200	25	.070	.138	3.6
13	Fss-3	.20	200	45	.134	.257	3.5
14	Fss-3	.20	200	70	.177	.350	3.6
[b]15	Fss-3	.15	200	100	.144	.314	4.0
16	Fss-4	.20	200	25	.034	.078	4.2
17	Fss-4	.20	200	45	.074	.165	4.1
18	Fss-4	.20	200	70	.128	.292	4.2
[b]19	Fss-4	.15	200	100	.092	.247	4.9
20	Fss-5	.20	200	25	.016	.046	5.5
21	Fss-5	.20	200	45	.040	.104	4.8
22	Fss-5	.20	200	70	.072	.196	5.0
[b]23	Fss-5	.15	200	100	.072	.228	5.7
24	Fss-6	.20	200	70	.023	.112	8.9
25	Fss-6	.15	200	100	.022	.112	9.3
26	C_2F-1	.20	200	70	.000	.026	----------
27	C_2F-1	.15	200	100	.000	.038	----------

[a] Temperatures ±0.5 °C except as follows: at 10 °C ±0.2 °C; at 100 °C, not determined.
[b] Precipitate formed on wall of flask during boiling.

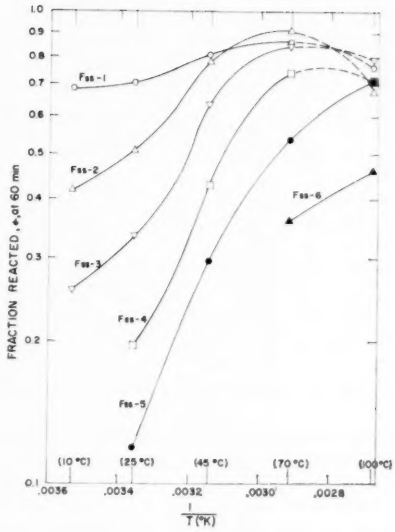

FIGURE 3. *Progress of reaction between calcium aluminoferrite preparations and water, on stirring for 60 minutes, as a function of temperature.*
1 gram per liter (except at 100 °C, where ratio was 0.75 gram per liter).

The results of analyses of the filtrates are given in table 5. It may be noted that the $CaO:Al_2O_3$ ratios for the solutions obtained by boiling are appreciably higher than the others. The precipitation mentioned above probably had an influence on these values. The other values for the $CaO:Al_2O_3$ ratio are in fair agreement with those reported in tables 2 and 4, and show no consistent trend with temperature.

The effect of temperature on the rate of solution is shown in figure 3. Here the fraction reacted, α, at 60 min is taken as a measure of the rate of the reaction, and plotted on a logarithmic scale against the reciprocal of the absolute temperature. In comparing the reactivities of the preparations, it should be noted that no correction has been made for the difference in surface area (see table 1).

3.4. Effect of Calcium Hydroxide Concentration

From the data given above (see table 3, for example) it is clear that the rate of solution falls off as the concentration increases, as would be expected. However, since this is not a case of simple solution, it is of interest to ascertain whether the reaction can be inhibited by a sufficiently high concentration of lime alone. A few tests were made with two of the preparations to obtain information on this point. Mixtures of the powdered materials were shaken with $Ca(OH)_2$ solutions of different concentrations in the ratio of 1 g/liter for 5 min at 25 °C and the filtrates were analyzed. Results are given in table 6. It is seen that the dissolution reaction is inhibited by increasing concentration of lime, but is not completely prevented even at saturation.

736-657—64——3

TABLE 6. *Dissolution of calcium aluminoferrites in* $Ca(OH)_2$ *solutions on shaking for 5 minutes at 25 °C*

Proportions: 1 g aluminoferrite per liter of solution

Expt. No.	Sample No.	CaO concn. at start	CaO in soln. at 5 min	Increase in CaO in soln.	Al_2O_3 in soln. at 5 min
1	Fss–1	0.000	0.180	0.180	0.120
2	Fss–1	.320	.411	.091	.068
3	Fss–1	.510	.561	.051	.048
4	Fss–1	.853	.860	.007	.019
5	Fss–1	1.150	1.149	−.001	.006
6	Fss–2	0.000	0.104	.104	.073
7	Fss–2	.425	.462	.037	.028
8	Fss–2	.700	.728	.028	.024
9	Fss–2	.924	.937	.013	.008

3.5. Effect of Composition on Reaction Rate

In the preceding experiments, any comparison of the reactivities of the samples is complicated by differences in surface area. In order to minimize this variable, a series of tests were run on the fractions passing a No. 200 and retained on a No. 325 sieve, which were assumed to be equal in surface area (probably of the order of 300 cm^2/g). To compensate for the lower surface area, the ratio of solid to water was increased to about 5 g/liter. The actual ratio was varied to make all the mixtures equivalent on a molar basis. The mixtures were stirred 10 min at 25 °C, then filtered and analyzed. The data are given in table 7. Sample Fss–1 reacted so rapidly that some precipitation occurred within the 10-min stirring period. The test therefore was repeated with one-fourth the original amount of solid (experiment 1a). Similarly, the experiment with sample Fss–2 was repeated with half the original amount. The results are shown in figure 4, in which the fraction reacted is plotted on a logarithmic scale against the initial composition of the solid expressed as $Al_2O_3/Al_2O_3+Fe_2O_3$. For this graph, the data for experiments 1a and 2a, rather than 1 and 2, were used, to minimize the concentration effect. This relationship will be discussed later.

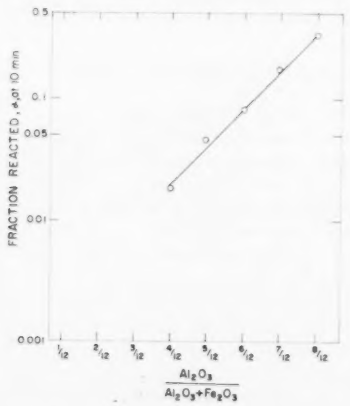

FIGURE 4. *Reactivity of calcium aluminoferrites with water as a function of composition.*

TABLE 7. *Comparison of rates of solution of calcium aluminoferrites (concentrations after stirring 10 minutes at 25 °C; fraction passing No. 200 and retained on No. 325 sieve)*

Expt. No.	Sample No.	Wt. of solid	Vol. of water	Al_2O_3 in solution	CaO in solution	CaO:Al_2O_3 (molar)
		g	*ml*	*g/liter*	*g/liter*	
1	Fss–1	1.00	200	0.416	0.562	2.5
1a	Fss–1	0.25	200	.127	.189	2.7
2	Fss–2	1.02	200	.151	.248	3.0
2a	Fss–2	0.51	200	.107	.182	3.1
3	Fss–3	1.03	200	.087	.164	3.4
4	Fss–4	1.05	200	.042	.094	4.1
5	Fss–5	1.08	200	.013	.037	5.2
6	Fss–6	1.12	200	.000	.005	---

3.6. Composition of Residue

It was shown in table 4 that the reaction between 1 g of aluminoferrite and 1 liter of water leaves a residue containing CaO and Fe_2O_3 in somewhat variable ratio, with less than 1 mole of CaO per mole of Fe_2O_3, and with no apparent relation to the composition of the original preparation. If this product is simply an adsorption complex, the CaO:Fe_2O_3 ratio should vary with the concentration of CaO in solution. To check this point, samples Fss–1 and Fss–2 were allowed to react with water in the ratio of 0.1 g/liter, one-tenth the previous amount. The concentrations of lime attained in solution were only 0.048 and 0.046 g/liter, respectively, as compared with 0.39 and 0.34 when 1 g was used. The residues, on analysis, showed CaO:Fe_2O_3 ratios of 0.3 and 0.2, respectively, as compared with the values 0.6 and 0.8 obtained at the higher concentration. This may be taken as evidence that the CaO is adsorbed on the Fe_2O_3, rather than chemically combined. This conclusion is confirmed, in a negative way, by the absence of any microscopic or x-ray diffraction evidence of a crystalline ferrite.

3.7. Compounds Precipitated From Solution

In the foregoing experiments, the ratio of solids to water was kept low to avoid precipitation. But it is important to know what solid phases would be precipitated if the concentration were increased slightly. On the assumption that the amount of Fe_2O_3 in solution is so small as to have no appreciable effect, the nature of the precipitate may be predicted from the known phase equilibria in the system $CaO-Al_2O_3-H_2O$ [7]. The concentrations are in the range where either or both of two phases would be expected to form: (1) the metastable C_2AH_8, or its solid solution, recently reported to extend to $C_{2.4}AH_n$, crystallizing as hexagonal plates; (2) the stable isometric C_3AH_6.

To check the validity of this supposition, a series of experiments were conducted in which the ratio of solid to water was increased sufficiently to assure a moderate amount of precipitation within 20 min. At 25 °C only the hexagonal plate phase was observed; at 45 °C, plate crystals were present at 20

min, isometric crystals after a few hours; at 70 °C, isometric crystals plus a few plates; at boiling temperature only the isometric. These results are in accord with published data on the system $CaO-Al_2O_3-H_2O$ [7].

The hexagonal plate phase was identified by x-ray diffraction as C_2AH_8 (or the limited solid solution mentioned above; no attempt was made to differentiate). The isometric crystals were identified by both x-ray diffraction and microscopic observation as being of the C_3AH_6 type. However, both the refractive index and the unit cell dimensions as calculated from the diffraction pattern were slightly larger than those that have been reported for C_3AH_6. It will be recalled that C_3AH_6 may be considered an end member of a quinary solid solution series [5, 7] in which Fe_2O_3 may replace Al_2O_3, and SiO_2 may replace H_2O. The Fe_2O_3 substitution results in an increase in both the refractive index and the unit cell size, while SiO_2 increases the refractive index but decreases the cell dimensions.

To eliminate the possibility of contamination by SiO_2 resulting from attack on glass, another series of reactions was run in polyethylene bottles. The proportion of solid was further increased, and the stirring was continued for 3–4 hr at 70 °C to get sufficient material for accurate measurement of the diffraction patterns. This procedure also yielded crystals large enough, in a few cases at least, for an accurate determination of refractive index. A preparation of C_3A was subjected to the same treatment, and the resulting hydrate, C_3AH_6, served as a basis for comparing the other products. The unit cell dimension of the C_3AH_6, calculated from measurement of the x-ray diffraction lines, was 12.573 Å. The results (see table 8) clearly show an increase in both index and cell dimensions, in comparison with C_3AH_6, which can be explained only by incorporation of Fe_2O_3 into the structure.

TABLE 8. *Data pertaining to isometric crystals precipitated from solutions from aluminoferrites in polyethylene at 70 °C*

Prepn. No.	Wt. of solid used	Vol. of water	Index of refraction	Unit cell edge, a_0	Remarks
	g	*ml*		Å	
Fss-1	1.0	500	[a] 1.61	12.591	
Fss-2	1.0	500	[a] 1.61	12.594	
Fss-3	2.0	500	[a] 1.61	12.585	
Fss-4	2.0	300	1.614	12.594	
Fss-5	3.0	300	1.615	12.606	Some crystals of higher index attached to Fss grains.
Fss-6	5.0	300	(b)	(b)	No isometric crystals observed; hexagonal plates present.
C_3A	2.0	500	1.605	12.573	Unreacted C_3A also present.

[a] Crystals too small to permit an accurate determination of index.
[b] No isometric crystals observed; x-ray pattern indicated probable presence in amount too slight for measurement of cell constant.

The relation between Fe_2O_3:Al_2O_3 ratio, index of refraction, and cell parameter is not known with sufficient precision to permit anything better than an estimate of the amount of Fe_2O_3 present. Assumption of a linear relation between the composition and index of refraction leads to the conclusion that the Fe_2O_3 constitutes about one-tenth of the total "R_2O_3" on a molar basis. Consideration of the unit cell size leads to a similar conclusion. Also, the ratio of the intensities of the 220 and 611 diffraction lines, recommended as a criterion by Zur Strassen, as reported by Jones [7], is compatible with this estimate.

Within the limits of precision of the measurements there was no apparent variation in composition of the isometric phase with the composition of the parent aluminoferrite, at least for the first four preparations. The fifth, Fss–5, yielded a product with appreciably larger cell size, but there was some broadening of the x-ray diffraction lines, possibly reflecting a variability in composition. Microscopic examination revealed isometric crystals, adhering to the aluminoferrite grains, with refractive index slightly higher than that of the dispersed crystals. Preparation Fss–6 reacted very slowly, yielding a few well formed hexagonal plates occurring mostly as a fringe around the original grains. Isometric crystals were not observed, but the x-ray pattern showed a few weak lines that could be attributed to this phase.

In view of the foregoing results, a re-examination of the solutions in regard to Fe_2O_3 concentration was indicated. Filtrates from some of the reaction mixtures were concentrated by evaporation and tested for iron by the thiocyanate method in comparison with a standard ferric chloride solution. The iron content was found to be in the range of 0.02 to 0.05 mg Fe_2O_3 per liter, without consistent trend with composition of the aluminoferrite. Although this is lower by several orders of magnitude than the concentration of Al_2O_3, it has an appreciable effect on the composition of the precipitate. The crystals typically were well formed, either dispersed or attached to the wall of the vessel, not attached to grains of the anhydrous aluminoferrite (except as noted above); hence there can be little doubt that they were precipitated from the solution phase, not formed at the solid-liquid interface.

3.8. Hydration in Paste Form

The reactions described above occurred under conditions permitting the Al_2O_3, most of the CaO, and a trace of Fe_2O_3 to go into solution, with ultimate disappearance of the original solid phase, leaving most of the Fe_2O_3 (possibly hydrated) with a little adsorbed CaO in finely dispersed form. These conditions are far different from those existing in cement pastes. A brief study of hydration with small amounts of water was therefore made. A small amount of the powdered sample (fine fraction) was placed in a weighed glass tube, the tube was reweighed, a few drops of water were added, and the tube was quickly sealed in a flame and again reweighed. The ratio of water to solid ranged from 0.5 to 1.1. The tubes were stored at three different temperatures, 1, 25, and 45 °C, all ±1 °C, for 2 months. The contents were then dried and examined microscopically and by x-ray dif-

fraction. Most of the tubes were found to be cracked, probably owing to expansion of the contents during hydration. Hydration appeared to be essentially complete or at least far advanced in all cases, thus it is apparent that the cracking had not interfered seriously with the process. However, a few of the x-ray diffraction patterns showed evidence of small amounts of calcium aluminate monocarbonate, probably indicating that some carbon dioxide had entered through the cracks.

The phases identified in the hydration products are listed in table 9. At 1 °C, C_2AH_8 is the major hydration product at the high-alumina end of the series. The high-iron members give the tetracalcium compound, presumably a solid solution containing both ferric oxide and alumina. At 25 °C, the isometric phase predominates, but is accompanied by C_2AH_8 in Fss–1 and by the other hexagonal phase in Fss–5, while in Fss–6 and C_2F–1 only the hexagonal is present. At 45 °C, the isometric phase was the only hydrate identified in the first five; the C_2F product showed only the hexagonal, and Fss–6 yielded both.

TABLE 9. *Phases present in hydration products of aluminoferrites after hydration for 2 months in paste form*

Sample No.	Stored at 1 °C	Stored at 25 °C	Stored at 45 °C
	[a]	[a]	[a]
Fss–1	C_2AH_8; little carb; little Fss; some unidentified material	HG; little C_2AH_8; little Fss	HG; very little Fss
Fss–2	Fss; little C_2AH_8	HG; trace carb.	HG; trace Fss
Fss–3	Fss; carb; little C_2AH_8; unidentified material	HG; little Fss; unidentified material	HG; trace Fss; unidentified material
Fss–4	$C_4(A,F)H_n$; trace carb; trace Fss	HG; trace Fss	HG
Fss–5	$C_4(A,F)H_n$; Fss	HG; $C_4(A,F)H_n$; little carb; unidentified material	HG; unidentified material
Fss–6	$C_4(A,F)H_n$; little hematite; trace carb.	$C_4(A,F)H_n$; Fss; unidentified material	HG; $C_4(A,F)H_n$; little Fss(?)
C_2F–1	C_4FH_n; unidentified material	C_4FH_n; unidentified material	C_4FH_n; unidentified material

[a] HG=hydrogarnet ($3CaO{\cdot}(Al_2O_3, Fe_2O_3){\cdot}6H_2O$), carb=$3CaO{\cdot}Al_2O_3{\cdot}CaCO_3{\cdot}11\ H_2O$, Fss=unaltered anhydrous material, "trace" indicates barely detectable by x-ray, C=CaO, A=Al_2O_3, F=Fe_2O_3, H=H_2O.

In general, the x-ray diffraction lines of the isometric phase were sharper the higher the temperature and the higher the alumina content. The patterns of the hexagonal phases were characterized by a very strong line from the 001 plane.

The cell constant, a_0, for the isometric phase was measured on partial x-ray diffraction patterns comprising the 431, 521, and 611 reflections, with tungsten present as internal standard. In figure 5 the cell constants for the 45-deg products are plotted against the composition of the anhydrous starting material, expressed as $\frac{Fe_2O_3}{Al_2O_3+Fe_2O_3\ (molar)}$. The

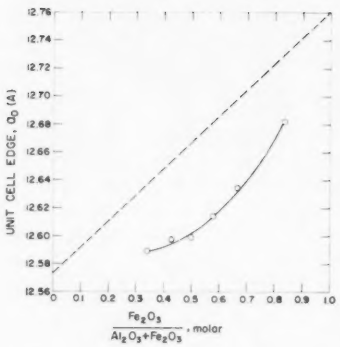

FIGURE 5. *Cell constant of isometric phase in product of paste hydration of calcium aluminoferrites as related to composition of anhydrous material.*

exact relationship between cell size and composition of the isometric phase is not known, but it is believed to be not far from linear. In the diagram, the dashed line represents a linear relationship from C_3AH_6 to C_3FH_6, based on the cell constants 12.573 for C_3AH_6 and 12.76 for C_3FH_6, the latter from data of Roberts reported by Jones [7]. The actual curve is below the dashed line, indicating that the hydration product is poorer in iron than the starting material.

The refractive index of the isometric phase in the hydration products also varies with composition, but because of other phases present it was difficult to determine with any precision. It ranged from 1.61 for Fss–1 up to about 1.67 for Fss–6.

4. Discussion

4.1. Nature of the Reaction

In the solution experiments described above, the ratio of water to solid was of the order of 1000:1. When the ferrite phase in portland cement is hydrated, in practice, the water-cement ratio is less than 1:1. The series of hydration experiments using small amounts of water was intended to simulate practical conditions, with the important exception that the other cement compounds were absent. The two conditions of solid:water ratio are widely divergent, but they coincide at one point, the instant of the first contact between solid and water, when the concentration of solute in the liquid phase is nil.

The leaching experiments described under section 3.1 demonstrated that the reaction begins practically instantaneously on contact. Exactly what takes place at the interface during the first fraction of a second is not revealed, but it is shown that CaO and Al_2O_3 go into solution immediately, leaving nearly all of the Fe_2O_3 in the solid state. The Fe_2O_3 is not totally insoluble, but the concentration is only about 0.05 mg/liter or less. If the Fe_2O_3 goes into solution initially along with the CaO and Al_2O_3, it must coagulate or crystallize into particles large enough to be retained on the filter, all within a fraction of a second. Such an explanation appears improbable.

It is more likely that the calcium and aluminum atoms are removed from the outer layers, by some unknown mechanism, leaving the iron at least momentarily in the original crystal structure. A small amount of calcium remains with the iron, the ratio being a function of the concentration of the solution in contact.[3]

Although the aluminoferrites do not dissolve congruently, the reaction rate is influenced in a similar manner by the concentration of the reaction products. That is, the rate decreases as the concentration of CaO and Al_2O_3 in solution increases. When the solid is leached with a stream of water, the concentration always remains low. Continued leaching should ultimately leave a residue of almost pure Fe_2O_3 (or a hydrate). When the solid is caused to react with a large volume of water, and the liquid phase is not removed, the concentration of CaO and Al_2O_3 in solution builds up to the point of supersaturation with respect to one or more of the calcium aluminate hydrates, whereupon precipitation will occur, though not necessarily at once. The concentration at which this happens depends on the temperature, the $CaO:Al_2O_3$ ratio, and the particular solid phase formed. The complexities of the phase equilibrium relations in the $CaO–Al_2O_3–H_2O$ system have been reviewed by Jones [7]. The experimental proportions in the present study were chosen to avoid precipitation of the hexagonal aluminates, but in a few cases, at 25 and 45 °C, it was apparent that a slight amount of precipitation had occurred, whether of hexagonal or isometric crystals being undetermined. At 70 and 100 °C, the precipitate was the isometric hydrate.

Hydration at low water-solid ratios, simulating paste hydration, may be assumed to follow the same course at first, but the concentration increases to the supersaturation range very rapidly, probably within the first minute for the more reactive members. In agreement with this assumption, preparations Fss–1 and Fss–2 exhibited what might be termed "flash set", while the rest of this series took increasingly long to stiffen as the Fe_2O_3 content increased. The initial stiffening is assumed to result from precipitation of a calcium aluminate hydrate.

Once the paste has stiffened, the movement of the liquid phase and the diffusion of ions through it must be greatly restricted. Hydration probably continues, however, provided sufficient water is present, until all the original anhydrous material has reacted, just as in the case of the other constituents of cement clinker.

The reaction products resulting from paste hydration are not the same as those produced by hydration in a large amount of water. When a small amount of the anhydrous material is dispersed in water, a supersaturated solution is formed, from which one or more hydrated phases then precipitate. At the higher temperatures, the precipitate contains the isometric phase, $3CaO·(Al_2O_3, Fe_2O_3)·6H_2O$. The ratio of Fe_2O_3 to Al_2O_3 in this phase is of the order of 1 to 10, and appears not to vary with the ratio in the anhydrous material. The ratio in the hydrated phase is therefore assumed to be controlled by the relative concentrations of the two components in solution. The ratio of Fe_2O_3 to Al_2O_3 in solution was found to be at least as low as 1 to 4000, with no apparent dependence on the composition of the anhydrous phase; thus the precipitate is strongly beneficiated with respect to iron.

In contrast, paste hydration yields an isometric phase in which the $Fe_2O_3:Al_2O_3$ ratio varies with that in the anhydrous starting material. However, they are not equal, the isometric hydrate being always poorer in iron than the starting material. These results are not entirely in agreement with those reported by Chatterji and Jeffery [9], who found no replacement of Al by Fe in the isometric phase when C_4AF was hydrated in paste condition. The data reported in the present paper indicate replacement of Al by Fe sufficient to enlarge the unit cell dimensions by about 0.2 percent in a comparable hydration of C_4AF. Because of minor differences in experimental conditions and in x-ray diffraction equipment, it is impossible to say, at present, whether this slight difference in results is apparent or real. There is agreement to this extent, at least, that even under conditions of paste hydration, the anhydrous structure is broken down and the components are selectively combined in the hydrate. Consideration of the stoichiometry of the reaction shows that this is necessary, since there is insufficient lime to combine with all the Fe_2O_3 and Al_2O_3 to form the isometric (hydrogarnet) phase. The effect of introducing excess lime into the paste was investigated by Chatterji and Jeffery [9], who obtained a cubic phase with unit cell dimension about 0.5 percent larger than that of C_3AH_6 by hydrating a paste of C_4AF with added lime.

The results obtained with preparation Fss–5 in water-solid ratio of 100 to 1 (table 8) show some indication of what might be termed a transition stage between the free dispersion and the paste conditions. Here there was evidence of formation of the isometric phase both by precipitation from solution and by growth on the edges of the parent material. The latter crystals were apparently richer in iron than the former, but still contained less iron than those formed by paste hydration of the same anhydrous preparation.

The products of hydration under the two extremes of reaction conditions also differ in respect to the hexagonal plate phases. Paste hydration permits formation of the tetracalcium series, $4CaO·(Al_2O_3, Fe_2O_3)·nH_2O$, from the iron-rich aluminoferrites, even at 45 °C in the case of Fss–6 and the C_2F end member (table 9). This phase was not observed in the hydration products precipitated from solution. This fact is understandable, since the CaO in solution never reached the high concentration necessary for precipitation of the tetracalcium series. It is reasonable to assume that in paste hydration the slow diffusion of the ions allows the concentration to build up sufficiently for formation of the tetracalcium series.

[3] The iron-free constituents of cement clinker, C_3S, C_2S, and C_3A, react in a different manner when subjected to the same leaching procedure, the ratio of components in the filtrate being approximately the same as in the solid compound.

The x-ray pattern of the hydrated tetracalcium aluminate-ferrite solid-solution series varies with composition but the displacement of the diffraction lines is relatively small, and the relationship not well established. The situation is complicated by the existence of two forms of C_4AH_{13} with slightly different spacings. For these reasons, no attempt was made to correlate the composition of the hexagonal plate phase with the composition of the parent material.

At the lower temperatures, the hexagonal plate phase C_2AH_8 (or its limited solid solution) was observed in the paste hydration products of the more alumina-rich members of the series. Similar plates were observed in stirred suspensions of the same preparations, also at the lower temperatures. Although too few for positive identification, they may be assumed to have been the same phase, since the CaO concentration was too low to permit precipitation of the tetracalcium compound of similar appearance. It would be interesting to know whether this phase also takes up Fe_2O_3 into solid solution, as does the hydrogarnet. Although there has been some speculation as to the possibility of such substitution [7] there appears to be no conclusive evidence that it occurs, and the question remains unanswered for the present.

It is of some interest to note (see table 9) that on hydration in paste form at 25 °C, the hexagonal plate phases appeared only at the high-alumina and the high-iron oxide ends of the series (dicalcium and tetracalcium compounds, respectively). The intermediate members, Fss–2 and Fss–3, yielded only the isometric phase.

The nature of the ferric oxide residue was not established. In a few of the precipitates examined by x-ray diffraction, numerous weak lines corresponding to the pattern of hematite were observed. In many other patterns only one or two lines attributable to hematite appeared, and in still others, none at all, even though the residue was known to contain a large amount of iron oxide not otherwise accounted for. Patterns of the hydrated ferric oxides were not observed. From these facts it may be inferred that the residual Fe_2O_3 is amorphous at first (with a variable amount of adsorbed CaO) and that it gradually changes to hematite.

It should be emphasized that the observations on the reactions of the aluminoferrites on paste hydration, as reported here, do not necessarily indicate that these materials would behave in the same way in the hydration of cement, in the presence of silica, calcium sulfate, excess calcium hydroxide, and other substances.

4.2. Rate of Reaction

The determination of reaction rates in heterogeneous systems is a complicated matter even for simple reactions occurring under carefully controlled conditions. The reaction between water and the aluminoferrites is not simple, and it appeared inadvisable to attempt to derive mathematical expressions for the true reaction rates. However, it was desirable to obtain at least an approximate idea of the variation of rate of reaction with composition.

The rate of solution of a solid in a liquid may be assumed to vary linearly with the area of the interface. As the reaction proceeds, both the volume and the surface area of the solid phase decrease. At the start, the percentage decrease in area is two-thirds that of the volume (which in turn is equal to that of the mass of the solid phase) assuming particles of regular shape and uniform size. Neither assumption holds in the present case. Furthermore, the solid does not dissolve congruently, and nothing is known as to the inhibiting effect of the residue. All that can be said on this point is that the surface area factor should cause a gradual decrease in reaction rate.

When a solid dissolves congruently, the rate decreases exponentially because of the increasing concentration of solute. In the present case, the solid does not dissolve congruently. It was shown experimentally that the reaction is slower in the presence of $Ca(OH)_2$ in solution, and it may reasonably be assumed that dissolved Al_2O_3 would have a similar effect. The dissolution of the aluminoferrite, unlike that of an ordinary soluble salt, does not reach an equilibrium concentration and then stop. Hydrated crystalline phases are precipitated from solution, permitting the decomposition of the anhydrous material to proceed to completion. These factors influence the reaction rate to an unpredictable extent. The rate was shown to fall off rapidly as the reaction progressed, and the concentration factor undoubtedly is the chief cause of the decrease.

Closely allied to the concentration factor is the rate of diffusion of solute away from the reaction zone, which in turn is controlled in large part by the rate of stirring. An attempt was made to subject all the suspensions to the same degree of agitation, but strict uniformity was not attained.

In view of the complicating factors discussed above, it is evident that any attempt to estimate reaction constants would not have much meaning. Therefore, in comparing the reaction velocities of the aluminoferrites, the concentration attained after a fixed period of stirring was arbitrarily taken as a measure of the reactivity. Under these experiental conditions, as shown in figure 4, the reactivity is strongly dependent on composition, increasing with the Al_2O_3:Fe_2O_3 ratio.

The kinetics of paste hydration are quite different. Here the diffusion of water molecules or the solute ions, or both, must be the most important factor in controlling the rate. Although there was but one series of experiments of this type, and all were of the same duration, it appears that the hydration of the different members of the series proceeded at something near the same rate, regardless of composition.

5. Summary

The initial reaction occurring immediately on contact between water and a member of the calcium aluminoferrite solid solution series is one of incongruent solution. The alumina, most of the calcium

oxide, and a trace of iron oxide pass into solution, and a residue of iron oxide (probably amorphous) with adsorbed calcium oxide remains.

At sufficiently high dilution, the reaction will proceed to completion. More concentrated suspensions give rise to supersaturation followed by precipitation. The major precipitated phase at room temperature is $2CaO \cdot Al_2O_3 \cdot 8H_2O$ (or a solid solution). At 70 °C the precipitate is chiefly a phase of the hydrogarnet type of approximate composition $3CaO \cdot 0.9Al_2O_3 \cdot 0.1Fe_2O_3 \cdot 6H_2O$.

The rate of reaction varies greatly with the composition of the aluminoferrite, being most rapid for the preparation highest in alumina.

The rate of reaction increases with temperature, the relative increase being more pronounced for the preparations high in iron oxide.

Hydration of the aluminoferrites in paste form progresses in a different manner. The hydrogarnet phase produced varies in composition with the aluminoferrite starting material, approaching but not reaching the Fe_2O_3:Al_2O_3 ratio in the anhydrous material. At the lower temperatures, $2CaO \cdot Al_2O_3 \cdot 8H_2O$ (or its limited solid solution) is produced from the aluminoferrite highest in alumina, hydrogarnet from intermediate members, and $4CaO \cdot (Al_2O_3, Fe_2O_3) \cdot nH_2O$ from those highest in iron oxide. The excess Fe_2O_3 remaining is believed to form hematite, possibly after an intermediate amorphous stage. The rate of hydration is less dependent on composition than is the case with highly dispersed suspensions.

Preparation of the main series of aluminoferrites and most of the work described under section 3.2 were done by Philip H. Bowles, student trainee at the National Bureau of Standards during one summer. X-ray diffraction patterns were made by H. E. Swanson and J. De Groot of the Crystallography Section. The assistance of these persons is gratefully acknowledged.

6. References

[1] W. C. Hansen, L. T. Brownmiller, and R. H. Bogue, Studies on the system calcium oxide-alumina-ferric oxide, J. Am. Chem. Soc. **50,** 396–406 (1928).

[2] R. W. Nurse, Phase equilibria and constitution of portland cement clinker, Proc. Fourth International Symposium on the Chemistry of Cement, NBS Mono. 43 (1962), pp. 9–37.

[3] D. K. Smith, Crystallographic changes with the substitution of aluminum for iron in dicalcium ferrite, Acta Cryst. **15,** 1146–1152 (1962).

[4] T. F. Newkirk and R. D. Thwaite, Pseudoternary system calcium oxide-monocalcium aluminate-dicalcium ferrite, J. Res. NBS **61,** 233–245 (1958).

[5] E. P. Flint, H. F. McMurdie, and L. S. Wells, Hydrothermal and x-ray studies of the garnet-hydrogarnet series and the relationship of the series to hydration products of portland cement, J. Res. NBS **26,** 13–33 (1941).

[6] G. Malquori and V. Cirilli, The hydrated calcium ferrites, and the complexes that originate from tricalcium ferrite by association with different salts of calcium (Note 4), (in Italian), Ric. Sci. **14,** 78–84 (1943).

[7] F. E. Jones, Hydration of calcium aluminates and ferrites, Proc. Fourth International Symposium on the Chemistry of Cement, NBS Mono. 43 (1962), pp. 204–246.

[8] M. H. Roberts, New calcium aluminate hydrates, J. Appl. Chem. **7,** 543–546 (1957).

[9] S. Chatterji and J. W. Jeffery, Studies of early stages of paste hydration of cement compounds, I, J. Am. Ceram. Soc. **45,** 536–543 (1962).

[10] H. G. Midgley, D. Rosaman, and K. E. Fletcher, X-ray diffraction examination of portland cement clinker, Proc. Fourth International Symposium on the Chemistry of Cement, NBS Mono. 43 (1962) pp. 69–74.

[11] Method 1101.1, Federal Test Method Standard No. 158a (1960).

[12] Method 2101.1, Federal Test Method Standard No. 158a (1960).

(Paper 68A5–293

JOURNAL OF RESEARCH of the National Bureau of Standards—A. Physics and Chemistry
Vol. 68A, No. 5, September-October 1964

Infrared Spectra of the Crystalline Inorganic Borates

C. E. Weir and R. A. Schroeder

(April 8, 1964)

Infrared absorption spectra of anhydrous, crystalline, inorganic borates were obtained in the 2000 cm^{-1} to 300 cm^{-1} range. Compounds with B^{10} and B^{11} isotopes were prepared to assist interpretation. Spectral bands for all orthoborates and pyroborates and some metaborates could be assigned satisfactorily. Borates with complex ring-type anions generally exhibited spectra of such complexity that only superficial interpretation was attempted. From correlations between spectra and structure it appears that boron in 3-fold or in 4-fold coordination can be identified with reasonable assurance on the basis of the infrared spectrum alone. Absorption bands are tabulated for about 80 borates and typical spectra are shown.

1. Introduction

The chemistry of systems containing boron oxide and the structures of glassy and crystalline inorganic borates are of considerable interest in this laboratory. In such work it is evident that the information available from infrared spectroscopy should be of considerable value. Such spectra are easily and rapidly obtained on very small quantities of material and contain direct information on the nature of the borate anion, the coordination of the boron, the strength of the B—O bonds, etc. Although this information is implicit in the absorption spectrum, an explicit derivation of the desired data requires a thorough understanding of the spectrum which is rarely available for any crystalline solid. This work is designed to advance the understanding of the spectra of the crystalline anhydrous borates by recording and correlating the spectrum with the structure of the crystal where this is known. Most structures are unknown so that the data obtained must be interpreted by comparisons, wherever possible, with spectra of crystals whose structure is known.

In addition to the general interest in borates, there is a specific interest here in crystals containing planar trigonal ions. Previous studies on the infrared spectra of carbonates, nitrates, and borates [57] [1] showed many close similarities, but demonstrated a striking difference in the spectra of the borates and the carbonate having the vaterite structure. The reason for the difference was left unresolved. Numerous absorption bands were found in low temperature spectra [48] of single crystals of carbonates and nitrates. These were attributed to combinations of fundamentals and lattice modes. The present survey was considered to be a preliminary requirement to a proposed study of crystals of the borates at low temperatures.

Previous work on the spectra of the borates will not be reviewed in detail here because the majority of such work consists of reports on only one or two materials. Such references will be discussed in connection with specific spectra. The only comprehensive study of the infrared spectra of anhydrous borates appears to be the recent work of Hart and Smallwood [18]. They studied a large number of borates, but the frequency range used did not extend to sufficiently low frequencies to observe all the fundamental vibrations of interest here. Hart and Smallwood concluded that assignment and interpretation of the more complex spectra was rather difficult. They did not examine several borates for which detailed crystal structures have been reported recently.

In this report, data are tabulated for infrared absorption bands of a number of inorganic borates. In many instances isotopic substitution was employed to assist in the interpretation of the spectra. The data are interpreted in terms of the structure of the anion wherever this is possible.

2. Experimental Method

Infrared spectra were obtained with a double-beam dual-grating spectrometer covering the range 2000 cm^{-1} to 200 cm^{-1}. Higher frequencies were not employed because it was known [18] that fundamentals and most strong overtones and combination bands did not fall above 2000 cm^{-1} in the crystalline compounds. Dry air was circulated through the spectrometer to eliminate interference from atmospheric moisture in the 400 cm^{-1} region. Although the range of the spectrometer extended to 200 cm^{-1} a practical limit of 300 cm^{-1} appeared to be imposed by the available energy.

Spectra were obtained under two conditions, first as a suspension in light petroleum oil, and second as a film produced by evaporation of a CCl_4 suspension. Both KBr and CsBr windows were used with a similar window being placed in the reference beam in all experiments. Mull spectra were used principally in the 1100 cm^{-1} to 300 cm^{-1} region while film spectra were found useful in the region above 1000 cm^{-1} where some interference by absorption in the mineral oil occurred. In the case of film spectra it was fre-

[1] Figures in brackets indicate the literature references at the end of this paper.

quently found useful to expand the absorption peaks along the intensity axis, a similar expansion for the suspension was not possible because of the undesirable magnification of weak absorption bands in the oil. In the region where the two spectra overlapped the positions of absorption bands frequently showed discrepancies of at most 2 cm^{-1}. Under these circumstances the mull spectra were assumed to be correct and a linear correction applied to the absorption bands of the film spectra. The correction is probably not linear if it arises from solubility effects in the alkali halide. However, the corrections are quite small and are not expected to affect the tabulated data appreciably.

3. Preparation of Borates

Borates were prepared using orthoboric acid and the metal carbonate or the metal oxide if the carbonate was unavailable. To reduce the loss of boric acid on ignition most reactions were initiated in aqueous suspensions. The residue on evaporation was subjected to several cycles of heating and grinding until reaction was judged to be complete. For most materials the maximum temperature employed was below the solidus temperature reported in the corresponding phase diagram. However, in the preparation of the alkali borates which crystallized as hydrates from solution, those specimens which melted congruently were melted prior to use. The resulting glasses were crystallized at temperatures below the melting points. The alkali borates that melted incongruently were dehydrated for 24 hr at temperatures 10–20 deg C below the reported incongruent melting points.

For isotope enrichment studies, specimens were prepared using $H_3B^{11}O_3$ (98.3% B^{11}) and $H_3B^{10}O_3$ (96.5% B^{10}) which were obtained from the Oak Ridge National Laboratory. Such pairs of specimens were synthesized in a limited number of cases, usually one for each major structure type expected except in the alkaline earth borates where more were prepared.

Powder x-ray diffraction patterns were obtained on all preparations. The diffraction patterns were checked against reported results where these were available. In many instances powder diffraction data were not available but the x-ray data served to check for contamination by metal oxide or related borates. In many instances the purity of the preparation was checked by means of a polarizing microscope.

In describing the composition of the borates prepared, the following system will be used here and to some extent throughout the paper: The molar ratios will be given with the metal oxide first and the borate as B_2O_3 last. Thus a 4:1 compound will contain 4 moles of metal oxide and 1 mole of boric oxide. Using this convention the following borates were prepared:

1. Lithium borates 1:1, 1:2, 1:3, 1:4, and 1:5 were prepared using the data of Mazzetti and Carli [38] as modified by Sastry and Hummel [46]. The recent data of Rollet and Bouaziz [45] which show additional 3:1 and 3:2 compounds could not be verified.

2. Sodium borates 2:1, 1:1, 1:2, 1:3, and 1:4 were synthesized in accordance with the phase diagram given by Morey and Merwin [40]. It should be noted that these authors report a 2:1 compound although it is not shown on the phase diagram.

3. Potassium borates 1:1, 1:2, 1:3, 1:4, and 1:5 were prepared using the data of Rollet [44].

4. Calcium borates 3:1, 2:1, 1:1, and 1:2 were prepared in accordance with the diagram given by Carlson [9].

5. Strontium borates 3:1, 2:1, 1:1, and 1:2 were prepared. A phase diagram for the system does not appear to be available to date although Hart and Smallwood [18] apparently have phase equilibrium data. The 1:4 compound corresponding to a known barium borate does not appear to exist.

6. Barium borates 3:1, 1:1, 1:2, and 1:4 were prepared in accordance with the results of Levin and McMurdie [34].

7. Magnesium borates 3:1, 2:1, and 1:1 were prepared using the diagram reported by Davis and Knight [10].

It should be noted that there is some confusion concerning the 1:1 compound which, according to Davis and Knight, decomposes at temperatures above 988 °C into B_2O_3 and the 2:1 compound. The powder diffraction pattern in the ASTM file is incorrectly labeled, a point which has been discussed in detail by Block, Burley, Perloff, and Mason [6]. A 1:1 mixture heated at 900 °C forms a product which yields a very complex powder diffraction pattern. It cannot be safely concluded that this pattern is free from the 2:1 borate. However, microscopic examination showed that the 1:1 compound prepared in this manner was a single phase differing from the 2:1 compound.

8. Cadmium borates 3:1, 2:1, and 1:2 were prepared. The phase diagram given by Subbarao and Hummel [53] reported 3:2 and 2:3 compounds but no 1:2 compound. The existence of the 3:2 compound was questioned by Hart and Smallwood [18] on the basis of x-ray and infrared data and later by Hand and Krogh-Moe [16]. Results here confirm the absence of the 3:2 compound. Hand and Krogh-Moe [16] have shown that the 2:3 compound is in fact a 1:2 compound.

9. Zinc borates 5:2, 4:3, and 1:2 were prepared. The original work of Ingerson, Morey, and Tuttle on the $ZnO—B_2O_3$ system [22] reported the existence of 5:2 and 1:1 compounds. Harrison and Hummel [17] later confirmed these findings and reported polymorphic forms of both compounds. However, Smith, Garcia-Blanco, and Rivoir [50, 51] showed from single crystal diffraction studies that the 1:1 compound of empirical formula $Zn(BO_2)_2$ had the structural formula $Zn_4O(BO_2)_6$ and was therefore a 4:3 compound. Recently Bauer [2], who appeared to be unaware of the previous reports of Smith et al. [50, 51], concluded that the compounds existing in the system were 3:1 (rather than 5:2), 1:1, and 1:2.

Data obtained here by x-ray diffraction and infrared absorption confirm the existence of the 1:2 compound reported by Bauer [2] but are in agreement with the 5:2 ratio rather than the 3:1 value.

10. Lead borates 2:1, 5:4, 1:1, and 1:2 were prepared. The data of Geller and Bunting [13] did not show a 1:1 lead borate but on the basis of x-ray data here it appears probable that this compound exists.

11. Rare earth borates having the ratios 3:1, 1:1, and 1:3 were prepared. Levin, Roth, and Martin [31] have reported on the 1:1 compounds and the 3:1, 1:1, and 1:3 compounds in the La_2O_3—B_2O_3 system were described by Levin, Robbins, and Waring [33]. Further work on the system by Levin and McDaniel [35] shows the existence of some compounds having nominal ratios of 3:1 and 1:3 for many of the other rare earths. Although the exact compositions and properties are not established to date, the materials were prepared for study.

12. Bismuth borates 2:1, 3:5, 1:3, and 1:4 were formed in accordance with the phase diagram of Levin and McDaniel [32].

13. Cobalt borates 3:1 and 2:1 were prepared using the findings of Konovalov [23].

14. Miscellaneous borates were prepared as follows:

a. beryllium borate, presumably of composition 3:1 [56].

b. indium borate, 1:1 [31].

c. nickel borate 3:1. This product was formed using NiO. Attempts to prepare the 2:1 nickel borate analogous to the cobalt compound met with no success. The failure to form other compounds might be attributed to the high temperature required to induce reactivity in NiO. The use of $NiCO_3$ might facilitate formation of other borates.

d. rubidium borate 1:5 [27].

e. cesium borates 1:3 and 1:9 [26].

f. two copper borates which appear in the system CuO–B_2O_3. One compound is apparently a 3:1 compound, forming large green crystals. The crystals are highly birefringent, biaxial, negative with $2V \approx 15°$, $\alpha = 1.78$, $\beta > 2.00$, $\gamma > 2.00$. The other compound is probably a 1:1 compound and is azure blue. The properties of these crystals have not been determined with certainty. They may be uniaxial negative or biaxial negative.

g. $TaBO_4$ reported by Zaslavskii and Zvinchuk [61] was prepared with some difficulty. The samples prepared here were not suitable for use because of impurities. The material actually used was supplied by Mrose [41] who has studied this compound in detail.

h. The two isostructural compounds BPO_4 and $BAsO_4$, were prepared according to the data of Schulze [49]. Attempts to prepare the antimony analog, $BSbO_4$ were not successful.

14. Several borates previously reported could not be prepared, in particular, ferrous and manganous borates [6]. Oxidation proceeding in the normal preparation techniques was probably responsible for the failure to obtain these borates.

4. Anion Structure and Vibrational Analysis

4.1. Structures

The fact that a number of borates are formed with the same cation is due to the polymeric behavior of the borate ion. Complex anions can arise from polymerization of basic triangular BO_3 or tetrahedral BO_4 units alone or in combination. The anion structures known to exist have been reported as follows:

The isolated planar anion BO_3^{-3} is found in $LuBO_3$, $InBO_3$, and $ScBO_3$ which have the calcite structure [31, 52], in $LaBO_3$ with the aragonite structure [31], and in $3MgO \cdot B_2O_3$ [5]. The borates isostructural with $3MgO \cdot B_2O_3$—$3CoO \cdot B_2O_3$, $3NiO \cdot B_2O_3$, and $3CdO \cdot B_2O_3$—must also have this anion [42].

The tetrahedral anion BO_4^{-5} has been reported in $TaBO_4$ [6] and in BPO_4 and $BAsO_4$ [49].

The pyroborate ion $B_2O_5^{-2}$ is formed by connecting two triangular BO_3 groups at one corner. This ion occurs in $2MgO \cdot B_2O_3$ [54] and in $2CoO \cdot B_2O_3$, $2MnO \cdot B_2O_3$, $2FeO \cdot B_2O_3$, and $2CdO \cdot B_2O_3$ [6, 16] which are isostructural.

An infinite chain of BO_3 triangles connected at one corner was shown to be present in $CaO \cdot B_2O_3$ by Zachariasen [36, 58, 59] and in α-$Li_2O \cdot B_2O_3$ [21].

The boroxol ring, a six-membered ring formed by $3BO_3$ groups, contains alternate boron and oxygen atoms and 3 oxygen atoms out of the ring, each connected to one of the boron atoms. This unit occurs in $K_2O \cdot B_2O_3$ [60] and $Na_2O \cdot B_2O_3$ [12, 37]. The rings are interconnected by means of the external oxygen atoms.

Two six-membered rings similar to the boroxol ring are coupled by means of a tetrahedral boron atom common to both rings to form the B_5O_8 anion. This ion is found in $K_2O \cdot 5B_2O_3$ and $Rb_2O \cdot 5B_2O_3$ [27]. Individual B_5O_8 units are interconnected by the external oxygen atoms.

A six-membered ring containing 2 triangular and 1 tetrahedral boron is known in $Cs_2O \cdot 3B_2O_3$. This unit is connected to similar units through the off-ring oxygen atoms [29].

The basic structural unit in $Li_2O \cdot 2B_2O_3$ is a $B_4O_7^{-2}$ group consisting of $2BO_4$ tetrahedra and $2BO_3$ triangles. The anion is an 8-membered ring in which the opposite tetrahedral BO_4 groups provide an oxygen bridge. Similar units are interconnected to form a 3 dimensional network [28].

The structure of $BaO \cdot 2B_2O_3$ has been reported to consist of a network containing rings similar to those found in $Cs_2O \cdot 3B_2O_3$ and $K_2O \cdot 5B_2O_3$. The two sets of rings are connected by means of the off-ring oxygen atoms and form a 3 dimensional network [7].

Lehmann and Teiss [30] have observed two additional forms of $Li_2O \cdot B_2O_3$ one of which denoted as the β form has a structure similar to that of cristobalite, the other denoted as the γ form appears to be similar to the cubic form of HBO_2.

Finally, the compound $4ZnO \cdot 3B_2O_3$ contains only tetrahedral boron atoms. The tetrahedra are coupled at certain corners to form a complex 3 dimensional array [50, 51].

The compounds $TaBO_4$ [61] and BPO_4 and $BAsO_4$ [49] also contain only tetrahedral boron atoms. In the latter two compounds the borate tetrahedra share corners with PO_4 and AsO_4 tetrahedra, respectively, so that each oxygen atom is part of two different tetrahedra. The empirical formulas of these two compounds could be written BO_2PO_2 and BO_2AsO_2. $TaBO_4$ is isostructural with zircon [61] and contains discrete BO_4 tetrahedra.

4.2. Vibrational Analysis

Both the planar triangle and the tetrahedral unit have been discussed in detail many times and only the results will be indicated here [19]. For an isolated, planar, trigonal BO_3 group of D_{3h} symmetry there are four fundamental modes of vibration; ν_1—the symmetrical stretch, ν_2—the out-of-plane bend, ν_3—the antisymmetric stretch, and ν_4—the in-plane bend. Both ν_3 and ν_4 are doubly degenerate and ν_1 is ordinarily inactive in the infrared. In a given crystalline environment ν_1 may become active and the degeneracies may be removed from ν_3 and ν_4. The nominal positions expected are ν_1—950 cm^{-1}, ν_2—750 cm^{-1}, ν_3—1250 cm^{-1}, and ν_4—600 cm^{-1} [57] with the exact positions varying somewhat with the crystal field. An isolated tetrahedral anion of symmetry T_d should also exhibit 4 fundamentals, a normally inactive symmetric stretch-ν_1, an inactive doubly degenerate mode-ν_2 which involves bond bending, a strongly active triply degenerate stretching mode-ν_3, and another active bending mode-ν_4 which is also triply degenerate. In a given crystal ν_1 and ν_2 may become active and the degeneracies may be removed from ν_2, ν_3, and ν_4. The expected locations of the bands can be inferred from data obtained on similar tetrahedral anions [19]. It is anticipated that ν_3 should occur near 1000 cm^{-1}, ν_1 below 950 cm^{-1}, ν_4 near 600 cm^{-1} and ν_2 below 600 cm^{-1}.

From isotope substitution in the trigonal ion it is expected that ν_1 will be unchanged, $\nu_2^{B^{10}}/\nu_2^{B^{11}} \approx 1.04$ and $\nu_3^{B^{10}}\nu_4^{B^{10}}/\nu_3^{B^{11}}\nu_4^{B^{11}} \approx 1.04$. For the tetrahedral anion ν_1 and ν_2 will be unchanged and $\nu_3^{B^{10}}\nu_4^{B^{10}}/\nu_3^{B^{11}}\nu_4^{B^{11}} \approx 1.04$. In the more complex anions it is possible that vibrations derived from those for the simple triangular or tetrahedral units might be detected. These vibrations would be shifted in frequency by the covalent bonding of the simple units into the complex anion structure but the isotopic frequency shift should serve to give some indication of the nature of the vibrations. As will be shown later, this type of identification which has been referred to as group frequency analysis in connection with spectra of organic materials, may have some justification.

In the pyroborate ion all B—O bonds are not equivalent, as shown by Block et al. [6] in $2MgO{\cdot}B_2O_3$, and there is no symmetry. The ion is therefore in point group C_1, all vibrations are of species A and all are infrared active. There are 15 normal modes of vibration and some idea of the nature of these modes may be obtained as follows:

Twelve normal modes would be expected from internal vibrations of the two coupled triangular units. There should be two each derived from the ν_1 and ν_2 type vibrations and 4 each from the ν_3 and ν_4 types. The extra 3 modes will be derived from the motions of one trigonal unit with respect to the other and arise essentially from the loss of the 3 translational modes of one unit. These latter three modes are expected to be of rather low frequency because of the large masses involved and might lie oustide the range of the present studies. The two modes derived from ν_1 and ν_2 can be visualized as in phase and out of phase motions in the coupled triangular units. Those derived from the originally degenerate ν_3 and ν_4 vibrations are somewhat difficult to visualize. However, the effect of isotopic substitution is expected to parallel the behavior of the isolated trigonal ion. Thus modes derived from ν_1 and ν_4 will be relatively unaffected, while those derived from ν_2 and ν_3 will be affected markedly. The three low frequency twisting or rocking modes should also be insensitive to isotopic substitution because of the relatively large masses involved.

The boroxol ring has been studied extensively by Goubeau and his coworkers [14, 15] who have proposed frequency assignments. The B_3O_6 ring is of point group symmetry D_{3h} and of the 21 total normal modes only a few are expected to be normally active in the isolated ring. The active modes are 2 of species A_2'' and 5 of species E'. In metaboric acid Goubeau and Hummel have assigned these bands as follows: species A_2''; ν_6—591 cm^{-1} ν_7—476 cm^{-1}; and species E'; ν_8—1375 cm^{-1}, ν_9—1150 cm^{-1}, ν_{10}—735 cm^{-1}, ν_{11}—456 cm^{-1}, ν_{12}—280 cm^{-1}. From these assignments it appears that not more than 6 fundamentals should be observed for this unit in these experiments, with, ν_{12} below the range studied here.

The other known metaborate structure consists of infinite chains of trigonal borate groups connected through two oxygen atoms. There is no symmetry and all vibrations will be infrared active in species A. The unit cell contains two chains, each of empirical formula $(BO_2)_4$. The spectrum, therefore, should resemble that of the pyroborate group, as the structural units consist of two coupled pyroborate groups. More bands can be expected because of the larger number of normal modes but the frequencies and isotope dependence should resemble similar data on the pyroborates.

The complex ring systems reported in $K_2O{\cdot}5B_2O_3$, $Cs_2O{\cdot}3B_2O_3$, $Li_2O{\cdot}2B_2O_3$, and $BaO{\cdot}2B_2O_3$ have no symmetry elements. Therefore, all modes are active and a very complex spectrum is to be expected. No detailed interpretation of these spectra are to be expected unless group frequency analysis should prove useful.

The zinc metaborate structure is very complex and complete analysis is not anticipated. From the x-ray structure analysis [50, 51], in a given tetrahedron one oxygen is connected to a zinc atom while the other 3 atoms are shared by 3 different tetrahedra. Although the structural analysis indicates all B—O

bonds to be similar, this appears to be most unlikely and it seems more reasonable to consider the oxygen coupled to the zinc to be unique. Under these circumstances it is useful to consider the symmetry of the tetrahedral unit to approximate C_{3v} rather than T_d. In this approximation the basic unit can be visualized as containing a central atom bonded to two different kinds of atoms, one the oxygen bound to zinc, and the other, the three oxygens connected into the network. The latter three atoms can be visualized as having large effective masses conferred by the coupling into the other tetrahedra. On the basis of these assumptions the spectrum would be expected to bear some resemblance to that of an XYZ_3 type molecule with allowances for network perturbation effects. As will be shown later this viewpoint permits a reasonable interpretation of the observed data.

5. Presentation of Data

The following system is adopted for presenting the data:

Observed absorption bands are tabulated for each material studied with the following abbreviations used to denote the character of the bands; s—strong, m—medium, w—weak, b—broad, sh—shoulder, v—very. It is understood that the bands may vary in character with the method of obtaining the spectrum, concentration, etc., so that the descriptions apply only to the bands observed here. The existence of the bands listed is considered to be well established because all spectra were obtained at least in duplicate by two different methods. Doubtful bands are indicated with a question mark.

Representative spectra are given for some but not all materials studied with frequencies in wave numbers indicated for the various bands. Two or more spectra are given in each figure with the spectra displaced vertically to eliminate overlapping. The transmittance axis, therefore, cannot be subdivided quantitatively but all spectra are referred to the same intensity scale and are directly comparable. Spectra shown are in most instances composite tracings of mull spectra below 1000 cm^{-1} and film spectra above 1000 cm^{-1}. In some instances film spectra are shown throughout the range used.

Borates are classified with respect to type of anion with all borates of a given type discussed together. Such a separation is desirable because spectra of compounds containing similar anions are expected to be comparable. Although the major separation is in terms of the empirical formula of the anion, subdivision in terms of actual structure is made where the structure is known.

6. Results and Discussion

6.1. Orthoborates

Orthoborates, $X_m(BO_3)_n$, are formed by the 3:1 divalent metal borates and the 1:1 trivalent metal borates. From the point of view of infrared spectroscopy these compounds may be interpreted, in many instances, in terms of the simple planar trigonal BO_3^{-3} ion.

a. Divalent Metal Orthoborates

The spectra of all of the divalent metal orthoborates with the exception of $3BeO \cdot B_2O_3$ can be interpreted in terms of the six fundamentals of the perturbed BO_3^{-3} ion. Typical spectra are shown in figures 1 and 2 and the observed bands and assignments are tabulated for the normal isotopic distribution in table 1. The assignments for the bands are supported by the isotopic shifts given in table 2 for some of the compounds. In figure 1 a definite split in the ν_3 band is noted for the B^{11} and B^{10} compounds. The split is not observed in the normal strontium borate although structure in the ν_3 band is apparent. All isotopically "pure" compounds showed such a split which produced two highly unsymmetrical ν_3 bands. The unsymmetrical nature of the bands caused some concern that the apparent splitting might be an artifact caused by variation of index of refraction of the specimen with frequency. Several different experiments were performed using different dispersing media without changing the position or shape of the splitting peak. The split of ν_3 is concluded to be real. Several weak bands in the 750 cm^{-1} — 1000 cm^{-1} region are of uncertain origin. Several of these bands observed in the normal strontium borate are eliminated in the B^{10} and B^{11} compounds so that they may arise from coupling of vibrations between trigonal ions containing different boron isotopes. Such effects have been discussed by Decius [11]. In addition it is not clear from the spectrum or the experiments on isotope substitution which band corresponds to ν_1. From comparisons with the carbonates and nitrates and from other data to be given later it is concluded that the weak band near 1000 cm^{-1} in these spectra corresponds to ν_1. The bands near 900 cm^{-1} are taken to represent combinations of lower frequency modes with ν_4 or ν_2 or overtones of a lower frequency mode. The alternate hypothesis that two dissimilar BO_3^{-3} groups are present in the unit cell and give rise to two different symmetric stretching modes is untenable in these compounds. The structure of $3MgO \cdot B_2O_3$ and $3CoO \cdot B_2O_3$ by Burger [35] shows that all BO_3^{-3} groups are equivalent. However, the B—O bonds are not identical and there is no trigonal symmetry. All modes should be active and nondegenerate as shown by the spectra of the isostructural magnesium, cobalt, nickel, and cadmium compounds.

In table 1 the data for $3BaO \cdot B_2O_3$ are incomplete. $BaCO_3$ contamination produced such strong interferences that the borate bands could not be located with certainty. The known carbonate bands [57] are not listed in table 1. The table lists only limits of the broad, strong ν_3 band. From figure 1 it is clear that the breadth of this band arises in part from overlapping of bands arising from the two boron isotopes. An additional source of strength is probably due to resonance with overtones of ν_4 which fall in this region.

The compounds $3MgO \cdot B_2O_3$, $3NiO \cdot B_2O_3$, $3CoO \cdot B_2O_3$, and $3CdO \cdot B_2O_3$ are isostructural with ortho-

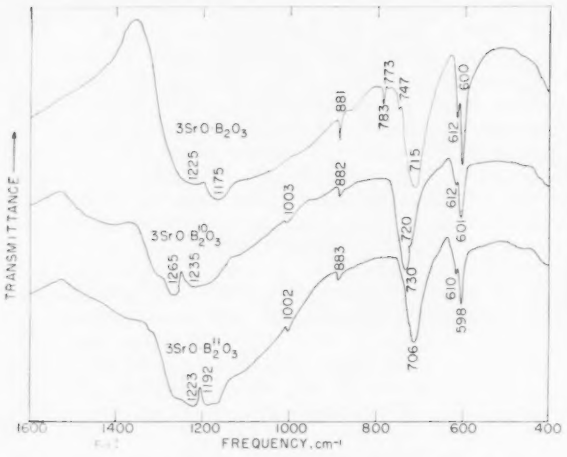

FIGURE 1. *Absorption spectra of strontium orthoborates.*

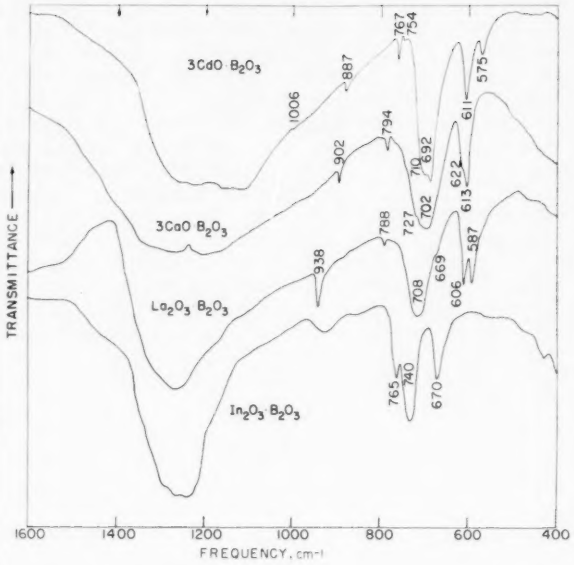

IGURE 2. *Absorption spectra for different crystal structures in the orthoborates.*

TABLE 1. *Infrared absorption spectra of divalent metal orthoborates*

(cm^{-1})

Radius of cation, Å	$3MgOB_2O_3$ 0.67	$3NiOB_2O_3$ 0.69	$3CoOB_2O_3$ 0.73	$3CdOB_2O_3$ 0.97	$3CaOB_2O_3$ 0.99	$3SrOB_2O_3$ 1.12	$3BaOB_2O_3$[1] 1.34	$3BeOB_2O_3$
ν_3	1090–1290	1080–1260	1020–1250	1100–1290	1140–1310	1090–1260	1140–1260	1240–1340
ν_1	1022w			1006vw				928m
–	907w	893w	893w	887w	902w	881w	908w	861s
–	836vw							837w
–	808w				794w	783w	808w	818wsh
								806m
								781m
								767s
		773w	773w	767w		773vw		740m
				754vw	752w	747w		727m
			719					708m
		709	700	710	727sh			700s
ν_2	719sb	691vs	676vs	692vs	702vs	715vs		672s
								667msh
								657m
								649m
ν_4	657m[2]	619s[2]	617s[2]	611m[2]	622m	612m		643m
								619w
ν_4'	606w	598m	587m	575w	613m[2]	600s[2]		600wb
								548wb
								420w
	500sb	400sb	400sb	350sb	420sb	350sb		400w

[1] All specimens of $3BaOB_2O_3$ were contaminated with $BaCO_3$. The known absorption bands for $BaCO_3$ are not tabulated here.
[2] The stronger of the two bands is denoted by the superscript.

TABLE 2. *Infrared absorption spectra of isotopically enriched divalent metal orthoborates*

(cm^{-1})

Assignment	$3MgOB_2O_3$		$3CaOB_2O_3$		$3SrOB_2O_3$		$3BaOB_2O_3$		$3CdOB_2O_3$	
	B^{10}	B^{11}	B^{10}	B^{11}	B^{10}	B^{11}	B^{10}	B^{11}	B^{10}	B^{11}
ν_3	1332	1264	1303	1261	1265	1223	1262	1222	1250	1210
ν_3'	1290	1224	1266	1227	1235	1192	1223	1185	1190	1160
ν_1	1025	1021	1014	1013	1003	1002				
					882?	883?				
ν_2	733	720	730	708	729	706	778	749	726	702
							792	761		
ν_4	659	655	624	619	612	610	602	599	608	606
ν_4'	608	604	617	612	601	598	568	567	574	572

rhomic cells having the parameters shown in table 3 [42]. From tables 3 and 1 it will be noted that as the unit cell dimensions decrease, the absorption frequencies generally shift to higher frequencies. This behavior parallels that found previously in isostructural carbonates and nitrates where it was attributed to the effect of anion repulsion in the closer packed structures [57]. For these compounds the behavior of the two components of ν_4 is of interest. It will be noted from table 1 that the higher frequency component of ν_4 is stronger in contrast to $3SrO \cdot B_2O$ and $3CaO \cdot B_2O$ (figs 1 and 2) in which the lower frequency component of ν_4 is stronger. The amount of splitting between the components of ν_4 appears to be least in the nickel compound and increases as the unit cell gets larger.

TABLE 3. *Unit cell parameters of isostructural orthorhombic orthoborates*

	a	b	c
	10^{-8}cm	*10^{-8}cm*	*10^{-8}cm*
$3MgOB_2O_3$	5.398	8.416	4.497
$3NiOB_2O_3$	5.398	8.305	4.462
$3CoOB_2O_3$	5.642	8.436	4.526
$3CdOB_2O_3$	5.967	9.010	4.785

In view of the reversal of intensities in the strontium, calcium, and barium orthoborates it is to be expected that the two groups of compounds are not isostructural. X-ray diffraction shows this to be true and indicates that $3SrO \cdot B_2O_3$, $3CaO \cdot B_2O_3$, and $3BaO \cdot B_2O_3$ might also form an isostructural group. However, even though the details of the structure are unknown, it can be concluded from the infrared spectra that all these compounds contain isolated planar BO_3^{-3} ions. In order for the splitting of ν_3 and ν_4 to occur, the ions must either be nontrigonal or be located in a crystal field of low symmetry.

The assignments given here differ considerably from those of Hart and Smallwood [18] who considered the weak sharp bands near 900 cm^{-1} to correspond to ν_2 and the strong band near 700 cm^{-1} to be ν_4. In view of the effects of isotopic substitution observed here, these assignments cannot be correct. The error appears to be due to the fact that ν_4 is located outside the spectral range available to Hart and Smallwood [18]. In view of these discrepancies the force constants were recalculated assuming valence forces [19] and the results are tabulated in table 4. The constants shown were calculated using the data of table 2 for compounds containing the B^{11} isotope. The splitting of ν_3 and ν_4 requires at least 2 values for the planar bending constant, K_δ/l^2, and in this calculation the higher frequency values of ν_3 and ν_4 were considered to represent a corresponding set and the lower frequency values the second set. The value of ν_1 for $3CdO \cdot B_2O_3$ was taken from table 1 and the value for $3BaO \cdot B_2O_3$ which was not observed was assumed to be equal to the value observed in $3SrO \cdot B_2O_3$. As this assumption may be incorrect, data depending on the value are enclosed in parentheses in table 4. The values for the force constants differ from these given by Hart and Smallwood [18] and are in reasonable good agreement with previous calculations based on the calcite and aragonite forms of the rare earth borates [57].

TABLE 4. *Force constants of orthoborate ions assuming valence forces*

	K_1	$K\lambda/l^2$	$K\delta/l^2$
	10^5 dyne/cm	*10^5 dyne/cm*	*10^5 dyne/cm*
$3MgOB_2O_3$	9.82	0.92	0.39 0.31
$3CaOB_2O_3$	9.67	0.89	0.35 0.32
$3SrOB_2O_3$	9.42	0.91	0.33 0.30
$3BaOB_2O_3$	(9.4)	1.0	(0.31) (0.26)
$3CdOB_2O_3$	9.54	0.87	0.31 0.26

The spectrum of $3BeO \cdot B_2O_3$ appears to be different from the spectra of the other divalent orthoborates, showing a large number of bands in the 600 cm^{-1} to 850 cm^{-1} range. The differences, however, may be more apparent than real because the spectrum is probably complicated by bands arising from Be-O vibrational modes. BeO itself exhibits broad absorption bands near 960 cm^{-1}, 880 cm^{-1}, and 750 cm^{-1} and the bands in beryllium borate appear to be superimposed on these bands which may arise from excess BeO or from Be-O vibrational modes in the borate itself.

b. Trivalent Metal Orthoborates

This series of orthoborates is of particular interest because of the formation of calcite-, aragonite-, and vaterite-type structures in the borates [31]. Earlier infrared studies demonstrated the similarity of the absorption spectra of the calcite and aragonite type structures [57] but showed no correlation in the spectra of the carbonate and borate vaterites. Later Levin, Roth, and Martin [31] found that the borate-type vaterites all exhibit a transition at elevated temperatures forming a nonquenchable high-temperature phase whose x-ray powder diffraction pattern is more nearly like that of the carbonate vaterite than the diffraction pattern of the room temperature phase. Although it is not possible, at present, to obtain the absorption spectrum of the high temperature phase, it seems probable that it will resemble the spectrum of the carbonate vaterite which can be interpreted on the basis of trigonal CO_3^{-2} ions. The previous data on the borate vaterites could not be interpreted readily in this manner and the problem was unresolved. Isotopic substitution data and comparison with the spectra of other borates permits some conclusions to be drawn at this time.

Considering first the results for calcite and aragonite-type structures, absorption data are compiled in table 5 for $Sc_2O_3 \cdot B_2O_3$ and $In_2O_3 \cdot B_2O_3$ which form calcite-type structures and for $La_2O_3 \cdot B_2O_3$ which forms the aragonite type structure. The spectra of

scandium and indium borates show the spectra associated with the calcite-type structure with ν_1 inactive and ν_4 degenerate and unsplit. Isotopic shifts found with the indium borate confirm the assignments. In the spectra shown in figure 2 the 765 cm^{-1} band observed in $In_2O_3 \cdot B_2O_3$ with a normal isotope distribution can be identified with the ν_2 band of the B^{10} compound by means of the data of table 5. The three bands below 600 cm^{-1} listed in table 5 did not appear in all preparations and were found to be present in In_2O_3. They presumably arise from excess In_2O_3.

TABLE 5. *Infrared absorption spectra of calcite and aragonite type borates*

(cm^{-1})

	$Sc_2O_3B_2O_3$ (calcite)	$In_2O_3B_2O_3$ (calcite)		$La_2O_3B_2O_3$ (aragonite)	
		B^{10}	B^{11}	B^{10}	B^{11}
ν_3	1198svb	1230svb	1202svb	1350sbsh 1289svb	1310sbsh 1244svb
ν_1				938m	938m
ν_2	722sb	765sb	740sb	733sb	708sb
				717msh	669wsh
ν_4	636m	672s	670s	610m	606m
				591m	587m
		596m 560m 533m	596m 561m 533m	In_2O_3	

The assignments and isotopic shifts in $La_2O \cdot B_2O_3$ confirm the behavior expected for the aragonite type structure. The symmetric stretch, ν_1, is active and unaffected by the boron isotope, ν_4, is split and affected slightly by the boron mass, and ν_3 is apparently split and strongly dependent on boron mass. Strong bands at 1350 cm^{-1} and 1310 cm^{-1} were taken to represent the high frequency components of ν_3 for the B^{10} and B^{11} compounds. Alternate assignments as combinations of ν_2 and ν_4 will not satisfy the isotopic dependence observed. In $La_2O_3 \cdot B_2O_3$ with the normal isotopic distribution a band is observed near 790 cm^{-1} (see fig. 2). This band is not found in the isotopically pure compounds and probably arises from coupling effects as noted by Decius [11]. This band was previously found in both neodymium and lanthanum borate and considered to be part of ν_2. The absence of the band in the isotopically "pure" compounds shows this is not correct. The results obtained here agree well with previous data reported by Steele and Decius [52].

In figure 2 the infrared spectra of the four different crystal structures are compared. The close similarities in the spectra are evident. It will be noted that the behavior of ν_4 in the different structures serves as a distinguishing feature. This band is split in $3CdO \cdot B_2O_3$ with the higher frequency the stronger, it is split in $3CaO \cdot B_2O_3$ with the separation small and the lower frequency the stronger, it is split in $La_2O_3 \cdot B_2O_3$ with both components of about equal intensity but separated about 30 cm^{-1}, and it is unsplit in $In_2O_3 \cdot B_2O_3$. In the first three compounds the position of ν_4 is about the same but in the $In_2O_3 \cdot B_2O_3$ it has shifted to much higher frequency, an indication of much tighter packing.

Absorption spectra of the rare earth borates having the vaterite type structure were studied only for the holmium, erbium, thulium, ytterbium, and lutecium compounds. Spectra for the holmium, thulium, and ytterbium borates were obtained with the normal isotopic distribution, for lutecium borate in the isotopically enriched compounds only, and for erbium borate in both the normal and enriched forms. Typical spectra are shown in figure 3 for the normal isotopic distribution and in figure 4 for the isotopically "pure" borates of erbium and lutecium. The observed bands are tabulated in table 6.

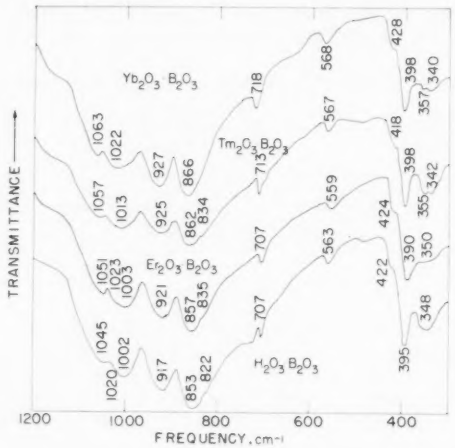

FIGURE 3. *Absorption spectra of rare earth vaterite-type borates.*

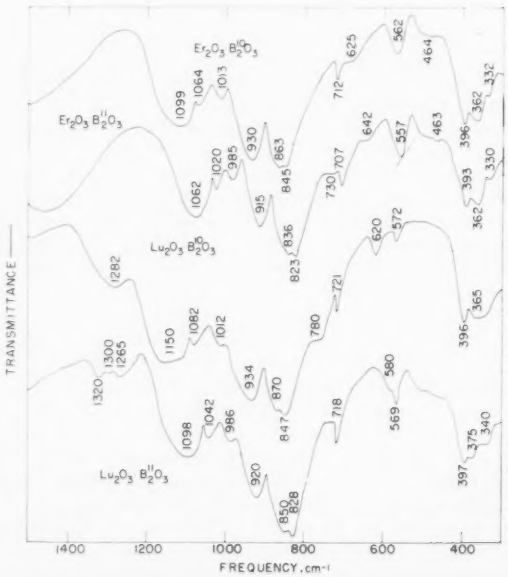

FIGURE 4. *Isotope effects in rare earth vaterite-type borates*

TABLE 6. *Infrared absorption spectra of vaterite type rare earth borates*

(cm^{-1})

$Ho_2O_3B_2O_3$	$Er_2O_3B_2O_3$			$Tm_2O_3B_2O_3$	$Yb_2O_3B_2O_3$	$Lu_2O_3B_2O_3$	
	$B^{10}+B^{11}$	B^{10}	B^{11}			B^{10}	B^{11}
		1099sb	1062sb			1282mvb 1150?mb	1320–1265wb 1098svb
1045sbsh	1051bsh	1064m	1020m	1057bsh	1063bsh	1082mb	1042mb
1020sbsh	1023sbsh						
1002svb	1003svb	1013m	985m	1013svb	1022svb	1012mb	986mb
917sb	921vsb	930sb	915sb	925vsb	927sb	934sb	920sb
853vsb	857vsb	863sb	836sb	862vsb	866vsb	870vsb	850vsb
822bsh		845s	823s 730vw?	834bsh		847vsb 780msh	828vsb
707m	707m	712m 625bsh	707m 642bsh	713m	718m	721m 620mb	718m 580msh
563mb	559mb	562mb 464bsh	557mb 463wsh	567mb	568mb	572mb	569mb
424wsh	424wsh			418wsh	428wsh		
395s	390s	396s	393s	398s	398s	396s	397s 375sb
348sb	350sb	362sb 332msh	362sb 330msh	355w 342w	357w 340wb	365sb	340mb

In figure 3 it will be noted that the four strong bands between 800cm^{-1} and 1100 cm^{-1} confirm the previous observations where only three of these bands could be detected with assurance in all the borates [57]. When isotope substitution is employed it is clear that at least six bands can be resolved in this region. In figure 4 it will be noted that almost without exception each band shifts to higher frequency as the cation mass increases from 167 in Er to 175 in Lu. The same tendency is apparent in figure 3 where the bands are not as well resolved. This shift has been attributed to increased anion repulsion produced by contraction of the unit cell dimensions. The bands between 800 cm^{-1} and 1100 cm^{-1} show marked shifts with change in mass of the boron. It is most likely that these bands are fundamentals for the following reasons: first, they are all quite strong, second, the dependence on mass is much greater than to be expected for overtones of low frequency modes, and third, there do not appear to be any reasonably constant differences between these bands. It may be concluded therefore that most of the six strong bands are fundamentals and correspond to a stretching type vibration. The weak bands in the 1300 cm^{-1} region may be combination modes or arise from contamination with the 3:1 borates whose spectra will be described later.

To interpret these spectra it is necessary to apply certain results which will be demonstrated later. First, every borate which is known to contain trigonal borate groups alone or in complex polymeric anions invariably exhibits strong absorption in the region of 1200 cm^{-1} or higher. The isotopic mass dependence of these bands shows that they may be considered to be derived from or due to the antisymmetric stretch of planar BO_3 groups. Second, there is always at least one band attributable to the out-of-plane bending mode of the trigonal group occurring in the 650 cm^{-1} to 750 cm^{-1} region which can be identified by its strong isotopic shift. The bands in the 700 cm^{-1} region for $Lu_2O_3 \cdot B_2O_3$ and $Er_2O_3 \cdot B_2O_3$ do not exhibit an isotopic shift sufficiently large for the trigonal ν_2 band. Third the spectrum of zinc borate which is known to contain only tetrahedrally coordinated boron shows strong broad fundamentals in the 900 cm^{-1} to 1100 cm^{-1} region and a band near 717 cm^{-1} with a small isotopic shift. From these considerations it is necessary to conclude that the spectra of the rare earth borates of the vaterite type are consistent with the presence of only four-fold coordinated boron in the structure. The longer B—O bonds in the tetrahedra would account for the shift of the strong stretching bands to frequencies below 1100 cm^{-1}. Furthermore, the number of fundamentals observed and their isotopic dependence cannot be reconciled with the behavior to be expected from isolated tetrahedra. These facts lead to the conclusion that the anion in these borates is a complex polymeric structure containing only BO_4 tetrahedra. It is suggested that a six-membered ring containing alternate B—O bonds with each boron connected to 2 off-ring oxygen atoms is not inconsistent with the empirical formula or the spectrum.

6.2. Metaborates

a. Alkali Metaborates

Of the alkali metaborates only the lithium, sodium, and potassium compounds were studied. The spectra of $Na_2O \cdot B_2O_3$ and $K_2O \cdot B_2O_3$ are very poor and are characterized by few resolvable bands. Typical spectra are shown in figure 5 and the data are given

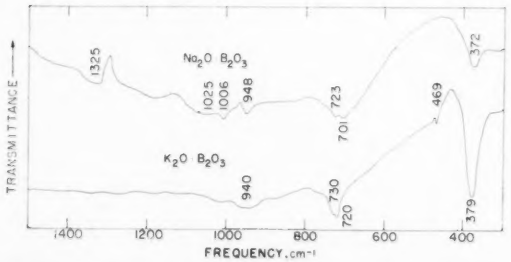

FIGURE 5. *Absorption spectra of alkali metaborates.*

in table 7. As shown in figure 5 few bands can be resolved in the 1000 cm^{-1} to 1400 cm^{-1} either because of overlapping bands or because of strong scattering. The distortion region below 800 cm^{-1}, however, shows several characteristic bands. From comparisons with previously reported spectra on $NaBO_2$ [8, 14, 25] it is clear that the present spectrum agrees reasonably well in the distortion region. The strong bands above 1200 cm^{-1} are not distinguishable in the present spectra, however, Using the terminology and assignments of Goubeau and Hummel [14] the 723 cm^{-1} and 701 cm^{-1} bands correspond to two components of ν_{10} in $NaBO_2$ and the corresponding bands in KBO_2 would be at 730 cm^{-1} and 721 cm^{-1}. The 469 cm^{-1} band observed in KBO_2 but not in $NaBO_2$ probably corresponds to ν_{11} while the 952 cm^{-1} band in $NaBO_2$ and the corresponding 940 cm^{-1} band in KBO_2 represent the 1st overtone of ν_{11}. The small discrepancy noted between calculated and observed values for the overtone is not considered significant in view of the breadth of the bands. The bands at 372 cm^{-1} in $NaBO_2$ and 379 cm^{-1} in KBO_2 are obviously similar but their assignments are not apparent from the data of Goubeau and Hummel [14] except possibly as combinations or overtones of lower frequency modes. Positions of higher frequency bands listed for $NaBO_2$ are so inexact that they have little significance.

TABLE 7. *Infrared absorption spectra of alkali metaborates*

(cm^{-1})

$NaBO_2$	KBO_2			$LiBO_2$		
	B^{10} &B^{11}	B^{10}	B^{11}	B^{10} &B^{11}	B^{10}	B^{11}
1323svb?				1400svb	1482sb	1435s
					1385sb	1345sb
				1157vsb	1358sb	1316sb
					1298wsh	1160sb
1025svb?					1166sb	1123sb
1006?					1073wb	1072wb
948w	940vb?	942m	942m	973m	986sb	967sb
	775sbs			882mb	915sb	895s
741wsh	730ssh	730sb	712sb	810vw	865wsh	877s
				775wsh	778wb	777wb
723s	720s			722sb	722mb	715sb
				685mbsh	715mb	677wsh
701ssh				626mb		620mb
	469w	473w	470w	522sb	545mb	538mb
372m	379m	382s	381s	420mb	510mb	510mb
				406msh	420mb	420mb
					410mb	410mb

As can be seen from table 7 the spectrum of $LiBO_2$ is completely different from those of the other alkali borates. In the 1000 cm^{-1} to 1400 cm^{-1} region there is overlapping and loss of resolution in the compound with the normal isotopic distribution but in the isotopically enriched specimens the resolution improves and the region is found to contain many bands. From the x-ray powder diffraction pattern, it appears that the $LiBO_2$ studied here is the α-form and contains anions consisting of chains of BO_3 groups sharing corners [21]. The spectrum should resemble that for $Ca(BO_2)_2$ to be discussed later. There are, in fact, many similarities in the spectra of these two compounds, but there are many more absorption bands present in $LiBO_2$ particularly at the lower frequencies. Because of the small mass of the lithium ion it is expected that vibrational modes arising from motion of the cation might be observed in this spectral region. Such vibrations and their combinations and overtones would be expected to produce a more complex absorption spectrum in $LiBO_2$ than in $Ca(BO_2)_2$. It is also of interest to note that strong bands extend to as high as 1400 cm^{-1} in $LiBO_2$. These bands appear to be fundamentals because of their strengths and the fact that their isotopic dependence is inconsistent with overtones and combinations of lower frequency bands. The presence of fundamentals in this range supports the supposition that some of the B—O bonds are much stronger than those found in the BO_3 trigonal ion.

b. Alkaline Earth Metaborates

Typical spectra for the alkaline earth metaborates are shown in figures 6 and 7 and the data for normal isotope distributions are given in table 8 and for isotopically enriched compounds in table 9. The structure of the anion of $CaO{\cdot}B_2O_3$ is known to consist of endless chains of triangles [36, 58, 59] which may be considered as coupled pyroborate groups. Consequently, the spectrum should resemble that of a pyroborate and the relationship of the bands

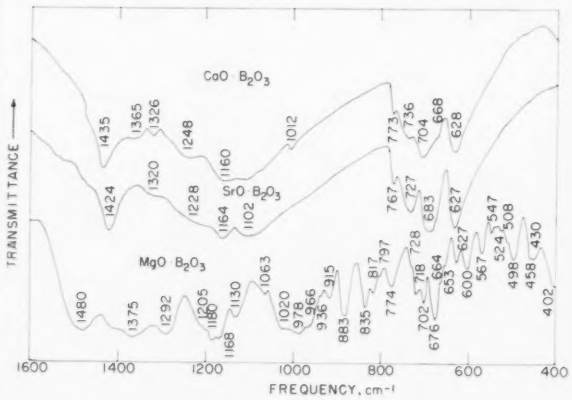

FIGURE 6. *Absorption spectra of alkaline earth metaborates.*

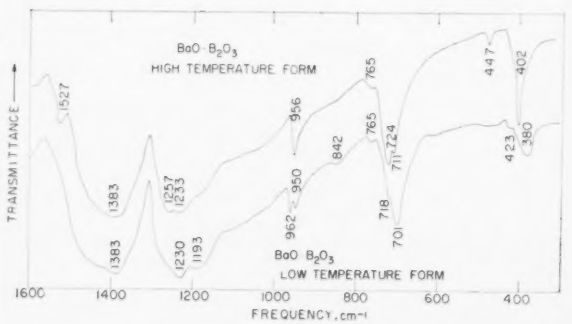

FIGURE 7. *Absorption spectra of two forms of barium metaborate.*

observed to the fundamentals of a trigonal group should be clear in many instances. Comparing the data of $CaO \cdot B_2O_3$ with that of $2CaO \cdot B_2O_3$ (table 12) it is apparent that the spectra show a close relationship. As in the pyroborate, the group of bands between 1100 cm^{-1} and 1450 cm^{-1} are strong, broad, and very strongly dependent on isotopic mass. These bands are therefore derived from ν_3 of the trigonal group. The 1012 cm^{-1} corresopnds to the symmetric stretch derived from ν_1 because it is isotope independent, and the bands below 800 cm^{-1} are derived from the distortion modes ν_2 and ν_4. The close similarity between the spectra of $CaO \cdot B_2O_3$ and $SrO \cdot B_2O_3$ is apparent in figure 6. This similarity led to the prediction that these compounds were probably isostructural. The prediction was verified by x-ray powder diffraction and it may be concluded that the strontium metaborate also contains anions consisting of chains of BO_3 groups. The spectra of $CaO \cdot B_2O_3$ and $SrO \cdot B_2O_3$ are very simple in view of the large number of active normal modes. Apart from the fact that some bands appear to overlap it seems that many bands must either be very weak or coincide in frequency with other bands to produce a spectrum of such apparent simplicity. Marezio, Plettinger, and Zachariasen [36] recently refined the structure of $CaO \cdot B_2O_3$ and showed that the unique oxygen atom attached to each boron atom in the chain is more tightly bonded than the oxygen atoms of the normal trigonal BO_3 group. This tighter bond can be used to account for the existence of fundamentals of much higher frequency than are normally found in isolated trigonal groups.

TABLE 8. *Infrared absorption spectra of alkaline earth metaborates with normal isotope content*

(cm^{-1})

$Mg(BO_2)_2$	$Ca(BO_2)_2$	$Sr(BO_2)_2$	$Ba(BO_2)_2$	
			High temp form	Low temp form
1480b	1435vs	1424s	1527m	
1375vbs	1365m	1320vb	1383sb	1383sb
1292sb	1326m	1228svb	1257s	
1205msh	1248mb			
1180s			1233sb	1230sb
1168s				
1130mb	1160svb	1164s		1193b
1063msh		1102sb		
1020s				
978s	1012vw	1002svb		962m
966s				
936s				
915m			956s	950m
883s				
835s				842wb
817m				
797w				
774m	773m	767m	765wb	765wb
728w				
718m	736mb	727mb	724s	
702s	704sb		711ssh	718ssh
676s				701s
664wsh	668wsh	683sb		
653wsh				
627m	628sb	627sb		
600m				
567m				
547w				
524wsh				
508wsh				
498m	475wb		477w	
458mb				423wsh
430m				
402m			402s	
375m				380mb
355m				

TABLE 9. *Infrared absorption spectra of isotopically enriched alkaline earth metaborates*

(cm^{-1})

$Ca(BO_2)_2$		$Ba(BO_2)_2$			
		Low temp form		High temp form	
B^{10}	B^{11}	B^{10}	B^{11}	B^{10}	B^{11}
				1461	
1483sb	1435s	1290	1245	1422	1367
1411sb	1365m	1271		1401	
		1210	1215	1287	1257
1374sb	1326m	1227	1188	1275	1230
1301sb	1248sb				
		966	962		
1163vsb	1168sb?	953	950	957	953m
1012vw	1012w	798		766w	766vw
		786			
781wsh	766m				
		723	700	738s	716s
750m	736m	712	688		
712sb	700s	603vw	604vw		
				480m	476m
675wsh	672sh	388m	388m	400s	400s
		378m	378m		
635sb	627s				

The spectrum of $MgO \cdot B_2O_3$ as shown in figure 6 is quite complex and not analogous to the calcium and strontium compounds. As noted earlier, it is believed that the spectrum is representative of the compound and is not complicated by the presence of other magnesium borates. It appears plausible that because of the tighter packing produced by the small Mg^{+2} ion, the chains present in $CaO \cdot B_2O_3$ and $SrO \cdot B_2O_3$ might be in such close proximity that cross linking by means of the unique atoms might occur. Cross linking would produce some tetrahedral boron atoms and give rise to strong absorption in the 800 cm^{-1} to 1000 cm^{-1} region as shown in figure 6. Some indirect support for this hypothesis may be drawn from the fact that a strongly cross-linked material might be expected to decompose at elevated temperatures, a behavior exhibited by $MgO \cdot B_2O_3$ which decomposes into B_2O_3 and the 2:1 compound. However, some strongly bonded oxygen atoms must be present in the structure as shown by strong absorption bands as high as 1480 cm^{-1}.

Barium metaborate undergoes a transition forming a quenchable high temperature phase and both forms were studied. From the spectra shown in figure 7 it may be concluded that the anion has high symmetry and is unlike the chain anions of $SrO \cdot B_2O_3$ and $CaO \cdot B_2O_3$. Both the low and high temperature forms give similar spectra with some evidence of lowering of the symmetry in the low temperature form as shown by the splitting of the 956 cm^{-1} band into two components at 962 cm^{-1} and 950 cm^{-1}. The isotopic substitution data of table 9 strengthen the indication that bands in the high temperature form split into two components in the low temperature form. Although the structure of the anion is not known in this compound it may be suggested on the basis of the spectrum alone that B_3O_6 rings of the boroxol type may constitute the anion in the high temperature form and that the rings are coupled in some manner in the low temperature form. Single crystal x-ray work, now under way, is expected to confirm or refute the correctness of this suggestion

in the near future. The x-ray powder diffraction pattern of the high temperature form indexes readily in the hexagonal system with the lattice parameters, $a=7.23\times10^{-8}$ cm, $c=39.17\times10^{-8}$cm [7].

c. Zinc Metaborate

Zinc metaborate, the 4:3 compound, has the structural formula $Zn_4O(BO_2)_6$ and represents one of the few anhydrous borates known to contain only tetrahedrally coordinated boron which have been studied in this investigation. Typical spectra for the compound are shown in figure 8 and the corresponding absorption frequencies are tabulated in table 10. The spectra appear to agree well with spectra given by Krogh-Moe [24]. From the structural analysis [50, 51] the B—O bond distance is known to be 1.48 Å and the maximum frequencies observed should be lower than those of any trigonal borate group which has B—O bonds of the order of 1.35 Å. From these considerations it appears likely that the 1082 cm^{-1} band is the highest fundamental and that the weaker bands observed at 1160 cm^{-1} and 1200 cm^{-1} are overtones or combinations. As noted earlier (see 4.2) the spectrum may be assigned completely in this frequency range by considering the bonded tetrahedra to be effective XYZ_3-type molecules. The assignments given in table 10 were made on this basis using the terminology of Hertzberg [19]. Although the specific assignments are subject to some uncertainty, they show that the three highest frequency bands, i.e., weak broad bands above 1100 cm^{-1} can be interpreted as combinations of the observed fundamentals and an unobserved ν_6 located near 230 cm^{-1}. The internal consistency of the assignments is indicated by the fact that application of the Teller-Redlich product rule [19] to the isotopically enriched specimens gives results in good agreement with the observed frequencies. It is required that $\nu_1\ \nu_2\ \nu_3/\nu_1'\ \nu_2'\ \nu_3' = \frac{11}{10} \approx \nu_4\ \nu_5\ \nu_6/\nu_4'\ \nu_5'\ \nu_6'$ where the unprimed frequencies refer to the B^{10} compound and the primed frequencies to the B^{11} compound. The values of the ratios agree within the experimental error of the measurements with the assumption that the ratio ν_6/ν_6' is unity. It may be noted that both the 470 cm^{-1} and 922 cm^{-1} bands of the B^{11} compound might arise from overtones and/or combinations in view of the derived 230 cm^{-1} frequency. The strength of the bands, however, makes this interpretation unlikely. Some of the internal structure observed in the 922 cm^{-1} band may arise from resonance effects between the fundamental and a combination of ν_4 and ν_6 which would be located near the same frequency.

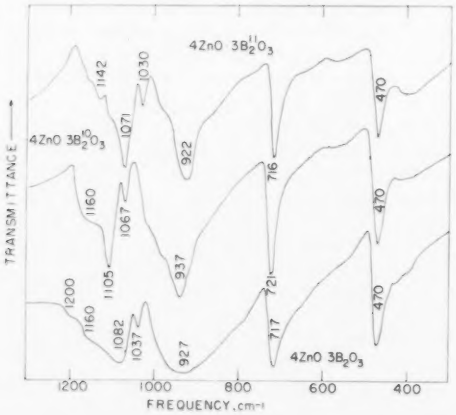

FIGURE 8. *Absorption spectra of zinc metaborate* ($Zn_4O(BO_6)_6$)

TABLE 10. *Infrared absorption spectra of zinc metaborate* [$Zn_4O(cm-1)(BO_2)_6$]

$4ZnO{\cdot}3B_2O_3$			Assignment [1]
B^{10} & B^{11}	B^{10}	B^{11}	
	1340vwb	1296vwb	$\nu_5+\nu_6$
1200wsh	1275wb	1232wb	$\nu_1+\nu_3$
1160wsh	1160wsh	1142wsh	$\nu_2+\nu_6$
1082svb	1105sb	1071sb	$\nu_3(E)$
1037m	1067m	1030m	$\nu_1(A_1)$
927vb	937svb	922svb	$\nu_2(A_1)$
717s	721s	716s	$\nu_4(E)$
470s	470s	470s	$\nu_3(A_1)$
		(230)	$\nu_6(E)$

[1] Assignments on basis of effective C_{3v} symmetry for BO_4 groups.

Regardless of the details of the assignment there is evidence for concluding that no fundamentals occur above 1100 cm^{-1} in the B^{11} compound, a conclusion which is in accord with the weak B—O bond obtained from the x-ray structure analysis. From this result and additional spectra to be discussed later, it is concluded that when tetrahedrally coordinated boron is present strong fundamentals derived from ν_3 of the tetrahedral ion should occur in the 800 cm^{-1} to 1100 cm^{-1} region. In these studies compounds containing three-fold coordinated boron always show strong fundamentals above 1100 cm^{-1} which can be considered as derived from the ν_3 of the trigonal ion. For purposes of determining coordination the region between 800 cm^{-1} and 1400 cm^{-1} is considered to be important. It may also be noted that the zinc metaborate shows a band in the 700 cm^{-1} region. This band might be misinterpreted as corresponding to the out-of-plane mode, ν_2 of a trigonal BO_3 group which falls in the same frequency region. However, isotopic substitution distinguishes these bands because the shift observed in the zinc metaborate is much smaller than the corresponding shift in the trigonal ions.

The rare earth vaterite-type borates (sec. 6.1.b) have spectra showing similarities with the spectrum of zinc metaborate both with respect to band position and with respect to isotope shift. The corresponding bands are 1042 cm^{-1}, 920 cm^{-1}, and 718 cm^{-1} in $Lu_2O_3{\cdot}B_2{}^{11}O_3$ and 1071 cm^{-1}, 922 cm^{-1} and 716 cm^{-1} in $Zn_4O(B^{11}O_2)_6$. These similarities were considered in

the previous conclusions concerning the presence of tetrahedrally coordinated boron in the vaterite structures.

d. Rare Earth Metaborates

The first few members of the rare earth series form borates having a nominal ratio of metal oxide to boric oxide of 1:3. The composition is known for lanthanum borate [33] but it is less certain for the other borates and the system is presently being studied by Levin and McDaniel [35]. Although the composition is uncertain all the borates will be considered to have the 1:3 ratio at this time. Assuming a 1:3 ratio, the empirical formula can be written $M(BO_2)_3$ and the compounds can be considered to be metaborates.

Typical absorption spectra are shown in figure 9 and the observed absorption bands are compiled in table 11. From figure 9 it will be observed that there are large numbers of bands throughout the frequency range extending as high as 1450 cm^{-1}. Further it can be observed that there is a very marked correspondence between the spectra, so that it is reasonably certain that the anions are the same or are very closely related in all compounds. The strong broad bands between 1100 cm^{-1} and 1500 cm^{-1} and their large shift with isotopic substitution is indicative of trigonal borate groups. Similarly the strong bands between 800 cm^{-1} and 1100 cm^{-1} and their strong isotopic dependence is indicative of tetrahedral boron. The bands at 725 cm^{-1} and 662 cm^{-1} in $La_2O_3 \cdot 3B_2{}^{11}O_3$ and their observed shifts may also be taken to indicate the presence of 4-fold and 3-fold coordinated boron, respectively. As shown later, these spectra have many similarities with these of the pentaborates.

TABLE 11. *Infrared absorption spectra of rare earth metaborates* [1]

(cm^{-1})

$La_2O_3 3B_2O_3$		$Nd_2O_3 3B_2O_3$	$Sm_2O_3 3B_2O_3$	$Eu_2O_3 3B_2O_3$
B^{10}	B^{11}			
1495sb	1445sb	1456sb	1470svb	1460svb
1410sb	1392sb	1376sb	1376sb	1380sb
1380svb		1308svb		
		1280svb		
		1210svb	1215sb	1215sb
1183svb	1167sb		1165svb	
1108sb				1115wsh
1053sb	1044sb	1042sb	1056svb	1048s
		972s	981s	975s
964sb	952sb	950m	937wsh	
905svb	870sb	890svb	911svb	903svb
		808s	863msh	861msh
			813s	810s
811sb	789sb	792msh	795wsh	795wsh
		767m	761s	770m
776	757m	755msh	756s	756msh
	744msh			
730s	725wsh	710mb	727s	
717wsh				
689sb	662s	672s	668s	670s
661s				
614s	605s	612s	612s	611s
578s	572s	580s	581m	583sb
523s	516s	522s	556m	
			525s	524sb
		492	492	490

[1] The molar ratio of only $La_2O_3 \cdot 3B_2O_3$ is known. The others are not known. X-ray diffraction and phase equilibrium data indicate that the europium and possibly samarium may have different compositions from that given here.

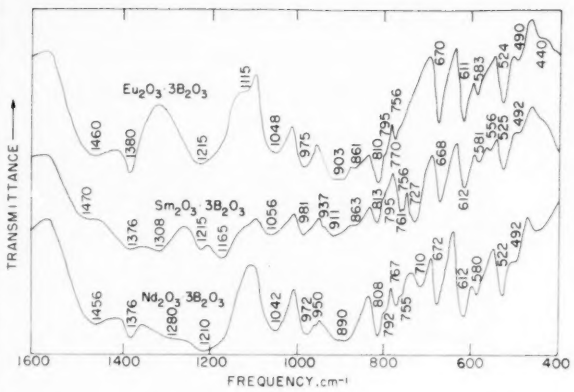

FIGURE 9. *Absorption spectra of rare earth metaborates.*

6.3. Pyroborates

The divalent metals form compounds with a 2:1 ratio of oxides which have empirical formulas $X_2B_2O_5$ and can be classed as pyroborates. Typical spectra are shown in figure 10 and the absorption bands are tabulated in table 12. From the figure it is observed that the spectra are quite similar and are of intermediate complexity. The lead pyroborate, however, as shown by the tabular data is somewhat different. Considering first the isotopic substitution data on $2CaO \cdot B_2O_3$, the two modes derived from ν_2 of the trigonal ion are probably represented by the 723 cm^{-1} and 713 cm^{-1} bands tabulated for the B^{11} compound. The 713 cm^{-1} band is not shown in figure 10 but is frequently resolved as a shoulder on the 723 cm^{-1} band. The overlap of the two modes is believed to produce the rather broad intense band above 700 cm^{-1} in all spectra of figure 10. The bands at 670 cm^{-1} and 618 cm^{-1} are identified by their relative independence of isotope mass as two of the modes derived from ν_4. The other two components of ν_4 are not apparent. They may be too weak to be observed, may coincide in frequency with the observed bands, or may overlap the band at 723 cm^{-1} which is apparently complex. The 474 cm^{-1} mode is probably an ionic distortion mode and may be tentatively assigned as the coupled bending mode. Two twisting modes probably are beyond the frequency range used. The symmetric stretch can be identified with the isotope independent frequency at 1012 cm^{-1}. The other mode derived from ν_1 is not apparent and may correspond to the 803 cm^{-1} band. This band, however, may also originate from combinations or overtones from a low frequency mode. The four modes derived from ν_3 of the trigonal ion are located between 1150 cm^{-1} and 1400 cm^{-1}. There are at least six bands observed in this region for $2CaO \cdot B_2{}^{11}O_3$ and at least two of these—1177 cm^{-1} and 1450 cm^{-1}—may be combinations or overtones. Therefore, with reasonable assurance the bands of table 12 can be assigned to the $B_2O_5{}^{-4}$ ion in terms of the corresponding vibrations of the

TABLE 12. *Infrared absorption spectra of divalent pyroborates*

(cm^{-1})

$2MgO·B_2O_3$	$2CaO·B_2O_3$			$2SrO·B_2O_3$	$2CdO·B_2O_3$	$2CoO·B_2O_3$	$2PbO·B_2O_3$
	B^{10}&B^{11}	B^{10}	B^{11}				
1450vsvb		1450msh	1450msh				
	1366	1411vs	1365vs	1350sb	1350svb	1400svb	1352w
	1328	1374s	1327s	1323sb			1315sh
1290m	1292	1335s	1290s	1261sh			1284s
1260m	1248	1302vs	1255vs	1220sb	1250sb	1250svb	1248s
		1208ssh	1177ssh				1233s
1150svb	1140svb	1172	1158svb	1161sb	1130svb	1150svb	
			1127sbsh	1092sb			
1022m	1011m	1012m	1012m	1000m	998m	1007	1017sb
975bsh	973vw						971s
							877vs
834wb							835
	806w	813m	803m	789w	800	817	
789wb	775vw			772w			
							744m
745msh				735msh			731m
				726msh	707		
712s	718s	738s	723s	717s	691s	698s	710
		735s				693	703
683s		728sh					
							685bsh
668msh	667m	671s	670s	656m	667s	658	661
							640
603s	618s	618s	618s	616s	591s	587	615
							595
568w						572	578
535wsh							547m
484s	475w	475	474w	460w	497w	449	

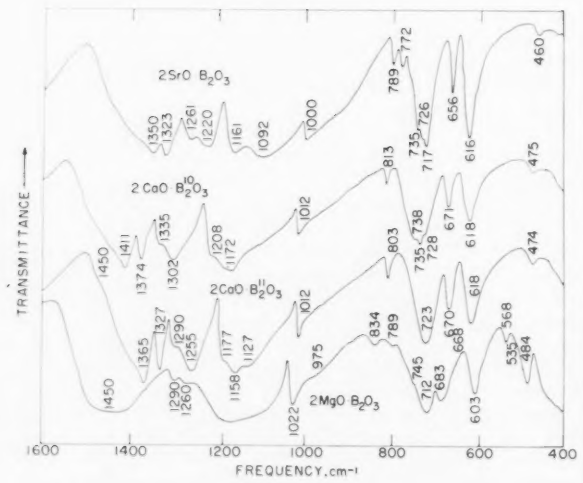

FIGURE 10. *Absorption spectra of pyroborates.*

parent BO_3^{-3} group. It is of interest to note that although the symmetric type stretching frequency in the pyroborates is essentially the same in the orthoborates, modes derived from ν_3 of the trigonal ion extend to much higher frequencies. The higher frequencies are not unexpected in this case because all B—O bonds are not equivalent in the pyroborates [6] and a greater partial double bond character may be attributed to some bonds.

From the data of table 12 it can be observed that the lead pyroborate exhibits a spectrum similar to the other pyroborates but containing more bands, particularly several strong bands in 800 cm^{-1} to 1100 cm^{-1} region. There are also other bands at lower frequencies not found in the other pyroborates. Therefore, the anion in this compound probably does not consist of two coupled trigonal groups. The bands in the 800 cm^{-1} to 1100 cm^{-1} region may be taken to indicate that tetrahedral boron is present and the low frequency bands are indicative of a large complex anion.

6.4. Triborates

Alkali borates formed with the 1:3 ratio of oxides have the empirical formula XB_3O_5. For purposes of this discussion they are classed as triborates. No structural data appear to be available on the compounds studied except $Cs_2O·3B_2O_3$ [29]. The anion is quite complex and is composed of six-membered rings each containing 2 triangular and one tetrahedral boron, with the tetrahedral boron atoms being shared by two rings. Typical spectra are given in figure 11 for the isotopically substituted lithium compounds with the observed data being tabulated in table 13. From figure 11 it can be observed that the spectra are complex and indicative of a low symmetry and a large anion. The spectra are consistent with the presence of both trigonal and tetrahedral boron. The persistence of absorption bands which appear to be fundamentals to high frequencies is indicative that at least some of the B—O bonds have partial double bond character. The spectra and the shifts observed are not inconsistent with the six membered ring found in $Cs_2O·3B_2O_3$ although the spectra are too complex to warrant any specific conclusions on this point without further information on the origin of the various bands.

TABLE 13. *Infrared absorption spectra of alkali triborates* (XB_3O_5)

(cm^{-1})

$Li_2O{\cdot}3B_2O_3$			$Na_2O{\cdot}3B_2O_3$	$K_2O{\cdot}3B_2O_3$	$Cs_2O{\cdot}3B_2O_3$
B^{10} & B^{11}	B^{10}	B^{11}			
1490sb	1540vsb	1490vsb	strong broad	strong broad	1455mb
1365sb	1410svd	1365svb	bands to 1450	bands to 1450	1350mb
1258sb	1280vsb	1258svb	1270svb	1250–1280	1320sb
			1228sb	1227sb	1250vsb
1083sb	1097sb	1080sb	1137mb	1110mb	
			1070sb	1073mb	1080sb
992sbsh	1007ssh	992ssh	1040sb	1030msh	1012msh
954vb	986sb	957sb	970bsh	966sb	967sb
	970sb		938s	937sb	
913b		913mb			
	928mb		901sb	892sb	907svb
882sb	900mb	885mb			
849b	864mb	847svb	850sb	862sb	847sb
771s	781m	774m	818s		797sb
755msh	762msh	758msh	777msh		777msh
			768s		759s
			757wsh	758w	749s
				746m	
730s	740m	723mb		735m	
723msh	730msh			720mb	
			701m	692m	702sb
682msh		680m	684m	686wsh	
667m		671m	673m	663w	
	686mb	662mb		654w	652mb
644m	653mb	639m	643w	646w	
			637w		
602w		600mb?		601w	
572s	575mb	567mb	564m	567wb	563w
547w			549m		547w
528m	528m	525m	530s	522s	530s
501w			507s		510s
			500wsh		
			493msh		
			469s		474msh
455s	455mb	454m	456wsh	450m	459s
	431m	430	431w		
412w	412m	410m			
382m	386m	380m			
355m					

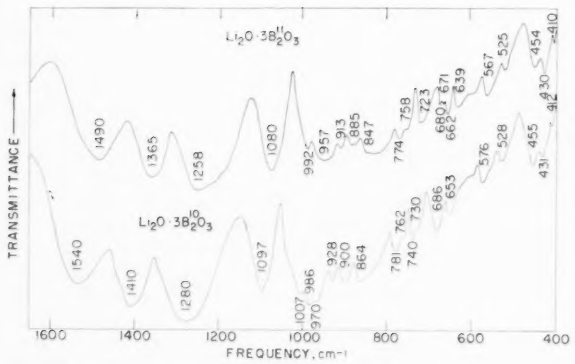

FIGURE 11. *Absorption spectra of lithium triborates.*

6.5. Tetraborates (XnB_4O_7)

Both monovalent (alkali) and divalent metals form borates in a 1:2 ratio of oxides which have empirical formulas $X_2B_4O_7$ and YB_4O_7, respectively. These compounds are classified as tetraborates.

a. Alkali Tetraborates

From the structure of lithium tetraborate reported by Krogh-Moe [28] it is expected that the spectra of the alkali tetraborates might give evidence for both 3- and 4-fold coordinated boron in a complex ring system of low symmetry. The spectra shown in figure 12 and the data of table 14 show that the results are in accord with the predictions. The strong bands and the isotopic shifts in $Li_2O{\cdot}2B_2O_3$ in the 800 cm^{-1} to 1100 cm^{-1} region are indicative of tetrahedrally coordinated boron and the similar bands in the 1100 cm^{-1} to 1400 cm^{-1} region are indicative of 3-fold coordination. Similarly the 773 cm^{-1} and 676 cm^{-1} bands of the B^{11} compound are taken as indicative of the presence of the two types of boron. These conclusions have been verified by the NMR data of Ring and Bray [43]. The absorption at higher frequencies is strong and broad and is not tabulated for the compounds with the normal isotopic distribution. These bands, however, are resolved in the two isotopically substituted lithium tetraborates. There is a very close correlation between the spectra of the sodium and potassium tetraborates and the anions in these compounds are apparently identical but it is not clear from the spectra that the anion in $Li_2O{\cdot}B_2O_3$ is similar. In the case of the sodium and potassium compounds the correlation is so close that it is suspected that they may be isostructural. The data obtained on $Na_2O{\cdot}2B_2O_3$ appear to agree reasonably well with the spectrum given by Krogh-Moe [25]. It may be noted that some of the apparent discrepancies between the data for the lithium tetraborate and the sodium and potassium tetraborates may arise from the tighter packing which presumably occurs with the small lithium ion.

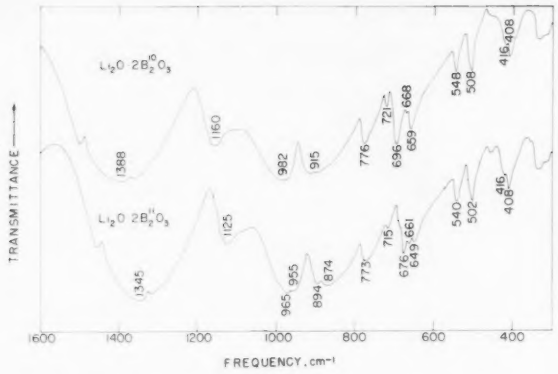

FIGURE 12. *Absorption spectra of alkali tetraborates.*

TABLE 14. *Infrared absorption spectra of alkali tetraborates* ($X_2B_4O_7$)

(cm^{-1})

$Li_2O\cdot 2B_2O_3$			$Na_2O\cdot 2B_2O_3$	$K_2O\cdot 2B_2O_3$
B^{10}&B^{11}	B^{10}	B^{11}		
	1388vsb	1345vsb		
	1160sb	1125sb	1148sb	1130msh
			1090sb	1085mb
			1046sb	1032sb
970sb	982svb	965sb	1010sb	978sb
886sb		955ssh	900—	915—
		894ssh		
861sb	915svb	874svb	836svb	835svb
				779
771s	776sb	773sb	767m	763
			745sh	748
			725	730
718msh	721m	715m	717	718
707msh				687s
678m	696s	676s	675mb	670msh
650mb	668w	661msh	661m	660m
	659s	649msh	636m	637m
			611m	612m
596msh			583m	596s
566wsh			554m	553m
543s	548s	540s	513m	517m
508msh			490w	492w
504s	508s	502s	472w	476w
455w				
	416sh	416sh		
	408s	408s		

b. Divalent Metal Tetraborates

The divalent metal tetraborates fall into two distinct groups with respect to their infrared spectra. Typical spectra for one type are shown in figure 13 and the data for all the compounds studied are compiled in table 15. From the tabulated absorption data it is clear that strong absorption occurs at much higher frequencies in the spectra of the calcium, barium, and zinc compounds than in those of strontium and lead. The presence of both 3-fold and 4-fold coordinated boron is indicated in the former compounds with a large anion of low symmetry. The structure reported for $BaO\cdot 2B_2O_3$ fulfills these requirements [7]. Although the tabular data indicate that the spectra of $CaO\cdot 2B_2O_3$, and $ZnO\cdot 2B_2O_3$ are very similar, this does not appear to be true. Comparison of the actual spectra shows marked differences in positions and relative intensities of many bands. On the basis of these

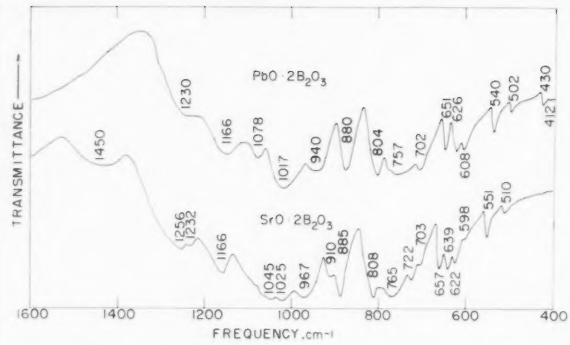

FIGURE 13. *Absorption spectra of divalent metal tetraborates.*

data it seems improbable that the anions in these compounds are identical.

From figure 13, however, it can be seen that the spectra of $SrO\cdot 2B_2O_3$ and $PbO\cdot 2B_2O_3$ are so similar that a structural relationship is indicated. X-ray powder diffraction patterns show that these two compounds are isostructural [7]. The spectra may be interpreted in the usual manner to indicate tetrahedrally coordinated boron. There appear to be bands in the region above 1100 cm^{-1} which would ordinarily be taken as indicative of the presence of boron in 3-fold coordination. However, bands in this region are not intense, being much weaker than expected for fundamentals presumed to be related to the ν_3 mode of triangular units. Therefore, it seems probable that these bands may represent overtones or combinations of some of the lower frequency modes. Although there is some evidence for the presence of boron in 3-fold coordination in the isotopic shifts observed for some bands in the 700 cm^{-1} region, the evidence cannot be considered unequivocal in the presence of such a complex spectrum. It is clear that the anions in these compounds are probably identical and complex. On the basis of the infrared spectrum it is concluded that the anions consist of tetrahedrally coordinated boron atoms with the presence of *any* boron in 3-fold coordination being doubtful. These conclusions are substantiated by the rather high density reported for $SrO\cdot 2B_2O_3$ [7].

Note added in proof: Work on the crystal structure of $SrO\cdot 2B_2O_3$ and $PbO\cdot 2B_2O_3$ has been completed by S. Block and A. Perloff. The structure, reported at the Annual Meeting of the American Crystallographic Association in Bozeman, Mont., July 1964, is found to contain only tetrahedral boron atoms. This result confirms the conclusions drawn from spectroscopic evidence alone. A paper on the structure is in preparation.

6.6. Pentaborates (XB_5O_8)

Some alkalies form compounds having a 1:5 ratio of the oxides and an empirical formula XB_5O_8 which are classified here as pentaborates. From the known structures [27] it is expected that the spectra should be complex and show evidence for both trigonal and tetrahedral boron. The spectra shown in figure 14 and the tabulated data of table 16 verify this prediction. In figure 14 it can be noted that the

TABLE 15. *Infrared absorption spectra of divalent metal tetraborates* (XB_4O_7)

(cm^{-1})

$CaO \cdot 2B_2O_3$	$BaO \cdot 2B_2O_3$	$ZnO \cdot 2B_2O_3$	$SrO \cdot 2B_2O_3$			$PbO \cdot 2B_2O_3$
			B^{10}&B^{11}	B^{10}	B^{11}	
1435sb	1443mb		1450mvb			
1390sb	1400mb	1390sb				
1363sb	1332–	1342sb				
1305sb	1292svb	1298sb				
1247sb	1245sb	1260sb	1256sb			
1188sb	1163m	1237sb	1232sb	1260sb	1223sb	1230sb
		1192msh				
	1107msh	1165sb	1166sb	1168sb	1157sb	1166s
1090sb	1082wsh	1072sb	1045sb	1080–	1060–	1078sb
1052sb	1068mb	1047wsh	1025sb	970vsvb	950vsvb	1017sb
993sb	995sb	988sb	967sb			940sb
942sb	926sb	965	910mb			
910sb	887sb	906sb			905msh	
850sb	835sb	858sb	885s	891s	880s	880sb
818mb		832m				
793wsh	790m	810mb	808s	811s	806s	804s
776mb	761m	763msh	765sb	769sb	750sb	757sb
728m	735sb					
706s	711m	716s	722m	731s	717ssh	
691wsh	679s	698msh	703m	702ssh	700ssh	702s
668m	660m	672w				
658wsh	653w	655w	657s	669s	653s	651s
632		643wb	639s	646m	636m	626s
600	606s			633vw	629vw	
	592w		622s	619s	618s	608s
585	580w	582w	598msh		601wsh	
567s	557m	561m			581w	
534m	529	545			566wsh	
505	496m		551s	549s	549s	540s
	483	469s			540msh	
	451s		510w	508s	508s	502s
	388m			442	435	430m
				411	411	412w
			358m	357s	356s	342w

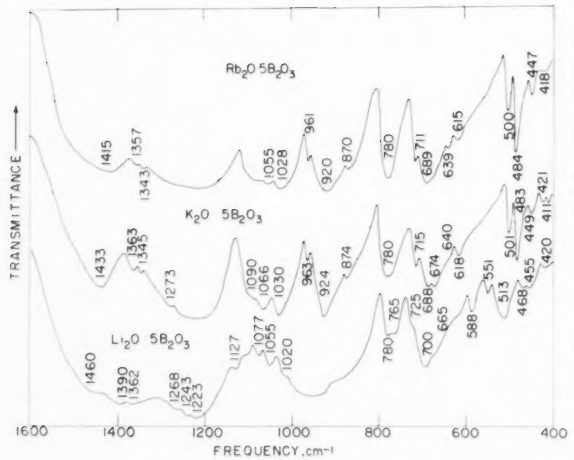

FIGURE 14. *Absorption spectra of alkali pentaborates.*

close similarity between the spectra of the rubidium and potassium compounds is indicative of their isostructural relationship [27]. The positions and isotopic shifts shown for the potassium pentaborate in table 16 are indicative of both 3-fold and 4-fold coordinated boron atoms. In the isotopically substituted compounds there appear to be several sets of "doublets" consisting of bands of equal strength, with a small separation, and similar isotopic shifts. Apparently overlapping of bands from B^{10} and B^{11} compounds obscure these doublets in the spectrum of the normal compound. In view of the fact that the anion is formed by coupling two six-membered ring by means of a tetrahedral boron atom common to both rings, the doublets may arise from similar coupled vibrations of the rings. The spectrum of $Li_2O \cdot 5B_2O_3$ is very similar to those of the other two borates and it would not be surprising if the anion structure in all three pentaborates studied was identical.

TABLE 16. *Infrared absorption spectra of alkali pentaborates* (XB_5O_8)

(cm^{-1})

$Li_2O \cdot 5B_2O_3$	$K_2O \cdot 5B_2O_3$			$Rb_2O \cdot 5B_2O_3$
	B^{10} &B^{11}	B^{10}	B^{11}	
1400–1300	1433sb	1468sb	1419sb	1415svb
1275–1175vsb	1363m	1405m	1359s	1357m
1127m	1345m	1387m	1338m	1343m
1077m	1273sh	1372m	1334m	
	1250–1190b	1257svb	1202svb	1250–1150svb
1055m	1090bsh	1084m	1061m	1055m
1020bsh	1066s	1040svb	1030svb	1028svb
1010–875svb	1030s	974ssh	962s	961m
	963m	940svb	923svb	920sb
	924sb	877s	872s	870s
	874s			
780s				
765s	780s	791s	780s	780sb
725msh	715s	732s	714s	711s
		711s		
700sb	688s	702s	684s	689sb
665ssh	674s	692msh	673ssh	670msh
	640wsh	660msh	635msh	639m
		636m		
588m	618m	630m	616m	615m
551m		508s	503s	509s
513m	501s	504s	500s	500s
468w	483s	489s	483s	484s
455w	449m	452w	449w	447m
420w	421w	422w	421w	418w
	411w	412w	412w	

The anions of the potassium and rubidium compounds may be considered as coupled modified boroxol rings. The presence of the tetrahedral boron should tend to decrease the strength of some of the B–O bonds in the ring and the coupling should tend to increase the effective mass of the coupling boron atom. Both effects would tend to decrease some observed frequencies below the corresponding modes of the boroxol ring. Furthermore from the lack of symmetry all modes of the modified boroxol ring should be active in this instance. Comparison of these spectra with those of the alkali metaborates is not too informative because of the poor spectra of the metaborates and their low infrared activity arising from symmetry. The only mode common to both compounds appears to be represented by the strong band identified as ν_{10} [14] in the alkali metaborates. This band occurs at 723 cm^{-1} in $NaBO_2$ at 712 cm^{-1} in KBO_2, 711 cm^{-1} in $Rb_2O{\cdot}5B_2O_3$, and 714 cm^{-1} in $K_2O{\cdot}5B_2^{11}O_3$. The position, character, and isotopic shift noted in the KBO_2 and $K_2O{\cdot}5B_2O_3$ compounds are so similar that this band can be assigned tentatively as corresponding to ν_{10} (E′). Comparing the present data with these of Goubeau and Keller; the following tentative assignments may be made in the pentaborates: for $Rb_2O{\cdot}5B_2O_3$, ν_1 (A_1') 1150–1250 cm^{-1}, ν_2 (A_1')—780 cm^{-1}, ν_3 (A_1')—500 cm^{-1} or 509 cm^{-1}, ν_{10} (E′)—711 cm^{-1}; for $K_2O{\cdot}5B_2O_3$, ν_1—1190 cm^{-1}—1250 cm^{-1}; ν_2 (A_1')—780 cm^{-1}, ν_3 (A_1')—501 cm^{-1} or 508 cm^{-1}, ν_{10} (E′)—715 cm^{-1}. It is also expected that ν_9 (E′) may fall in the regions given for ν^1 contributing to the strength and broadness of these bands. The bands at 484 cm^{-1} and 483 cm^{-1} in the pentaborates probably correspond to ν_7 (A_2'') which are strongly active in these compounds because of low symmetry. With this assignment it seems probable that the bands at 963 cm^{-1} and 961 cm^{-1} are the first overtones of ν_7. Although these assignments can only be taken as possibilities the relative insensitivity of these band positions to the substituents as demonstrated by Goubeau and Keller [15] lends some support to the proposed assignment.

6.7. Octoborates ($X_nB_8O_{13}$)

The alkali metals together with barium of the alkaline earth metals form borates with a 1:4 ratio of the oxides. The empirical formula of the anion is $B_8O_{13}^{-2}$, classified here as an octaborate. Typical spectra of these compounds are given in figure 15 and the data obtained are compiled in table 17. As expected and as shown in figure 15 a spectrum extremely rich with bands is obtained. All compounds show bands in positions taken to be characteristic of both 3-fold and 4-fold coordination of boron, and the isotopic shifts observed with lithium octaborate strengthens this conclusion. From the spectral data alone it seems very unlikely that the same anion is present in any of these compounds. Lithium octaborate in particular shows a large number of absorption bands but these may be due in part to Li–O vibrational modes, detected in this range because of the small mass of the cation. No structural data are available to assist in the interpretation and without some information of this type any attempt to explain these spectra is of dubious value.

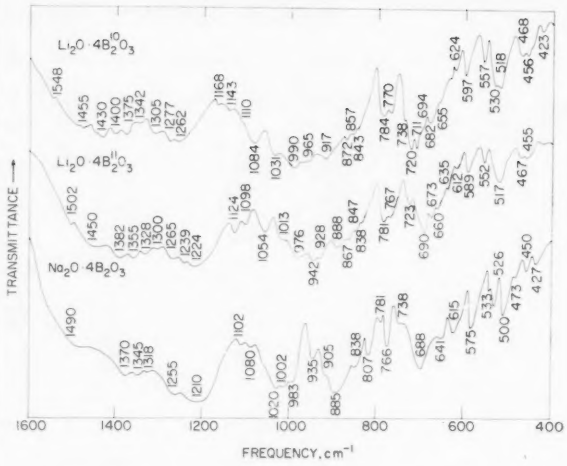

FIGURE 15. *Absorption spectra of alkali octaborates.*

TABLE 17. *Infrared absorption spectra of the octaborates* ($X_nB_8O_{13}$)

(cm^{-1})

$Li_2O{\cdot}4B_2O_3$		$Na_2O{\cdot}4B_2O_3$	$K_2O{\cdot}4B_2O_3$	$BaO{\cdot}4B_2O_3$
B^{10}	B^{11}			
1548sh	1502sh			
1455svb	1450svb	1490svb	1425svb	1420–1320svb
1430sh	1382sh	1370sh		
1400sh	1355sh	1345sh	1357svb	
1375sh	1328sh	1318mb	1312svb	
1342sh	1300svb			
1305sh	1265sh	1255sh		1268sh
1277sh	1239sh			
1262sh	1224sh	1210svb	1192svb	1227sh
1168sh	1124mb			1190sh
1143sh	1098m	1102mb		1095sh
1110msh	1074msh	1080mb	1066sh	1075mb
1084sh	1054m			
1031m	1013msh	1020sh	1034sh	
990sh	976sh	1002mb		
965sh	942sh	983msh	961msh	968svb
	928msh	935m	925svb	
		905msh		
917sh	888mb	885sh		890mb
872m	867bsh		872msh	865mb
857m	847bsh			
843msh	838ssh	838msh		
784sh	781s	807s	787mb	795mb
		781w		
770s	767s	766s	775mb	765mb
738msh	723m	738msh	716mb	723sh
720s		702msh		
711s	690s	688s	686mvb	698mb
694msh	673m			673mb
682m	660w		668m	655mb
655msh	635w	641m		
624m	612m	615m		593sh
597s	589m	575s		
557m	552m			544msh
530s		533m		
518s	518sb	526s	500s	515s
		500s		
468m	467m	473w	484s	490sb
456m	455m	450m	449m	
423w		427m		

6.8. Miscellaneous Borates

In this section data are presented for those borates which cannot be readily classified in the previous categories. These will represent in most instances individual borates of odd compositions or groups of borates whose classification as to anion type is obviously of no value.

a. Rare Earth 3:1 Borates

Levin and McDaniel [35] have observed that the rare earths form borates having a nominal oxide ratio of 3:1. There is doubt at this time that the ratio remains constant throughout the series of rare earth borates but there is no question that the compounds are formed. Inasmuch as the rare earth oxides produce no appreciable absorption in the frequency range used here, satisfactory spectra of the desired borates will be obtained if the quantity of oxide is in excess of the amount required for compound formation. If, as now appears likely, the compounds are of the 3:1 ratios or less, materials formed by a 3:1 oxide ratio should produce spectra of the borate only. From powder x-ray diffraction data on the compounds it is found that the 3:1 compounds of lanthanum, praseodymium, and neodymium are most probably isostructural. From samarium to ytterbium, however, a new structure or perhaps new structures (and probably different compositions) appear to form. This behavior is observed in typical spectra shown in figures 16 and 17 and the data tabulated in table 18. It is noted in figure 16 that the spectrum is characteristic of trigonal BO_3 groups with bands derived from the 4 modes of the trigonal ion apparent. The isotopic substitution effects shown for the lanthanum compound in figure 16 show that the bands in the 1200 cm^{-1} region are analogous to ν_3, the 937 cm^{-1} band to ν_1, the 700 cm^{-1} region bands to ν_2 and the 600 cm^{-1} region bands to ν_4 of the trigonal ion. However, at least 3 bands appear in each of the ν_3, ν_2, and ν_4 regions and the spectra are not typical of isolated trigonal ions. They are also not typical of either the pyroborate ion, the boroxol ring, or chains of triangular groups. It appears that the spectra of the first few members of the 3:1 rare earth borates are indicative of a new type of anion which is most probably a polymer formed of BO_3 groups.

Starting at $3Eu_2O_3{\cdot}B_2O_3$ and continuing to $3Tm_2O_3{\cdot}B_2O_3$ the marked change observed in figure 17 occurs in these spectra. Strong bands in the 800 cm^{-1} to 1100 cm^{-1} range occur which are indicative of boron with 4-fold coordination. Simultaneously new absorption bands appear in the 700 cm^{-1} to 800 cm^{-1} region which tend to confirm the indication. As the increase in atomic weight in the rare earth series is accompanied by a decrease in ionic radius, it would be expected that the packing in the unit cell increases as the mass of the cation increases. In the anion, however, closer packing can be accomplished by increase in coordination of boron from 3 to 4.

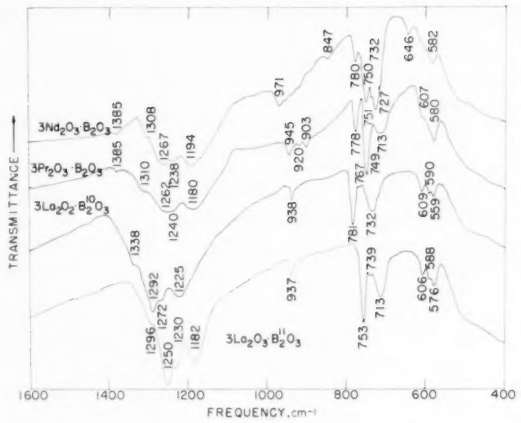

FIGURE 16. *Absorption spectra of 3:1 rare earth borates.*

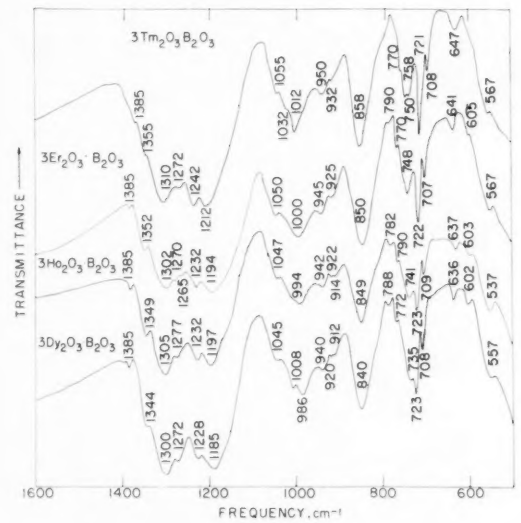

FIGURE 17. *Absorption spectra of 3:1 rare earth borates.*

Therefore, the increase in coordination indicated by these spectra is not surprising, and it would not be surprising if the composition of the compounds also changed. It should be noted, however, that there is still evidence for boron in 3-fold coordination in addition to the 4-fold coordination so that the anions are probably quite complex.

b. Bismuth Borates

The bismuth borates form in ratios of oxides which are unlike the other trivalent ions in most instances and the spectra of all the compounds are discussed here. No isotopically pure compounds were prepared for these compounds. Typical spectra are shown in figure 18 and the absorption frequencies are tabulated in table 19. The spectra of figure 18 all exhibit strong bands to low frequencies as well as

TABLE 18.—*Infrared absorption spectra of the 3:1 rare earth borates*

(cm⁻¹)

$3La_2O_3B_2O_3$		$3Pr_2O_3B_2O_3$	$3Nd_2O_3B_2O_3$	$3Sm_2O_3B_2O_3$	$3Eu_2O_3B_2O_3$
B^{10}	B^{11}				
		1385w	1385w	1386w	1386mb
				1325wsh	1325sbsh
1338msh	1296msh	1310msh	1308msh		
				1277svb	1279svb
1292s	1250svb	1262svb	1267svb		
1272ssh	1230sbsh	1240sb	1238svb	1242svb	
1225svb	1182svb	1180svb	1194svb	1200svb	
				1177svb	1177svb
					999sb
					969sb
938m	937m	945m	971m		
		920w			
		903m		910vw	904m
			847w		832sb
		778m	780m		
					768m
					760w
781s	753s	751s	750s	751s	750wsh
		749s		747s	
767w	739vw			740s	
			732s	726s	
732sb	713sb	713sb	727s	715s	707s
					688msh
			646m	650m	
					622mb
609m	606m	607bsh		587m	596s
590m	588msh	580mb	582mb		542sb
559m	576m				

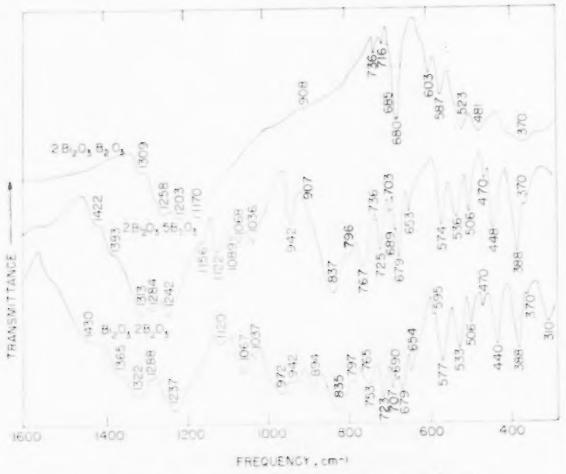

FIGURE 18. *Absorption spectra of bismuth borates.*

numerous bands which are nearly coincident in the different compounds. It was suspected that these bands might arise, in part from bismuth oxide impurities or from Bi—O bond modes. However, the pure oxide itself shows no absorption spectrum in this frequency range. The spectrum of the 2:1 compound is surprisingly simple and gives evidence of boron only in 3-fold coordination. The absence of strong bands just above 700 cm^{-1} (the ν_2 region for trigonal ions) and the apparent presence of modes derived from ν_2 at 685 cm^{-1} and 680 cm^{-1} may be taken to indicate that the anion is a complex polymer of trigonal BO_3 groups. The occurrence of low frequency bands supports this idea. Because of the simplicity of the spectrum it is probable that a highly symmetrical ion is present. The other bismuth borates show evidence of polymeric anions containing both 3-fold and 4-fold coordinated boron. It is apparent from the many points of similarity that the anions are very closely related in the 3:5, 1:3, and 1:4 compounds. Furthermore, the spectrum of the 1:3 bismuth borate is quite similar (but not identical) with the spectra of the 1:3 rare earth borates, and all the bismuth borate compounds except the 2:1 compound show spectra with marked

TABLE 18. *Infrared absorption spectra of the 3:1 rare earth borates*—Continued

(cm⁻¹)

$3Gd_2O_3B_2O_3$	$3Tb_2O_3B_2O_3$	$3Dy_2O_3B_2O_3$	$3Ho_2O_3B_2O_3$	$3Er_2O_3B_2O_3$	$3Tm_2O_3B_2O_3$
1392wb	1385w	1385w	1385w	1385w	1385vwsh
1325sbsh	1335sbsh	1344msh	1349msh	1352msh	1355msh
	1295sb	1300sb	1305sb	1302sb	1310sb
1280svb		1272ssh	1277msh	1270msh	
				1265msh	1272mb
	1220sbsh	1228ssh	1232ssh	1232sb	1242sb
			1197sb	1194sb	1212sb
1180svb	1180svb	1185sb			
	1045svb	1045ssh	1047ssh	1050ssh	1055ssh
					1032ssh
998sb	1008sb	1008msh			
968sb	982sb	986s	994sb	1000sb	1012sb
		940m	942m	945m	950sb
		920w	922w	925m	932m
905m	910sb	912w	914wsh		
830sb	840sb	840sb	849sb	850sb	858sb
		788wb	782wb	790wb	
770m	770m	772msh	770msh	770msh	770msh
767w		735sbsh	741ssh	748s	758s
752msh					750s
743msh					
734msh	723s	723s	723s	722s	721s
707s	708s	708s	709s	707s	708s
682mb	680wb				
		636mb	637m	641mb	647mb
598s	600w	602m	603m	605m	
550sb		557m	557sb	567sb	567sb

TABLE 19. *Infrared absorption spectra of the bismuth borates*

(cm⁻¹)

$2Bi_2O_3 \cdot B_2O_3$	$3Bi_2O_3 \cdot 5B_2O_3$	$Bi_2O_3 \cdot 3B_2O_3$	$Bi_2O_3 \cdot 4B_2O_3$
	1422msh	1430bsh	1448svb
	1383msh		1376svb
		1365bsh	
1309msh	1313sb	1322sb	
	1284sb	1288bsh	
1258sh	1242sb	1237vsb	1238svb
1203sb			1191ssh
1170sb	1156msh		
			1130msh
	1122sb	1120mb	
	1089s		
	1068sb	1067sb	1074sb
	1036sb	1037sb	
		972svb	
	942sb	942m	930msh
908w	907wsh	894mb	890svb
	837svb	835svb	835svb
	796m	797m	
	767s	765m	
		753m	750s
736m	736wsh		
716m	725s	723s	722s
	703m	707m	
685s	689m	690w	689mb
680s	679s	679s	
	655m	654m	653w
			623w
603sb			595msh
578sb	574s	577s	579s
	536s	533s	529s
523sb			
	506s	506s	503s
481svb			
	470m	470w	470w
	448s	440s	436sb
	388s	388s	389sb
370sb	370ssh	370ssh	
		310sb	

resemblances to the spectra the other metal borates that have high proportions of B_2O_3.

c. Odd Borates

Several borates are formed in systems already discussed in apparent odd ratios of metal oxide to boric oxide. These spectra are given here, together with those of compounds of doubtful composition. Representative spectra are not shown but the observed absorption bands are given in table 20. No detailed discussion of these spectra will be attempted. The questions concerning the composition of the 5:2 zinc borate have been noted previously (sec. 6.2.c). The spectrum would be consistent with boron in 3-fold coordination except for the strong band at 940 cm^{-1} which may indicate tetrahedral boron. In the 4:1 lead borate only trigonal boron is indicated. The 3:1 copper borate, whose exact composition is not established, gives indications of only 3-fold coordination of boron as would be expected from the nominal formula. The spectrum shows an interesting series of weak broad bands in the 858 cm^{-1} to 1032 cm^{-1} range which may be indicative of impurities. In the 5:2 zinc borate, the 4:1 lead borate and the 3:1 copper borate the spectra all indicate polymeric anions composed of trigonal BO_3 groups. The 5:4 lead borate spectrum indicates both coordinations of boron and the aluminum borate spectrum is complicated by the possibility of Al—O bond vibrations occurring in this spectral range. The 1:9 cesium borate spectrum shows very strong absorption throughout the range 500 cm^{-1} to 1500 cm^{-1} with no clearly resolved bands. At least a part of the broad absorption may arise from the glassy phase which is known to be present in small amounts. The only clearly recognizable feature of this spectrum consists of a complex group of bands near 460 cm^{-1}.

TABLE 20. *Infrared absorption frequencies of "odd" borates*
(cm^{-1})

$5ZnO2B_2O_3$	$4PbOB_2O_3$	$5PbO4B_2O_3$	$3CuOB_2O_3$	$9Al_2O_32B_2O_3$	$Cs_2O9B_2O_3$
1307svb	1329m	1292sb	1500m	1412sb	
1237svb	1278s		1480m	1390sb	
	1247s	1232sb	1340sb	1327sb	Very strong
1085sb	1179sb	1196m	1192mb	1260sb	broad
		1132m	1152sb	1230m	absorption
1040mb		1107m		1189s	1500cm⁻¹
		1037sb	1032wb	1100mbsh	to
991wsh	972m	975sb	980wb	1025mbsh	600cm⁻¹
		927sb	942wb		
940svb		900ssh	910wb		
	891w		888wb	875sb	
		820svb	858wb		
883w				827mvb	
863w		792sb		798sb	
	756s	765sb		775msh	
	728s	750msh	737msh	732s	
715sb		722m	722s	710msh	
	709w	711m	696s	693m	
672s	690s	702m	671s	669s	
	608s	681s	663s		
620mb		661s	648ssh		
		628m	611m		
955mb		609s	594m	601svb	
	559s	582s			
475s	521m	567msh	553m	552sb	
	503m	560msh		524m	
437s		509s	508s	493sb	505ssh
		476s	477s	458m	460sb
415s		434s	439ssh	443m	
	408sb	418s	433s	418m	
377vsb	356sb	409s			
		399s	397s		
		370s	375s		

d. Borates Containing Only Tetrahedrally Coordinated Boron

The three borates discussed in this section are known to contain boron only in BO_4 groups and consist of the 1:1 compounds of Ta_2O_5, As_2O_5, and P_2O_5 with B_2O_3. The structures are known for all of these compounds which have the empirical formulae ABO_4 with A representing Ta, P, or As. Both PBO_4 and $AsBO_4$ form crystals of space group $S_4^2 \equiv C_2$ [46] and $TaBO_4$, which is isostructural with zircon is of space group D_h^{19} [58]. The latter compound is expected to give a spectrum typical of tetrahedrally coordinated boron with all normal modes active. Coupling with the modes arising from Ta-O bonds is not expected to be important because of the relative weakness of these bonds and the large mass of the Ta atoms. It was determined experimentally that Ta_2O_5 showed no absorption in the frequency range used here. The compounds PBO_4 and $AsBO_4$ both contain two distinct types of tetrahedra, one of which is the BO_4 unit, the other either PO_4 or AsO_4 tetrahedra. The two types of tetrahedra are connected at corners and each oxygen is therefore shared by boron and either phosphorous or arsenic. The P—O and As—O bonds are expected to be similar in strength to the B—O bonds and the infrared spectrum will be expected to be representative of tightly coupled oscillators having at least some fundamentals nearly equal in frequency.

The spectra obtained on these compounds are shown in figure 19 and the observed absorption bands are tabulated in table 21. The spectrum of Ta_2O_5·B_2O_3 shows 3 strong bands at 840 cm^{-1}, 579 cm^{-1}, and 490 cm^{-1}, which have been assigned tentatively as corresponding to ν_3, ν_1, and ν_4, respectively. The missing ν_2 band may be located near 300 cm^{-1} and may correspond to the apparent absorption band observed in figure 19. However, the location of ν_2 or its presence in the spectrum is not certain because of the low energy available near 300 cm^{-1}. The assignments given are plausible and consistent with the expected strengths and complexities of the ν_3 and ν_4 bands. The assignments were not corroborated by isotopic substitution because of the difficulties involved in preparing the tantalum borate but it appears very probable that this spectrum should be characteristic of the isolated borate tetrahedral unit.

Although the spectra of PBO_4 and $AsBO_4$ are very simple in appearance their interpretation is not clear. First it should be noted that all bands in these compounds with one exception (the 858 cm^{-1} band) are very broad and the tabulated data are subject to considerable uncertainty. In addition it is possible that variations of index of refraction of the powdered specimens may produce artifacts in the observed spectra—the 858 cm^{-1} band is suspected in this connection. It should be noted that the normal frequencies of the isolated PO_4^{-3} ion are given as $\nu_1 \approx 980$ cm^{-1}, $\nu_2 \approx 363$ cm^{-1}, $\nu_3 \approx 1082$ cm^{-1}, and $\nu_4 \approx 515$ cm^{-1}. Comparing these values and those for $TaBO_4$ in table 21 with the observed frequencies for PBO_4 shows no clear correlation. The fact that

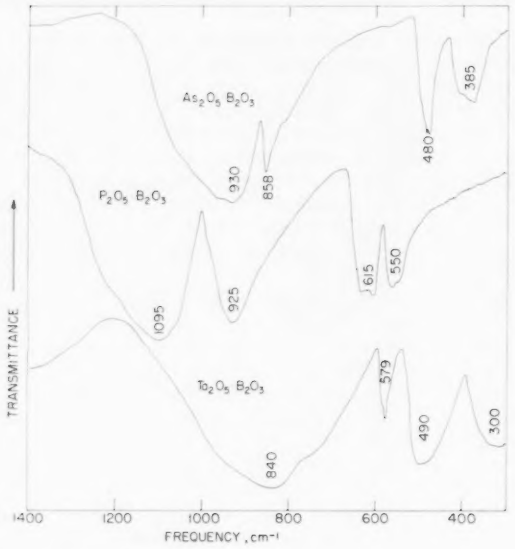

FIGURE 19. *Absorption spectra of compounds containing tetrahedrally coordinated boron.*

substitution of As for P in the structure produces strong shifts of *all* bands plus the fact that isotopic substitution of boron in a given compound results in shifts which appear to be in unexpected directions forces the conclusion that in a system of such tightly coupled oscillators, individual group frequencies cannot be recognized readily.

TABLE 21. *Infrared absorption spectra of compounds containing only tetrahedrally coordinated boron*

(cm^{-1})

$TaBO_4$	PBO_4			$AsBO_4$
	B^{11} & B^{10}	B^{10}	B^{11}	B^{11} & B^{10}
840vsvb,ν_3	1095vsb	1065vsb	1085vsb	930vsb
579s,ν_1	925vsb	925vsb	923vsb	858?s
490vb,ν_4	615sb	610sb	617sb	480s
300svb?,ν_2	550sb	535sb	537sb	385sb

7. Spectroscopic Identification of Borate Anions

From the studies described some generalizations on the character of the borate anion can be made on the basis of the observed spectrum. Under normal conditions the spectrum will be complicated by the presence of B^{10} and B^{11} isotopes in their natural abundance and recognition of the weaker, higher frequency bands arising from the B^{10} isotope is essential for purposes of identification.

As regards the problem of coordination of the boron, it can be concluded that the group frequency correlations may have certain validity in the spectra of the borates, regardless of the exact structure of the anion. Characteristic bands may shift by as much as 100 cm^{-1} or more depending on the structure so that conclusions must be made with caution particularly when very complex anions are involved.

With these reservations in mind, it can be concluded that boron in 3-fold coordination is characterized by the presence of strong, broad absorption in the region 1100 cm^{-1} to 1300 cm^{-1}. This band (or more generally bands) is one of the strongest and most prominent features of the spectrum. In addition there is always absorption in the 700 cm^{-1} to 780 cm^{-1} region (derived from ν_2 of the trigonal ion) which is strong, usually sharp, and frequently (but by no means always) consists of a single band. Both of these characteristic bands are strongly dependent on isotope mass and isotopic substitution can be used to differentiate the desired bands from others which occur in the same frequency region.

Boron in 4-fold coordination can be determined with much less certainty, particularly when boron in 3-fold coordination is also present. Based on the present (and previous work) it may be concluded that the most characteristic feature is the presence of strong, broad absorption in the 800 cm^{-1} to 1100 cm^{-1} region. This band (or bands) is very strong and broad and its position is strongly sensitive to isotope mass. Absorption in the 600 cm^{-1} to 800 cm^{-1} region can be distinguished from the absorption of boron in 3-fold coordination by the fact that it is relatively insensitive to isotopic mass. Caution must be exercised in this case to recognize overtones and combination bands which may be found in the region above 1100 cm^{-1} and be mistaken for fundamentals of trigonal borate groups. Overtones and combinations may be strongly dependent on isotope mass but may be differentiated from the fundamentals by their relative weakness compared to the fundamental bands. It appears to be characteristic of tetrahedral borates that reasonably strong absorption bands are found at much lower frequencies than in the trigonal borates (for example a band is generally observed near 470 cm^{-1} which may be derived from ν_4) but this observation is of little diagnostic value. Complex borate anions give rise to a large number of low frequency modes so that the tetrahedral boron bands, if present, cannot be identified with assurance.

The identity of individual anions can be determined with assurance in a limited number of cases only. The best identification can be made in the case of the planar BO_3 group. This spectrum is defined by the strong absorption above 1100 cm^{-1} which may be split into two bands, a strong band in the 700 cm^{-1} to 800 cm^{-1} region, and one or two weaker bands below 700 cm^{-1}. A weak sharp band near 1000 cm^{-1} may appear (see figs. 1 and 2).

The pyroborate ion can probably be recognized from its spectrum. In this case the diagnostic region appears to be the 600 cm^{-1} to 800 cm^{-1} region which exhibits three strong bands (see fig. 10). Additional bands may appear slightly above 800 cm^{-1} but they are much weaker. A sharp moderately strong band will also appear near 1000 cm^{-1}. Bands at still higher frequencies will occur but only

the appearance of the strong 3-fold coordination bands above 1100 cm^{-1} is of concern.

Compounds with infinite chains of triangles yield spectra very similar to those of the pyroborates. In the former, however, the bands appear to be broader, more complex in internal structure, and less easily resolved. The band near 1000 cm^{-1} is weak and may not be observed. The strong bands above 1100 cm^{-1} are also present but broader and less readily resolved than in the pyroborates.

Provided the spectrum obtained for $TaBO_4$ is typical of an isolated tetrahedral BO_4 group, the characteristics appear to be principally in the strong broad band near 840 cm^{-1} and the slightly weaker band near 490 cm^{-1}. The bands near 579 cm^{-1} and 300 cm^{-1} are not considered to be diagnostic features because they may be inactive in many instances.

Any attempt to identify more complex borate anions solely on the basis of their infrared spectra does not appear possible at this time. Spectra containing large numbers of bands, particularly in the region below 600 cm^{-1} may be taken to be indicative of structurally complex anions of low symmetry. Further detailed interpretations can be made only as x-ray structural data become available for more of the borates.

The authors are indebted to E. R. Lippincott for valuable suggestions.

8. References

[1] S. Anderson, R. Bohan, and D. Kimpton, J. Am. Ceram. Soc. **38,** 370 (1955).
[2] H. Bauer, Z. anorg alleg. Chem. **320,** 306 (1963).
[3] S. V. Berger, Acta Chem. Scan. **4,** 1054 (1950).
[4] S. V. Berger, Acta Cryst. **5,** 389 (1952).
[5] S. V. Berger, Acta Chem. Scan. **3,** 660 (1949).
[6] S. Block, G. Burley, A. Perloff, and R. D. Mason, Jr., J. Research NBS **62,** 95 (1959).
[7] S. Block, A. Perloff, and C. Weir, Acta Cryst. **17,** 314 (1964).
[8] A. Buchler and E. P. Marram, J. Chem. Phys. **39,** 292 (1963).
[9] E. T. Carlson, BS J. Res. **9,** 825 (1932).
[10] H. M. Davis and M. A. Knight, J. Am. Ceram. Soc. **28,** 97 (1945).
[11] J. C. Decius, J. Chem. Phys. **23,** 1290 (1955).
[12] S. M. Fang, Z. Krist. **99,** 1 (1938).
[13] R. F. Geller and E. N. Bunting, J. Research NBS **18,** 585 (1937).
[14] J. Goubeau and D. Hummel, Z. Physik. Chem. **20,** 15 (1959).
[15] J. Goubeau and H. Keller, Z anorg. alleg. Chem. **272,** 303 (1953).
[16] W. D. Hand and J. Krogh-Moe, J. Am. Ceram. Soc. **45,** 197 (1962).
[17] D. E. Harrison and F. A. Hummel, J. Electrochem. Soc. **103,** 496 (1956).
[18] P. B. Hart and S. E. F. Smallwood, J. Inorg. Nucl. Chem. **24,** 1047 (1962).
[19] G. Herzberg, Molecular Spectra and Molecular Structure, II, Infrared and Raman Spectra of Polyatomic Molecules (D. Van Nostrand Co., Inc., New York, N.Y. 1949).
[20] C. Hirayama and E. C. Subbarao, Phys. Chem. Glasses **3,** 111 (1962).
[21] E. Hohne and L. Kutschabsky, Z. Chem. **1,** 33 (1963).
[22] E. Ingerson, G. Morey, and O. F. Tuttle, Am. J. Sci. **246,** 38 (1948).
[23] P. F. Konovalov, Dokl. Akad. Nauk. SSSR **70,** 849 (1950).
[24] J. Krogh-Moe, Z. Krist. **117,** 166 (1962).
[25] J. Krogh-Moe, Arkiv f. Kemi **12,** 475 (1958).
[26] J. Krogh-Moe, Arkiv f. Kemi **12,** 247 (1958).
[27] J. Krogh-Moe, Arkiv f. Kemi **14,** 439 (1959).
[28] J. Krogh-Moe, Acta Cryst. **15,** 190 (1962).
[29] J. Krogh-Moe, Acta Cryst. **13,** 889 (1960).
[30] H. Lehmann and D. Tiess, Chem. Tech. **11,** 260 (1959).
[31] E. M. Levin, R. S. Roth, and J. B. Martin, Am. Mineral. **46,** 1030 (1961).
[32] E. M. Levin and C. L. McDaniel, J. Am. Ceram. Soc. **45,** 355 (1962).
[33] E. M. Levin, C. R. Robbins, and J. L. Waring, J. Am. Ceram. Soc. **44,** 87 (1961).
[34] E. M. Levin and H. F. McMurdie, J. Research NBS **42,** 131 (1949).
[35] E. M. Levin and C. L. McDaniel (private communication).
[36] M. Marezio, H. A. Plettinger, and W. H. Zachariasen, Acta Cryst. **16,** 390 (1963).
[37] M. Marezio, H. A. Plettinger, and W. H. Zachariasen, Acta Cryst. **16,** 594 (1963).
[38] C. Mazzetti and F. de Carli, Gazz. chim. ital. **56,** 23 (1926).
[39] F. A. Miller and C. H. Wilkins, Anal. Chem. **24,** 1253 (1952).
[40] G. W. Morey and H. E. Merwin, J. Am. Chem. Soc. **58,** 2248 (1936).
[41] M. E. Mrose, Geol. Soc. Am., Program Annual Meetings 1961, p. 111.
[42] A. Perloff and P. Shumate (private communication).
[43] P. J. Ring and P. J. Bray, Bull. Am. Phys. Soc. **9,** 24 (1964).
[44] A. P. Rollet, Compt. Ren. **200,** 1763 (1935).
[45] A. P. Rollet and R. Bouaziz, Compt. rend. **240,** 2418 (1955).
[46] B. S. R. Sastry and F. A. Hummel, J. Am. Ceram. Soc. **41,** 7 (1958).
[47] H. Scholze, Z. anorg. Chem. **284,** 272 (1956).
[48] R. Schroeder, C. E. Weir, and E. R. Lippincott, J. Research NBS **66A,** 407 (1962).
[49] G. E. R. Schulze, Z. Physik Chem. (B) **24,** 215 (1934).
[50] P. Smith, S. Garcia-Blanco and L. Rivoir, Ann. Fisica Quim. **57A,** 263 (1961).
[51] P. Smith, S. Garcia-Blanco and L. Rivoir, Z. Krist. **115,** 460 (1961).
[52] W. C. Steele and J. C. Decius, J. Chem. Phys. **25,** 1184 (1956).
[53] E. C. Subbarao and F. A. Hummel, J. Electrochem. Soc. **103,** 29 (1956).
[54] Y. Takeuchi, Acta Cryst. **5,** 574 (1952).
[55] Y. Takeuchi, Mineral. J. (Japan) **2,** 245 (1958).
[56] C. E. Weir and A. Van Valkenburg, J. Research NBS **64A,** 103 (1960).
[57] C. E. Weir and E. R. Lippincott, J. Research NBS **65A,** 173 (1961).
[58] W. H. Zachariasen, Pro. Nat. Acad. Sci. **17,** 617 (1931).
[59] W. H. Zachariasen and G. E. Ziegler, Z. Krist. **83,** 354 (1932).
[60] W. H. Zachariasen, J. Chem. Phys. **5,** 919 (1937).
[61] A. I. Zaspavskii and R. A. Zvinchuk, Doklad. Akad. Nauk. SSSR **90,** 781 (1953).

(Paper 68A5–294)

JOURNAL OF RESEARCH of the National Bureau of Standards—A. Physics and Chemistry
Vol. 68A, No. 5, September-October 1964

Effect of Pressure and Temperature Upon the Optical Dispersion of Benzene, Carbon Tetrachloride and Water

R. M. Waxler, C. E. Weir, and H. W. Schamp, Jr.

(May 26, 1964)

An interferometer has been used to measure the change in index of refraction with change in pressure or temperature. Absolute indices of refraction are reported to five decimals for benzene, carbon tetrachloride, and water at eight different wavelengths in the visible region of the spectrum at pressures as high as 1100 bars and temperatures as high as 55 °C. The data for benzene and carbon tetrachloride have been fitted to one term, dispersion equations of the Drude and Lorentz-Lorenz types. The observed changes in index of refraction for these two liquids have been attributed to change in density plus a shift in the fundamental absorption frequency, assuming that the oscillator strength remains constant. The data for water have been treated and explained in the same manner but with the additional postulate that water consists of two different molecular types.

1. Introduction

An interferometric technique has been described for use in precision measurements of index of refraction of liquids at pressures as high as 1100 bars in the range 0 °C to 55 °C by observing the shift in interference fringes as pressure and temperature are varied [1].[1] Data reported on the indices of benzene, carbon tetrachloride, and water at one wavelength were of such a nature as to warrant additional study of the effect of pressure and temperature upon the optical dispersion of these liquids. The present report describes the modifications of the instrument to permit simultaneous observation of the shift in interference fringes for eight spectral lines spaced to permit calculation of the change in index throughout the visible range of the spectrum. Data on indices for the three liquids, benzene, carbon tetrachloride, and water are reported and some of the implications of the results are discussed.

2. Experimental Method

The general experimental method has been described fully [1] and will be outlined only briefly here. It consists of placing an interferometer containing the liquid of interest inside a high pressure vessel equipped with glass windows. The shift in interference fringes is recorded photographically as the pressure is decreased from an elevated value to 1 bar. The refractive index is calculated from the relationship

$$\Delta\mu = \Delta n\lambda/2t \sin\theta \qquad (1)$$

where $\Delta\mu$ is the change in refractive index; Δn, the number of fringes passing a reference point during the pressure change; λ, the wavelength of the light employed; t, the distance between the optical flats; and θ, the angle of incidence of light which, in these experiments, was 90°.

In the interferograph developed by Saunders [2], light from the discharge tube is dispersed into its component spectral lines by a prism. Ordinarily all lines except the one in use are reflected by a mirror while the desired line passes through a slit in the mirror and is detected photographically. By rotating the camera through 90° and inserting a stop about 3 mm in width at the object position, several small images, one for each spectral line, are permitted to fall on the slit in the mirror and thus be detected by the film. The stop restricts the width of each line image and prevents overlapping. Thus each spectral line produces its own system of interference fringes, these systems being displaced vertically on the film. Each set of fringes will move as the pressure is varied, and a permanent record of the fringe shift is obtained on the film. The number of fringes can then be counted at leisure after the film is developed.

Using extremely high speed film it was found that the helium lines, 6678.15, 5875.62, 5015.68, and 4921.93 Å could be photographed successfully. To obtain additional lines a cadmium lamp was placed directly behind the helium tube and cadmium lines at 6438.47, 5085.82, 4799.92, and 4678.16 Å were also used. With the high speed film, it was found necessary to perform all experiments in a dark room to cut down the effects of extraneous light. It was also essential to shield the camera from the light emanating from the discharge tubes. Because of the great intensity of the helium yellow line at 5875.62 Å, a small filter was placed at the exit slit of the mirror where this radiation fell on the photographic film. A typical photographic record is shown in figure 1.

As shown by eq (1) only the changes in refractive index were measured, the initial indices at one bar were obtained from published data for benzene [3] and water [4]. Data of the required precision do not appear to be available for carbon tetrachloride, and its index was measured by the method of minimum deviation, the liquid being enclosed in a hollow glass prism [4].

[1] Figures in brackets indicate the literature references at the end of this paper.

736-657—64——5

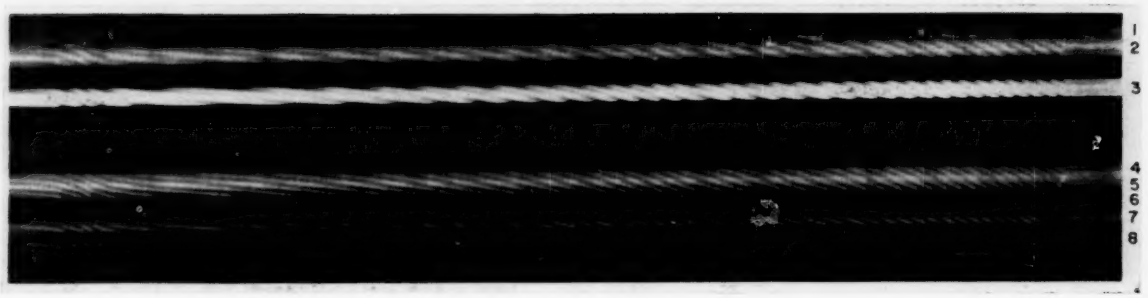

FIGURE 1. *Photograph of the shift in interference fringes for water from an elevated pressure to one atmosphere at constant temperature.*

Fringe shifts for eight spectral lines are shown: (1) A faint line, helium red of 6678.15 Å; (2) a strong line, cadium red of 6438.47 Å; (3) a very strong line, helium yellow of 5875.62 Å; (4), (5) two strong lines closely adjacent to each other, cadium green of 5085.82 Å and helium green of 5015.68 Å; (6) a very faint line, helium blue-green of 4921.93 Å; (7) a strong line, cadium blue of 4799.92 Å; (8) a strong line, cadium violet of 4678.16 Å.

3. Experimental Results

The experimental data for refractive index are given in tables 1, 2, and 3 as a function of pressure, temperature, and wavelength. It should be noted that the indices reported are absolute values. From previous experiments it has been found that the standard deviation of the index values is 0.00005 which corresponds to a limit of reproducibility of ± 0.0001 [1].

TABLE 1. *Absolute refractive index of benzene as a function of pressure, temperature, and wavelength*

Temperature	Pressure \ Wavelength Å / bars	6678.149	6438.4696	5875.618	5085.82	5015.675	4921.929	4799.92	4678.16	Specific volume
°C										ml/g
	1	1.49316	1.49455	1.49859	1.50704	1.50802	1.50941	1.51137	1.51350	1.14433
	250.1	1.50465	1.50616	1.51031	1.51891	1.51995	1.52139	1.52338	1.52557	1.11973
24.80	489.0	1.51413	1.51561	1.51982	1.52873	1.52969	1.53113	1.53320	1.52544	1.10057
	666.1	1.52021	1.52168	1.52593	1.53488	1.53593	1.53743	1.53952	1.54180	1.08828
	1	1.48684	1.48822	1.49221	1.50050	1.50151	1.50284	1.50477	1.50690	1.15805
	246.2	1.49879	1.50025	1.50438	1.51286	1.51391	1.51532	1.51724	1.51946	1.13187
34.50	484.8	1.50882	1.51029	1.51445	1.52316	1.52421	1.52557	1.52762	1.52986	1.11138
	757.2	1.51844	1.51991	1.52418	1.53305	1.53415	1.53555	1.53761	1.53992	1.09192
	1107.7	1.52903	1.53052	1.53489	1.54401	1.54514	1.54657	1.54867	1.55102	1.07112
	1	1.47390	1.47521	1.47910	1.48729	1.48817	1.48949	1.49128	1.49334	1.18757
	274.5	1.48888	1.49016	1.49422	1.50271	1.50361	1.50498	1.50681	1.50894	1.15350
54.34	484.4	1.49832	1.49972	1.50382	1.51251	1.51340	1.51483	1.51672	1.51889	1.13305
	770.2	1.50913	1.51060	1.51478	1.52362	1.52460	1.52606	1.52798	1.53018	1.11014
	1124.5	1.52059	1.52202	1.52633	1.53546	1.53644	1.53790	1.53988	1.54214	1.08705

TABLE 2. *Absolute refractive index of carbon tetrachloride as a function of pressure, temperature, and wavelength*

Temperature	Pressure \ Wavelength Å / bars	6678.149	6438.4696	5875.618	5085.82	5015.675	4921.929	4799.92	4678.16	Specific volume
°C										ml/g
	1	1.45476	1.45556	1.45791	1.46270	1.46322	1.46400	1.46511	1.46626	0.630927
	276.9	1.46762	1.46846	1.47089	1.47583	1.47635	1.47721	1.47831	1.47951	.614859
24.80	523.6	1.47706	1.47790	1.48037	1.48542	1.48598	1.48674	1.48794	1.48917	.603465
	797.4	1.48599	1.48683	1.48934	1.49404	1.49509	1.49591	1.49712	1.49835	.592991
	1116.7	1.49502	1.49591	1.49847	1.50371	1.50429	1.50515	1.50639	1.50767	.582760
	1	1.44890	1.44965	1.45197	1.45675	1.45723	1.45802	1.45908	1.46020	.638553
	255.4	1.46164	1.46243	1.46481	1.46975	1.47022	1.47104	1.47214	1.47329	.622336
34.50	480.9	1.47102	1.47182	1.47426	1.47928	1.47980	1.48059	1.48172	1.48292	.610937
	756.1	1.48045	1.48130	1.48381	1.48896	1.48949	1.49031	1.49146	1.49271	.599476
	1119.9	1.49098	1.49186	1.49441	1.49973	1.50028	1.50109	1.50229	1.50360	.587098
	1	1.43763	1.43844	1.44067	1.44534	1.44581	1.44663	1.44774	1.44879	.654959
	248.7	1.45181	1.45266	1.45493	1.45978	1.46025	1.46110	1.46225	1.46335	.636227
54.34	452.7	1.46107	1.46193	1.46428	1.46924	1.46975	1.47059	1.47176	1.47289	.624227
	751.9	1.47281	1.47371	1.47616	1.48118	1.48172	1.48257	1.48376	1.48497	.610060
	1059.2	1.48280	1.48371	1.48617	1.49135	1.49190	1.49281	1.49402	1.49520	.598302

TABLE 3. *Absolute refractive index of water as a function of pressure, temperature, and wavelength*

Temperature	Pressure / Wavelength	6678.149 Å	6438.4696 Å	5875.618 Å	5085.82 Å	5015.675 Å	4921.929 Å	4799.92 Å	4678.16 Å	Specific volume
°C	bars									ml/g
24.80	1	1.33077	1.33136	1.33293	1.33591	1.33624	1.33670	1.33734	1.33802	1.00288
	259.6	1.33438	1.33499	1.33653	1.33953	1.33987	1.34030	1.34096	1.34167	0.99152
	463.6	1.33714	1.33780	1.33943	1.34240	1.34278	1.34324	1.34389	1.34458	.98318
	762.8	1.34106	1.34163	1.34322	1.34630	1.34660	1.34710	1.34778	1.34846	.97180
	1108.6	1.34521	1.34581	1.34748	1.35053	1.35085	1.35133	1.35201	1.35271	.95973
34.50	1	1.32963	1.33020	1.33177	1.33474	1.33506	1.33552	1.33615	1.33683	1.00580
	259.3	1.33319	1.33375	1.33531	1.33830	1.33865	1.33908	1.33974	1.34043	0.99463
	480.9	1.33614	1.33679	1.33832	1.34132	1.34163	1.34213	1.34274	1.34344	.98572
	799.2	1.34007	1.34069	1.34228	1.34537	1.34567	1.34613	1.34676	1.34747	.97385
	1110.0	1.34367	1.34429	1.34589	1.34897	1.34928	1.34974	1.35042	1.35116	.96318
54.34	1	1.32655	1.32712	1.32866	1.33159	1.33191	1.33236	1.33299	1.33366	1.01415
	241.6	1.32985	1.33043	1.33192	1.33490	1.33523	1.33567	1.33633	1.33698	0.00372
	489.7	1.33307	1.33361	1.33518	1.33813	1.33849	1.33893	1.33960	1.34028	0.99371
	785.1	1.33667	1.33725	1.33883	1.34184	1.34216	1.34258	1.34327	1.34396	.98267
	1127.7	1.34053	1.34116	1.34274	1.34577	1.34609	1.34656	1.34718	1.34791	.97089
1.56	1	1.33220	1.33279	1.33438	1.33739	1.33772	1.33832	1.33882	1.33951	1.00004
	269.5	1.33635	1.33697	1.33857	1.34161	1.34197	1.34254	1.34305	1.34374	0.98712
	507.4	1.33989	1.34047	1.34212	1.34517	1.34552	1.34615	1.34663	1.34734	.97662
	768.5	1.34356	1.34415	1.34579	1.34887	1.34923	1.34985	1.35034	1.35106	.96577
	1049.7	1.34721	1.34785	1.34947	1.35255	1.35296	1.35359	1.35408	1.35479	.95522
7.64	1	1.33204	1.33263	1.33422	1.33724	1.33757	1.33803	1.33867	1.33935	1.00011
	256.1	1.33586	1.33645	1.33804	1.34108	1.34139	1.34186	1.34252	1.34325	0.98820
	497.8	1.33940	1.34002	1.34160	1.34466	1.34502	1.34544	1.34614	1.34688	.97788
	730.7	1.34267	1.34324	1.34494	1.34801	1.34828	1.34877	1.34944	1.35073	.96853
	1088.9	1.34698	1.34764	1.34928	1.35243	1.35273	1.35318	1.35391	1.35462	.95682

It will be noted in tables 1–3 that the behavior at each wavelength is similar to that reported earlier for observations using the helium yellow line, i.e., index increases with increasing pressure and decreases with increasing temperature. In addition it can be noted that in all cases the change in index with pressure is greater in the violet end of the spectrum than in the red end with the effect of wavelength being much smaller in water than in the organic liquids. There is some indication that the effect of wavelength is greater at higher temperatures for all three liquids. These results will be discussed in detail later.

4. Discussion

The data given in tables 1 through 3 can be analyzed by various methods. The obvious treatment is by one of the well-known dispersion relationships. From quantum mechanical considerations of the interaction between radiation and matter Kramers and Heisenberg have derived the equation

$$\mu^2-1=\sum_i \frac{e^2 f_i N_i}{m\pi(\nu_i^2-\nu^2)} \qquad (2)$$

where μ is the index of radiation of frequency ν, N_i the number of oscillators per unit volume, f_i the oscillator strength and e and m the charge and rest mass of the electron. This relationship takes the same form as the older, classical relationship developed by Drude where the optical electrons were regarded as being quasi-elastically bound to the nucleus. Despite the formal similarity of the two equations, the interpretation for ν_i in each case is different. In the Drude formulation the ν_i represent resonance frequencies of *different* electrons with different binding energies. In the Kramers-Heisenberg treatment the ν_i are values of the transition frequencies between states for the electronic system.

When an electric field at optical frequencies is applied to a dielectric the effective field which acts upon a given oscillator at the interior of the medium consists of the applied field plus the field created by the surrounding dipoles. In the usual derivation of the Drude formula no specific value is assigned to this polarization field, but Krishnan and Roy [5] have pointed out that the ν_i's, the fundamental absorption frequencies of the medium *include* the effect of the polarization field. On the other hand, according to the well-known Lorentz-Lorenz formula, the polarization field for a medium having cubic symmetry (or completely random symmetry as in a liquid) has been calculated to have the value $(4/3)\,\pi P$ where P is the polarization of the medium. Accepting this calculation the Lorentz-Lorenz equation has the form

$$\frac{\mu^2-1}{\mu^2+2}=\sum_i \frac{e^2}{3m\pi}\frac{f_i N_i}{(\Omega_i^2-\nu^2)} \qquad (3)$$

where the characteristic frequencies, the Ω_i's that appear, correspond to those of *isolated oscillators* unaffected by the polarization field.

Thus the Drude and the Lorentz-Lorenz equations are alternative formulas for the refractive index of a dense medium as a function of the frequency, the effect of the polarization field being taken into account in each equation in a different way. In order to visualize the effect of intermolecular interactions, it was decided to try to fit the experimental data to each of these dispersion formulas.

4.1. Benzene and Carbon Tetrachloride

If only a single term of an equation of the Drude type is used, the equation can be transformed into the following linear form

$$\frac{1}{\mu^2-1}=\frac{1}{A}(\nu_0^2-\nu^2) \tag{4}$$

where ν_0 is the absorption frequency and ν, the frequency at which μ applies; the factors other than $(\nu_i^2-\nu^2)$ which appear in eq 2 have been designated by A. Using the measured values of μ and the known frequencies it was found that for both benzene and carbon tetrachloride eq (4) satisfactorily represented the data with a residual standard deviation of $1/(\mu^2-1)$ of about 1×10^{-4} based on 6 deg of freedom. The curve fitting which was done on the computer yielded the values for the constants of eq (4) shown in tables 4 and 5 for benzene and carbon tetrachloride.

TABLE 4.—*Parameters of the Drude dispersion equation for benzene*

Temperature	Pressure bars	Specific volume	A x 10^{-31} [cycles/sec]^2	$A(V_p)$ x 10^{-31} [cycles/sec]^2 x ml/g	Fundamental frequency, ν_0 x 10^{-15}	Fundamental wavelength, λ_0
°C		ml/g			c/s	Å
	1	1.14433	0.543360	0.621783	2.1498	1394.6
	250.1	1.11973	.555574	.622093	2.1441	1398.2
24.80	489.0	1.10057	.565792	.622694	2.1399	1401.0
	666.1	1.08828	.572260	.622779	2.1371	1402.8
	1	1.15805	.537099	.621987	2.1537	1392.0
	246.2	1.13187	.549012	.621410	2.1463	1396.8
34.50	484.8	1.11138	.561588	.624138	2.1451	1397.6
	757.2	1.09192	.571678	.624227	2.1402	1400.8
	1107.7	1.07112	.581631	.622997	2.1329	1405.6
	1	1.18757	.522458	.620455	2.1583	1389.0
	274.5	1.15350	.538693	.621382	2.1517	1393.3
54.34	484.4	1.13305	.547908	.620807	2.1455	1397.3
	770.2	1.11014	.559651	.621624	2.1413	1400.1
	1124.5	1.08705	.571543	.621296	2.1349	1404.2

TABLE 5. *Parameters of the Drude dispersion equation for carbon tetrachloride*

Temperature	Pressure bars	Specific volume	A x 10^{-31} [cycles/sec]^2	$A(V_p)$ x 10^{-31} [cycles/sec]^2 x ml/g	Fundamental frequency, ν_0 x 10^{-15}	Fundamental wavelength, λ_0
°C		ml/g			c/s	Å
	1	0.630927	0.79919	0.50423	2.7131	1105.0
	276.9	.614859	.81931	.50376	2.7022	1109.4
24.80	523.6	.603465	.83860	.50607	2.7015	1109.7
	797.4	.592991	.85571	.50743	2.6991	1110.7
	1116.7	.582760	.86741	.50549	2.6879	1115.3
	1	.638553	.78865	.50359	2.7159	1103.8
	255.4	.622336	.81091	.50466	2.7089	1106.7
34.50	480.9	.610937	.82840	.50610	2.7055	1108.1
	756.1	.599476	.83943	.50322	2.6918	1113.7
	1119.9	.587098	.85388	.50131	2.6802	1118.5
	1	.654959	.76030	.49797	2.7072	1107.4
	248.7	.636227	.78591	.50002	2.7012	1109.9
54.34	452.7	.624227	.79956	.49911	2.6922	1113.6
	751.9	.610060	.82203	.50149	2.6893	1114.8
	1059.2	.598302	.83820	.50150	2.6822	1117.7

The derived value of the constant, A will vary with the density through its dependence on N. If it is assumed that $A(V_p)$ is constant where V_p is specific volume, then the density dependence can be eliminated and the values so obtained are given in column 5 of the tables. It can be observed from these values that there is no apparent systematic trend with either P or T. Because the lack of such a trend means that the oscillator strength is constant within the limits of error of the evaluation, it seems reasonable to assume that the oscillator strength is, in fact, constant. On the other hand the values of ν_0, the absorption frequency, derived from eq (4) and given in column 6 show a systematic shift to lower frequencies with increasing pressure. The values of the absorption frequencies derived are in the region where absorption is to be expected [6] and the shift with pressure is of the order of 10 Å/kb. However, this rate of shift is approximately twice the value observed by Oksengorn [7] for the benzene band in the region of 2500 Å although it is in the same direction. There do not appear to be data available for carbon tetrachloride for shifts with pressure.

From these findings it is apparent that the change of index with pressure can be described quantitatively by an equation of the Drude type in which the oscillator strength remains constant, but the apparent absorption frequency shifts to longer wavelengths at higher pressure. By plotting the fundamental wavelengths derived from eq (4) against the specific volume, an attempt was made to find the effect upon the fundamental absorption wavelength due solely to temperature. These plots are shown for benzene and carbon tetrachloride in figures 2 and 3. It was not found possible to evaluate the purely temperature effect in either case because of the scatter of the data. From the figures, however, it seems not unlikely that temperature effects of a small order of magnitude exist. These effects are to be attributed to the changes in the local field due to interaction between neighboring molecules at constant density.

The data for benzene and carbon tetrachloride were also fitted to a single term equation of the Lorentz-Lorenz type by inserting into the following linear form.

$$\frac{\mu^2+2}{\mu^2-1}=\frac{1}{B}(\Omega_0^2-\nu^2) \tag{5}$$

where Ω_0 is the fundamental absorption frequency of an isolated oscillator. The factors other than $(\Omega_i^2-\nu^2)$ which appear in eq (3) have been designated by B. The fittings were poorer than those obtained in using a single term Drude-type equation, because in each fitting of the data for a set of eight spectral lines the residual standard deviations of $(\mu^2+2)/(\mu^2-1)$ varied from 2×10^{-4} to 4×10^{-4} for benzene and from 1×10^{-4} to 4×10^{-4} for carbon tetrachloride which deviations are outside the experimental error. The values of the constants appearing in eq (5) are given in tables 6 and 7. In column 5 of these tables values of $B(V_p)$ are given, and it may be observed that there is no systematic trend with either P or

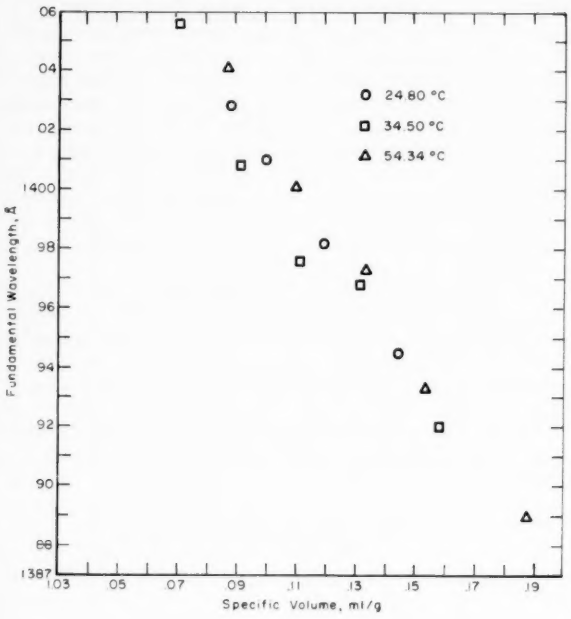

FIGURE 2. *Fundamental wavelength versus specific volume for benzene at three different temperatures.*

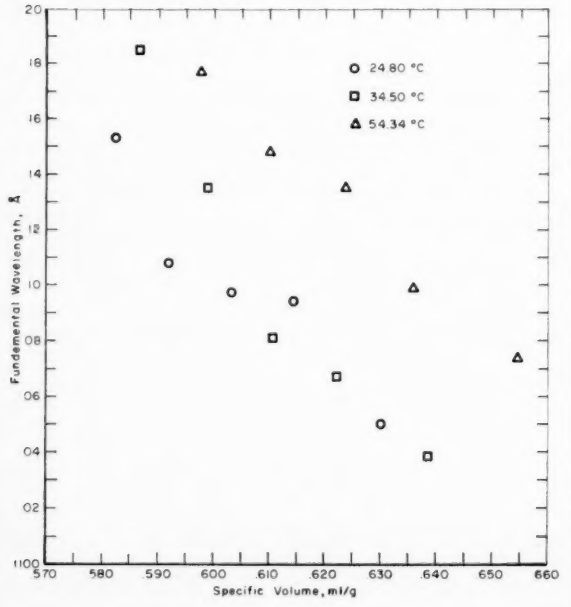

FIGURE 3. *Fundamental wavelength versus specific volume for carbon tetrachloride at three different temperatures.*

T so that it may be inferred again that the oscillator strength is constant within the limits of error of the evaluation. Although there is some scatter in the results, it appears that the values of Ω_0 given in column 6 show a trend toward higher frequencies with increasing pressure, in which case the shift is opposite in direction from that found earlier using a Drude-type equation.

TABLE 6. *Parameters of the Lorentz-Lorenz dispersion equation for benzene*

Temperature	Pressure bars	Specific volume	B x 10^{-31} [cycles/sec]^2	$B(V_p)$ x 10^{-31} [cycles/sec]^2 x ml/g	Fundamental frequency, Ω_0 x 10^{-15}	Fundamental wavelength λ_0
°C		ml/g			c/s	Å
24.80	1	1.14433	0.181121	0.207262	2.5363	1182.0
	250.1	1.11923	.185191	.207364	2.5395	1180.5
	489.0	1.10057	.188597	.207564	2.5427	1179.0
	666.1	1.08828	.190755	.207595	2.5445	1178.2
34.50	1	1.15805	.179033	.207329	2.5355	1182.4
	246.2	1.13187	.183004	.207137	2.5371	1181.6
	484.8	1.11138	.187196	.208046	2.5442	1178.3
	757.2	1.09192	.190559	.208075	2.5468	1177.1
	1107.7	1.07112	.193877	.207666	2.5472	1177.0
54.34	1	1.18757	.174153	.206819	2.5298	1185.0
	274.5	1.15350	.179564	.207127	2.5348	1182.7
	484.4	1.13305	.182636	.206936	2.5356	1182.3
	770.2	1.11014	.186650	.207208	2.5400	1180.3
	1124.5	1.08705	.190514	.207098	2.5422	1179.3

TABLE 7.—*Parameters of the Lorentz-Lorenz dispersion equation for carbon tetrachloride*

Temperature	Pressure bars	Specific volume	B x 10^{-31} [cycles/sec]^2	$B(V_p)$ x 10^{-31} [cycles/sec]^2 x ml/g	Fundamental frequency, Ω_0 x 10^{-15}	Fundamental wavelength, λ_0
°C		ml/g			c/s	Å
24.80	1	.630927	.266398	0.168078	3.1662	946.9
	276.9	.614859	.273104	.167920	3.1675	946.7
	523.6	.6003465	.279532	.168688	3.1771	943.6
	797.4	.592991	.285237	.169143	3.1840	941.6
	1116.7	.582760	.289136	.168497	3.1806	942.6
34.50	1	.639553	.262884	.167865	3.1631	947.8
	255.4	.622336	.270304	.168220	3.1688	946.1
	480.9	.610937	.276132	.168699	3.1750	944.2
	756.1	.599476	.279182	.167363	3.1692	946.0
	1119.9	.587098	.284625	.167103	3.1670	946.6
54.34	1	.654959	.253433	.165988	3.1406	954.6
	248.7	.636227	.261969	.166772	3.1490	952.0
	452.7	.624227	.266519	.166368	3.1485	952.2
	751.9	.610960	.274010	.167163	3.1579	949.3
	1059.2	.598302	.279401	.167166	3.1604	948.6

4.2. Water

A single term Drude-type dispersion equation will not fit the data for water within the experimental error, even though the dispersion for water is less than for the organic liquids. The results of the fitting processes showed that the residual standard deviations varied from 2×10^{-4} to 3×10^{-4}. In order to obtain a satisfactory fit a second term was required involving an absorption in the infrared. This frequency and its shift with pressure and temperature was obtained from the data of Giguère and Harvey [8] and Fishman and Drikamer [9]. Using the two-term equation, the data were fitted to within the experimental error and the derived values are

given in table 8. In contrast with the results obtained for benzene and carbon tetrachloride there is no systematic trend in the absorption frequency, and there appears to be a random fluctuation in the derived values. The effect of pressure on dispersion is much smaller than in the organic liquids and apparently the effect is lost by internal compensation in the curve fitting process.

TABLE 8. *Parameters of the Drude dispersion equation for water*

Temperature	Pressure bars	Specific volume	A $\times 10^{-31}$ [cycles/sec]^2	$A(V_p)$ $\times 10^{-31}$ [cycles/sec]^2 $\times$ ml/g	Fundamental frequency, ν_0 $\times 10^{-13}$	Fundamental wavelength, λ_0
°C		ml/g			c/s	Å
24.80	1	1.00288	0.75220	0.75437	3.1293	958.0
	259.6	0.99152	.75116	.74479	3.1278	958.5
	463.6	.98318	.74886	.73626	3.1086	964.4
	762.8	.97180	.76509	.74351	3.1215	960.4
	1108.6	.95973	.77690	.74561	3.1235	959.8
34.50	1	1.00580	.73536	.73963	3.1204	960.8
	259.3	0.99463	.74742	.74341	3.1265	958.9
	480.9	.98572	.75922	.74838	3.1349	956.3
	799.2	.97385	.76336	.74340	3.2290	960.0
	1110.0	.96318	.77383	.74534	3.1253	959.2
54.34	1	1.01415	.73179	.74214	3.1293	958.0
	241.6	1.00372	.74346	.74623	3.1360	956.0
	489.7	0.99371	.75017	.74545	3.1328	956.9
	785.1	.98267	.76033	.74715	3.1345	956.4
	1127.7	.97089	.77127	.74882	3.1363	955.9

Likewise, it was not found possible to fit the data for water to a single term equation of the Lorentz-Lorenz type; the residual standard deviations were found to vary from 6×10^{-4} to 10×10^{-4}. No attempt was made to fit the data to a Lorentz-Lorenz equation with two terms. Krishnan and Roy [5] have pointed out that the fundamental frequencies, the ν_i's that appear in the Drude equation are the experimentally observed absorption bands, and, although it would have been possible to take the data of Giguère and Harvey [8] and Fishman and Drikamer [9] and convert the ν_i's to the Ω_i's of the Lorentz-Lorenz equation, it appeared that the results would be too tenuous. The data on water can be considered from a somewhat different viewpoint as follows:

Many of the abnormalities of liquid water can be rationalized by the concept initially advanced by Röntgen [10] that water could be considered as a mixture of molecules of different degrees of association. In its simplest form this concept considers two types of water molecules, one having a greater density than the other with the relative proportions of the two types being influenced by temperature and pressure. The less dense form may be considered as analogous to the ice molecule which forms from water with an increase in volume. Many workers [11] have attempted to estimate the percentages of the types of molecules, but there is no agreement on either the size or percentage of the various species as the temperature is varied. It is generally accepted that the relative proportion of the less dense icelike molecules decreases with increasing temperature [11, 12]. Bridgman [13] from studies of viscosity at elevated pressure and Tammann from PVT data on water [14] concluded that the proportion of the less dense species also decreased with increasing pressure. Insofar as the index of refraction is concerned, there is no anomaly at the maximum density point and it is possible to regard the index of water as arising from the indices of its components using certain assumptions regarding the refractivity of the components [see Chéneveau, 12]. Such computations have been made with the present data and produce results in general agreement with those of previous workers [11, 12]. These data will not be reproduced here. It will suffice to note that, as shown earlier, for the wavelength of the helium yellow line [see reference 1, fig. 4] a plot of index against specific volume for water shows that the data separate into definite isotherms. At a constant specific volume the decrease in index with rising temperature is in full accord with the concept that there is a decrease in the relative proportion of the less dense molecules which have the higher refractivity.

4.3. Theoretical Considerations

These data on index of refraction are suitable for an analysis of the type proposed by Ramachandran [15, 16] who studied the thermo-optic behavior of solids. He assumed that the oscillator strength is invariant with changes in density and temperature, an assumption verified in part by the data of tables 4, 5, and 8 for the liquids studied here. He attributes the change in index with changing temperature to, partly, a change in the number of oscillators per unit volume (density effect) and partly a change in the absorption frequency arising from either change in density or change in temperature.

The data may be treated in a simpler manner and more analytically according to the method of Ramachandran and Radhakrishnan [16, 17] where the analysis proceeds as follows: starting with a simplified Drude equation applicable to a single wavelength they divide $d\mu/dT$, the observed change in index with temperature into three parts defined as (1) the change due to the number of oscillators per unit volume, (2) the change in polarizability of the oscillators arising from the change in density and (3) the change in polarizability due solely to the temperature change. Denoting these by P, Q, and R respectively they deduce the following values.

$$P=-\gamma\left(\frac{\mu^2-1}{2\mu}\right) \tag{6}$$

$$Q=-\gamma\left[\rho\left(\frac{d\mu}{d\rho}\right)-\frac{\mu^2-1}{2\mu}\right] \tag{7}$$

$$R=d\mu/dT+\gamma\rho(d\mu/d\rho) \tag{8}$$

where ρ is the density, μ the index, T the temperature and

$$\gamma=-\frac{1}{\rho}\frac{d\rho}{dT} \text{ and } d\mu/dT=P+Q+R.$$

In figures 4, 5, and 6 values of $(\mu^2-1)/\rho$ for the three liquids are given as a function of wavelength at 34.50 °C. This temperature was chosen because of the fact that the pressure range for benzene at 24.80 °C is limited by the freezing of benzene. The fact that the curves do not coincide for any of the liquids is indicative of the fact that the polarization field has changed due to the change in intermolecular spacing at the elevated pressures. The fact that the values for the higher pressures always are above the values at one bar can be explained by the fact that the increase in density brings about an increase in the strength of the polarization field acting upon an individual scattering center. The shift to longer wavelengths of the absorption frequency as the pressure increases in benzene and carbon tetrachloride is another manifestation of the same phenomenon. It is of interest to note that although no shift of absorption frequency could be detected in table 8 for water, figure 6 shows the same general picture for water as for the other liquids, the effect being much smaller with water. In fact, his discrepancy arises in part from the lower compressibility of water, but if comparisons are made for equal changes in volume it will be found that the separation of the curves for water is still much less than for benzene and carbon tetrachloride. The overall picture indicated by these figures can be obtained quantitatively by the use of eqs (6), (7), and (8). Such values are given in table 9 along with comparable values for cubic crystals [16, 17].

It will be noted that P, the purely density contribution, is much larger for the liquids than for most crystals. This is due largely to the fact that the expansivities of the liquids are larger than the crystals in most instances.

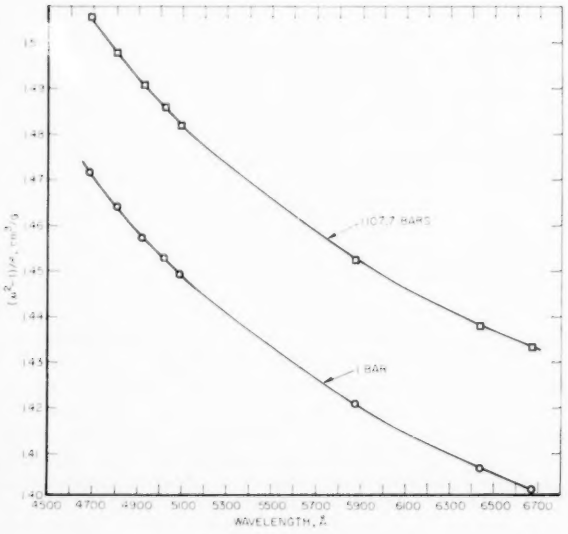

FIGURE 4. *$(\mu^2-1)/\rho$ versus wavelength at one bar and an elevated pressure for benzene at 34.50 °C.*

Q represents the change in refractive index arising from change in the polarizability of an oscillator which is brought about by change in volume. Q must also include the change in the polarization field acting upon a given oscillator which is likewise induced by change in volume. Q is opposite in sign for the liquids and the crystals. The values of Q for benzene and carbon tetrachloride are much larger in absolute value than values of Q for the solids, a fact probably due to the disparity in the values of the expansivities of liquid and solid. The value of Q for water is inordinately low in comparison with the Q values for the other two liquids. This observation may be explained by the fact that (1) the water is less compressible than the other two liquids, and there is a correspondingly smaller change in the local field, and (2) there is a smaller percentage of icelike molecules at higher pressures.

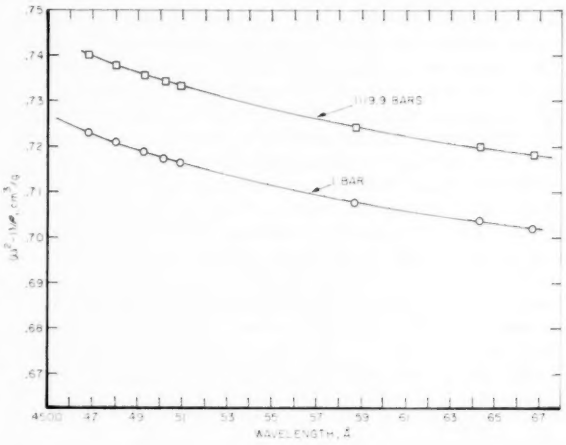

FIGURE 5. *$(\mu^2-1)/\rho$ versus wavelength at one bar and an elevated pressure for carbon tetrachloride at 34.50 °C.*

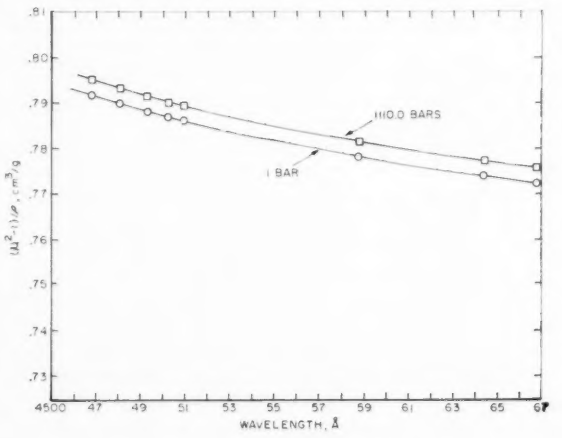

FIGURE 6. *$(\mu^2-1)/\rho$ versus wavelength at one bar and an elevated pressure for water at 34.50 °C.*

TABLE 9. *Values of γ, P, Q, and R for crystals and liquids**

Crystals	$\gamma \times 10^5$	$P \times 10^5$	$Q \times 10^5$	$R \times 10^5$
LiF	10.2	−3.4	2.4	−0.3
NaCl	12	−5.4	2.5	−0.9
KCl	11.4	−4.7	2.1	−1.0
KBr	12	−5.6	1.4	−0.2
KI	13.5	−7.2	1.4	+0.8
CaF_2	5.7	−2.1	0.7	+0.2
MgO	3.9	−2.2	3.6	+0.2
Diamond	1.3	−1.3	1.66	+0.6
Liquids				
C_6H_6	122.1	−50.8	−14.4	0
CCl_4	123.1	−47.5	−13.6	4.1
H_2O	25.2	−7.4	−0.6	−2.4

NOTE: The values for the crystals were derived from measurements made at 5893 Å while measurements on the liquids were made at 5876 Å, but the differences incurred are negligible.

*The data on crystals which are given in this table are taken from the book by R. S. Krishnan. See reference [16].

R in table 9 represents the contribution to refractive index which may be attributed solely to temperature change. It has been found heretofore for crystals that R may be of either sign and is usually two or three times smaller than Q in absolute value. In accordance with these results R is much less than Q for carbon tetrachloride and R was not measurable for benzene although it probably exists. For water, the high absolute value of R in comparison with the absolute value of Q is in keeping with the thought that at constant specific volume an increase in temperature causes a decrease in the proportion of icelike molecules with their high refractivity.

Some idea of the consistency of the data may be obtained as follows: a graph of index versus specific volume of water at one bar for the helium yellow line is given in figure 7. The data used were reported by Tilton [4]. At the specific volume of 1.00007 ml/g, which occurs at 1 °C and 7 °C, the change in refractive index with temperature is found to be $(\mu_{1\ °C}-\mu_{7\ °C})/6=2.18\times10^{-5}$/°C. At the corresponding specific volume for the temperature interval 1.56 °C to 54.34 °C. Where the specific volume is altered by compression [see ref. 1, fig. 4] a value of $(\mu_{1.56\ °C}-\mu_{54.34\ °C})/52.78=2.37\times10^{-5}$/°C, is obtained. The agreement between these results indicates that the same phenomenon is responsible for the data in the two cases. It is of interest to note that in the case of water both P and Q are zero at 4 °C because γ is zero at this temperature. Therefore, at 4 °C the quantity R is the only contributing factor to the change in index. From the data of Tilton [4] the value of the change in index with temperature at 4 °C is ascertained to be -2.1×10^{-5}/°C. Similar values of R based on the present data are at 1.56 °C, $R=-2.1\times10^{-5}$/°C; at 7.64 °C, $R=-2.2\times10^{-5}$/°C; and at 24.80 °C, $R=-2.4\times10^{-5}$/°C. The agreement between these data and the trends may be taken as indicative of the change in R with temperature.

In figures 8, 9, and 10, values of $(\mu^2-1)/(\mu^2+2)\rho$ for the three liquids are given as a function of wavelength at 34.50 °C. In these plots the effect of density has been accounted for in dividing by the factor ρ. Moreover, it must be borne in mind that in the Lorentz-Lorenz treatment the polarization field is assigned the calculated value of $(4/3)\pi P$. The fact that the two curves do not coincide on each plot may best be explained by assuming that an increase of density decreases the polarizability of

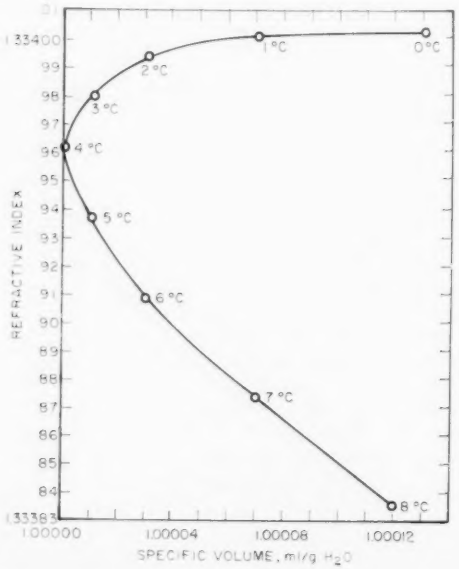

FIGURE 7. *Refractive index versus specific volume for water in the vicinity of the maximum density point at a pressure of one bar.*

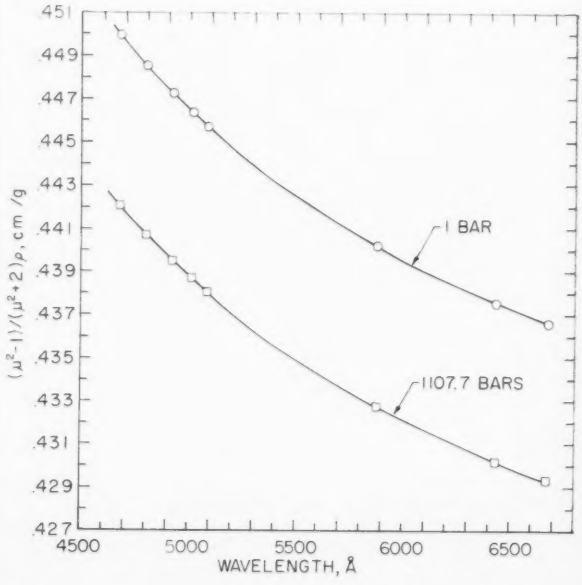

FIGURE 8. *$(\mu^2-1)/(\mu^2+2)\rho$ versus wavelength at one bar and an elevated pressure for benzene at 34.50 °C.*

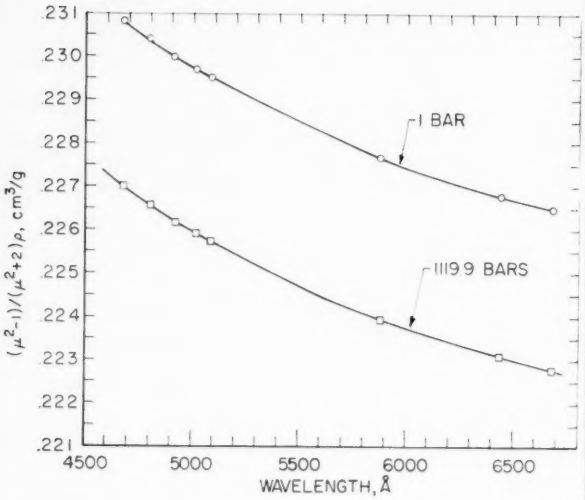

FIGURE 9. *$(\mu^2-1)/(\mu^2+2)\rho$ versus wavelength at one bar and an elevated pressure for carbon tetrachloride at 34.50 °C.*

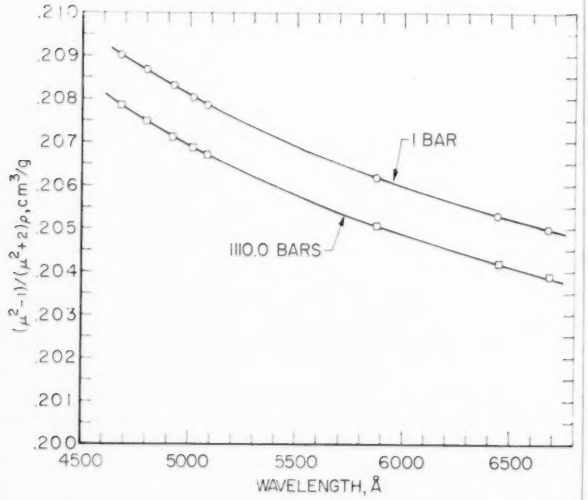

FIGURE 10. *$(\mu^2-1)/(\mu^2+2)\rho$ versus wavelength at one bar and an elevated pressure for water at 34.50 °C.*

the molecules. This assumption is a generalization of the rules of Fajans and Joos [18]; it is well known that the refraction of ions decreases as the distance of nearest neighbors gets smaller. Further, the assumption is in accord with the work of Ten Seldam [19] who has shown that the quantum mechanical theory of the atom-in-box model leads to a polarizability which decreases with increasing pressure.

It is interesting to compare these results with the results of investigations on solids. Pockels [20] has shown that for optical glasses the use of the Lorentz-Lorenz equation gives a considerably larger change of the index of refraction with density than do calculations made on the basis of photoelastic data. This discrepancy has also been noted in the study of crystals [21]. In fact for diamond [22] and MgO [23] the photoelastic data indicate that an increase in density results in an actual *decrease* in refractive index; i.e., in these crystals the contribution from decrease in polarizability of the ions must be even greater than the contribution from the increase in the number of ions per unit volume.

Mueller [24] has suggested that these changes in polarizability of solids are due to changes in energy levels and transition probabilities of optical electrons. Because the data for benzene and carbon tetrachloride indicate that the oscillator strengths (or transition probabilities) are constant within the limits of error of the evaluation, and because the fundamental absorption frequencies appear to show a trend toward higher values (see tables 6 and 7), it may be inferred that the failure of the curves to coincide in figures 8 and 9 is attributable essentially to changes in the energy levels, i.e., an increase in density creates a widening of the gap between the energy levels which determine the value of the fundamental absorption frequency.

In order to get a better understanding of the effect of density change at constant temperature in condensed phases one may compare an analysis of the data according to the Drude equation with an analysis according to the Lorentz-Lorenz equation, and then consider the situation both for the liquids studied here and for cubic crystals where data are available.

In figures 8, 9, and 10 (Lorentz-Lorenz equation) the curve representing the data at one bar lies above the curve for the data at an elevated pressure. The reverse of this order is shown by the curves in figures 4, 5, and 6 (Drude equation). In tables 6 and 7 (Lorentz-Lorenz equation) the fundamental absorption frequencies seem to show shifts towards higher values with increasing density; a shift in the opposite direction with increasing density appears to be the case in tables 4 and 5 (Drude equation).

In Table 9 (which represents an analysis according to Drude's equation but confined to one wavelength) the values of Q for crystals are always positive while the Q values for liquids are always negative. Burstein and Smith [21] have shown that for cubic crystals the experimentally determined change in refractive index is always smaller than the change calculated from either the Lorentz-Lorenz or Drude formulas.

From this evidence one might conclude that for both solids and liquids considered here a change in density produces two competing effects—a change in the polarization field and a change in the polarizability of the individual oscillator; in the liquids it is the first effect which is more important, while for the crystals the second effect is dominant. This situation is what one might reasonably expect considering the greater compressibility of the liquids.

The authors are indebted to Mr. Irving Malitson of the Refractometry Section of the National Bureau of Standards for his measurements of the refractive indices of carbon tetrachloride at one atmosphere.

5. References

[1] R. M. Waxler and C. E. Weir, J. Research NBS **67A** (Phys. and Chem.) No. 2, 163 (1963).
[2] J. B. Saunders, J. Research NBS **35,** 157 (1945) RP1668.
[3] A. F. Forziati, J. Research NBS **44,** 373 (1950) RP2085.
[4] L. W. Tilton and J. K. Taylor, J. Research NBS **20,** 419 (1938) RP1085.
[5] K. S. Krishnan and S. K. Roy, Phil. Mag. **43,** 1000 (1952).
[6] G. N. Lewis and M. Kasha, J. Am. Chem. Soc. **67–1,** 994 (1945).
[7] B. Oksengorn, Compt. rend. **242,** 2324 (1956).
[8] P. A. Giguère and K. B. Harvey, Canad. J. Chem. **34,** 798 (1956).
[9] E. Fishman and H. G. Drickamer, J. Chem. Phys. **24,** 548 (1956).
[10] W. C. Röntgen, Ann. d. Physik (Wied.) **45,** 91 (1892).
[11] N. E. Dorsey, Properties of ordinary water-substance (Reinhold Publishing Corp., New York, 1940).
[12] M. C. Chéneveau, Compt. rend. **156,** 1972 (1913).
[13] P. W. Bridgman, Proc. Am. Acad. Arts Sci. **61,** 57 (1926).
[14] G. Tammann, Z. Physik. Chem. **84,** 293 (1913); Z. anorg. Chem. **158,** 1 (1926).
[15] G. N. Ramachandran, Proc. Indian Acad. Sci. **A25,** 266 (1947).
[16] R. S. Krishnan, Progress in Crystal Physics, Volume I (Interscience Publishers, New York, London, 1958).
[17] G. N. Ramachandran and T. Radhakrishnan, Phil. Mag. **43,** 317 (1952).
[18] K. Fajans and G. Joos, Zeit. f. Physik. **23,** 1 (1924).
[19] C. A. Ten Seldam, Energies and Polarizabilities of Compressed Atoms (Van Gorcum & Co. N. Y., 1953).
[20] F. Pockels, Ann. d. Physik **7,** 745 (1902).
[21] E. Burstein and P. L. Smith, Proc. Indian Acad. Sci. **A28,** 377 (1948).
[22] G. N. Ramachandran, Proc. Indian Acad. Sci. **A32,** 171 (1950).
[23] E. Burstein, P. L. Smith, and B. Henvis, Phys. Rev. **73,** 1262 (1948).
[24] H. Mueller, Phys. Rev. **47,** 947 (1935).

(Paper 68A5–295)

JOURNAL OF RESEARCH of the National Bureau of Standards—A. Physics and Chemistry
Vol. 68A, No. 5, September-October 1964

Some Changes in Double-Bond Structure During the Vulcanization of Natural Rubber[1]

Frederic J. Linnig, Edwin J. Parks, and James E. Stewart[2]

(April 29, 1964)

Near-infrared studies indicate the absence or near-absence of isolated *cis* and terminal double bonds in rubber vulcanized either with or without accelerators, as well as in the squalene-sulfur reaction product. The use of purified natural rubber indicates a new absorption near 6.1 μ on reaction with sulfur, either with or without accelerators in the rubber system. This new absorption may be due either to a double bond with an attached sulfur atom or to conjugated double-bond systems that do not react readily with maleic anhydride. Ultraviolet spectra of chromatographic fractions show that squalene that has reacted with 15 percent of sulfur contains conjugated trienes, tetraenes, and possibly dienes, hexaenes, and heptaenes. The conjugated dienes, trienes, and tetraenes are probably present in sufficient proportions to account for a significant portion of the band at 10.4 μ. There is some evidence that the trienes and tetraenes, at least, may be largely all-*trans* in configuration. Other contributors to the band at 10.4 μ are possibly isolated, *trans* double bonds and heterocyclic sulfur structures along the chain.

1. Introduction

Evidence is accumulating that changes in double-bond structure occur during the vulcanization of natural rubber with sulfur. Sheppard and Sutherland [1][3] suggested that a band near 10.4 μ in the infrared spectrum of vulcanized rubber was due to an isolated *trans* double bond, indicating a shift of the original double bond. Recent work in our laboratory [2] has suggested the formation of conjugated double bonds. Consistent with our results, allo-ocimene, predominantly the *trans*-C_4, *cis*-C_6 isomer, a conjugated triene, has been isolated by Bateman et al. [3] from the reaction product of dihydromyrcene and sulfur. These authors also advanced evidence of other changes in double-bond structure [3].

The presence of conjugated double bonds in vulcanized rubber suggested [2] that they were, at least in part, responsible for the greater ease of oxidation of vulcanized rubber in comparison with unvulcanized rubber. Simple sulfur vulcanizates contain more conjugated double bonds and are more easily oxidized than accelerated vulcanizates. "Sulfurless" vulcanizates prepared with tetramethylthiuram disulfide [bis(dimethylthiocarbamoyl) disulfide] show no evidence of conjugation and are more stable than accelerated vulcanizates. The "sulfurless" and accelerated vulcanizates may, however, be somewhat stabilized by end products of the vulcanization. Other investigators [4] have related the differences in stability among these vulcanizates to differences in the assumed nature of the cross links.

The 10.4-μ band, if actually due to an isolated *trans* double bond, could indicate a 1,4 system which has been reported to be even more reactive towards oxygen than conjugated systems when attack is at the methylene carbon atom between the double bonds [5]. The presence of the 10.4-μ band in sulfur and accelerated vulcanizates and its absence in sulfurless vulcanizates are also consistent with the observed relative ease of oxidation of these vulcanizates.

Bateman et al. [3] indicated the presence of the 1,4 system among typical structures for cross-linked dihydromyrcene. These authors [3] also showed the presence of saturated structures and of ring structures containing a shifted double bond, but no adjacent original double bond and, hence, no 1,4 system.

The purpose of this paper is to examine more closely the possible changes in double-bond structure that occur during vulcanization.

2. Materials

(1) Natural rubber: NBS Standard Sample No. 385a.

(2) Highly purified natural rubber: No. 2103a obtained from United States Rubber Company.

(3) Synthetic *cis*-polyisoprene: "Coral" rubber made by Firestone Tire and Rubber Company.

(4) Squalene: (a) 98 percent, passed through silica gel, collected under nitrogen and stored under refrigeration. (b) 90 percent, passed through a column of silica gel; the best fractions were combined and an attempt was made at further purification by growing a single crystal, but, since the crystal was colored, the extent of purification was unknown. This sample also was stored under nitrogen and under refrigeration.

[1] This work was presented at the joint spring meeting of the American Chemical Society, Division of Rubber Chemistry and The Chemical Institute of Canada, Toronto, Canada, May, 1963, and in part, at the Pittsburgh Conference on Analytical Chemistry and Applied Spectroscopy, Pittsburgh, Pa., March 1962.

[2] Beckman Instruments, Inc., Fullerton, Calif.

[3] Figures in brackets indicate the literature references at the end of this paper.

3. Experimental Procedures

3.1. Sample Preparation

(1) Films of rubber were prepared by pressing the milled sample between two sheets of aluminum foil at 125 °C for about 1 min, using a pressure sufficient to give a film of suitable thickness, i.e., between 0.05 and 0.12 mm for infrared studies; three or four thicknesses were used for near-infrared studies. In general, accelerated stocks were vulcanized after the initial pressing for 24 hr, and unaccelerated stocks for 72 hr at 125 °C. Unless otherwise stated, all sulfur compounds contained 15 percent of NBS Standard Compounding Sulfur #371c, and accelerated compounds contained an additional 7 percent of accelerator.

(2) One squalene-sulfur reaction product was prepared as follows: Purified squalene 4(a) (8.44 g) and sulfur (1.52 g), purified by the method of Murphy, Clabaugh, and Gilchrist [6], were degassed five or six times, covered with about 0.7 atm of nitrogen, sealed in a glass container, and tumbled in an oven for 23 hr. Because the oven was vented, about 3 hr was required for the temperature to reach the reaction temperature of 150 °C after the sample had been introduced. The sample was held at 150 °C ±1.5 °C for 20 additional hours. A second squalene-sulfur reaction product was prepared in essentially the same manner with a 1.5 hr warmup period, using purified squalene 4(a) (8.47 g) and purified sulfur (1.54 g). A third squalene-sulfur reaction product, from 4(b) and 15 percent of compounding sulfur, was prepared by heating for 22.5 hr at 150 °C while nitrogen was bubbled through the mixture to exclude oxygen; this reaction product was used in the falling-film molecular distillation and in other studies.

3.2. Sample Treatment

(1) The first mentioned squalene-sulfur reaction product was separated chromatographically into 20 fractions, using a 50–50 (by weight) mixture of activated magnesia and diatomaceous earth [7]. The column was 20 cm long and packed in an 8-mm i.d. tube. Ten milligrams of the reaction product in 0.1 ml of spectrograde cyclohexane was added to the top of the column. After the material had been allowed to remain on the top of the column for a few minutes, the chromatogram was developed by adding about 14 ml of cyclohexane through the column, with intermittent suction, over a period of about 2.5 hr. The passage of the material down the column was followed by occasionally observing the fluorescence of the various fractions under an ultraviolet lamp. The fluorescent fractions progressed about 3.5 cm down the column. The remainder of the column and the material that passed through the column did not fluoresce. The upper part of the column was separated in terms of the six different, fluorescing zones (brown, tan, blue, white, blue, and yellow-green), and the remainder was cut into 13 arbitrary fractions, each 1.25 cm in length. The material passing through under these conditions was the 20th fraction. Each of the 20 fractions was dissolved in 3:1 cyclohexane-absolute ethanol and diluted to 5 ml. The absolute ethanol used was shown by its ultraviolet spectrum to have a low content of benzene. These solutions were diluted as much as 5:1 where necessary, and spectra of them were obtained between 210 and 500 or 600 mμ.

(2) The third squalene-sulfur reaction product was separated on a falling-film molecular distillation column at the temperature of boiling xylene (137–140 °C). Two distillate fractions were taken at different points along the column.

(3) (a) The second squalene–sulfur reaction product was reacted with maleic anhydride (Fisher certified reagent) as follows:

Sample No.	Reaction product (g)	Maleic anhydride (g)	Percent required, maleic anhydride	Reaction temperature
1	0. 2494	0. 0326	96	100
2	. 2266	. 0677	218	100
3	. 1999	----------	None	100
4	. 2559	. 0326	93	150
5	. 2337	. 0642	201	150
6	. 2874	----------	None	150

The percent of maleic anhydride required was based on the calculated percent of molecules containing conjugated dienes, trienes, and tetraenes, as determined from curve A in figure 5 and given in table 2. In all cases the reaction time was 5 hr. After reaction, it was possible to remove some unreacted maleic anhydride by heating under a vacuum in a hot-water bath.

(b) A film of NBS Standard Sample 385a, natural rubber, was vulcanized with 15 percent of sulfur for 20 hr at 150 °C. This film was put in a glass tube containing sufficient maleic anhydride to cover the film. The tube was evacuated, heated with a water bath above the melting point of the maleic anhydride, and degassed several times. The tube was sealed off, and the maleic anhydride was reacted with the vulcanized rubber for 70 hr at 100 °C. After reaction, the film was removed from the tube and rinsed several times with acetone.

3.3. Instruments Used

(1) Infrared spectra were obtained with a Perkin-Elmer Spectrophotometer Model 221, a grating-prism instrument, with the Model 21, and with the Infracord Model 137, all equipped with NaCl prisms.

(2) Near-infrared, ultraviolet, and visible spectra were obtained with a Beckman DK–1 spectrophotometer.

4. Results

4.1. Synopsis of Earlier Work

The following information was obtained in an earlier infrared study [2] of vulcanized rubber and the squalene-sulfur reaction product:

(1) The band at 10.4 μ was attributed to isolated, *trans* double bonds resulting from a shift of the original double bond.

(2) There was an increased absorption at 11.25 μ in the squalene–sulfur reaction product and not in vulcanized rubber. This absorption is probably related to terminal double bonds of the vinylidene type.

(3) New, small bands between 14 and 15 μ were related to skeletal vibrations, to C—S linkages, or to the hydrogen atoms on isolated, *cis* double bonds. It would appear that, if *trans* double bonds are formed as a result of a double-bond shift, *cis* double bonds should also be formed.

(4) A newly observed band at 6.25 μ that could be removed by reaction for 70 hr at 100 °C with maleic anhydride (done for the squalene–sulfur reaction product only) was related, therefore, to conjugated double bonds. Maleic anhydride reacts with conjugated double bonds to remove the conjugation.

(5) There was the appearance of an increased absorption near 6.1 μ, relative to the band at 6.0 μ, which could, however, be the result of a decreased absorption at 6.0 μ.

(6) The absorption near 6.1 μ in the original, unvulcanized material was found to result largely from an impurity.

In this and the following section, a number of points mentioned above will be further investigated and discussed.

4.2. Infrared Spectra

a. New Band Near 6.1 μ

Squalene and purified rubber, without definite absorptions near 6.1 μ, were used to determine whether a new band is produced here on reaction with sulfur.

As may be seen from figure 1, the band in the spectrum of the first squalene–sulfur reaction product at 6.10 μ (1639 cm^{-1}), cannot be related to anything in the spectrum of the unreacted squalene itself.

The difficulty with natural rubber is illustrated in figure 2 by the absorption at 6.15 μ (1626 cm^{-1}) in curve (A) for unvulcanized, natural rubber. This absorption, due largely to an impurity, manifests itself only as an unsymmetrical band with an irregularity on the long wavelength side in curve (B) for unvulcanized, purified rubber. The new band at 6.13 μ (1631 cm^{-1}) in curve (C) for purified natural rubber vulcanized with 15 percent of sulfur cannot be related to anything in the original material in curve (B). In this case, actual measurement, using a base-line technique, shows an increased absorbance at 6.13 μ and about the same absorbance near 6.0 μ

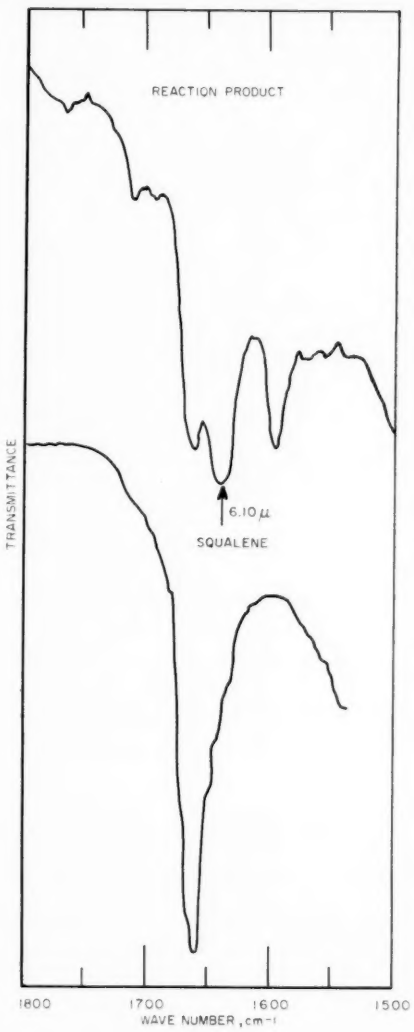

FIGURE 1. *Infrared spectra of squalene and first squalene-sulfur reaction product.*

(1666 cm^{-1}). Curves (D) and (E) are sulfur vulcanizates accelerated with ZnDBDC (zinc dibutyldithiocarbamate) and TMTD (tetramethylthiuram disulfide, NBS Standard Sample 374a), respectively. The small, sharp band at 6.13 μ is no longer present, but the measured absorbance at this wavelength is about the same in curves (C), (D), and (E). However, the absorbance at 6.0 μ is definitely greater in curves (D) and (E) than in curves (B) and (C). This, of course, might cause an increased absorbance near 6.13 μ through the effect of overlapping bands. On the other hand, absorbance is reduced near 6.0 μ in squalene after reaction with sulfur.

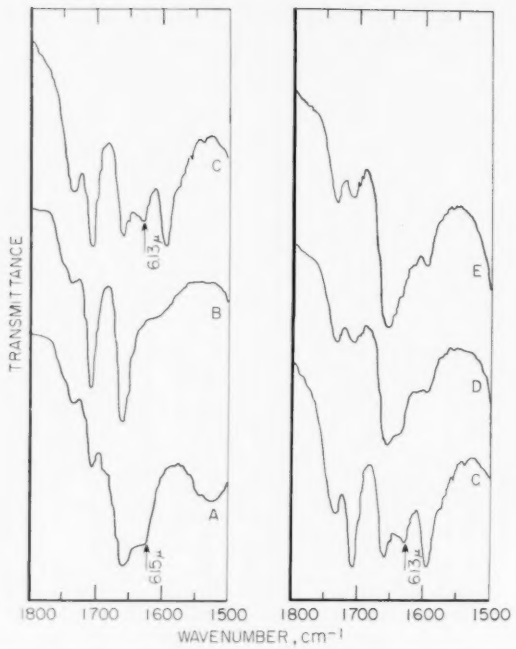

FIGURE 2. *Infrared spectra of unvulcanized and vulcanized natural rubber.*

A-unvulcanized NBS 385a, B-unvulcanized purified rubber, C-purified rubber vulcanized with 15 percent of sulfur, D-purified rubber vulcanized with 15 percent of sulfur and 7 percent of ZnDBDC, and E-purified rubber vulcanized with 15 percent of sulfur and 7 percent of TMTD.

Although the presence of a new band near 6.1 μ is not definite in the case of sulfur-vulcanized, unpurified rubber (NBS Standard Sample 385a), approximate measurements indicate increased absorbance at both 6.0 and 6.13 μ. Accelerated vulcanizates of NBS 385a show an increased absorbance at 6.13 μ and relatively small changes near 6.0 μ. The slight difference between 6.10 and 6.13 μ for the position of the band in the two systems may indicate the presence of two different groups.

Thus, it now appears likely that, as a result of vulcanization, there is new or increased absorption near 6.1 μ, even in the case of unpurified rubber.

b. Possible Interpretation of the 6.1-μ Band

This new absorption near 6.1 μ in vulcanized rubber and in the squalene-sulfur reaction product could be due to the *cis* double bonds or terminal double bonds mentioned earlier. Terminal double bonds of the vinylidene type, suggested by the increased absorption at 11.25 μ in the squalene–sulfur reaction product, may be partly responsible for the band at 6.1 μ in this case. According to Bellamy [8], *trans* double bonds absorb, on the average, very near 6.0 μ, where the original double bond absorbs, so that this structure should not be responsible for the new band. Substitution of sulfur for the hydrogen atoms on the original double bond should shift the carbon-to-carbon, double-bond stretching-frequency toward 6.1 μ or beyond. In fact, Mikawa [9] has found that methyl vinyl sulfide absorbs at 6.31 μ (1585 cm^{-1}). This type of structure is, therefore, a suggested cause of the new absorption. One other interpretation of the 6.1-μ band is that it is caused by conjugated double bonds. Two isomers of allo-ocimene, the *trans*-C_4, *trans*-C_6 and the *trans*-C_4, *cis*-C_6, have been reported by O'Connor and Goldblatt [10] to absorb at 6.06 and 6.08 μ, respectively. The *trans-cis* isomer was isolated from the dihydromyrcene-sulfur reaction product [3].

c. Relation of New Absorptions to Cross-linking

In an attempt to relate cross-linking to some of the new absorptions in the infrared spectra of the squalene–sulfur reaction-product, infrared spectra were obtained of the two distillate fractions and of the residue from the molecular distillation. The 6.25-μ band (related to conjugation) in the residue, presumably containing the cross-linked material, was stronger than in the distillates, which contained unreacted squalene and reacted monomolecular squalene [11]. The darker color of the residue is consistent with a higher concentration of conjugated double bonds. However, when allowances are made for the dilution effect of the unreacted material, as measured by the greater intensity of the characteristic bands at 6.0 and 12.0 μ in the distillates, it cannot definitely be concluded that there is a relationship between conjugation and cross-linking; it is, however, suggested. The band at 10.4 μ is probably somewhat stronger in both distillates than in the residue, but the shoulder on the long-wavelength side, at about 10.5 to 10.6 μ, is not as pronounced in the distillates. It is in this latter region that two of the tetrahydrothiophene ring compounds found in the dihydromyrcene–sulfur reaction product have been reported to absorb [12, 13].

d. Relation of Sulfur Content to the 6.25-μ Band

It has been found that, with NBS 385a, the intensity of the band at 6.25 μ, related to conjugation, increases with increased sulfur content up to about 20 percent, and then decreases with larger sulfur contents, with very little remaining at 32 percent of sulfur. On the other hand, with both purified rubber and the synthetic rubber, although there may be some decrease after a maximum at about 20 percent, a strong band still remains at 32 percent. This result is, presumably, due to the effect of the nonrubber constituents in the unpurified, natural rubber. An absorption still remains near 6.1 μ, even in purified rubber when vulcanized with 32 percent of sulfur. A band is present at this wavelength in both unpurified rubber and synthetic rubber vulcanized with 32 percent of sulfur.

4.3. Near-Infrared Spectra

Near-infrared studies have aided in clarifying the nature of the bands near 6.1 and 11.25 μ (in the squalene–sulfur reaction product only) and between 14 and 15 μ.

It will be noted in figure 3 that the spectrum of the first squalene–sulfur reaction product has a small band near 1.64 μ not exhibited in the unreacted squalene. This band is probably characteristic of terminal double bonds [14], and its presence is consistent with the increased absorption at 11.25 μ. A comparison of the two curves shows no evidence of a new absorption band in the lower curve, near 2.14 μ, characteristic of *cis* double bonds [14].

Curve A in figure 4 is of purified, natural rubber and contains no band at 1.64 or 2.14 μ. The absence of a band at 1.64 μ has been used by Fraga [15A] to indicate the absence of 3,4 structures in natural polyisoprenes. Binder [15B] from other evidence takes a contrary view. New absorption bands do not appear at 1.64 or 2.14 μ in curve B of purified rubber vulcanized with 15 percent of sulfur. Thus, the terminal double bonds in the squalene–sulfur reaction product are probably the result of end effects in the smaller molecule. There is only the barest suggestion of an absorption at 1.64 μ in curves C and D for vulcanizates accelerated with ZnDBDC and TMTD, respectively. Similar results are obtained when unpurified rubber (NBS 385a) is employed. Thus, except for the result of end effects in squalene, few or no *cis* or terminal double bonds result from reaction with sulfur, even in the presence of accelerators, and there cannot be much, if any, contribution of these structures to the band near 6.1 μ. Since there is no confirmatory evidence in the near-infrared of *cis* double bonds, the small bands between 14 and 15 μ are possibly due to skeletal vibrations or to C—S linkages.

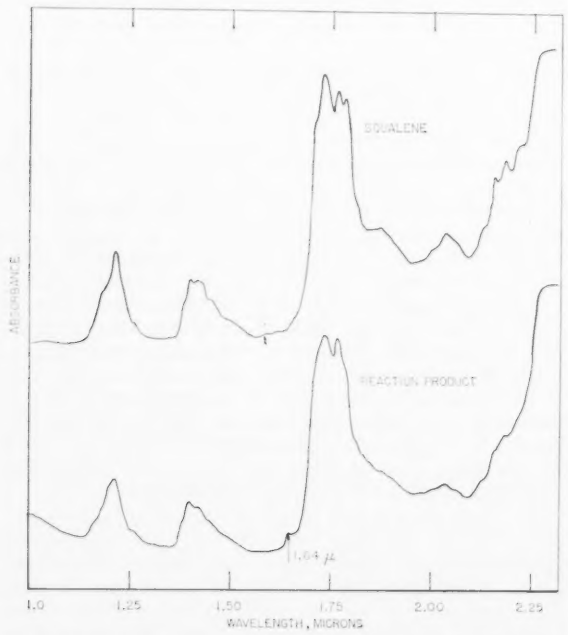

FIGURE 3. *Near-infrared spectra of squalene and squalene-sulfur reaction product: squalene, 200.4 g/liter; reaction product 203.7 g/liter; 1-cm path length.*

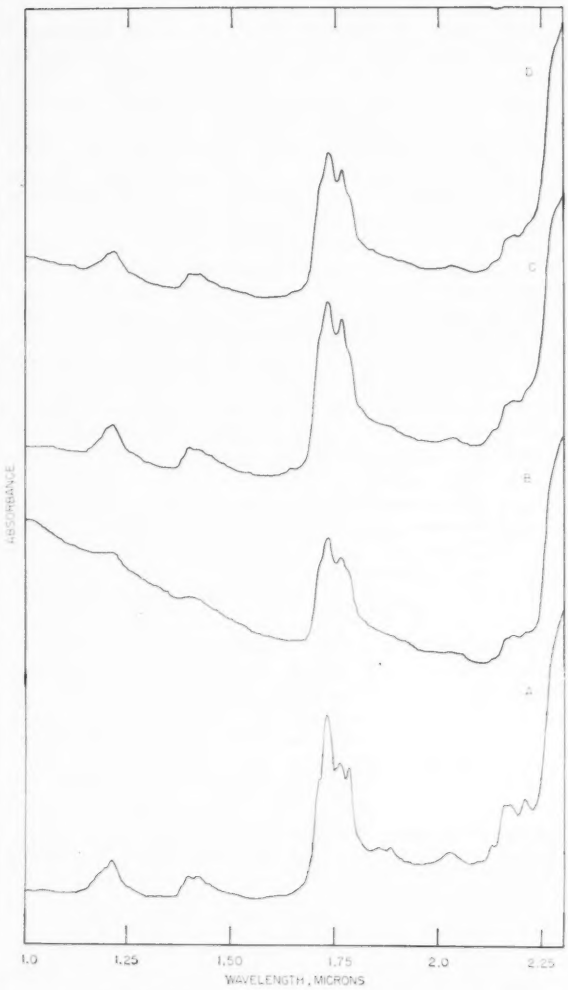

FIGURE 4. *Near-infrared spectra of unvulcanized and vulcanized purified natural rubber.*

A–unvulcanized rubber, B–rubber vulcanized with 15 percent of sulfur, C–rubber vulcanized with 15 percent of sulfur and 7 percent of ZnDBDC, and D–rubber vulcanized with 15 percent of sulfur and 7 percent of TMTD.

4.4. Ultraviolet Spectra and Chromatography

Vulcanized rubber and the squalene–sulfur reaction product presumably contain conjugated systems [2], free sulfur, and sulfur structures including heterocyclics, straight-chain monosulfides, and polysulfides [3]. Conjugated structures absorb in the ultraviolet, with conjugated dienes giving a single absorption, and the higher conjugated systems giving three-peak absorptions. These peaks occur at longer wavelengths with increasing numbers of conjugated double bonds in the systems [16]. Koch [17, 18], Davis [19], Minoura [20], and Baer and Carmack [21] have presented ultraviolet spectra of elemental sulfur and of a variety of sulfides and

polysulfides. Cyclic sulfides show an increased general absorption with decrease in wave length. Straight-chain mono-, di-, and polysulfides exhibit shoulders or broad maxima at wavelengths that increase with increasing numbers of sulfur atoms. Postovskaya, Salimov, and Kuzminskiĭ [22], and Dogadkin and Pavlov [23] have used these absorptions to determine the number of sulfur atoms in sulfide cross-links of vulcanized rubber.

The second squalene–sulfur reaction product, dissolved in spectrograde cyclohexane, gave the spectrum presented in A of figure 5. In the carotenoid or isoprenic series, such as might be present here, conjugated trienes are reported to absorb near 275, **285,** and 297 mμ and tetraenes near 305, **318,** and 332 mμ, [16], the boldface number being the strongest absorption. Similar conjugated dienes absorb near 240 mμ [16]. These absorptions very closely fit the curve given in figure 5. There are also

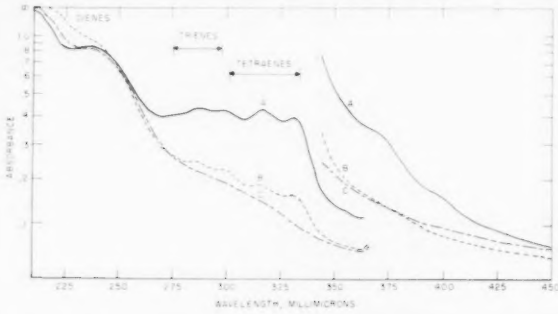

FIGURE 5. *Ultraviolet spectra of A-squalene-sulfur reaction product (53.3 mg/liter, 210–360 mμ; 0.178 g/liter, beyond 360 mμ), B-squalene-sulfur reaction product reacted with 218 percent of maleic anhydride at 100 °C (Sample No. 1–69.0 mg/liter, 210–360 mμ; 0.230 g/liter, beyond 360 mμ), and C-squalene-sulfur reaction product reacted with 201 percent of maleic anhydride at 150 °C (Sample No. 4–69.0 mg/liter, 210–360 mμ; 0.230 g/liter, beyond 360 mμ) at 1-cm path length.*

The concentrations given for curves B and C indicate the concentration of squalene-sulfur reaction product only in the reaction mixture.

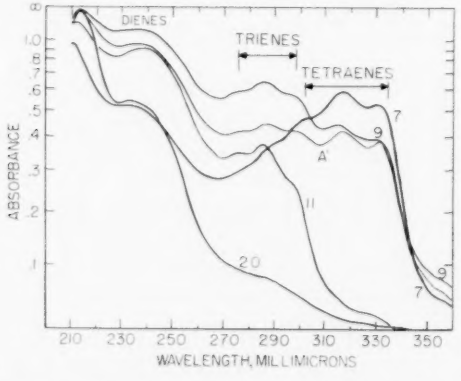

FIGURE 6. *Ultraviolet spectra of the original squalene-sulfur reaction product, A', and chromatographic fractions 7, 9, 11, and 20.*

shoulders, a slight but reproducible one at 356 mμ and others at 372, 398, and 420 to 425 mμ (these latter absorptions being more pronounced in the first reaction product), that could be due to conjugated hexaenes absorbing near 356, **376,** and 397 mμ and heptaenes absorbing near 378 **400,** and 425 mμ [16]. There is little evidence of pentaenes or, at this concentration, of systems with more than seven conjugated double bonds.

Chromatographic separation of the first reaction product into 20 fractions yielded the four significant fractions given in figure 6. The absorbance of the original reaction product is given by curve A'. In curve 7, reduced absorption in the triene region emphasizes the three absorptions at the wavelengths characteristic of tetraenes. On the other hand, the last two peaks characteristic of tetraenes are reduced in intensity in the curve for fraction 9, as would be the case if the concentration of the tetraenes were somewhat lowered, the third peak remaining unchanged presumably because of the proximity of the long-wavelength peak of the trienes. In the curve for fraction 11, there is only a shoulder in the tetraene region (that could be due either to tetraenes or a polysulfide) on the side of the triene peaks which are clearly revealed. Again, in the curve for fraction 20, there is merely a shoulder on the 236-mμ peak, characteristic of dienes or sulfide structures, which is also present in the spectra of the other fractions. None of the fractions contained more than shoulders in the region beyond 360 mμ. Thus, if hexaenes and heptaenes are actually present, they are not present in sufficient proportions to give well defined, characteristic, three-peak spectra in any of the fractions.

The ultraviolet spectrum of the first reaction product was nearly identical with that of the second. The third reaction-product was not as dark as the first two, and when it was kept in a capped bottle under nitrogen in a freezer (−26 °C) for several years after preparation, it resembled fraction 9 in the region between 210 and 360 mμ. The first reaction product, after a similar period of storage, also gave a curve similar in shape to that of fraction 9, with reduced absorption in the triene and tetraene regions.

The separation of the reaction product into fractions exhibiting the three-peak absorption spectra characteristic of trienes and tetraenes is strong evidence of their presence. In view of this conclusion, it is reasonable to suppose that the peak at 236 mμ is probably due, in part as least, to conjugated dienes. Analysis of the first squalene–sulfur reaction product by the method of Bartlett and Skoog [24] showed the presence of about 0.4 percent of elemental sulfur, a proportion shown not to affect the ultraviolet spectrum of the reaction product. In the qualitative interpretation, interference from sulfur structures seems most likely in the case of conjugated dienes, although part of the general absorption throughout the region studied here is probably due to sulfur structures. The Russian authors [22, 23] were able to use ultraviolet studies to estimate the number of sulfur atoms in polysulfide cross-links, probably

because their compounds had been vulcanized for relatively short periods of time, compared to the 20 to 23 hr used here for the squalene–sulfur reaction product. There is evidence that polysulfides tend to decompose to shorter sulfidic links on extended reaction [3, 25], whereas conjugation tends to increase with reaction time.

4.5. Treatment With Maleic Anhydride

a. Discussion

Maleic anhydride reacts with conjugated systems, through a Diels–Alder reaction, to remove the conjugation. The band at 6.25 μ in the spectrum of the squalene–sulfur reaction product was completely removed in 70 hr at 100 °C, suggesting that it was due to conjugation; whereas the bands at 6.0 and 6.1 μ remained largely unchanged, except for an apparent increase in the absorption at 6.0 μ relative to 6.1 μ which could be related to increased absorption in the adjacent carbonyl region. This situation suggests that the band near 6.1 μ is due to some structure other than conjugated double bonds. Sterically unhindered systems, such as those containing *trans-trans* conjugation, react readily at this temperature. Sterically hindered systems, such as those containing *cis-cis* and *cis-trans* conjugation, are usually much more difficult to react, but are sometimes isomerized into the more reactive *trans-trans* form at higher temperatures [26]. There is, unfortunately, at least one exception in what is apparently a *cis-trans* isomer of 2,6-dimethyl-3,5-octadiene [27]. The structure of this compound is similar to structures that might be expected in the squalene–sulfur reaction product, and the compound reacts with maleic anhydride when reated in a water bath for 15 hr.

The effect of temperature on the infrared and ultraviolet spectra of the maleic anhydride reaction-product was investigated, along with the effect of maleic anhydride on vulcanized rubber.

Preliminary work had suggested that reaction of the squalene–sulfur reaction product with maleic anhydride at 100 °C for only 5 hr was sufficient to remove the band at 6.25 μ. Consequently, reactions were carried out for this period of time using the second squalene–sulfur reaction product and the indicated amounts of maleic anhydride at 100 and 150 °C, to determine whether any of the unreactive types that would not react at 100 °C could be isomerized at the higher temperature to the more reactive *trans-trans* isomers.

b. Squalene-Sulfur Reaction Product; Infrared Spectra

In the samples included in section 3.2, removal of the band at 6.25 μ was complete in 5 hr, only at 150 °C. In addition, at the higher temperature, the band at 6.01 μ is reduced relative to the one at 6.10 μ, instead of the converse that would have been expected. There is indeed, in these cases, some additional reaction at the higher temperature, as indicated (in the ultraviolet studies to follow) by the reduced absorbance in curve C of figure 5 in the triene and tetraene regions. This change is probably in part related to the more complete removal of the band at 6.25 μ.

Possible interpretations of the small effect that is observed on the bands near 6.0 and 6.1 μ are discussed below. This effect could suggest that some of the conjugated systems are absorbing near 6.0 rather than 6.1 μ. Shifting of double bonds in 1,4 or 1,5 systems at the higher temperature could also cause reduction in the intensity of the 6.0-μ band, because the absorption at this wavelength, characteristic of the original double bond or the shifted *trans* double bond, could be removed. Direct reaction with maleic anhydride to remove the isolated, original, double-bond systems is highly unlikely, since uninitiated reactions related to isolated double bonds have been reported to take place only at temperatures above 150 °C and to involve the hydrogen atoms on the α-carbon atom instead of the double bond itself [28]. It should be noted that Binder [15B] gives evidence for the removal of the double bond, but does not give the temperature of the reaction. Pinazzi, Cheritat, and Pautrat [29] obtained a reaction product with rubber and maleic anhydride, using heat alone, in which part of the double bonds are shifted to the methyl side chain at temperatures above 180 °C. If this reaction were to take place to any extent at 150 °C, it could explain the relative increase in the intensity of the band near 6.1 μ, since the shifted terminal double bond would be expected to absorb here.

Maleic anhydride has a strong band at 14.4 μ. As judged by removal or reduced intensity of this band, reaction at 150 °C does reduce the amount of unreacted maleic anhydride to an unexpected extent, considering the amounts present. Treatment of the blank at 100 and 150 °C, or distillation of the blank following treatment, does not change the infrared spectrum appreciably. Apparently, further reaction does not occur, and the structures causing absorption at 6.1, 6.25, and 10.4 μ are not volatile.

c. Squalene-Sulfur Reaction Product; Ultraviolet Spectra

The ultraviolet absorption spectrum of the maleic anhydride reaction-product, obtained at 100 °C with 218 percent maleic anhydride (Sample No. 1) and dissolved in cyclohexane, is given in curve B of figure 5. Curve C in the same figure was made by using the reaction product obtained at 150 °C with 201 percent maleic anhydride (Sample No. 4), dissolved in 3:1 cyclohexane-absolute ethanol; this reaction product was not quite completely soluble. It had been shown that the curve for the squalene-sulfur reaction product was identical in both solvents. Absorbance measurements given in table 1 were made at 236, 287, and 317 mμ, as being indicative of changes in absorbance in the diene, triene, and tetraene regions, respectively. The measurements on curves B and C were corrected for the dilution effect of the added maleic anhydride, and for the differences in concentration of the material used, in

an effort to put them on a basis comparable with those made on curve A. Data for the other samples are not presented.

TABLE 1. *Comparison of ultraviolet absorbances* [a]

Treatment with maleic anhydride	mμ		
	236	287	317
Untreated (Curve A)[c]	0.839	0.430	0.426
100 °C (Curve B) [b d]	.943	.250	.186
150 °C (Curve C) [b d]	.808	.218	.144

[a] Data obtained from curves in figure 5.
[b] Data corrected for the dilution resulting from the addition of maleic anhydride and for differences in concentration from curve A.
[c] Squalene-sulfur reaction product.
[d] Squalene reaction product, reacted with maloic anhydride.

In both curves B and C, there is little change in absorption in the region characteristic of dienes, but a pronounced decrease in absorption in the regions characteristic of trienes, tetraenes, hexaenes, and heptaenes. The reduced absorption and, where noted, decreased detail in curve C when compared to curve B in these regions, is presumably consistent with reduced absorption at 6.25 μ in the infrared region when the reaction is carried out at 150 °C.

In other tests of the first squalene-sulfur reaction product (not listed in section 3.2), in which the band at 6.25 μ was removed at 100 °C, there was little change in the ultraviolet absorption on going from 100 to 150 °C, except for somewhat less detail in the triene and tetraene regions and a 12–16 percent reduction in absorbance in the diene region.

Decreasing the proportion of maleic anhydride caused little change in the ultraviolet spectra. At the lower concentration, there was an unexplained crossing over of the curves for the 100- and 150 °C-reaction products near 342 mμ in the short wavelength section but not in the other. Distillation indicating that the structures responsible for the bands are not volatile. The only time that distillation resulted in an appreciable reduction in absorption was for the spectrum beyond 340 mμ of sample 4 containing 93.1 percent of maleic anhydride and reacted at 150 °C. The difference was most pronounced at the longer wavelengths.

These results offer further confirmation of the assignment of the original, pertinent, ultraviolet bands to conjugated trienes and tetraenes. There appears to be little confirmation of the presence of dienes. However, maleic anhydride shows an absorbance of 0.176 at 236 mμ for 15.2 mg/liter, corresponding to about the 200 percent level. The contribution of the maleic anhydride structure in the reaction product to the absorbance at 236 mμ is not known, but, to the extent that free maleic anhydride is present, it would increase the absorbance at this wavelength. For the distilled samples, the solutions were prepared assuming that no maleic anhydride had been removed. In cases where appreciable amounts of maleic anhydride had been removed, this method of preparation would increase the actual concentration of squalene-sulfur reaction product beyond the amount intended and thus increase absorption in general, including that in the diene region. Thus, there is reason to assume some reduction in absorption in the diene region, too. The picture is further complicated, however, by the fact that interference from sulfur compounds is most likely in this region. Thus, complete support of the hypothesis is dependent on whether maleic anhydride also reacts with the sulfur compounds present to give reduced absorbance in the diene region. As an example, tetrahydrothiophene, the parent compound of the substituted materials found in the dihydromyrcene-sulfur reaction product [12, 13], does not react with maleic anhydride in 90 min at 125 °C [30]. This type of compound shows an increased general absorption at shorter wavelengths. Because of the extended reaction time, polysulfides having large numbers of sulfur atoms would not be expected to be present [3]. Since large numbers of sulfur atoms are probably not involved, reduced absorption and removal of the shoulders beyond 340 mμ suggest that the shoulders are due to hexaenes and heptaenes.

The residual absorption after reaction with maleic anhydride may, of course, still be due to unreactive conjugated systems. However, reactions above 150 °C would not be meaningful, since this was the temperature at which the squalene–sulfur reaction product was formed. Furthermore, Bloomfield and Naylor [31–33] have indicated that polysulfides decompose, and react with olefins, at temperatures from 140 to 180 °C. Another possible cause of this residual absorption is scattering.

On the other hand, the ultraviolet curve for the maleic anhydride reaction product obtained at 150 °C is quite similar to those of some of the sulfur compounds mentioned earlier, and may, quite possibly, be due largely to this type of material. If such is, indeed, the case, the band at 6.1 μ cannot, of course, be due to unreactive conjugated double bonds. The other possibility, suggested earlier, is isolated double bonds with attached sulfur atoms. In the squalene–sulfur reaction product, there is also some contribution from terminal double bonds to the band at 6.1 μ.

d. Vulcanized Rubber; Infrared Spectrum

Reaction of the film of vulcanized rubber with maleic anhydride removed the band at 6.25 μ in the infrared spectrum, as had been found earlier for the squalene–sulfur reaction product [2].

The band reported by Mikawa [9] at 6.31 μ in methyl vinyl sulfide could cast doubt on the interpretation of the 6.25-μ band as being due to conjugation, if the band at 6.31 μ is removed by reaction with maleic anhydride.

5. Discussion

5.1. Mechanisms

The first formula given below shows two adjacent

isoprene units of a rubber molecule, and the second, the *trans* double bond resulting from a shift of the original double bond through a free-radical mechanism, as originally proposed by Sheppard and Sutherland [1]. If *trans* double bonds to which the 10.4-μ band has been attributed are actually present, they must be produced by a shift of the original double bond, since the introduction of a new double bond would automatically produce a cumulative or conjugated system. The new *trans* double bond produces a 1,4 system. Two shifts of two double bonds toward each other, or two successive shifts of one double bond, are, barring more involved mechanisms, necessary to produce the conjugated dienes suggested by the ultraviolet spectra.

On the other hand, the observed conjugated trienes could be produced by the introduction of a new double bond midway between two original double bonds. The observed conjugated tetraenes could be produced by the introduction of a new double bond at this same point, combined with two successive shifts of another original double bond toward these three. Similar reasoning applies to the more highly conjugated polyenes suggested by the ultraviolet spectra. Of course, similar numbers of conjugated double bonds could also result simply from many different shifts alone. However, the introduction of new double bonds is consistent with the work with dihydromyrcene of Bateman, Glazebrook, and Moore [3], in which they isolated, among other compounds, alloocimene, and with our work with propylene, in which we isolated propadiene (allene) [34].

In any event, regardless of whether isolated *trans* double bonds exist, shifts of double bonds by some mechanism are necessary for the production of some of the observed conjugated systems, e.g., conjugated dienes, tetraenes, and hexaenes, as well as other even-numbered systems. Whether longer conjugated systems would be produced, with the same proportion of sulfur, in the larger molecule, rubber, is not known.

The observed different degrees of conjugation could result from reaction at a single point, as part of a chain mechanism. They could also be related to the statistical probability of producing the observed concentration of the different systems as a result of stepwise, individual reactions at certain necessary sites with the proportion of sulfur used. This would be difficult to determine, since many sulfur atoms may go into one cross-link [25].

5.2. Interpretation of the 10.4-μ Band

The band at 10.4 μ, previously attributed to isolated *trans* double bonds [1, 2], presents an interesting problem. It has also been attributed by Glazebrook and Saville [13] and by Bateman, Glazebrook, Moore, and Saville [12] to the substituted tetrahydrothiophenes that were formed in their studies with dihydromyrcene. It is instructive to follow through the implications of the data presented here and in our previous paper [2], in terms of an interpretation of the 10.4-μ band.

a. Isolated Trans Double Bonds

In figure 6 of the earlier paper [2], there was some residual band present at 10.4 μ in the spectrum of the maleic anhydride reaction-product. Spectra of some of the other samples of this reaction product have also shown residual absorption here, indicating the presence either of unreacted conjugation (see section 5.2c) or of some isolated *trans* double bonds and, therefore, of the 1,4 double-bond structure. The actual proportion present of structures absorbing at 10.4 μ may be greater than that indicated by these spectra, because of the effect of increased absorption on both sides of the band [2] due to reaction with the maleic anhydride.

b. Tetrahydrothiophene Structures

The substituted tetrahydrothiophenes isolated in the reaction of dihydromyrcene with sulfur have been reported to absorb near 10.5 to 10.6 μ, with one absorbing at 10.44 μ, also [12, 13]. The breadth of the band at 10.4 μ in the spectra of rubber and the squalene-sulfur reation product does allow for the presence of structures of the type absorbing at 10.44 μ, and even for some of those absorbing between 10.5 and 10.6 μ. This latter situation is especially true in the spectrum of the squalene-sulfur reaction product, where there is a definite shoulder between 10.5 and 10.6 μ. The shoulder here, its absence from vulcanized rubber, and the isolation of tetrahydrothiophenes in the dihydromyrcene-sulfur reaction product might suggest that these structures are more likely in smaller compounds and less likely in larger molecules, such as rubber. As indicated previously [2], the band at 10.4 μ in vulcanized rubber shifts toward longer wavelengths with increasing sulfur content. This result is in agreement with the findings of Sheppard and Sutherland [1]. With unpurified natural rubber, the band showed, with 32 percent of sulfur, a flat spot between 10.5 μ and 10.55 μ, with what appeared to be a slight shoulder at 10.35 μ. On the other hand, purified rubber and synthetic rubber showed a maximum absorption at about 10.47 μ with 32 percent of sulfur. These effects might be interpreted as resulting from an increase in tetrahydrothiophenes with increased sulfur content. The longer wavelength for the unpurified rubber could presumably also be related to the reduced amount of conjugation (near-absence of the band at 6.25 μ and consequent reduction in the band at 10.35 or 10.4 μ; see section 5.2 c) in natural rubber vulcanized with 32 percent of sulfur, as compared with the amount present when purified or synthetic rubber is used. It must also be remembered that the tetrahydrothiophenes in different structural environments could absorb at wavelengths other than those reported above.

c. Conjugated Double Bonds

Many conjugated polyenes absorb near 10.4 μ. Lunde and Zechmeister [35] showed that, in the case of conjugated diphenyl polyenes, at least one *trans* double bond had to be present to produce an appreciable band between 10.0 and 10.6 μ. This absorption is sometimes a single band, sometimes shifted from its usual position near 10.4 μ, and sometimes split into two bands. Unfortunately, it is difficult to predict with certainty, from theory, the types of conjugated systems that would or would not lead to shifting or splitting of this band. Some pertinent experimental evidence on this point follows:

(1) Conjugated *cis-trans* systems of the —CH=CH— type common in fatty acids have been found to exhibit splitting, as in the case of *cis-trans*-octadecadienoates (absorptions at 10.18 and 10.55 μ), whereas *trans-trans* isomers show a single stronger absorption at 10.12 μ [36].

(2) Lunde and Zechmeister [35] showed that, in a series of conjugated diphenylpolyenes, splitting occurred in this region for *cis-trans* conjugation, but that only shifting of the band to shorter wavelengths occurred in the all-*trans* isomers. The split bands lay closer together in the higher conjugated systems tested (up to four double bonds) than in the lower ones. These authors suggest that "the two bands may coincide or even exchange places in still higher conjugated systems" [35].

(3) O'Connor and Goldblatt [10] showed that both *trans*-(C_4), *trans* (C_6) and *trans*-(C_4),*cis*-(C_5) isomers of the isoprenoid, conjugated triene, allo-ocimene, show splitting, with bands at 10.13 and 10.46 μ. These are structures similar to those presumably present in the squalene-sulfur reaction product and in vulcanized rubber.

(4) Lunde and Zechmeister [37] showed that many long-chain carotenoid pigments exhibit only a single absorption near 10.4 μ, and that the presence of a central *cis* double bond adjacent to two —CH= groups produced a doublet absorbing at 10.35 and 10.47 μ.

The above information and the single absorption at 10.4 μ in the present case suggest the presence of some fairly long conjugated systems, absorbing primarily at this wavelength. The work of Lunde and Zechmeister [35] indicates that these systems contain at least one *trans* double bond. The breadth of the present band should allow for some of these systems to exhibit shifted or split absorptions. No further definition is possible from the position and shape of this band.

An attempt has been made to estimate the percentage of the molecules of squalene-sulfur reaction product containing dienes, trienes, and tetraenes, from their ultraviolet absorbances; and, from this, to estimate the fraction of the band at 10.4 μ due to conjugated systems in the squalene-sulfur reaction product. It must be remembered in the following discussion that large variations in the values of molar absorptivities of given groups, in both the ultraviolet and the infrared, can occur from molecule to molecule. In addition, large variations have been observed, especially in the infrared, in the absorptivities of the same compound reported by different laboratories. These variations reduce the value of the quantitative aspect of these calculations.

The details of the calculation are discussed below:

The ultraviolet molar absorptivities used as reference for 100 percent of molecules absorbing as conjugated dienes and trienes, respectively, were taken from the data for ocimene and for the average of the two isomers of allo-ocimene given in the paper by O'Connor and Goldblatt [10]. A value of 57,500 liters/mole cm was used for the molar absorptivity of tetraenes, based on the average of data taken from an article by Braude [38] for tetraenes in decatetraenol and for pentaenes in vitamin A. The contribution to the band at 10.4 μ of dienes and trienes, respectively, was estimated from the absorbance of ocimene and the allo-ocimene isomers at 10.4 μ, and the data for absorptivities of these compounds were taken from the article by O'Connor and Goldblatt [10]. A value of 34 liters/mole cm was used for the molar absorptivity of the tetraenes, based on a comparison of band strengths for bands near 3.3 and 10.4 μ in the spectrum of the conjugated tetraene compound designated 4,5-*trans*-XVIa by Oroshnik and Mebane [39] and the fact that the absorptivities for the 3.3-μ band for many nonaromatic hydrocarbons seem to average about 45 liters/mole cm as indicated by the data of O'Connor and Goldblatt [10]. The results of the calculations are given in table 2. In the absence of knowledge of the molecular weight of the reaction product, the molar absorptivities were calculated by using the molecular weight and density of squalene and the concentration of the squalene part of the molecule in the reaction product. If there is a split absorption in the diene actually present in the squalene-sulfur reaction product, such as is present in the model compound ocimene, a more definite shoulder would be expected at 10.10 μ in the reaction product. If this stronger band of the two is closer to 10.4 μ, the effect of the dienes may be increased about threefold, thus allowing conjugation to account for about 59 percent of the band at 10.4 μ in the spectrum of the reaction product. On the same basis, if only that part of the conjugation removed with maleic anhydride is considered (Curve C fig. 5), and using the absorptivity of the stronger band in ocimene as the absorptivity for dienes, about 14 percent of the band at 10.4 μ is accounted for by conjugation. There is some reason to consider only that part of the ultraviolet absorbance removed with maleic anhydride, because of the interference due to sulfur structures discussed in sections 4.4 and 4.5c. This may, however, give low values for dienes because of absorption by maleic anhydride as indicated in section 4.5c.

TABLE 2. *Conjugated double bonds in squalene-sulfur reaction product*

	Molecules with conjugated double bonds, percent [a]		Molar absorptivity at 10.4 μ — liters / mole cm	
	Total [b]	Removed with maleic anhydride [c]	Total [b]	Removed with maleic anhydride [c]
Dienes	45.8	1.7	3.9	0.1
Trienes	9.5	4.7	4.1	2.0
Tetraenes	6.8	4.5	2.3	1.5
Total molar absorptivity			10.3	3.6
% of the molar absorptivity of band at 10.4 μ			[d] 30.5	[d] 10.7

[a] Indicates percent of molecules containing dienes, trienes, or tetraenes.
[b] Based on absorbance data from curve A in figure 5, as given in table 1.
[c] Based on values corrected for maleic anhydride (curve C in figure 5).
[d] Based on total molar absorptivity of 33.7 for band at 10.4 μ.

The point of this calculation and discussion is to show that, with this much completely reacted sulfur, the material is rather heavily conjugated, and there is good reason to believe that a significant percentage of the band at 10.4 μ is due to conjugated double bonds. There is, of course, room for contribution from isolated *trans* double bonds and from tetrahydrothiophene structures, especially in the dimer reaction-product where they have been isolated [3], in the squalene-sulfur reaction product where there

is a shoulder at 10.5–10.6 μ, and in unpurified rubber vulcanized with larger proportions of sulfur, where the absorption occurs at longer wavelengths and little absorption at 6.25 μ due to conjugation is noted. Unfortunately, no correlation for isolated *trans* double bonds is available in the near-infrared at the present time [14].

d. Other Related Work

Shipman and Golub [40], in an excellent article, have analyzed the nature of this band, using *cis*-polyisoprene and partially and wholly deuterated *cis*-polyisoprene to isolate these three effects, and have concluded that the band at 10.4 μ is due largely to conjugated double bonds and tetrahydrothiophenes, with some contribution from isolated *trans* double bonds.

Apparently, the situation is different in accelerated vulcanizates containing 15 percent of sulfur and 7.5 percent of TMTD, because the conjugation is greatly reduced, as judged by the intensity of the band at 6.25 μ, while the band at 10.4 μ is of about the same intensity as in the case of simple sulfur vulcanizates, the reaction presumably being carried nearly to completion in both cases.

Kuz'minskiĭ and Borkova [41], on the basis of infrared studies with ebonite, concluded that the band at 10.4 μ is due to a new double bond that is produced as a secondary reaction of the polysulfides originally formed on reacting rubber with sulfur. They also note the existence of considerable unsaturation remaining in completely vulcanized ebonite as a result of the above sequence. The presence of considerable unsaturation in completely vulcanized ebonite is in agreement with our present and with our earlier findings [2].

Craig, Diller, and Rowe [42] suggested that terminal conjugation, presumably of dienes, could be produced by cleavage of the chain at a radical site on an α-methylene carbon atom.

Klauzen and Dogadkin [43] regard the band at 10.4 μ as being due to a *trans* double bond which, in part, accounts for the difference in physical-mechanical properties between vulcanized and unvulcanized rubber. These authors also consider the band at 6.1 μ to be related to the *trans* double bond absorbing at 10.4 μ.

Except for the absence of a band at 6.25 μ, Dale and Artun [44] obtained an infrared spectrum of squalene following dehydrogenation on hydrogenation catalysts that was remarkably similar to that of our squalene-sulfur reaction product. Ultraviolet studies showed that their material, nevertheless, contained conjugated dienes, tetraenes, and hexaenes. The authors considered these changes to have resulted from double-bond migration. This work constitutes further evidence that conjugated systems can absorb near either 6.0 or 6.1 μ, since these wavelengths were the only places where bands were observed in the —C=C— stretching region.

Dale [45] showed that squalene could be dehydrogenated by *N*-bromosuccinimide to give a wide range of conjugated systems, including those containing 3, 5, 7, 9, and 11 conjugated double bonds.

The last two studies and the present work are striking examples of how widely different reagents may produce very similar results. They suggest that similar mechanisms may possibly be operating in all three cases.

5.3. Configuration of Conjugated Double Bonds

Although rubber is almost entirely *cis*-polyisoprene, squalene is probably largely *trans*. In fact, Nicolaides and Laves [46] indicate that it is all-*trans*. The rather recent near-infrared method of Corish [47] for determining *cis* and *trans* configurations in polyisoprenes, when applied to squalene in this laboratory, gave a value of about 43 percent of *cis*. However, end effects, for example, in the smaller molecule may reduce the quantitative value of this method.

The isomer of allo-ocimene reported by Bateman, Glazebrook, and Moore [3] in their work with dihydromyrcene was predominantly the *trans*-C_4,*cis*-C_6 isomer, suggesting that the new double bond required for forming a conjugated triene would be *trans*. In squalene, if nearly all *trans*, the introduction of a new *trans* double bond would yield, usually, the all-*trans* triene. This does not, however, rule out the presence of *cis-trans* conjugation in the squalene-sulfur reaction product or the all-*trans* variety in *cis*-polyisoprene-sulfur vulcanizates, since various treatments, including the use of heat, have been known to isomerize carotenoid materials [48, 49, 50], suggesting the possibility of a mixture of all-*cis*, *cis-trans*, and all-*trans* isomers.

As indicated above, Bateman, Glazebrook, and Moore [3] reported finding the *trans*, *cis* isomer of allo-ocimene in the dihydromyrcene-sulfur reaction product. Nevertheless, Chipault and Hawkins [50] indicated that small proportions of sulfur will convert *cis* into *trans* conjugated systems at room temperature, as in the case of the conversion of *trans-trans-cis* α-eleostearic acid into the all-*trans* β-isomer. Thus, if this latter statement is generally true, it may be that, regardless of whether *cis*- or *trans*-polyisoprene is the starting material, conjugated systems in the reaction product will be largely *trans*.

Some inferences may be attempted from the ultraviolet spectra of the squalene-sulfur reaction product presented here. First, the absorption maxima are remarkably close to those for the presumably all-*trans* isomers of natural products given by Dale [16], provided that the substitution of cyclohexane or cyclohexane-alcohol for hexane does not affect the wavelengths of the absorption. It has been noted that the first two solvents are interchangeable. Isomers containing *cis* double bonds absorb, generally, at somewhat shorter wavelengths and tend to lose their distinctive fine structure [49]. Second, the fact that the long-wavelength band for the tetraenes in curve 7 of figure 6 is more intense than the third band suggests the presence of an all-*trans* or nearly all-*trans* isomer [16]. Increasing numbers of *cis* double bonds tend to cause a reversal of this

band shape [16]. The opposite appears to be true for the trienes pictured in curve 11 of the same figure, but the absorption in the diene region undoubtedly increased the absorption for the short-wavelength band. Furthermore, the work with allo-ocimene would suggest largely, at least, an all-*trans* triene in the case of squalene. It seems likely that both the trienes and the tetraenes are, for the most part, all-*trans*. The *cis* peak [49] present in certain compounds containing *cis* double bonds in conjugation with *trans* double bonds cannot be used here, since it is either obscured by the lower polyenes or else would come at too short a wavelength for the instrument to detect. No evidence was found concerning the effect of attached sulfur atoms on the wavelengths of absorptions of conjugated systems, so their presence or absence cannot be indicated.

6. Conclusions

Near-infrared studies indicate the absence or near-absence of isolated *cis* and terminal double bonds in rubber vulcanized either with or without accelerators, as well as in the squalene-sulfur reaction product. The use of purified natural rubber indicates a new absorption near 6.1 μ on reaction with sulfur either with or without accelerators in the rubber system. This new absorption is presumably due either to a double bond with an attached sulfur atom or to conjugated double-bond systems that do not react readily with maleic anhydride. Ultraviolet spectra of chromatographic fractions show that squalene reacted with 15 percent of sulfur contains conjugated trienes and tetraenes and, possibly, dienes, hexaenes, and heptaenes. The conjugated dienes, trienes, and tetraenes are probably present in sufficient proportions to account for for a significant portion of the band at 10.4 μ. There is some evidence that the trienes and tetraenes, at least, may be largely all-*trans* in configuration. Other contributors to the band at 10.4 μ are probably isolated *trans* double bonds and heterocyclic sulfur structures along the chain. It had previously been shown [2] that the band at 6.25 μ, attributed to conjugation, first appears with about 5 percent of sulfur and that the band at 10.4 μ first appears at about 2 percent of sulfur. It may, therefore, be assumed that the structures attributed to these bands are formed at considerably smaller concentrations of sulfur than those used here. Variations in the relative proportions of the various conjugated systems with sulfur content are to be expected.

7. References

[1] N. Sheppard and G. B. B. M. Sutherland, J. Chem. Soc. **1947,** 1699; Rubber Chem. Technol. **21,** 799 (1948).

[2] F. J. Linnig and J. E. Stewart, J. Res. NBS **60,** 9 (1958); Rubber Chem. Technol. **31,** 719 (1958).

[3] L. Bateman, R. W. Glazebrook, and C. G. Moore, J. Chem. Soc. **1958,** 2846; Rubber Chem. Technol. **31,** 1065 (1958).

[4] E. T. McDonel, J. R. Shelton, J. Chem. Eng. Data **4,** 360 (1959).

[5] J. L. Bolland and Geoffrey Gee, Trans. Faraday Soc. **42,** 244 (1946); Rubber Chem. Technol. **20,** 617 (1947).

[6] T. J. Murphy, W. S. Clabaugh, and R. Gilchrist, J. Res. NBS **64A,** (Phys. and Chem.) 355 (1960).

[7] Association of Official Agricultural Chemists, Official Methods of Analysis of the Association of Official Agricultural Chemists, 9th edition, p. 654 (Association of Official Agricultural Chemists, Washington, D.C., 1960).

[8] L. J. Bellamy, The Infra-red Spectra of Complex Molecules, p. 36 (John Wiley & Sons, Inc., New York, N.Y., 1958).

[9] Y. Mikawa, Bull. Chem. Soc. Japan **29,** 110 (1956).

[10] R. T. O'Connor and L. A. Goldblatt, Anal. Chem. **26,** 1726 (1954).

[11] G. F. Bloomfield, J. Chem. Soc. **1947,** 1546.

[12] L. C. Bateman, R. W. Glazebrook, C. G. Moore, and R. W. Saville, Proceedings of the Third Rubber Technology Conference p. 298 (W. Heffer and Sons, Limited, Cambridge, London, 1954); Rubber Chem. Technol. **30,** 397 (1957).

[13] R. W. Glazebrook and R. W. Saville, J. Chem. Soc. **1954,** 2094; Rubber Chem. Technol. **28,** 109 (1955).

[14] R. F. Goddu and D. A. Delker, Anal. Chem. **32,** 140 (1960).

[15A] D. W. Fraga, J. Polymer Sci. **41,** 522 (1959); Rubber Chem. Technol. **33,** 982 (1960).

[15B] J. L. Binder, J. Polymer Sci. **1,** 37 (1963).

[16] J. Dale, Acta Chem. Scand. **8,** 1235 (1954).

[17] H. P. Koch, J. Chem. Soc. (London) **1949,** 387.

[18] H. P. Koch, *ibid,* **1949,** 394.

[19] R. E. Davis, J. Org. Chem. **23,** 1380 (1958).

[20] Y. Minoura, J. Inst. Polytech., Osaka City University, Ser. C **5,** 206 (1956); Rubber Chem. Technol. **31,** 808 (1958).

[21] J. E. Baer and M. Carmack, J. Am. Chem. Soc. **71,** 1215 (1949).

[22] A. F. Postovskaya, M. A. Salimov, and A. S. Kuzminskiĭ, Dokl. Akad. Nauk SSSR **114,** 586 (1957); Rubber Chem. Technol. **31,** 747 (1958)

[23] B. A. Dogadkin and N. N. Pavlov, Vysokomolekul. Soedin. **3,** 613 (1961); Rubber Chem. Technol. **36,** 262 (1963).

[24] J. K. Bartlett and D. A. Skoog, Anal. Chem. **26,** 1008 (1954).

[25] C. G. Moore and M. Porter, Paper presented at Conference Internationale sur le Caoutchouc, Paris, May 14–18, 1962.

[26] L. F. Fieser and M. Fieser, Advanced Organic Chemistry, p. 206 (Reinhold Publishing Corp., New York, 1961).

[27] G. Dupont, R. Dulou, V. Desreux, and R. Picoux, Bull. Soc. Chim. France [5] **5,** 322 (1938).

[28] L. H. Flett and W. H. Gardner, Maleic Anhydride Derivatives—Reactions of the Double Bond, p. 6, (John Wiley & Sons, Inc., New York, N.Y., 1952).

[29] C. Pinnazi, R. Cheritat, and R. Pautrat, Paper presented at Conference Internationale sur le Caoutchouc, Paris, May 14–18, 1962.

30] D. Craig, B. F. Goodrich, Research Center (private communication).

[31] G. F. Bloomfield, J. Polymer Sci. **1,** 312 (1946); Rubber Chem. 4 Technol. **20,** 360 (1947).

[32] G. F. Bloomfield, J. Chem. Soc. **1947,** 1547; Rubber Chem. Technol. **22,** 348 (1949).

[33] G. F. Bloomfield and R. F. Naylor, Proc. XIth Intern. Congr. Pure Appl. Chem., Volume II, p. 7, Organic Chem., Biochem. London, England, 1947.

[34] F. J. Linnig, E. J. Parks, and L. A. Wall, J. Res. NBS **65A,** 79 (1961).

[35] K. Lunde and L. Zechmeister, Acta Chem. Scand. **8,** 1421 (1954).

[36] J. E. Jackson, R. F. Paschke, W. Tolberg, H. N. Boyd, and D. H. Wheeler, J. Am. Oil Chemists' Soc. **29,** 239 (1952).

[37] K. Lunde and L. Zechmeister, J. Am. Chem. Soc. **77,** 1647 (1955).

[38] E. A. Braude, Ann. Rept. Progr. Chem., (Chem. Soc. London) **42,** 105 (1945).

[39] W. Oroshnik and A. D. Mebane, J. Am. Chem. Soc. **76,** 5719 (1954).
[40] J. J. Shipman and M. A. Golub, J. Polymer Sci. **58,** 1063 (1962).
[41] A. S. Kuz'minskiĭ and L. V. Borkova, Zh. Prikl. Khim. **31,** 648 (1958); J. Appl. Chem. USSR (English Trans.) **31,** 635 (1958).
[42] D. Craig, D. Diller, and E. H. Rowe, J. Polymer Sci. **28,** 435 (1958).
[43] N. A. Klauzen, and B. A. Dogadkin, Zavodsk. Lab. **28,** 438 (1962).
[44] J. Dale and T. Artun, Acta Chem. Scand. **10,** 439 (1956).
[45] J. Dale, Arch. Biochem. Biophys. **41,** 475 (1952).
[46] N. Nicolaides and F. Laves, J. Am. Chem. Soc. **76,** 2596 (1954).
[47] P. J. Corish, Spectrochim. Acta **1959,** 598 Rubber; Chem. Technol. **33,** 975 (1960).
[48] P. Karrer and E. Jucker, Carotenoids, p. 38 (Elsevier Publishing Co., Inc., New York, 1950).
[49] L. Zechmeister, Experientia **10,** 1 (1954).
[50] J. R. Chipault and J. M. Hawkins, J. Am. Oil Chemists' Soc. **37,** 176 (1960).

(Paper 68A5–296)

JOURNAL OF RESEARCH of the National Bureau of Standards—A. Physics and Chemistry
Vol. 68A, No. 5, September-October 1964

Dislocations in Polymer Crystals

H. D. Keith[1] and Elio Passaglia

(April 20, 1964)

The role that dislocations are likely to play in chain-folded polymer crystals is examined, particularly with regard to their influence on plastic deformation. It is assumed that primary bonds cannot be broken in backbone molecular chains; and this restriction, together with further restrictions brought about by chain folding, limits substantially the number of permissible dislocations and glide processes. It is shown that deformations of appreciable magnitude in chain-folded polymer crystals almost certainly cannot be attributed solely to dislocation mechanisms. Crystals of the *n*-alkanes and "extended chain" polymer crystals are also discussed briefly.

1. Introduction

The recent discoveries that high polymers are capable of forming chain-folded lamellar single crystals when deposited from dilute solution, and that lamellar crystals of a similar nature are present in many bulk polymers [*1*],[2] have aroused considerable interest in the growth and properties of chain-folded molecular crystals. These crystals have been most widely studied in polyethylene, but attention has been confined, for the most part, to what may be considered properties of the *ideal* crystal. That is to say, for the interpretation of most observations recorded to date, it is sufficient to represent a lamellar single crystal as a perfectly alined array of uniformly folded molecules which is bounded on two sides by flat surfaces consisting of regularly packed molecular folds. Properties sensitive to defect structures within *real* crystals have not yet been investigated thoroughly or systematically. It is known that giant screw dislocations are commonly present during growth and often give rise to growth spirals or terraced growth pyramids, and that Moiré patterns occasionally reveal features probably indicative of the presence of edge dislocations. But there is little evidence beyond this relating to possible defects in the crystals, or to frequencies of their occurrence.

However, there is precedence from experience with metallic and ionic solids for the view that such defects may contribute significantly to the physical properties of polymer crystals, and particularly to processes of annealing, recrystallization and plastic deformation. As early as 1958, the possible role of dislocation mechanisms in the deformation of polyethylene was discussed extensively by Frank, Keller, and O'Connor [*2*]; however, the influence of chain folding was not considered. More recently, dislocation mechanisms have been proposed to account for plastic flow in nylons [*3*] and for the thickening of polyethylene crystals on annealing [*4*] but, in both cases, in terms of dislocations of new types which have no direct counterparts in simpler solids. Our purpose here is to re-examine the part that dislocations might play in crystalline polymers, now taking chain folding into account. We shall point out that the applicability of dislocation concepts to these materials can easily be exaggerated if not examined critically. We shall be concerned principally with the enumeration of dislocations which are geometrically permissible in polymer crystals and with assessing the likelihood of their participating in plastic deformation. Indeed, not much more is possible at present since neither the energies associated with dislocations nor the stresses required to move them can be estimated with confidence in these systems.

The prime consideration to be borne in mind is that no dislocation is allowed which demands that primary bonds be broken for its formation or motion. As we shall see, this limits the number of permissible dislocations and slip systems quite substantially. We shall see also that further restrictions are imposed by chain folds at external surfaces of the crystals. For simplicity we proceed in three stages. First we consider an "infinite chain" crystal, that is, a crystal composed of *very long* chains which are not folded. Secondly, we consider crystals of long chain hydrocarbons (*n*-alkanes) which consist of layers each having a structure differing from the infinite chain crystal only insofar as the chains (which are of uniform length) are relatively short. Finally, we consider chain-folded polymer crystals. As a specific model for discussion, we assume the crystals in each instance to have orthorhombic subcells identical to that of polyethylene [*5*]. As a further simplification, we limit our discussion in the cases of hydrocarbons and polymers to flat, as distinct from pyramidal, crystals [*6*, *7*]. Although our results are directly applicable only to a small range of materials, they will nevertheless serve to illustrate how dislocation processes are restricted in long chain molecular crystals in general. Extension of our analysis to other structures would in most instances be a simple matter.

[1] Bell Telephone Laboratories, Murray Hill, N.J.
[2] Italized figures in brackets indicate the literature references at the end of this paper.

2. "Infinite Chain" Crystals

Under the restriction that primary bonds must not be broken during deformation, or that chains do not remain bent after deformation, the only possible slip planes are ($hk0$) planes. But, of these, we may confine our attention to the more closely packed low index planes (100), (010), and (110), for it is unlikely that planes of higher index will be effective as slip planes. It is now relatively easy to enumerate the dislocations which can give rise to slip on these planes.

In table 1 we have listed possible screw and edge dislocations, but limiting ourselves, for simplicity, to dislocations of unit strength (Burgers vector equal to a primitive translation of the lattice), and omitting other dislocations obtainable from those listed by trivial change, as in the sign of a Miller index or a Burgers vector. Given in the table are the orientations of the Burgers vector, b, and of the line, l, of each dislocation, together with its associated glide plane. For the four screw dislocations (1–4), b and l are, of course, identical and, in all respects save one, the entries in the table are arrived at by simple considerations such as would apply in a metal crystal [*8, 9*]. The notable exception is the assignment of specific glide planes to the screw dislocations 2, 3, and 4. Whereas a screw dislocation in a metal or an ionic crystal can glide in any plane of the zone defined by the dislocation line as axis, dislocations 2, 3, and 4 in an infinite chain crystal can glide easily only in the planes we have indicated. If they were to glide in any other planes they would leave behind in their wakes planes of disorder in which molecular chains suffer a sigmoid bending (see later); the only alternative to such a bending would be the breaking of bonds. We shall now consider each of the dislocations listed in more detail.

TABLE 1.

	Burgers vector	Dislocation line	Glide plane
Screw dislocations			
(1)	[001]	[001]	Any plane of the [001] zone
(2)	[100]	[100]	(010)
(3)	[010]	[010]	(100)
(4)	[110]	[110]	($1\bar{1}0$)
Edge dislocations			
(5)	[100]	[001]	(010)
(6)	[010]	[001]	(100)
(7)	[110]	[001]	($1\bar{1}0$)
(8)	[001]	[100]	(010)
(9)	[001]	[010]	(100)
(10)	[001]	[110]	($1\bar{1}0$)

2.1. Screw Dislocations

Screw dislocations of type 1 are unique in the infinite chain crystal in that they are the only screw dislocations possible which do not require any distortion or bending of molecular chains. They could exist, indeed, in a crystal composed of closely packed rigid rods. These dislocations, therefore, are free to glide in any plane of the [001] zone; but, of course, close-packed planes will be favored. Except in that they have a relatively small Burgers vector (2.54 Å) they are topologically similar to the giant screw dislocations which contribute significantly to crystal growth in polyethylene lamellae formed in dilute solution [*1*].

As already mentioned, dislocations of types 2, 3, and 4 are different. Here the dislocation lines are perpendicular to the chains and, since the stress field of a screw dislocation is confined to shears acting along the direction of the dislocation line [*8, 9*], there must be associated with these dislocations shear stresses which cause the chains to bend. For example, let us now consider a dislocation of type 2, shown schematically in figure 1. This dislocation can glide in the (010) plane without doing more than causing the shear field (whose form is obvious from fig. 1) to move with it, and at the same time causing chains to slip past one another over the plane swept out by the glide motion. But, if it were to glide in the (001) plane, say (that is, in or out of the plane of the paper in fig. 1), it would leave behind it in the region swept out by glide a plane of sigmoid bends (shaded area in fig. 2). In other words, such a motion of the dislocation would not only cause chains to slip past one another in (010) planes, but would also allow the upper part of the crystal to move relative to the lower part (by a translation b) *only at the expense of bending every chain in that part of the crystal through which the dislocation has passed.* It is clear on energetic grounds that such a slip process will not figure prominently in the behavior of real crystals. Moreover, such a process implies that a stress exists over the whole plane of bent bonds instead of being localized near the dislocation line. It is a plane defect rather than a line defect and hence difficult to classify as a perfect dislocation [8, 9].

A word may be said in passing about the means whereby chains close to a dislocation line may bend in the cases of dislocations of types 2, 3, and 4 (see again fig. 1). In our opinion, this distortion is most likely brought about by bond stretching and by slight distortion of valence bond angles. We are led to this view by noting that, whereas rotations about bonds would be favored in terms of intra-chain energy, they would not lead to a slight elongation of the chain as is required (quite the opposite) and, in addition, they would give rise to larger inter-chain conflicts.

2.2. Edge Dislocations

The six edge dislocations listed in table 1 represent the only ones likely to participate in slip processes in an infinite chain crystal. The first three (5–7) involve no bond distortion and, like screw dislocations of type 1, could exist in a lattice of rigid rods. They require little comment, other than to remark (a) that their energies of formation (proportional to b^2) increase in the order 6, 5, and 7; (b) that a dislocation

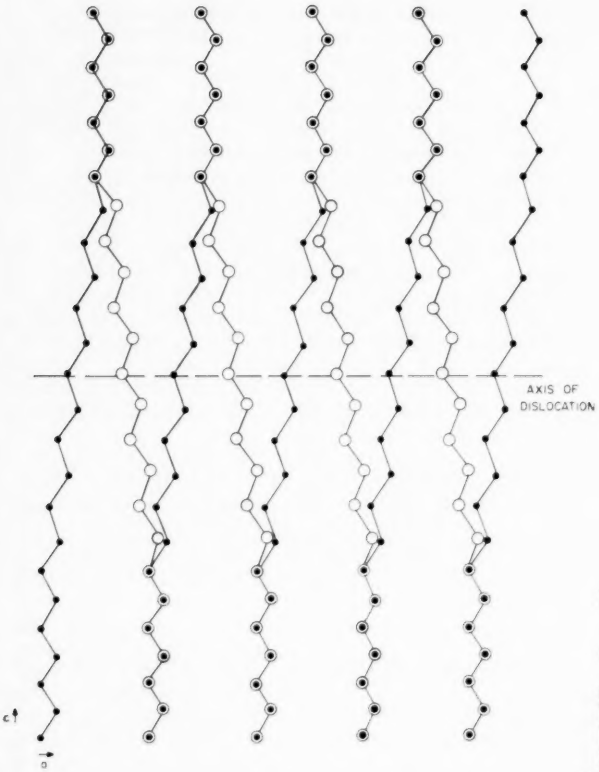

FIGURE 1. *A schematic representation of a screw dislocation with [100] Burgers vector in polyethylene.*

The chains are projected on the (010) plane and for clarity only the chains at the corners of the unit cell are shown.

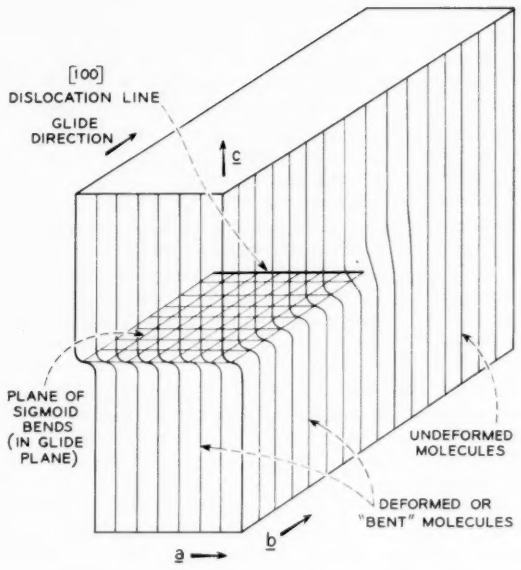

FIGURE 2. *A schematic representation of the effect of a screw dislocation with [100] Burgers vector gliding in a (001) plane.*

Notice that a plane of sigmoid bends is left as a result of this motion, which accordingly is considered to be energetically most unlikely.

of type 7 might well dissociate into a pair of partial dislocations [2]; and (c) that, regarding an edge dislocation of unit strength as arising by the insertion of a half-plane of molecules into an otherwise perfect lattice, then, on account of the "body centered" character of the unit cell we are considering, what must be inserted is two half-planes which may be of (110), (100), or (010) type. With reference to (b) it may be pointed out that dissociation of a dislocation of type 7 into partials is limited by the energy required to generate a ribbon of stacking fault between the separated partials. Although this energy might be expected to be appreciable for polyethylene, the possibility exists that it may become quite small at elevated temperatures because of rotation (perhaps even fairly free rotation) of molecular chains in the lattice. Dislocations might then split readily into partials at higher temperatures and, despite unfavorable energetics, these partials may remain separated, for the most part, on cooling again to room temperature.[3]

The remaining dislocations (8–10) require more detailed discussion. These dislocations involve strains in the chain direction which are opposed by relatively strong forces, and would inevitably be ones with which substantial line energies must be associated. Indeed, we are uncertain of the likelihood of their ever being formed. But, in the absence of these dislocations, it may be noted, the only dislocation mechanism which would lead to slip in the [001] direction under the action of a simple shear on an (hk0) plane would involve the glide of screw dislocations of type 1.

We suggest that, if b=[001] edge dislocations do occur, they are probably formed by bond stretching and bond angle distortion. Dislocations as recently proposed to account for slip bands in nylon 66 [3] we consider to be much less likely. In the latter, planes of molecules are considered to "bulge" at the dislocations, thus giving rise to large cavities in the crystal. In negotiating these bulges, molecules must undergo rotations about bonds such as would give rise to severe inter-chain conflicts (this is easily demonstrated with a Hirschfelder model). The longer the repeat distance along the chain (~17A for nylon 66) the larger the cavities and the more severe the conflicts become; at the same time, the resistance to glide motion increases correspondingly. In these terms it would appear that edge dislocations whose Burgers vectors are parallel to a molecular chain axis are likely only in polymers in which the chemical repeat distance is fairly short.

3. Long Chain Hydrocarbon Crystals

In this section we again use as a model for discussion hydrocarbon crystals of orthorhombic structure. For these crystals two unit cells may be

[3] Note added in proof: Recent studies by V. F. Holland (J. Appl. Phys. **35**, (1964)) show that appreciable densities of such partials are produced in chain-folded polyethylene crystals by heat treatment.

distinguished; a primary unit cell which incorporates in its c direction the full length of two hydrocarbon chains and a subcell which in its c direction incorporates two CH_2 groups and has a length 2.54 Å [*10*]. The a and b dimensions are the same for both cells and apart from slight variations in a and b, the subcell is identical with those of the infinite chain crystal and of polyethylene.

The uniform length of the hydrocarbon chains clearly introduces as a new glide plane the plane on either side of which lie terminal methyl groups of the extended molecules. In the system defined by the primary cell these are (002) planes [*10*]. The existence of this glide plane, across which there are no molecular ties, obviously brings several new dislocations into play.

Screw dislocations similar to type 1, but with Burgers vectors equal to integral multiples of that of dislocation 1, can occur in hydrocarbon crystals just as they might arise in an infinite chain crystal. But now, as a special case, these would include the screw dislocation which gives rise to the well known growth steps in hydrocarbon crystals and has a Burgers vector equal to the length of one or more extended molecules. In addition to this dislocation, there are dislocations which may glide in the new glide plane. These are the screw dislocation 2–4 listed earlier, and three new edge dislocations with Burgers vectors [100], [010], [110], and lines [010], [100], and [1$\bar{3}$0], respectively. For the third of these to be strictly an edge dislocation, its line must be normal to b; it must therefore lie close to the [1$\bar{3}$0] direction in this structure. Any of these dislocations cause individual layers of molecules to slip over one another, leading to a "card-deck" type of deformation which, *a priori*, would seem a likely process in these crystals.

4. Chain-Folded Polyethylene Single Crystals

Proceeding now to the case of a polyethylene single crystal, we recognize immediately that slip processes must be limited in many cases by the fact that neighboring lengths of chain may be connected by virtue of molecular folding. Moreover, the geometry of this folding will be an important consideration. To illustrate this, we consider a crystal with molecules folded regularly in {110} planes, and in figure 3 we show a boundary between different fold domains for one of the possible folding regimes of this type [*11*].

It is evident in this case that the only planes on which repeated slip is possible without disruption of the structure are {110} planes, and of these there is but one suitable plane in each domain. This is the fold plane [*11*], which lies parallel to the growth front by the advance of which the particular domain in question was initially formed. Since there are no primary bond connections between molecular segments in a given fold plane and segments in either of the adjacent fold planes, the given plane is clearly

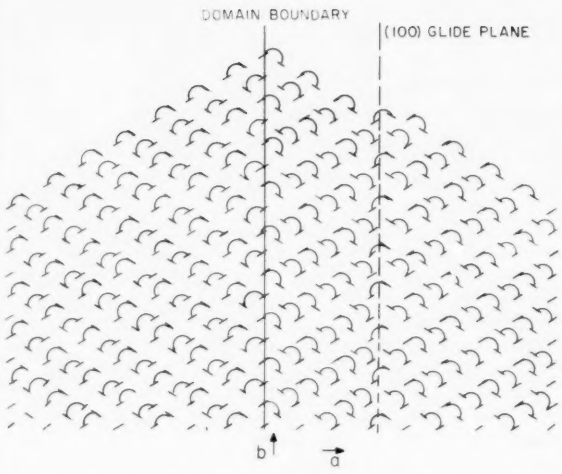

FIGURE 3. *A schematic representation of the chain-folded surface of a lamellar polyethylene crystal.*

The only true glide planes are the fold planes. In the right hand half of the crystal a dislocation with [010] Burgers vector has glided in a (100) plane and resulted in a modification of the folding scheme. Note that subsequent slip in this plane is impossible without a drastic rearrangement of the molecules and of the fold geometry.

a possible glide plane. The dislocations which may glide in this plane are obviously the same as those which can glide in the corresponding plane of an infinite chain crystal and have already been listed in table 1. However, any departure from regular folding which gives rise to connectivity between fold planes is potentially a barrier to glide. Fold domain boundaries, in particular, are impenetrable barriers to the passage of dislocations in this structure other than screw dislocations of type 1 which could conceivably approach a boundary along a fold plane in one domain, change direction at the boundary and then glide in the (different) fold plane of the adjacent domain. For example, a screw dislocation might approach the boundary in figure 3 from the left along a (1$\bar{1}$0) plane and, having passed through the boundary, continue to the right along a (110) plane. Favorable stresses for generating such a motion might well arise in the drying down of pyramidal crystals (see later), but it is difficult to see how they would otherwise be produced in any concerted fashion.

As is evident from figure 3, a limited amount of slip is possible in [010] or conceivably in [100] directions. However, these motions are restricted to translations of one unit cell and, even then, to translations in specific directions. For, if (110) is the fold plane, as in the right of figure 3, then the part of the crystal lying to the right of a (010) slip plane may move upward by one unit with respect to the remainder of the crystal because the folds may be rearranged to lie in the [110] rather than the [1$\bar{1}$0] direction. But these folds cannot easily be stretched the distance required either for slip in the opposite direction, or for multiple slip processes, to occur.

An interesting situation arises if slip takes place in the *c* direction in a plane such as the (010) plane and, in principle, this could be caused by the glide of dislocations of types 1 or 9. Because of the continuity of folded molecules, configurations such as shown in figure 4 must result. Motion of these dislocations in adjacent planes, successively, might occur in the collapse of pyramidal or ridged crystals which become flat as a result of shear deformations in the course of drying down from suspension in solvent [*1*]. For it is clear that stress will be concentrated at boundaries between the deformed, and as yet undeformed, regions of these crystals and may generate the dislocations required for this process. In later stages of collapse of an initially pyramidal crystal, continuing collapse could be brought about by a screw dislocation of type 1 circuiting the boundary of the undeformed region in an ever decreasing spiral.

Repeated passage of dislocations along the same (010) glide plane in a case such as shown in figure 4, however, would have the effect of partly disrupting the structure but leaving those parts of the crystal which lie on opposite sides of the glide plane connected by sections of alined chains. If such a process were to occur within a chain folded crystallite in bulk polyethylene it would doubtlessly be accompanied by a reorientation of the molecular chain about the *a* axis as is often observed in fibers drawn to moderate elongations [*12*].

It is convenient at this point to consider briefly the questions of the climb motion and the intersection of dislocations [*8*, *9*]. Our remarks are applicable not only to polymer crystals but also to the infinite chain crystal and to hydrocarbon crystals of appreciable chain length ($n>20$, say). First we note that climb involves diffusion of vacancies or interstitials, but in the conventional sense these defects have no significance in the various crystals under consideration. (Vacancies could exist at chain ends in a polymer crystal, but would be immobile in the sense that they cannot diffuse independently of the specific chains with which they are associated.) Since diffusional motion in these structures would require the displacement of entire chains (or of extended lengths of chain in a polymer crystal) dislocation climb will be an insignificant process except perhaps in chain-folded crystals at elevated temperatures.

The intersection of dislocations in long chain molecular crystals would require considerable space for thorough discussion. Suffice it to say that we have examined all possible intersections of the dislocations listed in table 1, and that the results may be summarized as follows. Intersections lead in general to the formation of jogs, which in some instances offer little resistance to the further motion of dislocations and in other instances immobilize dislocations by being constrained to move only by climb. The climb of such a jog is forbidden for the reason that it would involve the diffusion, not of entire chains or extended lengths of chain, but of interstitials or vacant lattice sites. Certain intersections are physically impossible since, as in the case of dislocation 3 intersecting dislocation 5, they would lead to jogs which cannot be formed without primary bonds being broken. In this situation the dislocations are pinned. The following rules apply. Half of the conceivable screw-screw intersections are physically impossible and only those are allowed in which a dislocation of type 1 intersects dislocations of types 2, 3, and 4. Even in these cases, the first dislocation acquires a jog which has to glide out of the crystal along the screw axis before the dislocation as a whole can glide; the other dislocation (2, 3, or 4) is totally immobilized. Edge dislocations, on the other hand, may intersect one another without immobilization. Of the 17 conceivable screw-edge intersections, 7 are physically impossible, 7 involve immobilization of the screw, and in only 3 can the screw and edge both move freely after intersection. In hydrocarbon crystals, of course, some of these restrictions are relaxed on account of the presence of unique glide planes lying between molecular layers.

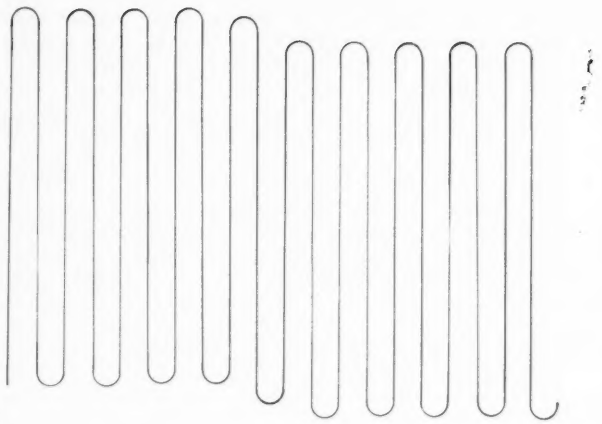

FIGURE 4. *A schematic representation of the configuration of a chain folded molecule in a polyethylene crystal after the passage of a dislocation with [001] Burgers vector.*

To summarize, it is clear that dislocations are unlikely to play a major part in bringing about deformations of appreciable magnitude in chain-folded polymer crystals. As we have seen, repeated slip on a given glide plane is impossible unless there are attendant readjustments in the disposition and packing of folds. Our remarks concerning intersections make it evident that extended movement of dislocations will in general be severely restricted. Moreover, the relatively small number of dislocations likely to be present initially in polymer crystals as grown (whose volumes are usually small, 10^{-12} cm^3 or less) would soon be used up in quite small deformations; and we note that their replacement by mecha-

nisms such as might operate in metal crystals is in the present case highly improbable. A Frank-Read source [*13*], for example, requires for its operation an area of glide plane of the order of a 1 μ square, and the only planes of sufficient extent in chain-folded polymer crystals are not permissible glide planes.

A possible deformation mechanism which could give rise to substantial and more or less uniform shear strains in these crystals is twinning. This involves a rearrangement in packing requiring no more than a slight translation of one chain relative to its neighbors, and what little evidence is currently available does indeed suggest that deformation by twinning is a common occurrence [*2, 14*]. As has already been pointed out, in chain-folded polyethylene crystals the only unrestricted glide planes are the fold planes. Thus in these crystals twinning would be expected to occur on (110) planes, and this does appear to be the case [*14*]. On the other hand, in oriented bulk polyethylene, where regular chain folding does not exist, other twin planes are possible, and (310) twins have been reported [*2*]. Here, as in simpler solids, the mechanism by which twinning occurs remains uncertain; the successive generation and motion of dislocations on adjacent glide planes may be involved, but, of necessity, it must be a cooperative process.

Very large plastic deformations, such as occur in the drawing of fibers, most likely involve various complex catastrophic processes. But, in the event that tensile stress is applied normal to the *c* axis of a crystal, one might expect a simple "unzippering" of folded chains to give rise to fine fibrillar texture, a process for which there is already some experimental evidence [*15, 16*].

It seems reasonable to conclude that *appreciable* deformations of chain-folded polymer crystals cannot be attributed solely or simply to dislocation mechanisms. Molecular rearrangements other than slip in an otherwise undisturbed lattice must be involved, and these require careful consideration. Dislocations may make important contributions to plastic deformation in hydrocarbon crystals, however, or in "extended chain" polymer crystals such as have recently been reported in some samples of bulk polyethylene [*17*].

We are very grateful to Drs. F. Khoury of the National Bureau of Standards and P. H. Lindenmeyer of the Chemstrand Research Center for many critical comments and numerous helpful discussions.

5. References

[1] H. D. Keith "Crystallization of long-chain polymers" in The Physics and Chemistry of the Organic Solid State, ch. 8, Interscience, New York (1963).
[2] F. C. Frank, A. Keller, and A. O'Connor, Phil. Mag. **3,** 64 (1958).
[3] D. A. Zaukelies, J. Appl. Phys. **33,** 2797 (1962); M. F. Bender and M. L. Williams, J. Appl. Phys. **34,** 3329 (1963).
[4] D. H. Reneker, J. Polymer Sci. **59,** S39 (1962).
[5] C. W. Bunn and T. C. Alcock, Trans. Faraday Soc. **41,** 317 (1945).
[6] A. Keller, Phil. Mag. **6,** 329 (1961).
[7] D. C. Bassett and A. Keller, Phil. Mag. **6,** 345 (1961).
[8] W. T. Read, Dislocations in crystals (McGraw-Hill Book Co., Inc., New York, N.Y., 1953).
[9] A. M. Cottrell, Dislocations and plastic flow in crystals (Oxford, 1953).
[10] P. W. Teare, Acta. Cryst. **12,** 294 (1959).
[11] D. H. Reneker and P. H. Geil, J. Appl. Phys. **31,** 1916 (1960).
[12] S. L. Aggarwal and O. J. Sweeting, Chem. Rev. **57,** 665 (1957).
[13] F. C. Frank and W. T. Read, Phys. Rev. **79,** 722 (1950).
[14] P. H. Geil (in press).
[15] A. Keller, Phil. Mag. **2,** 1171 (1957).
[16] H. D. Keith and F. J. Padden, Jr., J. Polymer Sci. **41,** 525 (1959).
[17] P. H. Geil, F. R. Anderson, B. Wunderlich, and T. Arakawa (in press).

(Paper 68A5–297)

JOURNAL OF RESEARCH of the National Bureau of Standards—A. Physics and Chemistry
Vol. 68A, No. 5, September–October 1964

Dependence of Mechanical Relaxation on Morphology in Isotactic Polypropylene

Elio Passaglia and Gordon M. Martin

(June 2, 1964)

The shear modulus and logarithmic decrement at approximately 1 c/s have been measured from −180 °C to about 150 °C for a series of samples of isotactic polypropylene prepared by various thermal treatments. The samples had varying densities (degrees of crystallinity) and morphologies as characterized by spherulite size. All of the samples exhibited the three relaxations characteristic of polypropylene. The maxima in the three measures of relaxation (logarithmic decrement, G'', and J'') occur at about −60 °C, 0–10 °C, and 50 to 100 °C for the three processes. However, the relation between crystallinity and the magnitude of the peak value of the particular measure of loss depends upon the relaxation and the function used to measure the loss. The loss is almost independent of density and morphology for all three relaxations when G'' is used to characterize the loss, whereas the loss increases monotonically as the density decreases when using J'' to characterize the loss behavior. The logarithmic decrement behaves in a more complicated manner. The implications of this behavior are discussed, and it is shown that the primary effect of changing density is to change the equilibrium modulus rather than the relaxation processes.

1. Introduction

Mechanical relaxation in amorphous and crystalline polymers has been extensively studied because of its intrinsic and practical importance and because its correct intrepretation can elucidate the nature of molecular motions in these systems. In amorphous polymers, a great deal of experimental and theoretical work has been carried out, and agreement between experiment and molecular theories of relaxation has been achieved.

In crystalline polymers, the situation is much more complex. The complicated morphological nature of these polymers has permitted only qualitative interpretation of various relaxation processes in molecular terms [1, 2].[1] Indeed, most of the interpretation has been in terms of an amorphous-crystalline two-phase model of polymer morphology using the degree of crystallinity (as determined by density or some other means) as the primary parameter for comparison of different samples. The effort has gone primarily into inferring the phase in which the relaxation process occurs and the probable size and type of relaxing species. Such a model may be too restrictive for highly crystalline polymers such as linear polyethylene, where electron microscope [3] and heat of fusion [4] results indicate a very small amorphous component which can, in fact, be regarded primarily as in the crystalline phase imperfections such as chain folds [5]. Moreover, even on the basis of the two phase model, there is considerable disagreement as to the site of various relaxations in specific cases. Thus, for example, McCrum [6] deduces that the high temperature (see below) relaxation in polypropylene involves a "crystal disordering," while Flocke [7] attributes the same relaxation to a process occurring in the amorphous regions. Other evidence [8, 9], also indicates that the degree of crystallinity is not a sensitive enough criterion for comparing samples of varying thermal treatment, and that some of the relaxation processes are related to more subtle aspects of the morphology.

In most of the work relating mechanical behavior to morphology, comparison of various samples has been made on the basis of tan δ (the ratio of the imaginary part of the complex modulus to the real part) or some related quantity such as the logarithmic decrement (which in this paper we shall denote by the symbol Δ), primarily because most of the experiments have been carried out by the methods of forced or free oscillation in which the behavior of the specimen is governed by this quantity. However, it is well known that the maximum value of tan δ against frequency (or, more commonly, temperature) is not a good measure of the strength of the relaxation [2] unless the change in G', the real part of the complex modulus, is very small compared to the static modulus, G_e. This is not the case in most polymer systems. The correct quantity to use would be the area under the G'' peak in a G'' versus $\ln\omega$ plot, where ω is the frequency. This type of data is not usually available, and the area under a $G''-1/T$ curve at constant frequency (which would be equivalent if all the relaxation times had the same temperature dependence) is often very difficult to obtain because the peaks are unresolved. In some cases G'' has been used as a measure of the relaxation strength when comparing samples of different crystallinity or morphology [10]. However, even in this case there is no *a priori* reason to use G'' rather than J'', the imaginary part of the complex compliance. When comparing samples in which the modulus changes, the two methods, as will be seen, may lead to quite different conclusions.

[1] Figures in brackets indicate the literature references at the end of this paper.

[2] By "strength of the relaxation" we mean the difference between the moduli at very high and very low frequencies, i.e., $G_\infty - G_e'$.

In order to clarify some of these points a study was made of mechanical relaxation in polypropylene. This is a good material for study in that it can be obtained in both atactic (i.e., noncrystallizable) and isotactic (crystallizable) forms. It is known from the work of Keith and Padden [11] that atactic polypropylene mixed with isotactic is excluded from the crystalline phase when the isotactic component crystallizes. Hence, a density defect (density lower than the crystal density) in such a mixed system may be fairly unambiguously identified with the presence of a true amorphous phase. A thorough study of mechanical relaxation in such a system has already been carried out by Flocke [7]. Our own aims were threefold. These were: (a) to compare the behavior of a quenched isotactic specimen with that of a mixed isotactic-atactic specimen of the same density; (b) to compare the behavior of a sample which had been quenched and subsequently annealed to a given density, with that of one in which the same density had been achieved by isothermal crystallization (it is well known that such treatments produce widely different morphologies); (c) to compare the various viscoelastic functions for these samples.

2. Experimental Details

2.1. Apparatus and Method

All the measurements reported here were taken using a torsion pendulum based on the design of Nielsen [12]. In this type of torsion pendulum the inertial member is supported by a fine wire of negligible elastance and is counterbalanced so that the sample is under no longitudinal stress. The inertial member was designed so that the frequency would be 1 c/s for a sample with a shear modulus of 10^9 N/m^2 and the chosen dimensions (see below).

The primary quantities measured in such an apparatus are the period of the oscillation and the rate of decay of the vibration amplitude. In some of the experiments the amplitude decay and the frequency were measured by a galvanometer lamp and scale arrangement. In a later development a strain gage was added to the system to provide an electrical signal proportional to displacement. This signal was then recorded on a recording oscillograph. There was no discernible difference in the results obtained by the two methods.

In both methods of operation the period was determined by timing the swings, either by a stop watch in the first case, or by timing-markers on the recorder chart in the second. The logarithmic decrement, Δ, in both cases was determined by plotting the logarithm of the amplitude against the number of the swing and determining the slope of the resulting line. In practically all cases good straight lines were obtained.

The real part of the complex modulus, G', was determined from the frequency, the known moment of inertia of the inertial member of the pendulum, and the sample dimensions (see "Sample Preparation" below). The approximate equation

$$G' \cong \frac{\omega^2 I}{k}$$

where ω is the angular frequency, I the moment of inertia and k a form factor depending on sample dimensions [12], was used. The maximum error this approximation produced was about 1 percent. From G' and Δ, G'' and J'' were calculated by the equations

$$G'' = \frac{G'\Delta}{\pi} \tag{1}$$

and

$$J'' = \frac{G''}{(G')^2 + (G'')^2}. \tag{2}$$

2.2. Material and Sample Preparation

The material was an experimental sample of isotactic polypropylene kindly provided by the AviSun Corporation. This had a viscosity average molecular weight of 207,700 and contained 2.56 percent material extractable by C_7 hydrocarbon fraction. It contained 0.02 percent of stabilizer.

The samples were in the form of flat strips, with nominal dimensions $10 \times 2 \times 0.125$ cm. This rather long flat shape was chosen to permit easy quenching of the specimens. The latter were prepared in the following manner. Flat sheets about 15×15 cm and of the proper thickness were prepared by compression molding. From these a specimen about 12 cm long and 2 cm wide was cut. This was then mounted between two aluminum strips of the proper dimensions and the sandwich tightly wrapped in aluminum foil. This wrapped sandwich was then mounted between two 0.8 mm thick sheets of phosphor-bronze held together by slight spring tension. The whole assembly was heated to 200 °C for a few minutes either in a silicone oil bath or an oven, and then either quenched in dry-ice acetone or isothermally crystallized. This arrangement was chosen over a conventional mold to reduce the mass and provide fast quenching. From the resulting strip the final specimen was shaped by machining. The variation in width was negligible. The thickness was measured at several places along the sample and the results averaged. The maximum variation in thickness over the sample was about 5 percent. Since the thickness enters the form factor for calculating G' as the cube, an average of the cube of the thickness was used.

The primary means of comparison of the state of various specimens was the degree of crystallinity, χ, as determined by density. This was determined by hydrostatic weighing and converted to crystallinity by the crystallinity-density scale of Danusso and Maraglio [13]. Because of effects such as static charge on the specimen which affected the weighing, χ has an estimated standard error of about ± 1 percent.

As mentioned in the introduction, one of the aims of this work was to compare samples of the same χ, but achieved in different ways, i.e., by the quench-anneal technique and isothermal crystallization. The quench-anneal experiments were carried out on one specimen which had been quenched by the procedure outlined above. After measurement in the torsion pendulum, this specimen was annealed for a certain time, remeasured, etc. The history of this sample is reported in table 1. During the run in the torsion pendulum the specimens of course crystallized somewhat, particularly at the lower crystallinities. This limited the temperature range of the experiments for the lower crystallinity samples. Furthermore, the curves for the lower crystallinity samples are once-through curves. The change in χ during the measurements on the torsion-pendulum is also reported.

TABLE 1. *Thermal treatment and crystallinity of samples*

Sample No.	Treatment	χ %	
		Before run	After run
1	Quenched	44	47
1A	No. 1+1 hr at 70 °C	50.3	51.1
1B	No. 1A+1 hr at 90 °C	55.2	56.2
1C	No. 1B+4 hr at 135 °C	64.4	65.8
1D	No. 1C+4 hr at 150 °C	70.3	
2	Isothermal; 40 hr at 135 °C	68.5	

One other sample was crystallized isothermally. It is also reported in the table. In addition to these, other specimens were used to check and amplify the results. They will be mentioned in the text.

X-ray diffraction studies [3] were carried out on specimens 1, 1C, and 2, and flat film transmission patterns are shown in figure 1. Specimen No. 1 contained a small amount of polypropylene in the hexagonal crystal form [14], which disappeared on annealing. Although not apparent from the photographs shown in figure 1, specimens 1 and 2 showed a small amount of preferred orientation, determined by more precise diffractometer measurements. This was probably caused by multiple nucleation at the walls of the quenching apparatus, and is not expected to affect the results significantly.

The gross morphology of specimens 1, 1C, and 2 was observed by studying thin sections of these specimens under the polarizing microscope, and photomicrographs are shown in figure 2. The results are as expected; specimens 1 and 1C show a highly irregular, granular morphology, with some indication of spherulites, albeit ill-formed and irregular. Specimen 2 shows typical well-formed spherulites of mixed positive and negative character [15].

3. Results and Discussion

As mentioned in the introduction, Δ is not a good quantity to use to determine the strength of a relaxation, nor the average relaxation time of the process. Nevertheless, we shall delay discussion of G'' and J'', which are more directly related to the relaxation parameters, and discuss the relaxations in terms of Δ. This will be more nearly comparable to much of the discussion in the literature, and make comparison with it easier.

[3] We are highly indebted to Mr. Norman M. Walter of the American Viscose Corporation for carrying out these studies for us.

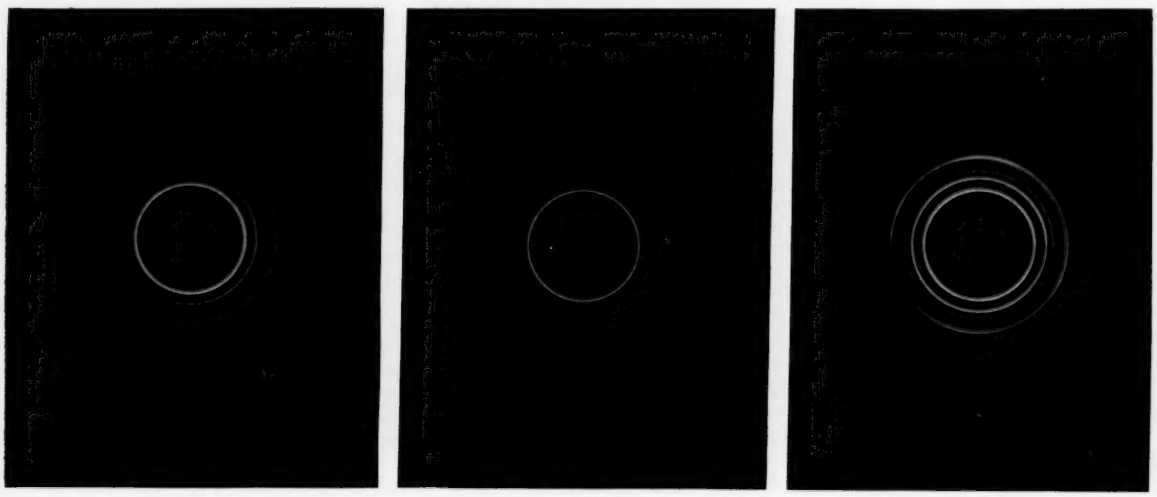

FIGURE 1. *X-ray diffraction patterns of samples 1, 1C, and 2 in table 1.*
More precise diffractometer measurements show a small amount of preferred orientation in samples 1 and 2.

736-657—64——7

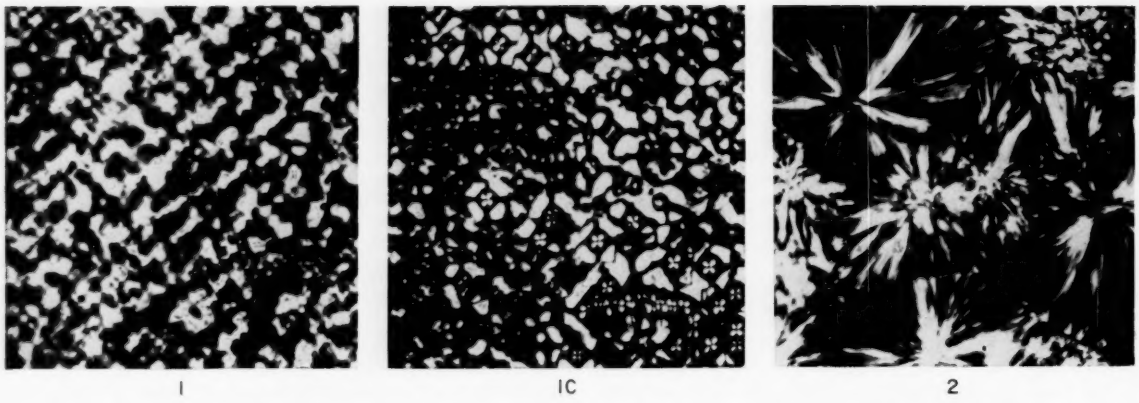

FIGURE 2. *Optical micrographs under crossed polaroids of thin sections of samples 1, 1C, and 2 in table 1.*

The magnification is 290 × in each case. Note the well formed spherulites in sample 2.

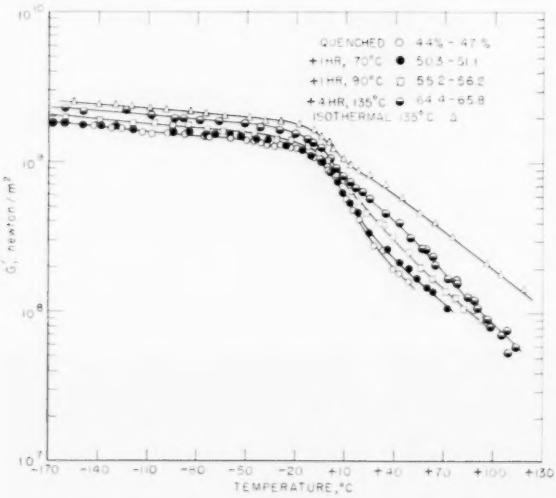

FIGURE 3. *The real part of the complex modulus as a function of temperature for five of the specimens listed in table 2: 1—○, 1A—●, 1B—□, 1C—◒, 2—△.*

The numbers denote degrees of crystallinity before and after the run.

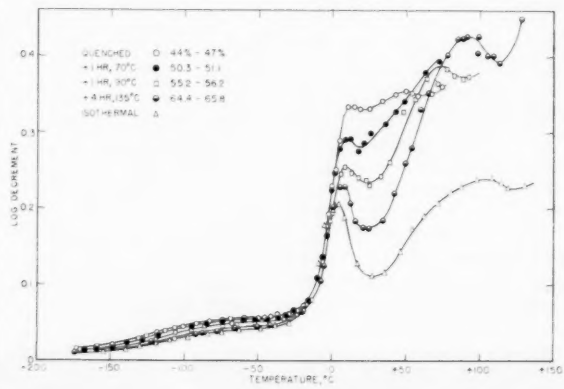

FIGURE 4. *The logarithmic decrement as a function of temperature for the same specimens shown in figure 3.*

Note the behavior with crystallinity of the high temperature relaxation.

The results for G' and Δ are shown in figures 3 and 4 for samples 1, 1A, 1B, 1C, and 2. Sample 1D is omitted for clarity but is reported in table 2 (see below). Sample No. 1 was measured only to 53 °C, but the data for Δ were later extended and checked by similar samples whose dimensions, unfortunately, were not uniform enough to permit unambiguous calculation of G'.

The Δ versus T curve shows the three peaks indicating three relaxation processes characteristic of other crystalline polymers. (The lowest temperature peak is small and very broad, appearing almost as a shoulder on the low temperature side of the intermediate temperature peak.) These relaxations have been referred to in almost as many ways as there are authors in the field. Indeed, they have been called transitions, although they are not necessarily related to true thermodynamic transitions, except in some cases. We prefer to use the term "relaxation" for these peaks, and adopt the nomenclature of Scott et al. [9] for them. Thus, the low temperature peak we call the "low-temperature relaxation" (LTR), the medium temperature peak we call the "glass transition relaxation" (GTR) since it occurs near the dilatometric glass transition temperature, and the high temperature peak we call simply the "high-temperature relaxation" (HTR).

3.1. Low Temperature Relaxation

This is a very broad relaxation with a maximum in Δ (Δ_{max}) occurring at approximately −60 °C. It has been previously observed by other workers [6, 7, 16, 17]. The pertinent information for this and

TABLE 2. *Experimental parameters for the three relaxations observed*

Sample No.	LTR				GTR				HTR					
	T_{max}	Δ_{max}	G'	ν	T_{max}	Δ_{max}	G'	ν	T_{max} [a]	Δ_{max}	G'	ν	G''_{max}	T_{max} [b]
	°C		*newton/m²*	*c/s*	°C		*newton/m²*	*c/s*	°C		*newton/m²*	*c/s*	*newton/m²*	
1	−60	0.057	1.42×10^9	1.070	12	0.334	0.52×10^9	0.650	50	0.355		0.383		
1A	−60	.055	1.52	1.111	11	.292	.55	.665	72	.373	0.104×10^9	.294		
1B	−55	.052	1.80	1.104	9	.254	.76	.785	74	.369	.124	.323	0.25×10^8	47
1C	−50	.045	1.80	1.204	7.5	.230	.85	.823	93	.426	.100	.275	.25	57
1D	−50	.043	2.05	1.36	4	.212	1.14	1.020	108	.468	.106	.312	.28	66
2	−50	.043	2.04	0.888	4	.203	1.12	0.671	105	.240	.170	.258	.23	57

[a] The temperature of the maximum in Δ.
[b] The temperature of the maximum in G''.

the other relaxations are given in table 2. The curves for the real part of the shear modulus (fig. 3) do not show any inflection point within the temperature range of this relaxation. However, it will be noticed that, with the exception of sample 1D, Δ_{max} decreases and G' increases as the density increases. This is even more evident in the data of Flocke [7], where the different densities were obtained by differing polymerization procedures and hence refer to samples of varying tacticity, and he was therefore able to study samples of lower density. Where comparison is possible the present data agree with those of Flocke to within about 10 percent.

The difference in density between samples 1D and 2 is just outside experimental error. The slightly higher values of Δ_{max} than would be expected for sample 1D from the behavior of the other samples indicates that some imperfections in the crystal for the quench-annealed samples may be the cause of a small amount of relaxation. The same difference occurs in the GTR.

Now, as mentioned in the introduction, it is well known from the work of Keith and Padden [11, 18] that atactic polymer in the presence of isotactic polymer is excluded from the crystalline phase when the isotactic component crystallizes. This atactic component segregates at interspherulitic boundaries, between lamellae or fibrils, etc., and exists as a true amorphous phase coexisting with the crystalline phase. Thus, reasoning from the behavior of Δ_{max} with crystallinity one would conclude, at least from the data of Flocke, that whatever process is responsible for the LTR, it is occurring in the amorphous phase, since Δ_{max} decreased with increasing crystallinity. And, to the extent that mechanical behavior as exemplified by Δ can be used to infer the thermodynamic state of a polymer, one would conclude that the quenched isotactic polymer is in the same state as the mixed atactic-isotactic polymer. This would be a fairly good reason for adopting a two-phase model for the fine morphological structure of a quenched polymer.

Moreover, the behavior of Δ in the LTR region is almost independent of the grosser details of the morphology. The behavior of specimen 2 is essentially what would be predicted from the behavior of the various specimens 1. This behavior would follow from the mechanisms proposed to explain the LTR in other polymers [1, 2, 8]. The relaxing unit is presumably small, consisting of only a few chain segments, and involves no motion of more complex morphological units.

3.2. Glass-Temperature Relaxation

The GTR is the next that occurs on the temperature scale. Again with the slight exception of the Δ_{max} value for sample 1D, the magnitude Δ_{max} decreases and G' increases as density increases in all cases, independently of how the density is achieved. Again these data are in agreement with those of Flocke, and the same remarks that have been made for the LTR apply also to this relaxation.

There is an easily discernible difference in the temperature of the maximun in Δ. It is unfortunately difficult to discuss this in quantitative terms since "mixing" of this peak with that due to the HTR undoubtedly raises the temperature of the GTR maximum somewhat. (See, however, the $G''-T$ curves in figure 6. The same temperature difference exists for the maximum in the $G''-T$ curve, with much less mixing of peaks.) Without data at different frequencies these two peaks are difficult to separate. However, the behavior persists even with samples 1C, 1D, and 2 where mixing is less likely to influence the temperatures of the maximum and it is tempting to ascribe this variation to a more fundamental cause. It is known that the glass transition temperature in isotactic polypropylene is somewhat higher than in atactic polypropylene [19, 20]. The present sample of polypropylene contains 2.5 percent extractable material which is presumably all atactic, and may contain more atactic either as high molecular weight atactic chains or (as is more likely) atactic sequences in the main chains which would make the main chain a stereoblock copolymer. If this is true, and, as discussed above, atactic sequences are excluded from crystallites, then as the degree of crystallinity is increased the composition of the resulting amorphous component is changed, becoming richer in atactic material, and the glass-transition temperature falls. Since this relaxation is associated with the glass transition, the temperature of the maximum in Δ also falls.

This may be put into somewhat more quantitative terms. We assume that the whole polymer contains a fraction f of atactic material and $(1-f)$ of isotactic material, with glass transition temperatures T_a^g and T_i^g respectively. The glass transition is a property only of the amorphous polymer, and for a mixture of atactic and isotactic components can be related for our purposes to the glass transition temperature of the pure atactic and pure isotactic components by the equation [21]

$$T_m^g = \varphi T_a^g + (1-\varphi) T_i^g \tag{3}$$

where φ is the fraction of atactic polymer in the amorphous component. With these assumptions it is easy to show that

$$T_m^g = \frac{f}{1-\chi}(T_a^g - T_i^g) + T_i^g \tag{4}$$

where χ is the degree of crystallinity. It is now reasonable to expect that T_{max}, the temperature of the maximum in Δ, is displaced by the same amount from the dilatometric T_g for each of the pure components and for the mixture, provided the frequency of measurement is the same, as is very nearly true in these experiments. Figure 5 shows a plot of the observed T_{max} against $(1-\chi)^{-1}$, and it will be seen that the fit is surprisingly good. Extrapolating the curve to the (physically impossible) value of $(1-\chi)^{-1}=0$ gives a value of 21 °C for T_i^g for this frequency. If we accept the value of 2 °C for T_a^g from the 16.1 percent isotactic sample (measured at 2.0 c/s) of Flocke, then we calculate the not unreasonable value of 0.27 for f. Although the agreement is almost certainly fortuitous, this is in striking agreement with the value of 0.25 for the same quantity deduced by Wyckoff [22] from x-ray determinations on a similar polymer.

Further elaboration of this point would be inappropriate, considering the drastic nature of the approximations. However, the reasonable value of the quantities calculated indicate that some validity may be attached to this interpretation of the dependence of T_{max} on χ.

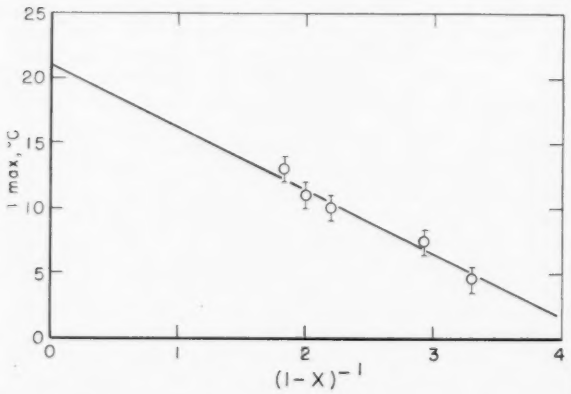

FIGURE 5. *A plot of the temperature of the maximum in* Δ *in the glass temperature relaxation against* $(1-\chi)^{-1}$ *(see text).*

3.3. High-Temperature Relaxation

This is the most complex of the relaxations. It is quite evident from the Δ-T curves that the behavior is quite intimately associated with the method of sample preparation. Arguing from the curves for specimen 1, one would be tempted to ascribe the source of this relaxation to some process occurring within the crystal, for the magnitude of Δ_{max} increases with sample crystallinity, and the temperature of the maximum also rises. This, however, cannot be the case, for specimen 2, which is more highly crystalline than any of the No. 1 specimens shown on the figure, has a lower peak than any of the latter. Indeed, specimen 1D, which had a χ of 0.70 shows a value of 0.468 for Δ_{max} whereas specimen 2 with essentially the same χ has a value of 0.24 for Δ_{max}.

This strong dependence on the gross morphology is unquestionably the basis of the conflicting interpretations found in the literature about the source of this process. Thus McCrum [6] ascribed this relaxation to "crystal disordering," Flocke [7] to a process in the amorphous regions, and Scott et al., ascribed the analogous relaxation in poly(chlorotrifluoroethylene) to "lamellar surfaces or interlamellar interactions." We are inclined to consider the last interpretation as being the most nearly correct.

The behavior of G' requires little comment. It is worthwhile to point out, however, that G' is higher throughout the whole temperature range for the higher crystallinity samples.

3.4. Behavior of Other Viscoelastic Functions

The various relaxation processes have been discussed with respect to the behavior of the logarithmic decrement, although the relationship of this quantity to the fundamental parameters of the relaxation is not very direct. That is to say, Δ_{max} may change not only because of a change in $\Delta G(G_\infty - G_e)$, but also because of a change in G_e alone. The more appropriate quantities for discussing the relaxation behavior are either G'' or J'' both of which have a direct relation to the relaxation strength.

However, in the case of a material such as a crystalline polymer, even the behavior of G'' and J'' is not sufficient to describe the situation completely. This is because such polymers are in a sense composite materials, consisting, on scale almost observable by optical microscopy, of a high modulus crystalline phase and some less well defined regions of lower modulus. In a polymer such as isotactic polypropylene there is evidence, as we have seen, for what amounts to a true amorphous phase. In a polymer such as polyethylene, which is much more highly crystalline, there exists a low modulus region consisting probably of some tie-molecules and certainly of juxtaposed chain-fold planes between lamellae. We

shall call these different modulus regions "phases," without meaning to imply that they both are true thermodynamic phases. In either case the evidence is that such materials are composites on a fairly gross scale.

Now, before mechanical relaxation can be observed, the applied stress, or strain, must be coupled to the relaxing species. And it will be clear that if the relaxing species exists primarily in one of the phases, then the connectivity between the phases is of paramount importance in determining the extent of relaxation. This problem of connectivity has already been discussed by Sasaguri and Stein [23] with reference to the optical behavior, and by Takayanagi [10] with respect to mechanical behavior of spherulites under deformation. The latter author has developed a phenomenological model which accounts for the behavior of filled polymer systems and mixtures of two polymers. Unfortunately, its application to the problem of relaxations in crystalline polymers presupposes a knowledge of the viscoelastic properties of the two phases over the whole range of temperatures, and this is usually not known.

In the absence of a detailed knowledge of the viscoelastic properties of the two phases, or of the details of the connectivity (which in principle could make their properties calculable from the properties of the composite if one could solve the formidable mechanical problem), we have chosen to compare the different samples studied at equivalent *macroscopic* strains and stresses. At a macroscopic sinusoidal strain $\epsilon_0 \sin \omega t$, the energy lost per cycle per unit volume is given by

$$W = \pi G'' \epsilon_0^2. \tag{5}$$

At a macroscopic sinusoidal stress of $\sigma_0 \sin \omega t$, the energy lost per cycle per unit volume is given by

$$W = \pi J'' \sigma_0^2. \tag{6}$$

Hence the correct quantities for comparing the loss at equivalent macroscopic strains and equivalent macroscopic stresses are G'' and J'' respectively. Plots of these quantities against temperature are shown in figures 6 and 7.

The differences between the Δ and G'' curves are striking; those between the Δ and J'' curves are not as great. The only distinct relaxation in the G'' curves is the GTR, the LTR and HTR appearing only as shoulders on this. Moreover, the order of the samples has been reversed in the GTR. Samples Nos. 2 and 1D (not shown) now have the highest value of G'' at the peak, with very little difference between the other No. 1 samples.

As shown in table 2, the differences in G''_{max} in the HTR are very much smaller than the differences in Δ_{max}, and above 125 °C, G'' for sample No. 2 is higher than for any of the No. 1 samples. This again is to be contrasted with the behavior of Δ. Moreover, in the HTR the temperature at which the maximum in G'' occurs is from 27 to 48 °C lower than the temperature at which the maximum in Δ occurs (table 2). This is due to the fact that G''_{max} and Δ_{max} are different functions of the relaxation times and the relaxing moduli, and Δ_{max} is also a function of the equilibrium modulus. These quantities change by varying and unknown amounts as the crystallinity and morphology change.

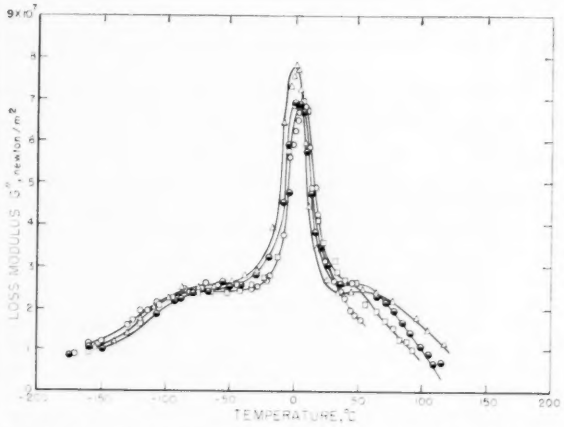

FIGURE 6. *The loss modulus of four of the samples in figure 4 as a function of temperature.*

The symbols are the same as in figure 4. Note the reversal in the behavior with crystallinity both in the glass temperature relaxation and in the high temperature relaxation as compared with figure 4.

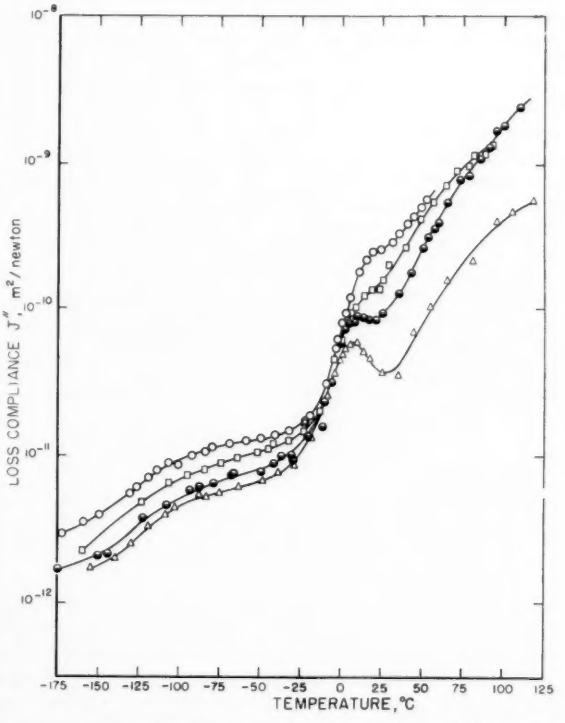

FIGURE 7. *The imaginary part of the complex compliance as a function of temperature for the same four samples as in figure 6.*

Figures 4, 6, and 7 indicate that for this material analysis of the effect of morphology upon the various relaxation processes depends upon the viscoelastic function chosen to characterize the relaxation.

The LTR is less complex, and to the precision of the data in this region these samples must be considered the same. In essence, the G'' curves have minimized the differences in the samples demonstrated by Δ, and, in fact, inverted the behavior.

The J'' curves, on the other hand, magnify the differences among the curves as compared to the Δ plot.

From these sets of curves, and bearing in mind that the samples in question had different degrees of crystallinity, one would be led to quite conflicting conclusions. Reasoning from the J'' curves one would conclude that the LTR, GTR, and HTR are all processes which occur in amorphous regions since all three processes are more prominent in the least crystalline specimens. Reasoning from the Δ curves one would conclude, as previously discussed, that the LTR and GTR are properties of an amorphous phase, while the HTR is a complex process depending very strongly on the morphology. Reasoning from the G'' curves, however, one would conclude that the differences among the samples are small, and what differences do exist are such that more relaxation is taking place in the more crystalline specimens and that hence the site of the relaxation process is in the crystal.

Such conflicting conclusions show the degree of caution which must be exercised when using any one mechanical experiment to deduce something about the nature of the relaxation processes in crystalline polymers. Not only must any one viscoelastic function be measured but the others must be computed from it and their behavior taken into consideration. To go beyond this one would need a molecular or phenomenological model on the basis of which the behavior of the viscoelastic functions could be calculated. With present knowledge of the details of the morphology of crystalline polymers this would be a formidable task.

It is relatively easy to show what conditions are necessary to have G' change and G'' not change over the whole temperature (and hence frequency) range as the degree of crystallinity is changed. This is approximately the behavior shown by the curves in figure 6. From linear viscoelasticity we have

$$G' = G_e + \sum_i \frac{G_i \omega^2 \tau_i^2}{1+\omega^2 \tau_i^2} \tag{7}$$

and

$$G'' = \sum_i \frac{G_i \omega \tau_i}{1+\omega^2 \tau_i^2} \tag{8}$$

where G_e is the equilibrium (low frequency) modulus, the τ_i are the relaxation times with associated relaxation moduli G_i, and ω is the frequency. For the purposes of this analysis we assume (as is approximately true) that the temperature dependence of G' and G'' comes only from the temperature dependence of the τ_i. Since ω and τ appear symmetrically in these equations, G' and G'' are the same functions of ω as they are of τ. Hence asking that a change in crystallinity produce no change in G'' over the whole temperature range at constant frequency is equivalent to asking that no change be produced over the whole frequency range at constant temperature.

Now, we expect G_e, the G_i, and the τ_i all to be functions of the degree of crystallinity, χ. Hence we have

$$\frac{dG'}{d\chi} = \frac{dG_e}{d\chi} + \sum_i \frac{\omega^2 \tau_i^2}{1+\omega^2 \tau_i^2} \frac{dG_i}{d\chi} + \sum_i \frac{2G_i \omega^2 \tau_i}{(1+\omega^2 \tau_i^2)^2} \frac{d\tau_i}{d\chi} \tag{9}$$

$$\frac{dG''}{d\chi} = \sum_i \frac{\omega \tau_i}{1+\omega^2 \tau_i^2} \frac{dG_i}{d\chi} + \sum_i \frac{G_i(\omega - \omega^3 \tau_i^2)}{(1+\omega^2 \tau_i^2)^2} \frac{d\tau_i}{d\chi}. \tag{10}$$

The vanishing of $dG''/d\chi$ at all frequencies (and hence at all temperatures) implies that both $dG_i/d\chi$ and $d\tau_i/d\chi$ are zero. If this is the case, then the only variation in G' comes about from the variation in G_e with crystallinity. This would imply that the G' curves for the various crystallinities are parallel to one another when plotted on a linear scale. A plot of the data shown in figure 3 shows that this is indeed approximately the case, at least below the GTR, where the G'' curves are very similar. Above this temperature the curves approach one another more closely, a reflection, no doubt, of the real differences that exist in the G'' curves in the HTR region.

These results imply that the main effect of changing χ is to change the static modulus, G_e, and that the differences observed in the $\Delta - T$ and $J'' - T$ curves for different χ are primarily, although not entirely, due to the variation of this quantity. This seems to be the case below and through the GTR, but above this temperature, both G_i and τ_i may change with χ. This behavior is understandable on the two-phase crystalline-amorphous concept of polymer morphology.

3.5. Conclusions

Three relaxation processes are observed for isotactic polypropylene in plots of G'', Δ, or J'' against T: one below the temperature at which the dilatometric glass transition is observed (the LTR), one near the dilatometric glass transition temperature (the GTR), and one above this temperature (the HTR).

Changing the crystallinity and morphology by annealing quenched specimens on the one hand, or preparing isothermally crystallized specimens on the other hand, has only a small effect on the behavior of G'' with temperature.

On the other hand, J'' for the less crystalline specimens is higher at all temperatures than for the more crystalline specimens, quite independently of the morphology. The behavior of Δ is more complicated, the LTR and GTR decreasing with crystallinity, while the HTR may increase or decrease. It is concluded that when comparison of different samples is made, completely different results will be obtained if comparison is made at equivalent macroscopic strains (G'') or equivalent macroscopic stresses (J''). This is presumably due to the un-

known microscopic connectivity of the composite material which is the crystalline polymer. It is incorrect, therefore, to say that changing the degree of crystallinity increases or decreases the magnitude of a given relaxation process; whether it does or does not depends primarily upon the mode of comparison. It is shown from these results that the primary effect of changing the degree of crystallinity is to change the static modulus, G_e.

4. References

[1] J. A. Sauer and A. E. Woodward, Rev. Modern Phys. **32,** 88 (1960).
[2] R. K. Eby and K. W. Sinnott, J. Appl. Phys. **32,** 1765 (1961).
[3] See, for example, F. R. Anderson, J. Appl. Phys. **35,** 64 (1964).
[4] E. Passaglia and H. K. Kevorkian, J. Appl. Polymer Sci. **7,** 119 (1963).
[5] J. D. Hoffman, to be published.
[6] N. G. McCrum, Makromol. Chemie.
[7] H. A. Flocke, Kolloid Z. **180,** 119 (1962).
[8] J. D. Ferry, Viscoelastic Properties of Polymers, p. 338 (John Wiley & Sons, New York, N.Y., 1961).
[9] A. H. Scott, D. J. Scheiber, A. J. Curtis, J. I. Lauritzen, Jr., and J. D. Hoffman, J. Res. NBS **66A,** (Phys. and Chem.) No. 4, 269 (1962).
[10] M. Takayanagi, Memoirs of Faculty of Engineering, Kyushu University **XXIII,** 42 (1963).
[11] H. D. Keith and F. J. Padden, J. Appl. Phys. **34,** 2409 (1963).
[12] L. E. Nielsen, Rev. Sci. Instrum. **22,** 690 (1951).
[13] F. Danusso and G. Moraglio, Chimica e industria **41,** 748 (1959).
[14] H. D. Keith, F. J. Padden, N. M. Walter, and H. W. Wyckoff, J. Appl. Phys. **30,** 1485 (1959).
[15] F. J. Padden and H. D. Keith, J. Appl. Phys. **30,** 1479 (1959).
[16] A. E. Woodward, Trans. N. Y. Acad. Sci. **24,** 250 (1962).
[17] K. H. Illers, Rheol. Acta **1,** 616 (1961).
[18] H. D. Keith and F. J. Padden, J. Appl. Phys. **35,** 1270–1296 (1964).
[19] E. Passaglia and H. K. Kevorkian, J. Appl. Phys. **34,** 90 (1963).
[20] F. S. Dainton, D. M. Evans, F. E. Hoare and T. P. Melia, Polymer **3,** 286 (1962).
[21] E. A. DiMarzio, Private communication.
[22] H. W. Wyckoff, J. Polymer Sci. **62,** 83 (1962).
[23] K. Sasaguri and R. S. Stein, to be published.

(Paper 68A5–298)

JOURNAL OF RESEARCH of the National Bureau of Standards—A. Physics and Chemistry
Vol. 68A, No. 5, September–October 1964

Precision Density Measurement of Silicon [1,2]

Ivars Henins[3]

(June 10, 1964)

The densities of 22 large highly perfect silicon single crystals have been measured by hydrostatic weighing in water, yielding an average value of

$$d_{Si}(25\ ^\circ C) = 2.329002 \pm (7 \times 10^{-6})\ g/cm^3.$$

An experimental precision has been achieved which exceeds the accuracy with which the absolute density of water is known. The effect of variations of the water surface tension force on the suspension wire has been mimized by using a 0.001 in. suspension wire coated with platinum black, and by doing a large number of repeated weighings of each crystal.

1. Introduction

Measurement of density is one of the most basic of physical measurements, and is often intrinsic in the determination of other physical constants. For instance, the density together with the lattice spacing and molecular weight of a crystal can be used to determine Avogadro's number [1].[4] Similarly, it is possible to determine relative atomic or molecular weights from the densities and lattice constants of different crystals [2]. Density has also been used as an indication of the lattice perfection of crystals [3]. In a different type of experiment, the density of a crystal has been used as a factor in determining e/m of the electron from the index of refraction of x rays [4].

One of the most direct methods of determining the density of solid bodies is by hydrostatic weighing in a liquid of known density, and conversely, the density of a liquid can be measured by hydrostatic weighing of a solid body of known mass and volume. Aside from the usual problems associated with precision weighing, the main difficulty encountered is due to the variation of the surface tension effects of the liquid on the suspension wire passing through the surface. These effects must be minimized by using minimum diameter suspension wire and by keeping a constant contact angle of the liquid against the wire.

This paper describes the procedure which has been used to measure the density of silicon crystals up to 18 g in size. Primary attention is paid to the apparatus and methods used for the hydrostatic weighing in water. In another paper [5] the result of this density determination has been used in conjunction with x-ray lattice spacing measurements of the same crystals to determine the absolute scale of x-ray wavelengths.

[1] This work was supported by the U.S. Atomic Energy Commission.
[2] This paper is based in part on a doctoral dissertation submitted to the Department of Physics, The Johns Hopkins University, 1961.
[3] Present address: Los Alamos Scientific Laboratory, University of California, Los Alamos, N. Mex.
[4] Figures in brackets indicate the literature references at the end of this paper.

2. Experimental Procedure

Accurate density measurement consists of a precise determination of the mass and the volume of an object. The mass can be determined by direct weighing, but the volume must usually be determined indirectly by determining the mass of water that the object displaces. Kohlrausch [6] was the first to use this method for accurate density determination, and it usually bears his name. The density, d_0, of the object of mass M_0, then is given by

$$d_0 = M_0 d_{H_2O}/(M_0 - M_{0w})$$

where M_{0w} is its apparent mass in water, and d_{H_2O} the density of water at the time of weighing. Thus the accuracy of the density determination depends to a large extent on the accuracy of the weighings. This accuracy depends on the precision and sensitivity of the balance, the accuracy of the weights, and the care with which the weighings are made. A good discussion of the weighing process and the construction of precision balances has been presented by Corwin [7].

As already stated, the main difficulty with the weighings in water is due to the surface tension effects on the suspension at the liquid surface. The surface tension of water at 25 °C against air is 71.97 dyn/cm. Thus if a 0.001 in. wire is wetted perfectly, the downward force on it due to surface tension is 0.574 dyn, which is equivalent to 586 μg of weight. Since this force on the wire varies as the cosine of the liquid contact angle, it is desirable to maintain a nearly zero contact angle, thus minimizing the force variations due to small changes in the angle. In general, the contact angle varies with the cleanliness of the metal surface and with the direction of motion of the water surface. Usually, for a receding water surface, the contact angle is very nearly equal to zero [8]. Therefore the usual procedure in hydrostatic weighing has been to clean the suspension wire very carefully and to use exactly the same portion of the wire in each weighing [9]. It has also been

suggested that the contact angle should be observed during the measurements to insure its constancy [10]. The associated problems of this method are that a zero contact angle is very difficult to attain, it depends on the direction of travel of the contact line relative to the metal surface, and minute traces of foreign matter on the metal surface will alter the contact angle considerably. On the other hand, the contact angle against a rough metal surface may be zero due to capillary attraction of the liquid to the surface. This fact was utilized in this experiment and has also been applied by various other observers who have coated their suspensions with either a rough gold [11] or platinum black [12] coating.

The following paragraphs describe the equipment and procedures used in this experiment.

2.1. The Balance

A Mettler M–5 microbalance was chosen for this experiment primarily because of its automatic weight changing feature and because it can be obtained with an under the pan weighing attachment. The capacity of this balance is 20 g. The balance was enclosed in an additional sheet aluminum case to exclude air currents, and the experiment was performed in a room where the temperature was controlled to within ± 0.2 °C of 25 °C.

Because the weights are housed inside the balance, and not easily removable, they were calibrated by weighing a set of National Bureau of Standards certified class M weights [13]. The procedure for calculating the weight corrections from these weighings has been developed by Lashof and Macurdy [14]. These calculations also yield (exclusive of the standard weight errors) the probable error of weighing with the balance. On this particular balance the probable error of a weighing was approximately 1 μg.

2.2. Air Bouyancy Corrections

Because of different densities of the object being weighed and of the weights, the buoyant force on the two may be different. The true mass, M_o, of the object then is given to a good approximation by

$$M_o = M_w + M_w\,(1/d_o - 1/d_w)\,\rho,$$ [5]

where M_w is the true mass of the weights, ρ is the density of air, and d_o and d_w the densities of the object and the weights respectively [16]. The density of air with the normal CO_2 content of 0.04 percent by volume is given by [17]

$$\rho = 1.2930\ (273.15/T)\ [(B - 0.3783e)/760] \times 10^{-3}\ \text{g/ml},$$

where

e=vapor pressure of the water in air (mm Hg),
T=absolute temperature (°K) [273.15 °K=0 °C]
B=barometric pressure (mm Hg).

Under normal atmospheric conditions each of the following variations will produce approximately one μg/cm^3 change in the density of air: 0.6-mm change in barometric pressure, 0.2 °C change in temperature, and 7-percent change in relative humidity at 25 °C. Obviously, the error that the uncertainties in the above quantities introduce in the weight determination, is proportional to the difference in volume of the object and the weights.

During this experiment, the air temperature was measured to ± 0.1 °C with a thermometer inserted inside the aluminum shroud of the balance. Later a thermistor thermometer [18] was constructed which could be inserted inside the balance case. The relative humidity was measured inside the balance case with an electrical resistance type hygrometer. The probable error in this measurement was estimated to be approximately 3 percent. The atmospheric pressure was measured to ± 0.2 mm Hg probable error with an aneroid barometer which was calibrated against a mercury barometer.

2.3. Density of Water

Historically, water was chosen as the density standard because of its universal availability and because it was believed to have constant density. The International Prototype Kilogram was constructed to have as nearly as possible the mass of 1000 cm^3 of water at its maximum density. Then the liter was defined as the volume of 1 kg of pure, air-free water at standard atmospheric pressure and at the temperature of its maximum density, approximately 4 °C. It was left to experiment to determine the exact relationship between the liter and 1000 cm^3.

The determination of the absolute density of water at any given temperature was carried out in two steps. First, the density relative to the maximum density was determined by Chappuis [19] and by Thiessen et al., [20] from measurements of thermal expansion. Tilton and Taylor [21] have recalculated the relative densities based on Chappuis' data. According to this recalculation, the density of water at 25° relative to that at 4° is 0.9970751 g/ml, and the change in density with temperature in the range from 25.0 °C to 25.1 °C is -256×10^{-6} g/ml per °C. The absolute density of water was determined in three very painstaking experiments by hydrostatic weighing of objects with known masses and volumes [22, 23, 24]. From these experiments it was determined [25] that 1 liter=1000.028 cm^3. Unfortunately at the time of the above experiments nothing was known about isotopes, and consequently, no precautions were taken to avoid isotopic fractionation during the distillation of the water. Chappuis makes the statement that his usual procedure was to redistill good quality commercially available

[5] Using this approximate equation for calculating the mass of an object, the error is only 0.18 parts per million in weighing silicon with stainless steel weights.

distilled water [26]. In view of this, DuMond, Cohen, et al., have assigned to this value a probable error of 3 ppm [27]. Even this error may be optimistic, and actually may be worse. Based on the above values, the absolute density of water at 25 °C is $0.997047 \pm (3 \times 10^{-6})$ g/cm^3.

Natural waters from different parts of the world have been found to vary in density by only a few parts in ten million [28]. The effect of dissolved air on the density of water at 25 °C is also only a few parts in ten million [29]. However, because of bubble formation on surfaces, the air must be removed from the water before hydrostatic weighings can be made. The average compressibility of water at the pressure of 1 to 10 atm, at 25 °C is 47.6×10^{-6} per atm [30].

For the present experiment ordinary tap water was triply distilled according to a procedure suggested by Bauer and Levin [31], and boiled before use to expel the absorbed air. The probable error in the density due to fractionation and the remaining impurities is estimated to be less than 1 ppm. The purity of the water was checked by conductivity measurements [32], which gave values as low as 1.1×10^{-6} $(\Omega \text{ cm})^{-1}$ and never exceeded 1.7×10^{-6} $(\Omega \text{ cm})^{-1}$.

2.4. Weighing Chamber

The weighing chamber for this experiment consisted of a triple walled glass container as shown in figure 1. The thermostating water from a constant temperature bath flowed at a rate of approximately 3 gal per minute around the inner chamber and returned via the outer jacket. The bath temperature was measured with two calibrated calorimeter type (0.01 °C divisions) thermometers. The thermometers were calibrated for total immersion, but in these measurements they were only partially immersed. Therefore it was important to correct for the hydrostatic pressure difference on the thermometer bulbs. This pressure effect was measured to be 0.10 °C/atm. No stem temperature corrections were necessary, because the room was maintained at the same temperature as the bath. The total probable error in the temperature determination in the weighing chamber is estimated to be 0.004 °C, which corresponds to approximately 1 ppm error in the water density.

Because the crystals had flat faces, it was possible to support them on a simple stirrup made of 3 mm glass rod. The crystals could be lifted from this stirrup for the "empty" weighings by means of the lifter which was raised by thin nylon lines leading to the outside. Thus it was possible to check the repeatability of the weighings by doing a series of weighings without removing the crystal from the weighing chamber. In addition to this, the balance could be deflected magnetically, thus producing motion of the suspension wire through the water surface, thus making possible repeated weighings without arresting the balance. Repeatability indicated that the surface tension forces on the suspension were remaining constant. The most frequent problem encountered was due to small dust particles floating on the water surface attaching themselves to the suspension, and thus changing the effective diameter of the suspension. To eliminate errors from this, the weighings on each crystal were taken in several groups, the water level being lowered after each group of weighings. Weighings were continued until there was good agreement among the weighings in each group and among the averages of these groups.

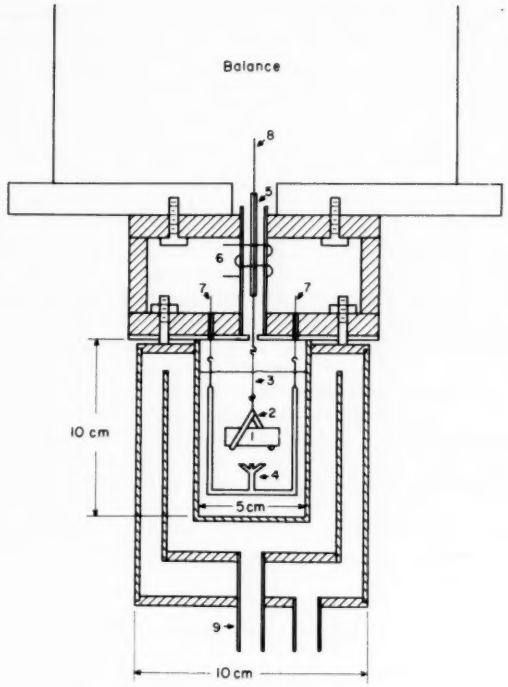

FIGURE 1. *Details of the weighing chamber.*

Legend: (1) crystal to be weighed, (2) crystal supporting stirrup, (3) suspension wire, (4) lifter for raising crystal from stirrup, (5) nickel wire spot welded to support wire, (6) coil for magnetically deflecting the balance, (7) strings for raising crystal lifter, (8) support wire attached to balance pan hook, and (9) inlet for thermostating water.

2.5. Preparation of the Suspension

As already stated, the suspension wire passing through the water surface should be of minimum diameter to minimize the total surface tension force on it, its surface should be wetted by the water, and it should be easily replaceable. In this experiment, 0.001 in. diam 92 percent platinum, 8 percent tungsten alloy wire was used [35]. This wire is quite ductile and has a tensile strength of approximately 300,000 psi. Thus a 1-mil diameter wire of this alloy will support approximately 100 g of weight. The hooks for the suspension wire were made by flattening the end of a short (8 mm) piece of 1-mm diameter stainless steel wire and then filing a hook out of it.

A longitudinal slot was cut in the body of the hook, the fine wire placed in the slot and then the slot crimped closed. First a hook was crimped onto one end of a 3-cm long piece of the 1-mil wire. The wire was then cleaned in a sulfuric acid and sodium dichromate solution [38] and washed in distilled water. Next, the platinum black coating was applied from a plating solution of 3-percent platinum chloride dissolved in 0.025-percent lead acetate solution [37]. A No. 18 platinum wire was used as the positive electrode and a 6-V dry cell with a 1000 Ω resistor in series supplied the current. The suspension wire was immersed up to the hook, and approximately 5 mA of current allowed to flow for 40 sec, with the wire being agitated to retard bubble formation. The coating should be even and uniformly rough and approximately 0.1-mil thick. This was verified by examination under a microscope of 200 × magnification. If the coating was satisfactory, the suspension was again cleaned in the acid solution, washed in distilled water, and a hook crimped on the other end. This last cleaning was necessary because a freshly coated wire without cleaning did not exhibit a constant contact angle with the water surface.

3. Experimental Results

3.1. Silicon Crystals

A group of 22 large silicon single crystals ranging in weight from 5 to 18 g were available for this experiment [38]. These crystals were grown from high purity intrinsic silicon and had low dislocation densities, as specified by the suppliers. The main impurity was oxygen which varied in concentration from as low as 1.3×10^{17} to as high as 8.8×10^{17} atoms/cm^3. This was determined by measuring the infrared absorption at 9 μ [39]. Before weighing, the crystals were ground to remove any foreign matter and jagged corners. Etching in 1 : 3 : 3 solution (by volume) of HF, HNO_3, and glacial acetic acid for about 1 min. removed any loose silicon particles from the surfaces. After being washed the crystals were kept under distilled water. Vacuum was applied to remove air bubbles from any small crevices.

3.2. Density of Silicon

The results of all the density determinations are shown in the form of a histogram in figure 2. The average density at 25 °C was calculated to be

$$d_{Si}(25\ ^\circ\text{C})=2.329002\pm(7\times10^{-6})\text{g/cm}^3.$$

The probable error of this value consists of approximately 0.5-ppm random error of the average, computed from $p=0.67[\Sigma_{i=1}^{k}(d_i-d_{av})^2/(k-1)k]^{\frac{1}{2}}$ and 3-ppm systematic error in the water density. The individual density determinations had a random probable error of approximately 3 μg/cm^3, as computed by combining the errors in the various quantities used in the density calculations. This high precision of the experiment is also indicated in figure 2 by the close grouping of the density values obtained in separate measurements on the same crystals, such as, on crystals 3, 7, 8, 9, and 11. Also crystals 19, 20, 21, and 22 were obtained from the same source at the same time, and the close grouping of their densities indicates that they were probably cut from the same ingot.

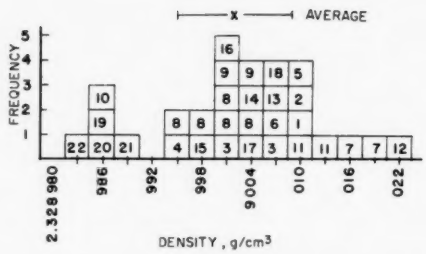

FIGURE 2. *The density of silicon single crystals at 25 °C.*
Each square represents one independent density determination, and the numbers in the squares identify the crystals.

Thus the variations in the densities of the different crystals are quite real, but so far, no correlation of these variations with any of the known properties of these crystals has been found. It has already been demonstrated by Smakula and Kalnajs [40] that the oxygen impurity does not affect the density of silicon. This is also indicated by the present results, although in this case, no really oxygen-free crystals were available for comparison.

The above density value can be compared to $d_{Si}(25\ ^\circ\text{C})=2.32902\pm(3\times10^{-5})$ g/cm^3 obtained by Smakula and Sils [9]. It also is in agreement with the lower precision value of $d_{Si}(25\ ^\circ\text{C})=2.3289\pm0.0001$ g/cm^3 obtained by Straumanis et al. [3]. It disagrees however, with an earlier measurement of $d_{Si}(25\ ^\circ\text{C})=2.3282\pm0.003$ g/cm^3 by Straumanis and Aka [41].

4. Conclusions

In this experiment the density of silicon single crystals was measured by hydrostatic weighing with a precision of approximately one part per million. This high precision is due to the following factors: (a) the precision of the balance and an accurate calibration of the weights; (b) accurate water temperature control and measurement; (c) the platinum-black coated small diameter suspension wire, and (d) the ease with which repeated weighings could be made, thus making it possible to detect any erratic behavior of the surface tension effects on the suspension. At the present this precision exceeds the accuracy with which the absolute density of water is known, therefore it may be worthwhile to redetermine the absolute density of water with known isotopic composition.

The densities of the invididual crystals showed variations which were larger than the experimental precision. However, the average of all these values should be a good indication of the true density of silicon. This average value agrees quite well with the precision measurement by Smakula and Sils [9].

This work was done under the direction of Professor J. A. Bearden, and the author wishes to express appreciation for his advice and assistance. The cooperation of Dr. W. C. Dash of General Electric Company, Dr. Morris Tanenbaum of the Bell Telephone Laboratories, and Dr. Walter Runyan of Texas Instruments, Inc., in providing the crystals is greatly appreciated. Also the author is indebted to Mr. L. B. Macurdy and Mr. J. F. Swindells of the National Bureau of Standards for providing the certified weights and the calibration of the thermometers.

5. References and Notes

[1] R. T. Birge, Am. J. Phys. **13,** 69 (1945).
[2] H. L. Johnston, D. A. Hutchison, Phys. Rev. **62,** 32 (1942); D. A. Hutchison, J. Chem. Phys. **13,** 383 (1945).
[3] A. Smakula, J. Kalnajs, V. Sils, Phys. Rev. **99,** 1747 (1955); M. E. Straumanis, P. Borgeaud, W. J. James, J. Appl. Phys. **32,** 1382 (1961).
[4] J. A. Bearden, Phys. Rev. **54,** 698 (1938).
[5] I. Henins and J. A. Bearden, in press.
[6] F. Kohlrausch and W. Hallwachs, Wied. Ann. d. Phys. **50,** 118 (1893).
[7] A. H. Corwin, in Physical Methods of Organic Chemistry, 3d ed., Part I, p. 71, A. Weissberger, ed. (Interscience Publishers, Inc., New York, 1959).
[8] F. E. Bartell and J. T. Smith, J. Phys. Chem. **57,** 165 (1953); D. J. Trevoy and H. Johnson Jr., J. Phys. Chem. **62,** 833 (1958).
[9] A. Smakula and V. Sils, Phys. Rev. **99,** 1744 (1955).
[10] W. Primak, Rev. Sci. Instr. **29,** 177 (1958).
[11] P. Hidnert and E. L. Peffer, NBS Circular No. 487 (U.S. Government Printing Office, 1950).
[12] O. Redlich and J. Bigeleisen, J. Am. Chem. Soc. **64,** 758 (1942).
[13] The writer is indebted to L. B. Macurdy of the National Bureau of Standards for the loan of these weights, and for a very enlightening discussion of precision weighing.
[14] T. W. Lashof and L. B. Macurdy, Analytical Chemistry **26,** 707 (1954).
[15] T. W. Lashof and L. B. Macurdy, NBS Circular No. 547, sec. 1, p. 10 (1954).
[16] NBS Circular No. 3, 3d ed. (1918).
[17] F. W. J. Whipple, International Critical Tables (1928), vol. I, p. 71.
[18] K. S. Cole, Rev. Sci. Instr. **28,** 326 (1957).
[19] P. Chappuis, Trav. mém. bur. int. poids mes. **13,** D1–D40 (1907).
[20] M. Thiessen, K. Scheel, and H. Diesselhorst, Wiss. Abh. phys.-techn. Reichsanst. **3,** 1–70 (1900).
[21] L. W. Tilton and J. K. Taylor, J. Res. NBS **18,** 205 (1937) RP 971.
[22] C. E. Guillaume, Trav. mém. bur. int. poids mes. **14,** A1–A276 (1910).
[23] P. Chappuis, Trav. mém. bur. int. poids mes. **14,** B1–B163 (1910).
[24] J. Mace de Lepinay, H. Buisson, and J. R. Benoit, Trav. mém. bur. int. poids mes. **14,** C1–C127 (1910).
[25] C. E. Guillaume, La Creation du Bureau Int. des Poids et Mes. (Gauthier-Villars, Paris, 1927), 256.
[26] P. Chappuis, Trav. mém. bur. int. poids mes. **14,** D46 (1910).
[27] J. W. M. DuMond, E. R. Cohen, and K. M. Crowe, The Fundamental Constants of Physics, p. 5 (Interscience Publishers, Inc., New York, 1957).
[28] C. H. Greene and R. J. Voskuyl, J. Am. Chem. Soc. **61,** 1342 (1939).
[29] W. Marek, Ann. d. Physik (3) **44,** 171 (1891).
[30] N. E. Dorsey, Properties of Ordinary Water Substance, p. 243 (Reinhold Publishing Corp., New York, 1940).
[31] N. Bauer and S. Z. Levin, in Physical Methods of Organic Chemistry, A. Weissberger, ed., vol. I, part I, p. 136 (Interscience Publishers, Inc., New York, 1959).
[32] According to I. Kirshenbaum (ref. 33) the conductivity of water sufficiently pure for analysis with 0.1 ppm accuracy should be of the order of magnitude of 1×10^{-6} $(\Omega\ \mathrm{cm})^{-1}$. Voskuyl (ref. 34) has found that a slight impurity which changed the conductivity from 1.2×10^{-6} to 2.2×10^{-6} $(\Omega\ \mathrm{cm})^{-1}$ changed the density by 0.7 ppm.
[33] I. Kirshenbaum, Physical Properties of Heavy Water, pp. 295, 296 (McGraw-Hill Book Company Inc., New York 1951).
[34] R. J. Voskuyl, quoted by I. Kirshenbaum, op. cit., p. 295.
[35] The author wishes to thank the Sigmund Cohn Corp. of Mount Vernon, N.Y., for suggesting the use, and providing a length of this wire (their alloy No. 479).
[36] 35 ml saturated sodium dichromate to 1 liter of H_2SO_4.
[37] "Platinizing solution" sold by A. H. Thomas Co., Philadelphia, Pa.
[38] Most of these crystals were obtained previously by Professor J. A. Bearden for determining the feasibility of using silicon as a standard x-ray diffraction crystal. We are greatly indebted to the following individuals and laboratories for providing the crystals, and for the cooperation without which this study would have been severely limited: the late Dr. W. C. Dash, of the General Electric Co., for supplying four of the crystals, Dr. Morris Tanenbaum of the Bell Telephone Laboratories for six crystals, and to Dr. Walter Runyan of Texas Instruments, Inc., for ten of the crystals. In addition, two crystals were purchased from Knapic Electro-Physics, Inc., of Palo Alto, Calif.
[39] W. Kaiser and P. H. Keck, J. Appl. Phys. **28,** 882 (1957).
[40] A. Smakula and J. Kalnajs, J. Phys. Chem. Solids **6,** 46 (1958).
[41] M. E. Straumanis and E. Z. Aka, J. Appl. Phys. **23,** 330 (1952).

(Paper 68A5–299)

JOURNAL OF RESEARCH of the National Bureau of Standards—A. Physics and Chemistry
Vol. 68A, No. 5, September–October 1964

Franck-Condon Factors to High Vibrational Quantum Numbers IV: NO Band Systems

R. W. Nicholls[1]

(June 5, 1964)

Franck-Condon factor arrays have been computed numerically to highest known vibrational quantum numbers for the following NO band systems.

β : ($B^2\Pi$–$X^2\Pi$)	Feast 1: ($D^2\Sigma^+$–$A^2\Sigma^+$)
γ : ($A^2\Sigma^+$–$X^2\Pi$)	Feast 2: ($E^2\Sigma^+$–$A^2\Sigma^+$)
δ : ($C^2\Pi$–$X^2\Pi$)	Ogawa 1: ($B'^2\Delta$–$B^2\Pi$)
ϵ : ($D^2\Sigma^+$–$X^2\Pi$)	Ogawa 2: ($b^4\Sigma^+$–$a^4\Pi$)
β': ($B'^2\Delta$–$X^2\Pi$)	"M": ($a^4\Pi$–$X^2\Pi$)
γ': ($E^2\Sigma^+$–$X^2\Pi$)	

1. Introduction

The NO molecule has a rich spectrum of electronic transitions which extend from the vacuum ultraviolet region into the infrared. In addition, a vibration-rotation spectrum in the infrared is well known. The disposition of energy levels and transitions between them have been extensively studied by Miescher [1962 and references therein] and many others. A partial energy level diagram is displayed in figure 1, and transitions are indicated on it which give rise to the best known band systems which are treated in this paper. The NO molecular spectra have important applications to a wide range of chemical and physical situations of contemporary interest; for example, radiation from hot air and chemiluminescent gas reactions.

It is well known that the Franck-Condon factors $q_{v'v''}=|\int \psi_{v'}\psi_{v''}\, dr|^2$, which are the squares of the overlap integrals of vibrational wave functions, exert a dominating and proportional influence on intensity distributions of molecular spectra [Nicholls and Stewart, 1962]. It is thus the purpose of this paper to present tables of Franck-Condon factors (calculated on the basis of the Morse model) for the NO band systems listed in table 1.

TABLE 1. *Band systems treated*

NO β ($B^2\Pi$–$X^2\Pi$)	NO Feast 1 ($D^2\Sigma^+$–$A^2\Sigma^+$)
NO γ ($A^2\Sigma^+$–$X^2\Pi$)	NO Feast 2 ($E^2\Sigma^+$–$A^2\Sigma^+$)
NO δ ($C^2\Pi$–$X^2\Pi$)	NO Ogawa 1 ($B'^2\Delta$–$B^2\Pi$)
NO ϵ ($D^2\Sigma^+$–$X^2\Pi$)	NO Ogawa 2 ($b^4\Sigma^-$–$a^4\Pi$)
NO β' ($B'^2\Delta$–$X^2\Pi$)	NO "M"(1) ($a^4\Pi$–$X^2\Pi$)
NO γ' ($E^2\Sigma^+$–$X^2\Pi$)	

Note: (1) See Peyron and Broida (1960).

This paper is one of a series which treat astrophysically and aeronomically important band systems. Earlier papers have treated O_2 Schumann-Runge [Nicholls, 1960], N_2 and N_2^+ transitions [Nicholls, 1961], Oxides [Nicholls, 1962a], Vacuum Ultraviolet transitions [Nicholls, 1962b], CO^+ transitions [Nicholls, 1962c], I_2 [Nicholls, 1963], CN transitions [Nicholls, 1964a]. Papers are in preparation on O_2, C_2, and H_2 transitions.

2. Method

Details of the method of computer calculations of the Franck-Condon factor arrays have been discussed in earlier papers of this series (see e.g., Nicholls 1961). The input data are ω_e, $\omega_e x_e$, r_e, μ_A, $v_{\max}$ for each electronic state involved and a Morse model is assumed for the potential. This is admittedly an empirical expedient but is adequate in many cases. $v_{\max}$ values appropriate to the spectroscopically highest known levels as summarized in Wallace's [1962] compilation and Pearse and Gaydon's [1963] compilations and in the original papers listed therein, have been adopted.

The input data used in the calculations (which were performed on the IBM 7094 computer in the NBS Computation Center), and the sources of these data are summarized in table 2.

TABLE 2. *Basic data*

State	ω_e(cm^{-1})	$\omega_e x_e$(cm^{-1})	r_e(A)	$v_{\max}$	α_e(cm^{-1})	B_e(cm^{-1})	Reference
$X^2\Pi$	[1] 1903.85	[1] 13.97	[1] 1.1508	23	[1] 0.018	[1] 1.707	[1]
$A^2\Sigma^+$	2374.8	16.46	1.0637	15	0.0192	1.9972	[2]
$B^2\Pi$	1037.69	7.603	1.415	19			[2]
$C^2\Pi$	2395	15	1.062	4	0.03	2.002	[3]
$D^2\Sigma^+$	2323.9	22.895	1.062	11	0.021	2.0026	[2]
$E^2\Sigma^+$	2373.66	15.87	1.066	5	0.0182		[4]
$B'^2\Delta$	1216.6	15.88	1.303	6	0.109	1.33	[5]
$b^4\Sigma^-$	1168	13.3	[2] (1.300)	3	[2] (0.02)	[2] (1.335)	[6]
$a^4\Pi$	1019	12.8	[2] (1.407)	3	[2] (0.02)	[2] (1.14)	[6]

$\mu_A=7.46881$ for all states.

Notes:
[1] Average value of two components of the doublet state.
[2] See text for discussion of these data.

References:
[1] Ogawa (1955).
[2] Barrow and Miescher (1957).
[3] Lagerqvist and Miescher (1958).
[4] Feast (1950).
[5] Miescher (1956).
[6] Ogawa (1954).

[1] Department of Physics, University of Western Ontario, London, Ontario; visiting Professor at Stanford University, Stanford, Calif.

In the case of the $b^4\Sigma^-$ and $a^4\Pi$ states, Ogawa [1954] gives ω_e and $\omega_e x_e$ values but not r_e values. In order to obtain r_e values for these states, recourse had to be made to an iteration method previously used by Nicholls, Fraser, Jarmain, and McEachran [1960] which involves the use of Pekeris' [1934] relation

$$B_e = \frac{1}{\omega_e x_e}\left[\frac{\alpha_e \omega_e}{6B_e} + B_e\right]^2 \qquad (1)$$

where the symbols are as defined by Herzberg [1950]. Some knowledge of the α_e values for the $b^4\Sigma^-$ and $a^4\Pi$ states is required before eq (1) may be used iteratively to determine the B_e values and thus, the r_e values from eq (2)

$$B_e = \frac{h}{8\pi^2 c\mu r_e^2}. \qquad (2)$$

It is clear from table 2 that $\alpha_e \sim 0.02$ cm^{-1} for most of the NO states. Further, the close similarity between the structure and energy level array of NO and O_2^+ pointed out by Vanderslice, Mason, and Maisch [1959], and the close equality between α_e values for all O_2^+ states, including $b^4\Sigma^-$ and $a^4\Pi$, led to the adoption of 0.02 cm^{-1} for the α_e values of the corresponding NO states. The B_e values for the O_2^+ states were then respectively used as starting values for the iterative use of eq (1). A very few (3 or 4) cycles of iteration were then required before convergence was respectively obtained to the B_e values listed in table 2 for these states.

3. Results

Franck-Condon factors for the band systems listed in table 1 are displayed in tables 3–13. The Condon loci are clearly indicated on them by setting the local maximum values in boldfaced type. In each of the tables, the negative number in each entry is the power of ten by which the entry is multiplied.

4. Discussion

The Condon loci of tables 3–13 agree closely in each case with the commonly observed distribution of emission bands where they are known. [See Wallace 1962, and Pearse and Gaydon, 1963].

Franck-Condon factors for a few bands on the primary locus of some of the systems treated in table 3–13 which contribute to the absorptivity and emissivity of heated air have been discussed recently [Nicholls, 1964b] with other similar data of aeronomically important spectra at the Aeronomy Symposium on Laboratory Studies held at the International Association of Geomagnetism and Aeronomy meetings, Berkeley, August 1963.

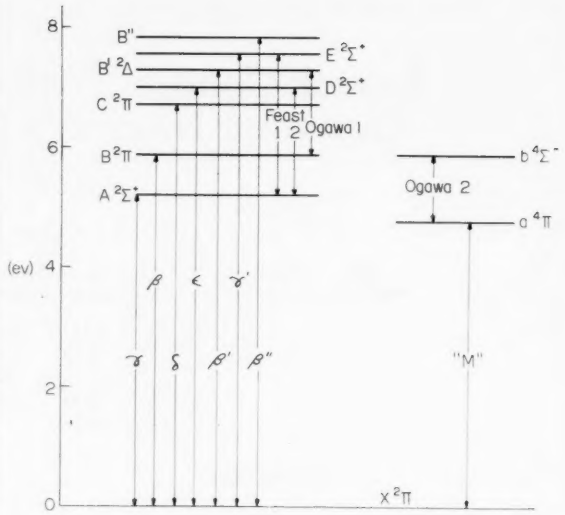

FIGURE 1

Previously published arrays for the β and γ systems [Nicholls, 1961] are here extended to higher quantum numbers using better constants. They are in good agreement with the recent calculations of Ory, Gittleman, and Maddox [1964]. Marr [1964] has recently used these data in a critical discussion of NO β and γ band strengths and his conclusions have been reviewed by Nicholls [1964], Ory [1964] has recently reported NO δ and ϵ arrays which agree well with the more extensive ones presented in tables 5 and 6. An interpolation procedure, which will be discussed in detail elsewhere, has recently been set up, using the data of this paper and others reviewed in section 1, has recently been developed which allows interpolation of Franck-Condon factors (to moderate quantum numbers) for systems for which arrays have not yet been calculated.

The great assistance to this work of Miss R. Zucker of the NBS Computational Laboratory is gratefully acknowledged.

The work has been mainly supported through research grants from The National Aeronautics and Space Administration (NsG–349) and The Air Force Office of Scientific Research (AF–AFOSR 62–236). Some support was also supplied by Contracts with The Air Force Cambridge Research Center (AF 19(628)–2820) and The Defence Research Board of Canada, and grants from The National Research Council of Canada.

TABLE 3. *Franck-Condon factors to high vibrational quantum numbers for the* NOB ($B^2\Pi - X^2\Pi$) *band system*

v' \ v''	0	1	2	3	4	5	6	7	8	9	10	11
0	2.2641−5	3.1095−4	2.0460−3	8.5693−3	2.5605−2	5.7994−2	**1.0327−1**	**1.4802−1**	**1.7347−1**	**1.6790−1**	**1.3507−1**	9.0595−2
1	1.8507−4	2.0886−3	1.0933−2	3.4872−2	7.4613−2	**1.1026−1**	1.0966−1	6.4327−2	1.1898−2	4.5902.3	5.3129−2	**1.1554−1**
2	7.9208−4	7.2777−3	2.9747−2	6.9589−2	**9.8353−2**	7.7835−2	2.2280−2	1.4296−3	4.3261−2	**8.2242−2**	**5.6926−2**	7.1534−3
3	2.3640−3	1.7488−2	5.4452−2	**8.8170−2**	7.0117−2	1.4830−2	5.9847−3	**5.2637−2**	**6.0405−2**	1.2960−2	7.9981−3	**5.9707−2**
4	5.5296−3	3.2490−2	7.4499−2	7.5692−2	2.1921−2	3.2797−3	4.7031−2	4.8606−2	3.9214−3	2.0276−2	**5.8742−2**	2.6351−2
5	1.0802−2	4.9585−2	**7.9752−2**	4.1836−2	3.7157−5	3.3852−2	**4.8235−2**	4.9013−3	1.9158−2	**5.0219−2**	1.2252−2	1.0677−2
6	1.8342−2	6.4437−2	6.7470−2	1.0719−2	1.3818−2	**4.9225−2**	1.3360−2	9.9095−3	**4.5081−2**	1.2101−2	1.0996−2	**4.6567−2**
7	2.7819−2	**7.2876−2**	4.3780−2	2.3794−5	3.7263−2	3.0752−2	6.8564−4	**3.7234−2**	2.0120−2	4.8586−3	**4.0709−2**	1.1249−2
8	**3.8444−2**	7.2602−2	1.9422−2	9.9449−3	**4.3958−2**	5.0880−3	1.9595−2	3.2580−2	1.0085−6	**3.2189−2**	1.7899−2	6.3211−3
9	**4.9137−2**	6.3933−2	3.6587−3	2.7687−2	3.0196−2	1.2400−3	**3.5473−2**	7.9236−3	1.6005−2	2.8670−2	2.8389−4	**3.2754−2**
10	5.8772−2	4.9435−2	2.9977−4	**3.9271−2**	1.0517−2	1.5594−2	2.7802 2	8.2478−4	**3.1758−2**	4.6967−3	1.9531−2	2.1129−2
11	6.6403−2	3.2817−2	7.3542−3	3.8256−2	2.8930−4	2.9905−2	8.9732−3	1.5262−2	2.1772−2	3.0509.3	**2.9308−2**	5.1501−4
12	7.1413−2	1.7689−2	1.9359−2	2.7069−2	4.0595−3	**3.0554−2**	5.3481−6	**2.7836−2**	3.8248−3	2.0008−2	1.2639−2	9.9564−3
13	**7.3571−2**	6.6513−3	3.0450−2	1.2957−2	1.5812−2	1.8994−2	6.7309−3	2.3689−2	1.4319−3	**2.5947−2**	5.6462−5	**2.4982−2**
14	7.2996−2	9.0715−4	**3.6607−2**	2.8272−3	2.6140−2	5.7878−3	1.9242−2	9.6232−3	1.3388−2	1.4008−2	8.1734−3	1.8479−2
15	7.0071−2	3.4677−4	3.6490−2	7.3785−5	**2.8933−2**	2.9455−2	**2.5371−2**	4.6136−4	**2.2955−2**	1.5109−3	**2.0787−2**	3.2791−3
16	6.5333−2	3.9283−3	3.1067−2	4.1473−3	2.3758−2	3.6267−3	2.1099−2	2.8819−3	2.0191−2	2.0937−3	2.0154−2	1.3501−3
17	5.9370−2	1.0150−2	2.2610−2	1.1976−2	1.4337−2	1.2312−2	1.0996−2	1.2232−2	9.4610−3	1.2049−2	8.8015−3	1.1875−2
18	5.2740−2	1.7466−2	1.3658−2	1.9905−2	5.4717−3	2.0021−2	2.4494−3	1.9680−2	1.1169−3	**1.9368−2**	4.7738−4	**1.9226−2**
19	4.5918−2	**2.4574−2**	6.2527−3	**2.5168−2**	5.6450−4	**2.2715−2**	8.8207−5	**1.9366−2**	1.0485−3	1.7461−2	2.5012−3	1.5252−2

v' \ v''	12	13	14	15	16	17	18	19	20	21	22	23
0	5.0680−2	2.3597−2	9.1027−3	2.8878−3	7.4549−4	1.5431−4	2.5096−5	3.1173−6	2.8377−7	1.7756−8	6.8421−10	1.3104−11
1	**1.4289−1**	**1.2329−1**	7.9833−2	4.0015−2	1.5714−2	4.8388−3	1.1594−3	2.1269−4	2.9090−5	2.8443−6	1.8574−7	7.1708−9
2	1.2322−2	7.5864−2	**1.3042−1**	**1.2986−1**	8.8602−2	4.4083−2	1.6385−2	4.5704−3	9.4761−4	1.4263−4	1.4943−5	1.0123−6
3	**6.8819−2**	1.8319−2	4.7608−3	6.5497−2	**1.2784−1**	**1.2901−1**	8.4249−2	3.8424−2	1.2571−2	2.9539−3	4.8919−4	5.4748−5
4	1.6224−3	**4.9422−2**	**6.8023−2**	1.7696−2	6.9462−3	7.5792−2	**1.3454−1**	**1.2204−1**	6.9882−2	2.7081−2	7.2370−3	1.3185−3
5	**5.3768−2**	2.6914−2	2.0392−3	**5.2566−2**	**6.2060−2**	8.4628−3	1.9486−2	1.0119−1	**1.4083−1**	1.0463−1	4.8636−2	1.4846−2
6	1.2174−2	1.1883−2	**5.2743−2**	1.8414−2	8.0290−3	**6.3074−2**	**4.6872−2**	1.4697−4	5.0250−2	**1.3195−1**	**1.3361−1**	7.5724−2
7	1.2526−2	**4.3854−2**	5.9108−3	2.1177−2	**5.0030−2**	5.5485−3	2.5526−2	**6.9044−2**	2.0771−2	1.0895−2	9.9568−2	**1.4868−1**
8	**3.8668−2**	5.1603−3	2.1119−2	**3.7423−2**	1.3630−4	**3.7517−2**	**3.6602.2**	5.2480−4	**5.3480−2**	**5.3560−2**	3.8131−4	5.7535−2
9	1.0370−2	1.3545−2	**3.3789−2**	7.1077−5	**3.4275−2**	2.1768.2	6.4394−3	**4.8990−2**	1.1683−2	2.0438−2	**6.9370−2**	1.6505−2
10	3.6263−3	**3.2974−2**	1.8543−3	**6.0339−2**	2.0389−2	6.1236−3	**4.0558−2**	3.1124−3	**3.0510−2**	**3.8206−2**	8.0584−4	**5.8834−2**
11	**2.6162−2**	9.7428−3	1.3830−2	2.5200−2	1.7025−3	**3.4698−2**	3.3557−3	**2.6629−2**	2.5301−2	5.4405−3	**4.9403.2**	6.8086−3
12	2.2465−2	1.9396−3	**2.8637−2**	4.8447−4	**2.7188−2**	8.5052 3	1.7183−2	2.4509−2	3.9466−3	**3.9391−2**	1.6645−3	**3.6562−2**
13	2.8160−3	2.0608−2	9.3923−3	1.3518−2	1.8548−2	5.6115−3	**2.7767−2**	3.4153−4	**3.3007−2**	2.7896−3	**2.9233−2**	1.8219−2
14	3.8203−3	**2.2451−2**	8.6198−4	**2.5221−2**	5.3306−5	**2.5973−2**	2.3389−3	**2.3817−2**	8.7590−3	1.8041−2	2.0035−2	8.9963−3
15	1.8480−2	5.8506−3	1.5834−2	9.3064−3	1.2750−2	1.3723−2	9.2113−3	1.9137−2	5.3677−3	**2.5428−2**	1.7733−3	**3.1991−2**
16	**2.0625−2**	7.1007−4	**2.1427−2**	2.3282−4	**2−2458.2**	4.5613−6	**2.3633−2**	1.8138−4	**2.4827−2**	1.0716−3	**2.5782−2**	3.3045−3
17	8.6593−3	1.1749−2	8.8898−3	1.1678−2	9.4554−3	1.1646−2	1.0397−2	1.1612−2	1.1841−2	1.1487−2	1.4040−2	1.1104−2
18	1.6500−4	**1.9296−2**	2.8616−5	**1.9595−2**	1.5027−6	**2.0148−2**	5.1225−5	**2.1003−2**	1.5523−4	**2.2251−2**	2.8413−4	**2.4061−2**
19	4.1831−3	1.3281−2	6.0357−3	1.1478−2	8.0662−3	9.7961−3	**1.0301−2**	8.2149−3	**1.2773−2**	6.7481−3	**1.5520−2**	5.4418−3

TABLE 4. *Franck-Condon factors to high vibrational quantum numbers for the* NO γ ($A^2\Sigma^+ - X^2\Pi$) *band system*

v' \ v''	0	1	2	3	4	5	6	7	8	9	10	11
0	1.6725−1	**2.6456−1**	**2.3741−1**	**1.5978−1**	9.0065−2	**4.5066−2**	2.0735−2	8.9783−3	3.7184−3	1.4904−3	5.8326−4	2.2439−4
1	**3.3431−1**	1.0242−1	1.1580−3	7.4263−2	**1.3583−1**	**1.3330−1**	**9.7259−2**	5.9428−2	3.2279−2	1.6143−2	7.6040−3	3.4276−3
2	2.9262−1	1.7957−2	**1.5684−1**	1.1223−2	1.7613−4	3.7296−2	9.0778−2	**1.0578−1**	**8.8529−2**	6.0987−2	3.6946−2	2.0450−2
3	1.4727−1	2.0259−1	4.2298−2	4.3396−2	**1.1315−1**	4.6214−2	9.8246−5	2.6352−2	6.8918−2	**8.6432−2**	**7.8866−2**	5.8111−2
4	4.7062−2	**2.4039−1**	4.6886−2	**1.2242−1**	6.9213.4	**6.1636−2**	**8.5428−2**	2.8433−2	2.0659−5	**6.3115−2**	5.6663−2	**7.2814−2**
5	9.9525−3	1.2656−1	**2.1521−1**	5.6888−4	**1.1140−1**	4.1408−2	8.1102−3	**6.8293−2**	**6.3115−2**	1.6371−2	5.1617−4	2.1236−2
6	1.4083−3	3.7778−2	1.9572−1	1.2393−1	4.2608−2	4.8568−2	**8.3044−2**	4.8751−3	2.5923−2	**6.5414−2**	**4.5018−2**	8.6661−3
7	1.3177−4	6.9230−3	8.2277−2	**2.2299−1**	3.9266−2	**9.5223−2**	4.7082−3	**8.0926−2**	3.5837−2	1.1101−3	3.9436−2	**5.7040−2**
8	7.8608−6	7.9343−4	1.9317−2	1.3398−1	**2.0249−1**	1.3818−3	**1.1050−1**	5.9887−3	**4.6390−2**	**6.2561−2**	7.5553−3	1.0899−2
9	2.7802−7	5.5665. 5	2.6807−3	4.0138−2	1.8008−1	1.4909−1	1.1266−2	**8.5860−2**	8.6115−2	1.2055−2	**6.3411−2**	3.1088−2
10	5.0323−9	2.2372−6	2.1883−4	6.6919−3	6.8965−2	**2.0966−1**	8.6078−2	4.6944−2	**8.2605−2**	**6.5703−2**	1.1286−2	**4.2137−2**
11	3.1794−11	**4.4416−8**	9.9004−6	6.3044−4	1.3747−2	1−0341−1	**2.1685−1**	3.4125−2	8.2605−2	1.1286−2	**7.5315−2**	1.1680−2
12	1.0538−14	2.9465−10	2.1360−7	3.1855−5	1.4852−3	2.4584−2	1.3968−1	**2.0170−1**	5.1603−3	**1.0092−1**	5.2344−6	**6.2003−2**
13	5.9817−16	**4.3432−14**	1.4460−9	7.4066−7	8.3254−5	3.0310−3	3.9587−2	1.7345−1	1.6912−1	1.2674−3	**9.6855−2**	1.0133−2
14	7.5344−16	1.9828−15	3.9044−14	5.0256−9	2.0707−6	1.8743−4	5.5490−3	5.8691−2	**2.0072−1**	1.2680−1	1.6959−2	**7.5373−2**
15	3.5559−16	1.1501−15	**4.3289−14**	4.0394−14	1.3928−8	4.9547−6	3.7671−4	9.3270−3	8.1363−2	**2.1848−1**	8.3053−2	4.2871−2

v' \ v''	12	13	14	15	16	17	18	19	20	21	22	23
0	8.5321−5	3.2200−5	1.2103−5	4.5436−6	1.7076−6	6.4374−7	2.4383−7	9.2921−8	3.5672−8	1.3808−8	5.3939−9	2.1276−9
1	1.4955−3	6.3699−4	2.6664−4	1.1026−4	4.5231−5	1.8468−5	7.5271−6	3.0692−6	1.2545−6	5.1486−7	2.1247−7	8.8272−8
2	1.0599−2	5.2320−3	2.4900−3	1.1530−3	5.2316−4	2.3391−4	1.0351−4	4.5502−5	1.9930−5	8.7193−6	3.8184−6	1.6768−6
3	3.8016−2	2.2703−2	1.2681−2	6.7373−3	3.4464−3	1.7131−3	8.3333−4	3.9895−4	1.8882−4	8.8677−5	4.1452−5	1.9336−5
4	**6.8746−2**	5.3940−2	3.7374−2	2.3698−2	1.4072−2	7.9528−3	4.3281−3	2.2886−3	1.1839−3	6.0252−4	3.0300−4	1.5113−4
5	4.8783−2	**6.2751−2**	**6.0844−2**	4.9624−2	3.5983−2	2.3973−2	1.4995−2	8.9412−3	5.1390−3	2.8715−3	1.5702−3	8.4479−4
6	1.4526−3	2.0410−2	4.3056−2	**5.4915−2**	**5.4193−2**	4.5567−2	3.4317−2	2.3857−2	1.5620−2	9.7696−3	5.8983−3	3.4653−3
7	3.1024−2	4.1023−3	2.5505−3	1.9679−2	3.8461−2	**4.8531−2**	**4.8541−2**	4.1881−2	3.2604−2	2.3544−2	1.6064−2	1.0494−2
8	**4.5363−2**	**4.6723−2**	2.0772−2	1.6488−3	3.5524−3	1.8797−2	3.4499−2	**4.3134−2**	**4.3666−2**	**3.8564−2**	3.0944−2	2.3138−2
9	1.4810−6	2.2000−2	**4.5125−2**	**3.6747−2**	1.3627−2	5.0016−4	4.2935−3	1.7682−2	3.0914−2	3.8431−2	**3.9387−2**	**3.5569−2**
10	**4.9878−2**	9.3400−3	3.9025−3	2.9486−2	**4.1250−2**	2.8229−2	8.8623−3	7.7910−5	4.6979−3	1.6330−2	2.7569−2	3.4225−2
11	1.6139−2	**5.1337−2**	2.7800−2	7.2225−4	1.1148−2	**3.2700−2**	**3.5873−2**	2.1503−2	5.8073−3	2.8993−7	4.7560−3	1.4768−2
12	3.4143−2	1.2195−3	**3.6912−2**	**4.1425−2**	1.0967−2	7.6408−4	1.7442−2	**3.2675−2**	**3.0367−2**	1.6473−2	3.9313−3	3.8995−5
13	**3.7595−2**	**5.2056−2**	3.0281−3	1.7060−2	**4.2315−2**	2.5738−2	2.3872−3	4.4728−3	2.1384−2	**3.0738−2**	**2.5451−2**	1.2866−2
14	3.2091−2	1.3825−2	**5.6247−2**	1.6982−2	2.9801−3	**3.1414−2**	**3.5468−2**	1.2730−2	1.3328−5	8.6620−3	2.3068−2	**2.7953−2**
15	**4.6484−2**	**5.3923−2**	1.1027−3	**4.6382−2**	3.3404−2	5.5857−4	1.5809−2	**3.5165−2**	**2.4487−2**	4.7740−3	9.1640−4	1.1894−2

736–657—64——8

TABLE 5. *Franck-Condon factors to high vibrational quantum numbers for the* NO δ ($C^2\Pi$–$X^2\Pi$) *band system*

v′ \ v″	0	1	2	3	4	5	6	7	8	9	10	11
0	1.5303–1	**2.5430–1**	**2.3802–1**	**1.6619–1**	9.6817–2	4.9932–2	2.3636–2	1.0519–2	4.4751–3	1.8427–3	7.4117–4	2.9329–4
1	**3.1826–1**	1.1664–1	3.4184–8	6.0911–2	**1.2789–1**	**1.3451–1**	**1.0312–1**	6.5614–2	3.6935–2	1.9091–2	9.2807–3	4.3144–3
2	2.9469–1	7.9811–3	**1.4637–1**	**8.5132–2**	2.7400–3	2.5826–2	8.0610–2	**1.0384–1**	**9.2717–2**	6.7154–2	4.2452–2	2.4415–2
3	1.6035–1	1.7343–1	6.0846–2	2.6051–2	**1.0916–1**	**6.0224–2**	2.7988–3	1.6040–2	5.8190–2	**8.2801–2**	**8.0896–2**	6.3852–2
4	5.7021–2	**2.3879–1**	2.3254–2	**1.2922–1**	7.2589–3	4.3165–2	**8.7758–2**	4.2110–2	1.6656–3	1.2539–2	4.5861–2	**6.8255–2**

v′ \ v″	12	13	14	15	16	17	18	19	20	21	22	23
0	1.1482–4	4.4676–5	1.7338–5	6.7318–6	2.6214–6	1.0259–6	4.0423–7	1.6060–7	6.4411–8	2.6109–8	1.0705–8	4.4435–9
1	1.9412–3	8.5299–4	3.6861–4	1.5751–4	6.6851–5	2.8281–5	1.1960–5	5.0690–6	2.1574–6	9.2372–7	3.9846,7	1.7339–7
2	1.3117–2	6.7023–3	3.2999–3	1,5807–3	7.4226–4	3.4367–4	1.5764–4	7.1906–5	3.2722–5	1.4895–5	6.7968–6	3.1150–6
3	4.3869–2	2.7359–2	1.5905–2	8.7778–3	4.6592–3	2.4021–3	1.2119–3	6.0200–4	2.9580–4	1.4435–4	7.0177–5	3.4085–5
4	7.0512–2	5.9148–2	4.3297–2	2.8806–2	1.7873–2	1.0527–2	5.9615–3	3.2773–3	1.7621–3	9.3202–4	4.8729–4	2.5281–4

TABLE 6. *Franck-Condon factors to high vibrational quantum numbers for the* NO ϵ ($D^2\Sigma^+$ $X^2\Pi$) *band system*

v′ \ v″	0	1	2	3	4	5	6	7	8	9	10	11
0	1.6588–1	**2.5830–1**	**2.3329–1**	**1.6030–1**	9.3089–2	4.8237–2	2.3038–2	1.0357–2	4.4465–3	1.8421–3	7.4210–4	2.9239–4
1	**3.5011–1**	1.0080–1	9.9080–4	6.8939–2	**1.2782–1**	**1.2813–1**	**9.6030–2**	6.0461–2	3.3872–2	1.7458–2	8.4579–3	3.9080–3
2	3.0414–1	2.7624–2	**1.5930–1**	6.5280–2	6.1723–5	3.5537–2	8.5003–2	**9.9710–2**	**8.4761–2**	5.9552–2	3.6842–2	2.0812–2
3	1.3914–1	2.4466–1	2.6133–2	5.7407–2	**1.0916–1**	3.7944–2	1.7524–5	2.7373–2	6.5869–2	**8.1111–2**	**7.3182–2**	5.4780–2
4	3.5527–2	**2.4918–1**	9.4737–2	**1.0409–1**	1.2430–3	**7.3266–2**	**7.5852–2**	1.9318–2	8.0186–4	2.5773–2	5.5977–2	**6.8586–2**
5	4.9046–3	9.9762–2	**2.7168–1**	1.1081–2	**1.2446–1**	1.7093–2	2.2750–2	**7.2794–2**	**4.9239–2**	7.8166–3	2.8982–3	2.6240–2
6	3.1618–4	1.8287–2	1.7000–1	**2.2885–1**	4.2543–3	**9.1441–2**	5.4692.2	4.7379–4	4.3883–2	**6.1092–2**	2.8727–2	1.9091–3
7	5.7018–6	1.3859–3	4.0353–2	2.2847–1	1.6074–1	3.5644–2	4.5282–2	**7.6794–2**	7.7805–3	1.5239–2	**5.1876–2**	**4.4812–2**
8	9.6899–9	2.3825–5	**3.4892–3**	6.8911–2	**2.6769–1**	9.6204–2	**7.0993–2**	1.2617–2	**7.5117–2**	2.7981–2	1.1079–3	3.2171–2
9	5.6809–9	1.8790–7	5.2947–5	6.6130–3	1.0096–1	**2.8811–1**	4.8315–2	**9.3543–2**	3.2044–4	**5.7738–2**	**4.5765–2**	2.2409–3
10	7.3032–12	**3.8313–8**	1.3231–6	7.9711–5	1.0461–2	1.3381–1	**2.9422–1**	1.8977–2	**1.0018–1**	3.8388–3	3.5876–2	**5.3909–2**
11	7.9047–12	3.3321–10	1.2892–7	5.5882–6	8.4722–5	1.4540–2	1.6551–1	**2.9157–1**	4.6190–3	**9.4486–2**	1.5442–2	1.7394–2

v′ \ v″	12	13	14	15	16	17	18	19	20	21	22	23
0	1.1317–4	4.3176–5	1.6279–5	6.0774–6	2.2498–6	8.2658–7	3.0156–7	1.0925–7	3.9284–8	1.4005–8	4.9415–9	1.7208–9
1	1.7402–3	7.5254–4	3.1788–4	1.3174–4	5.3748–5	2.1642–5	8.6174–6	3.3975–6	1.3275–6	5.1422–7	1.9744–7	7.5088–8
2	1.0987–2	5.5063–3	2.6493–3	1.2340–3	5.5994–4	2.4870–4	1.0852–4	4.6661–5	1.9810–5	8.3178–6	3.4577–6	1.4238–6
3	3.6149–2	2.1781–2	1.2258–2	6.5436–3	3.3506–3	1.6593–3	7.9981–4	3.7705–4	1.7450–4	7.9524–5	3.5765–5	1.5901–5
4	**6.3385–2**	4.9235–2	3.3939–2	2.1443–2	1.2682–2	7.1239–3	3.8415–3	2.0043–3	1.0181–3	5.0583–4	2.4675–4	1.1853–4
5	4.9996–2	**5.9522–2**	**5.5314–2**	4.3907–2	3.1215–2	2.0455–2	1.2593–2	7.3819–3	4.1611–3	2.2725–3	1.2093–3	6.2997–4
6	5.9169–3	2.7203–2	4.5736–2	**5.2484–2**	**4.8597–2**	3.9086–2	2.8435–2	1.9189–2	1.2219–2	7.4313–3	4.3562–3	2.4783–3
7	1.4425–2	2.8285–5	9.2474–3	2.7989–2	4.2235–2	**4.6703–2**	**4.2927–2**	3.4823–2	2.5802–2	1.7850–2	1.1705–2	7.3565–3
8	**4.8059–2**	2.0026–2	5.6900–3	7.0713–4	1.2367–2	2.8320–2	3.9070–2	**4.1769–2**	**3.8083–2**	3.1091–2	2.3399–2	1.6546–2
9	1.3544–2	**3.9989–2**	**3.7873–2**	1.6437–2	1.3354–3	2.7327–3	1.4937–2	2.8119–2	3.6069–2	**3.7458–2**	**3.3906–2**	2.7839–2
10	1.2408–2	2.5127–3	2.6501–2	**3.8493–2**	2.6214–2	7.8228–3	1.4750–5	5.2175–3	1.6798–2	2.7422–2	3.3180–2	**3.3642–2**
11	**5.2147–2**	2.4534–2	1.3430–4	1.3426–2	**3.2452–2**	**3.1465–2**	1.6044–2	2.8045–3	5.1857–4	7.5892–3	1.7928–2	2.6317–2

TABLE 7. *Franck-Condon factors to high vibrational quantum numbers for the* NO β' ($B'^2\Delta - X^2\Pi$) *band system*

v′ \ v″	0	1	2	3	4	5	6	7	8	9	10	11
0	1.8358–2	8.3318–2	**1.7687–1**	**2.3362–1**	**2.1342–1**	**1.4749–1**	7.7849–2	3.2466–2	1.0877.2	2.9605–3	6.5948–4	1.2076–4
1	5.8594–2	**1.5426–1**	1.4162–1	3.4431–2	6.8166–3	9.3789–2	**1.7119–1**	**1.6350–1**	1.0405–1	4.8403–2	1.7244–2	4.8310–3
2	1.0320–1	1.3858–1	2.4259–2	2.4264–2	**1.0688–1**	6.5626–2	3.5856–4	5.3227–2	**1.4300–1**	**1.5775–1**	1.0719–1	5.1162–2
3	1.3331–1	7.1848–2	5.6975–3	**8.8161–2**	3.8636–2	8.5167–3	**8.6451–2**	**6.5503–2**	1.0381–3	4.7414–2	**1.3547–1**	**1.5018–1**
4	**1.4163–1**	1.6810–2	5.0973–2	5.7444–2	2.7502–3	**7.3045–2**	3.2065–2	9.8989–3	**8.2331–2**	**5.4804–2**	1.4135–5	5.6873–2
5	1.3163–1	2.4605–5	**7.5678–2**	7.0741–3	**4.7790–2**	3.9753–2	7.4184–3	**6.9260–2**	1.8513–2	1.9357–2	**8.2901–2**	3.7695–2
6	1.1117–1	**1.3118–2**	5.9638–2	5.5592–3	**5.9402–2**	1.8304–4	**5.4105–2**	2.0365–2	**1.9830–2**	**6.3426–2**	5.1730–3	3.6551–2

v′ \ v″	12	13	14	15	16	17	18	19	20	21	22	23
0	1.8210–5	2.2607–6	2.3052–7	1.9206–8	1.2959–9	7.0744–11	3.1971–12	9.1352–14	6.7896–16	1.4617–15	1.0247–17	7.7555–16
1	1.0812–3	1.9507–4	2.8509–5	3.3782–6	3.2389–7	2.5016–8	1.5473–9	7.5319–11	2.7691–12	9.4006–14	2.9641–15	4.3000–16
2	1.8234–2	5.0168–3	1.0863–3	1.8714–4	2.5790–5	2.8460–6	2.5088–7	1.7569–8	9.6709–10	4.0835–11	1.3275–12	3.9485–14
3	1.0035–1	4.6455–2	1.5884–2	4.1519–3	8.4605–4	1.3586–4	1.7272–5	1.7388–6	1.3806–7	8.5618–9	4.0909–10	1.5428–11
4	**1.3853–1**	**1.4128–1**	8.8042–2	3.8075–2	1.2130–2	2.9401–3	5.5198–4	8.1016–5	9.3256–6	8.4029–7	5.8892–8	3.1800–9
5	2.4457–3	7.5874–2	**1.4415–1**	**1.2892–1**	7.2534–2	2.8579–2	8.3082–3	1.8329–3	3.1160–4	4.1104–5	4.2111–6	3.3356–7
6	**7.9081–2**	1.8448–2	1.3839–2	1.0006–1	**1.4617–1**	1.1210–1	5.5842–2	1.9706–2	5.1460–3	1.0180–3	1.5437–4	1.8019–5

TABLE 8. *Franck-Condon factors to high vibrational quantum numbers for the* NO $\gamma^1(E^2\Sigma^+ — X^2\Pi)$ *band system*

v′ \ v″	0	1	2	3	4	5	6	7	8	9	10	11
0	1.8292–1	**2.7657–1**	**2.3718–1**	**1.5256–1**	8.2230–2	3.9369–2	1.7346–2	7.1987–3	2.8604–3	1.1012–3	**4.1436–4**	1.5345–4
1	**3.4419–1**	8.8265–2	4.8132–3	9.0257–2	**1.4532–1**	**1.3244–1**	9.1120–2	5.2865–2	2.7374–2	1.3087–2	5.9058–3	2.5550–3
2	2.8488–1	2.8268–2	**1.6337–1**	5.8596–2	6.1843–4	5.0870–2	**1.0194–1**	**1.0809–1**	**8.4501–2**	5.4997–2	3.1674–2	1.6735–2
3	1.3638–1	2.1667–1	3.0458–2	5.8301–2	**1.1413–1**	3.4941–2	8.4098–4	3.8518–2	7.9760–2	**8.9988–2**	**7.5535–2**	5.2958–2
4	4.1780–2	**2.3390–1**	6.1865–2	**1.1475–1**	1.8000–4	**7.5107–2**	**8.1670–2**	1.8913–2	1.9603–3	3.3693–2	6.6678–2	**7.6744–2**
5	8.5623–3	1.1620–1	**2.2212–1**	1.5384–4	**1.1958–1**	3.0105–2	1.6595–2	**7.6998–2**	5.6403–2	8.9686–3	3.6710–3	3.1358–2

v′ \ v″	12	13	14	15	16	17	18	19	20	21	22	23
0	5.6232–5	2.0476–5	7.4344–6	2.6992–6	9.8222–7	3.5895–7	1.3195–7	4.8862–8	1.8247–8	6.8785–9	2.6195–9	1.0084–9
1	1.0717–3	**4.3949–4**	1.7738–4	7.0817–5	2.8084–5	1.1100–5	4.3843–6	1.7347–6	6.8886–7	2.7500–7	1.1053–7	4.4774–8
2	8.3041–3	3.9337–3	1.8002–3	8.0297–4	3.5152–4	1.5186–4	6.5028–5	2.7698–5	1.1770–5	5.0020–6	2.1304–6	9.1099–7
3	3.2889–2	1.8737–2	1.0020–2	5.1101–3	2.5150–3	1.2051–3	5.6609–4	2.6212–4	1.2016–4	5.4738–5	2.4852–5	1.1273–5
4	**6.7155–2**	4.9581–2	3.2599–2	1.9720–2	1.1215–2	6.0882–3	3.1904–3	1.6277–3	8.1396–4	4.0107–4	1.9558–4	9.4721–5
5	5.7873–2	**6.6675–2**	5.9894–2	4.5962–2	3.1634–2	2.0118–2	1.2061–2	6.9141–3	3.8302–3	2.0672–3	1.0939–3	5.7045–4

TABLE 9. *Franck-Condon factors to high vibrational quantum numbers for the* NO *Feast 1* $(D^2\Sigma^+ — A^2\Sigma^+)$ *band system*

v′ \ v″	0	1	2	3	4	5	6	7	8
0	**9.9969–1**	1.8711–4	1.2792–4	4.2490–7	1.9841–7	5.0558–8	6.3344–9	6.0985–10	4.3012–11
1	1.8680–4	**9.9943–1**	2.3871–7	3.8609–4	2.6853–6	7.9047–7	2.4905–7	3.5216–8	3.8579–9
2	1.2809–4	7.3738–7	**9.9843–1**	6.3266–4	8.1095–4	1.0154–5	1.8354–6	7.1982–7	1.1145–7
3	3.5713–7	3.8558–4	7.2150–4	**9.9407–1**	3.3205–3	1.4801–3	2.9837–5	3.1627–6	1.5993–6
4	5.8411–7	1.1705–7	7.2576–4	3.8448–3	**9.8354–1**	9.3034–3	2.5250–3	7.5208–5	4.3234–6
5	5.0012–8	2.6448–6	6.7206–7	1.0513–3	1.1049–2	**9.6385–1**	1.9746–2	4.1490–3	1.7088–4
6	2.7548–9	3.5170–7	6.7176–6	9.1700–6	1.2300–3	2.4096–2	**9.3205–1**	3.5616–2	6.6496–3
7	2.2567–10	2.5801–8	1.3823–6	1.2174–5	3.9537–5	1.1380–3	4.4657–2	**8.8552–1**	5.7506–2
8	3.7741–11	2.2890–9	1.3468–7	3.9507–6	1.6793–5	1.0863–4	7.3893–4	7.4031–2	**8.2227–1**
9	8.7194–12	3.7557–10	1.3324–8	5.1088–7	9.0455–6	1.7403–5	2.2596–4	2.0102–4	1.1279–1
10	2.1009–12	9.1238–11	2.1272–9	5.8012–8	1.5584–6	1.7336–5	1.2044–5	3.7816–4	4.1487–5
11	5.0514–13	2.3801–11	5.2379–10	9.2181–9	2.0777–7	4.0169–6	2.8339–5	3.2728–6	5.1520–4

v′ \ v″	9	10	11	12	13	14	15
0	1.6911–12	2.3259–16	3.1030–14	1.3183–14	1.3826–15	1.6314–16	5.8860–16
2	3.0600–10	1.3939–11	3.8679–14	1.8562–13	1.5501–13	6.4102–14	1.5042–14
3	1.3713–8	1.2183–9	6.2007–11	1.8049–13	8.9484–13	7.0660–13	3.0022–13
4	2.6348–7	3.5901–8	3.5164–9	2.0186–10	8.4664–13	3.1340–12	2.5370–12
5	3.0336–6	5.1616–7	7.7344–8	8.2311–9	5.2672–10	3.4074–12	8.4579–12
6	4.6428–6	5.2018–6	8.8229–7	1.4520–7	1.6592–8	1.1609–9	1.0351–11
7	3.6005–4	3.5015–6	8.3708–6	1.3538–6	2.4566–7	2.9855–8	2.2503–9
8	1.0440–2	7.1600–4	1.1120–6	1.3002–5	1.8932–6	3.8328–7	4.9008–8
9	8.5431–2	1.6061–2	1.3587–3	2.7157–7	1.9942–5	2.4248–6	5.6189–7
10	**7.4152–1**	1.1859–1	2.4178–2	2.4779–3	9.8849–6	3.0794–5	2.8234–6
11	1.6033–1	**6.4412–1**	1.5518–1	3.5529–2	4.3617–3	5.1516–5	4.8609–5
12	1.2692–3	2.1446–1	5.3305–1	1.9223–1	5.0831–2	7.4293–3	1.7076–4

TABLE 10. *Franck-Condon factors to high vibrational quantum numbers for the* NO *Feast 2*$(E^2\Sigma^+ — A^2\Sigma^+)$ *band system*

v′ \ v″	0	1	2	3	4	5	6	7	8
0	**9.9870–1**	1.2883–3	1.0997–5	4.9375–9	1.0915–9	1.0213–10	5.6952–12	3.3202–13	2.4765–14
1	1.2730–3	**9.9633–1**	2.3741–3	3.4489–5	3.2079–8	4.7978–9	6.0333–10	4.0994–11	2.8670–12
2	2.5361–5	2.3180–3	**9.9433–1**	3.2624–3	7.1876–5	1.1942–7	1.2403–8	2.0753–9	1.6988–10
3	3.2103–7	7.3484–5	3.1471–3	**9.9271–1**	3.9593–3	1.2441–4	3.3486–7	2.4348–8	5.3691–9
4	2.7010–9	1.2658–6	1.4188–4	3.7731–3	**9.9144–1**	4.4718–3	1.9316–4	7.8683–7	3.9737–8
5	9.3350–13	1.4230–8	3.1152–6	2.2815–4	4.2094–3	**9.9050–1**	4.8079–3	2.7895–4	1.6346–6

v′ \ v″	9	10	11	12	13	14	15
0	3.2792–15	1.4501–15	4.7722–16	7.8604–17	1.0406–15	6.2341–16	4.5463–19
1	2.8291–13	3.0768–14	6.4091–16	2.0026–16	1.6107–17	2.9577–18	6.4610–17
2	1.2876–11	1.1715–12	1.5147–13	1.4358–14	2.0644–16	1.2891–15	2.6996–18
3	5.1906–10	4.4829–11	4.1309–12	4.6474–13	6.8501–14	5.5006–15	4.0016–16
4	1.1648–8	1.3082–9	1.2731–10	1.3003–11	1.4734–12	2.0122–13	2.7711–14
5	5.6031–8	2.2302–8	2.8997–9	3.1344–10	3.5110–11	4.2122–12	5.4726–13

TABLE 11. *Franck-Condon factors to high vibrational quantum numbers for the* NO *Ogawa* 1 ($B'^2\Delta - B^2\Pi$) *band system*

v' \ v''	0	1	2	3	4	5	6	7	8	9	10
0	2.2557–1	**2.8877–1**	**2.2351–1**	**1.3509–1**	7.0194–2	3.2915–2	1.4329–2	5.8961–3	2.3208–3	8.8114–4	3.2453–4
1	**4.0580–1**	4.6505–2	2.3550–2	1.1453–1	**1.4223–1**	**1.1537–1**	7.3699–2	4.0680–2	2.0291–2	9.3929–3	4.1043–3
2	2.7386–1	1.1578–1	**1.5641–1**	1.7228–2	1.6543–2	7.7701–2	**1.0553–1**	**9.3033–2**	6.4867–2	3.8907–2	2.0992–2
3	8.3679–2	**3.3228–1**	3.4276–3	**1.2714–1**	**7.4062–2**	2.3923–3	2.1451–2	6.6632–2	**8.5455–2**	**7.5983–2**	5.4691–2
4	1.0751–2	1.8393–1	**2.6978–1**	1.7606–2	5.9222–2	**9.5322–2**	2.7899–2	5.3014–4	2.8988–2	6.2000–2	**7.2264–2**
5	3.5658–4	3.1720–2	2.6413–1	1.8477–1	5.8488–2	1.4888–2	**8.1219–2**	5.2826–2	5.4958–3	6.7032–3	3.6077–2
6	1.2371–6	1.0260–3	5.7520–2	**3.1892–1**	**1.1736–1**	8.5432–2	3.5003–4	**5.4379–2**	**6.3103–2**	2.0003–2	1.9756–5

v' \ v''	11	12	13	14	15	16	17	18	19
0	1.1640–4	4.0756–5	1.3947–5	4.6642–6	1.5223–6	4.8350–7	1.4867–7	4.3883–8	1.2264–8
1	1.7124–3	6.8749–4	2.6702–4	1.0068–4	3.6917–5	1.3170–5	4.5652–6	1.5331–6	4.9592–7
2	1.0467–2	4.9076–3	2.1894–3	9.3698–4	3.8680–4	1.5457–4	5.9913–5	2.2531–5	8.2092–6
3	3.4207–2	1.9338–2	1.0124–2	4.9879–3	2.3382–3	1.0510–3	4.5528.4	1.9072–4	7.7389–5
4	**6.2697–2**	4.5351–2	2.8935–2	1.6827–2	9.1070–3	4.6524–3	2.2655–3	1.0587–3	4.7706–4
5	5.8454–2	**6.1900–2**	5.1823–2	3.7208–2	2.3934–2	1.4165–2	7.8501–3	4.1227–3	2.0693–3
6	1.6053–2	4.1013–2	**5.4306–2**	**5.2854–2**	4.2646–2	3.0243–2	1.9496–2	1.1672–2	6.5842–3

TABLE 12. *Franck-Condon factors to high vibrational quantum numbers for the* NO *Ogawa 2* ($b^4\Sigma - a^4$)II *band system*

v' \ v''	0	1	2	3
0	2.5072–1	**2.8316–1**	**2.0542–1**	**1.2337–1**
1	**4.1515–1**	3.3835–2	2.6702–2	1.0337–1
2	2.5352–1	1.3774–1	**1.5569–1**	1.9506–2
3	7.0990–2	**3.3382–1**	3.7309–3	**1.2598–1**

TABLE 13. *Franck-Condon factors to high vibrational quantum numbers for the* NO *M* ($a^4\Pi - X^2\Pi$) *band system*

v' \ v''	0	1	2	3	4	5	6	7	8	9	10	11
0	3.0173–5	4.7769–4	2.9981–3	1.1897–2	3.3501–2	7.1222–2	**1.1875–1**	**1.5923–1**	**1.7473–1**	**1.5884–1**	**1.2064–1**	7.7007–2
1	2.5281–4	2.7560–3	1.3784–2	4.1550–2	8.2978–2	**1.1254–1**	9.9641–2	4.7787–2	3.8815–3	1.2840–2	6.9130–2	**1.2510–1**
2	9.4105–4	8.4217–3	3.3078–2	7.3176–2	**9.5485–2**	6.6157–2	1.2844–2	5.6499–3	5.3302–2	**8.1755–2**	4.7163–2	3.0844–3
3	2.4832–3	1.8123–2	5.4838–2	**8.4501–2**	6.1186–2	9.2341–3	1.0044–2	**5.6171–2**	**5.4831–2**	8.3969–3	1.1585–2	**6.2308–2**

v' \ v''	12	13	14	15	16	17	18	19	20	21	22	23
0	4.1458–2	1.8860–2	7.2505–3	2.3524–3	6.4232–4	1.4695–4	2.7999.5	4.4077–6	5.6743–7	5.8971–8	4.8694–9	3.1368–10
1	**1.4096–1**	**1.1536–1**	7.2979–2	3.6789–2	1.5015–2	5.0007–3	1.3628–3	3.0351–4	5.4999–5	8.0468–6	9.4035–7	8.6529–8
2	1.7871–2	8.1174–2	**1.2954–1**	**1.2693–1**	8.8657–2	4.6953–2	1.9434–2	6.3833–3	1.6746–3	3.5112–4	5.8594–5	7.7164–6
3	**6.6459–2**	1.7411–2	3.9705–3	5.8645–2	**1.1957–1**	**1.2921–1**	9.3582–2	4.9531–2	1.9941–2	6.2278–3	1.5213–3	2.9088–4

5. References

R. F. Barrow and E. Miescher (1957), Proc. Phys. Soc. **70,** 219.
M. W. Feast (1950), Can. J. Res. **A28,** 488.
G. Herzberg (1950), Spectra of Diatomic Molecules (D. Van Nostrand, New York).
A. Lagerqvist and E. Miescher (1958), Helv. Phys. Acta. **31,** 221.
G. V. Marr (1964), Proc. Phys. Soc. **83,** 293.
E. Miescher (1956), Helv. Phys. Acta. **29.**
E. Miescher (1962), J. Quant. Spectr. Radiative Transfer **2,** 421.
R. W. Nicholls (1960), Can. J. Phys. **38,** 1705.
R. W. Nicholls (1961), J. Res. NBS **65A** (Phys. and Chem.) No. 5, 451.
R. W. Nicholls (1962a), J. Res. NBS 66A (Phys. and Chem.) No. 3, 227.
R. W. Nicholls (1962b), J. Quant. Spect. Rad. Transf. **2,** 433.
R. W. Nicholls (1962c), Can. J. Phys. **40,** 1772.
R. W. Nicholls (1963), J. Chem. Phys. **38,** 1029.
R. W. Nicholls (1964a), J. Res. NBS **68A** (Phys. and Chem.) No. 1, 75.
R. W. Nicholls (1964b), Ann. Geophys. **20,** 144 (1964).
R. W. Nicholllls and A. T. Stewart (1962), Ch. 2 of Atomic and Molecular Processes (ed. D. R. Bates) (Academic Press, New York).
R. W. Nicholls, P. A. Fraser, W. R. Jarmain, and R. P. McEachran (1960), Astrophys. J. **131,** 399.
M. Ogawa (1954), Sci. Light **3** No. 1, August 1954, 39.
M. Ogawa (1955), Sci Light **3** No. 2, 90.
H. Ory (1964), J. Chem. Phys. **40,** 562.
H. Ory, A. P. Gittleman, and J. P. Maddox (1964), Astrophys. J. **139,** 346.
R. W. B. Pearse and A. G. Gaydon (1963) The Identification of Molecular Spectra (3d Edition) (Chapman and Hall, London).
C. L. Pekeris (1934) Phys. Rev. **45,** 98.
M. Peyron and H. P. Broida (1960), J. Chem. Phys. **32,** 1068
J. T. Vanderslice, E. A. Mason, and W. G. Maisch (1959), J. Chem. Phys. **31,** 738.
L. V. Wallace (1962), Astrophys. J. Suppl. **7,** 165.

(Paper 68A5–300)

JOURNAL OF RESEARCH of the National Bureau of Standards—A. Physics and Chemistry
Vol. 68A, No. 5, September–October 1964

Publications of the National Bureau of Standards*

Selected Abstracts

Thermodynamics of perfect elastic fluids, B. Bernstein, E. A. Kearsley, and L. J. Zapas, *J. Res. NBS* **68B** (*Math. and Math. Phys.*), *No. 3, 103–113 (July–Sept. 1964). 75 cents.*
A simple nonequilibruim thermodynamics is developed and a particular example is studied. The theory is formulated to describe a viscoelastic fluid, capable of finite deformation, which need not be locally in or near a state of thermodynamic equilibrium. This fluid may support shear stresses only when away from local thermodynamic equilibruim. A notion of time-temperatures superposition is contained in the formulation of the constitutive equations. Conservation of energy is obeyed and the second law of thermodynamics is satisfied as a consequence of simple requirements on the constitutive relations. In an adiabatic isochoric motion the temperature increases when work is done on the material and decreases when the material does work. For given volume and temperature, entropy decreases when the material is deformed from equilibrium. It is shown in what general way viscosity depends upon temperature. For infinitesimal strain, the special form of the stress-strain relations are derived in order to determine how temperature and time-temperature superposition enter in this case.

Theory of radiation from sources immersed in anisotropic media, J. R. Wait, *J. Res. NBS* **68B** (*Math. and Math. Phys.*), *No. 3, 119–136 (July–Sept. 1964). 75 cents.*
The electromagnetic fields produced by an electric dipole immersed in an anisotropic medium are considered. Various approaches to the problem are outlined with special reference to a cold plasma. An attempt is made to show the close relationship between previously published work on this subject.

Response of highly precise balances to thermal gradients L. Macurdy, *J. Res. NBS* **68C** (*Eng. and Instr.*), *No. 3* 135–140 (*July–Sept. 1964*). *75 cents.*
As small thermal gradients often cause large instabilities in the indications of the more precise balances, an investigation was made of the effects of various types of thermal gradients on several such balances. It was found that the largest instabilities result when the air at the top of the balance case is cooler than that at the bottom, and further that the best performance is obtained when air at the top is warmer, rather than in a state of thermal equilibrium throughout the case. The desired thermal gradients, i.e., top warmer than the bottom, can be achieved through proper insulation of the balance case, with provision being made for some flow of heat in through the lower front of the case and entrapment of warm air at the top of the case. These results apply directly to the equal-arm type of balance; a separate study would be required for balances of different design. However, the general nature of the effects of thermal gradients is applicable to some degree to all types of the more precise balances.

A new high resolution small-angle x-ray camera, H. Brumberger and R. Deslattes, *J. Res. NBS* **68C** (*Eng. and Instr.*), *No. 3,* 173–175 (*July–Sept. 1964*). *75 cents.*
A novel small-angle x-ray camera, utilizing the Borrmann effect in the 220 Laue reflection from germanium to form the incident beam, has been designed and tested. A test pattern of amorphous carbon showed angular resolution of 0.8 milliradian. In principle, an improvement of resolution by an order of magnitude is possible.

Creep and drying shrinkage and lightweight and normal-weight concretes, T. W. Reichard, *NBS Mono. 74 (Mar. 4, 1964), 30 cents.*
This is the first edition of a standard on requirements for reinforced masonry. It is a complete code of minimum requirements for reinforced masonry construction, including definitions and requirements for materials, structural design, and allowable stresses. This document, prepared by American Standards Association Sectional Committee A41, under the sponsorship of the National Bureau of Standards, is one of a series of related standards being developed by various committees under the jurisdiction of the Construction Standards Board of the American Standards Association.

Quantum field theoretic techniques and the electromagnetic properties of a uniformly magnetized electron gas, L. A. Steinert, *NBS Tech. Note 207 (Apr. 6, 1964), $1.50.*
Field theoretic operators for the charge, ρ, and current, $\vec{j}$, densities of the electron gas were obtained using the Darwin Hamiltonian in "second quantized" form. Temperature dependent Green's functions were formed from certain averaged combinations of the field creation and annihilation operators. Equations of motion were obtained for these Green's functions, and ρ and $\vec{j}$ were written in terms of the Green's functions.

In order that ρ and $\vec{j}$ might be expressed explicitly in terms of the perturbing field, formal functional series expansions were obtained for ρ and $\vec{j}$ in terms of the potentials. Connecting relations obtained from the requirements of gauge invariance and charge conservation were used to show the general result that ρ and $\vec{j}$ reduce to functionals of the electric field alone.
Using the "self-consistent field" approximation, calculations were performed determining $\vec{j}$ explicitly to an order linear in the perturbing electric field. Specific calculations are given for a zero temperature gas and for classical high temperatures. Discussed briefly was the "dielectric screening" as induced by a magnetized electron gas. The Green's functions equation of motion for the "spin magnetization" was obtained. Brief mention is made of diagrammatic techniques.

Mechanism of the photolysis of ethane at 1470 A, R. F. Hampson, Jr., J. R. McNesby, H. Akimoton, and I. Tanaka, *J. Chem. Phys.* **40,** *No. 4, 1099–1105 (Feb. 15, 1964).*

A complete analysis of the products of the photolysis of ethane at 1470 Å has been carried out. Isotopic analyses of products of the photolysis of $C_2H_6+C_2D_6$ and of CH_3CD_3 have led to the following conclusions.

1. It is possible to explain the bata on the basis that nearly all molecular hydrogen produced in the primary process comes from the end carbon atom.

$$CH_3CD_3 \rightarrow H_2 + CHDCD_2^*$$

$$CH_3CD_3 \rightarrow D_2 + CH_2CHD^*$$

The HD can be accounted for by the decomposition of excited $CHDCD_2^*$ and CH_2CHD^*.

$$CH_2CHD^* \rightarrow HD + CHCH$$

$$CD_2CHD^* \rightarrow HD + CDCD$$

2. Other primary processes are

$$CH_3CD_3 \rightarrow CH_3 + CD_3$$

$$CH_3CD_3 \rightarrow H + D + CH_2CD_2$$

The importance of the latter, relative to the molecular elimination, is about 15:85.

3. Propane and butane arise from ethyl radicals formed by addition of H and D atoms to ethylene.

4. The excited state of ethane has a lifetime smaller than 10^{-8} seconds.

Continuum theory of a plasma, J. L. Jackson and L. S. Klein, *Phys. Fluids* **7**, *No. 2, 232–241 (Feb. 1964).*
A continuum description of a classical plasma in equilibrium is presented. Thermodynamic properties and equilibrium fluctuations are discussed in terms of the fluctuations of the net charge density function $n(r)$. The probability distribution function of the potential at a typical point, and the joint distribution of the potential at two points are calculated. As was noted in the preceding paper, these results lead to the chemical potential and two-particle distribution function of classical Debye-Hückel theory. A first order correction to the potential distribution of the continuum theory is obtained by treating the nearest neighbor charge as a discrete charge and the remainder of the plasma as a continuum. The corresponding correction to the free energy is obtained and compared with the results of diagrammatic calculations, to which the present results are similar.

Pressure broadening of DCl by HCl and of HCl by DCl. A comparison of experimental results with Anderson's theory, T. C. James and R. J. Thibault, *J. Chem. Phys.* **40**, *No. 2, 534–540 (Jan. 15, 1964).*
Line widths in the 1–0 band of DCl broadened by HCl and in the 1–0 band of HCl broadened by DCl are reported for rotational levels up to $|m|=15$ and 13, respectively. These experimental results are compared with calculated values using Anderson's theory as amplified by Tsao and Curnutte. Calculations are made at 300 °K for quadrupole moments of 2, 4, and 6 Debye angstroms and calculations at 194.5 °K are also made for a Q of 6 Debye angstroms.

Energy losses and elastic resonances in electron scattering from H_2, C. E. Kuyatt, S. R. Mielczarek, and J. A. Simpson, *Phys. Rev. Letters* **12**, *293 (1964).*
Recently developed techniques of high-resolution spectroscopy have been applied to molecular hydrogen. Inelastic scattering measurements for the first time show well resolved vibrational levels of several electronic states of H_2. Elastic scattering measurements show at least eight narrow resonances in the elastic cross section.

Intensity of the forbidden $X^2\Pi_{3/2}$–$X^2\Pi_{1/2}$ satellite bands in the infrared spectrum of nitric oxide, T. C. James, *J. Chem. Phys.* **40**, *No. 3, 762–771 (Feb. 1, 1964).*
Satellite lines in the spectrum of nitric oxide which correspond to transitions $^2\Pi_{1/2}$, $v=0$, $J\rightarrow{}^2\Pi_{3/2}$, $v=1$, J^1 were observed. Intensities were measured and found to be in agreement with the theoretical predictions. Frequency measurements and line width measurements are also reported. A value for the intensity of the fundamental of 138 cm^{-2}/atm at 273°K has been obtained.

Energy spectra and angular distribution of electrons transmitted through sapphire (Al_2O_3) foils, M. J. Berger and S. M. Seltzer, *Natl. Aero. Space Admin. Spec. Publ. SP3008, p. 1–107 (1964).*
Monte Carlo results are presented, in the form of 72 tables, pertaining to the transmission of electrons incident with energies of 1, 2, 2.954, 4, 5.907 and 8 Mev on sapphire foils with thicknesses of 0.1, 0.2 and 0.3 g/cm². Two types of beam geometry are treated for all source energies: (a) perpendicular incidence; (b) beams with an initial cosine-law angular distribution (corresponding to an isotropic electron flux). For a source energy of 2 Mev, various incident beam obliquities are also treated, ranging from grazing to perpendicular incidence. The physical factors taken into account include the energy losses due to collisions with atomic electrons (mean value and fluctuations), the mean energy loss due to bremsstrahlung, and the angular deflections and path detours due to multiple Coulomb scattering by atoms.

Effects of anharmonicity on vibrational energy transfer, F. H. Mies, *J. Chem. Phys.* **22**, *No. 2, 523–531 (Jan. 15, 1964).*
Certain diagonal matrix elements which enter into the quantum theory of vibrational energy transfer generally have been assumed to be identical. If morse potentials are used to describe the molecular forces, the elements are approximately but not identically equal. The transition probability is found to decrease markedly when the ratio of the diagonal elements is allowed to deviate even slightly from one. Morse potentials were choosen to reproduce the observed anharmonicities of a variety of diatomic molecules and an anharmonic correction factor was calculated. It is found that the generally used transition probabilities should be reduced by a factor of the order of 10^{-1}–10^{-2}.

High-resolution infrared determination of the structure of carbon suboxide, W. J. Lafferty, A. G. Maki, and E. K. Plyler, *J. Chem. Phys.* **40**, *No. 1, 224–229 (Jan. 1, 1964).*
High resolution spectra have been obtained and the vibration-rotation absorption spectrum has been analyzed for a $\Sigma_u-\Sigma_g$ and a $\Pi_g-\Pi_u$ transition in C_3O_2 between 3142 cm^{-1} and 3195 cm^{-1}. The absorption region studied contains a parallel combination band and a series of associated "hot bands." The successive "hot bands" are displaced toward high frequencies in such a manner that the $\Sigma-\Sigma$ and $\Pi-\Pi$ bands are relatively free of overlapping lines. The analysis shows that the molecule must have $D_{\infty h}$ symmetry with $B_o=0.073206$ cm^{-1}. The large number of "hot bands," their variation with temperature, and the large value of the l-doubling constant q all indicate that the lowest frequency bending mode must lie at quite low wave numbers.

Infrared spectra and the structures and thermodynamics of gaseous LiO, Li_2O, and Li_2O_2, D. White, K. S. Seshadri, D. F. Dever, D. E. Mann, and M. J. Linevsky, *J. Chem. Phys.* **39**, *No. 10, 2463–2473 (Nov. 15, 1963).*
The vapor above heated lithium oxide (Li_2O) has been investigated mass spectrometrically and by infrared matrix-isolation spectroscopy. The vapor composition and Knudsen effusion rates were measured as functions of temperature, and the matrix spectra of the principal lithium oxide species—Li_2O, LiO, Li_2O_2—identified and analyzed for different isotopic abundances. The predominant vapor species $Li^7{}_2O$ is probably linear with $r(Li–O)=1.59$ Å, and has fundamentals ν_1, ν_2, ν_3 at [760], [140], and 987 cm^{-1}, respectively. Its heat of formation $\Delta H_0°(f)=-43.7\pm2.5$ kcal/mole. The diatomic molecule Li^7O has $\nu=745$ cm^{-1}, and estimated bond length $r=1.62$ Å, and $\Delta H_0°(f)=+16.0\pm5$ kcal/mole. The previously undetected molecule $Li^7{}_2O_2$ is shown to resemble the alkali halide dimers in having a planar rhombic (V_h) structure for which the O–Li–O angle and Li–O bond length are estimated to be 116° and 1.90 Å, respectively. Its B_{2u} and B_{3u} frequencies are found at 324 and 522 cm^{-1}, respectively, in a krypton matrix. The remaining unobserved modes are estimated in cm^{-1} as follows: $\nu_1(A_g)=400$, $\nu_2(A_g')=250$, $\nu_3(B_{1g})=300$, $\nu_4(B_{1u})=270$. Its $\Delta H_0°(f)=+27.5+6$ kcal/mole.

Exact conditions for the preservation of a canonical distribution in Markovian relaxation processes, H. C. Andersen, I. Oppenheim, K. E. Shuler, and G. H. Weiss, *J. Math. Phys.* **5** *No. 4, 522–536 (Apr. 1964).*
Necessary and sufficient conditions have been determined for the exact preservation of a canonical distribution characterized by a time dependent temperature (canonical invariance) in Markovian relaxation processes governed by a master equation. These conditions, while physically realizable, are quite restrictive so that canonical invariance is the exception rather than the rule. For processes with a continuous energy variable, canonical invariance requires that the integral master equation is exactly equivalent to a Fokker-Planck equation with linear transition moments of a special form. For processes with a discrete energy variable, canonical invariance requires, in addition to a special form of the level degeneracy, equal spacing of the energy levels and transitions between nearest neighbor levels only. Physically, these con-

ditions imply that canonical invariance is maintained only for weak interactions of a special type between the relaxing subsystem and the reservoir. It is also shown that canonical invariance is a sufficient condition for the exponential relaxation of the mean energy. A number of systems (hard sphere Rayleigh gas, Brownian motion, harmonic oscillators, nuclear spins) are discussed in the framework of the above theory. Conditions for *approximate* canonical invariance valid up to a certain order in the energy are also developed and then applied to nuclear spins in a magnetic field.

Changes in relation between refractive index and Young's modulus as the result of successive heat treatments, E. H. Hamilton, *J. Am. Ceram. Soc.* **47,** *No. 4, 167–170 (Apr. 1964).*
The relation between refractive index and elastic modulus is found to be a sensitive indicator of the nucleation and separation of submicroscopic phases in glass. While studying the changes in properties with heat treatments of a wide variety of glasses containing SiO_2, B_2O_3 and ZnO as major constituents, large decreases in Young's moduli were observed that were not accompanied by decreases in refractive indices of the magnitude usually observed. The abnormal changes in properties were the result of a sequence of two heat-treatments. The results indicate that during the first heat-treatment an immiscible phase is nucleated which on subsequent heat-treatment at a higher temperature develops into heterogeneous regions producing the changes in the refractive index versus elastic modulus relation.

Calorimetry of portland cement. I. Effects of various procedures on determination of heat of solution, H. A. Berman and E. S. Newman, *ASTM Proc.* **63,** *830–851 (1963).*
Nine calculation procedures for correcting the observed temperature rise in a solution calorimeter are compared. Eight of these procedures are used in various specifications for determining the heat of hydration of hydraulic cements by the heat-of-solution method.
The best reproducibility was found with methods that use long rating periods and reading intervals rather than short ones, that use constants of stirring energy and heat leakage that are independently calculated from calibrations or other pertinent tests of the apparatus or that are obtained in part from temperatures of the initial rating period rather than from temperatures of the final rating period (provided that they are accurately obtained), and that are not restricted by definitely specified duration times for the solution and rating periods. The best accuracy was found in methods that employ solution periods longer than 20 min and in methods that employ the most rigorous possible approach to the heat-leakage integration calculation consistent with the data available.

Calorimetry of portland cement. II. Application of various heat-of-solution procedures to determination of heat of hydration, E. S. Newman and H. A. Berman, *ASTM Proc.* **63** *852–860 (1963).*
The heats of hydration of two cement samples were determined using three types of heat-of-solution calorimeter. The three calorimeters were the ASTM standard air-bath Dewar, a submerged Dewar with a metal cover, and a submerged metal precision calorimeter using a resistance thermometer. The data were taken in sufficient detail to permit the computation of the corrected temperature rise by eight different methods, all based on Newton's law of cooling, recommended by various authorities in the United States and abroad. The determinations were made in two different rounds of duplicates, and the accuracy and precision of the calorimeters and of the methods are discussed on the basis of the results obtained. Differences among the calorimeters and methods found in heat-of-solution determinations largely disappeared in computing the heats of hydration. By the most rigorous method, standard deviations of 1.45, 1.38, and 0.70 cal/g were found for the heat of hydration as determined by the air-bath Dewar, the submerged Dewar, and the precision calorimeter, respectively.

Relative oscillation strengths of some O II and O III lines from measurements on shock-heated plasmas, H. F. Berg, K. L. Eckerle, R. W. Burris, and W. L. Wies, *Astrophys. J.* **139** *No. 2, 751–757 (Feb. 15, 1964).*
The layer of plasma behind reflected shock waves, which were produced in a T-tube filled with a helium-oxygen mixture, served as a high-temperature light source for the measurement of relative oscillator strengths of some O II and O III lines. Densities and temperatures were determined using the line-broadening data of some neutral and ionized helium lines as well as their relative intensities. Some relative O II and O III oscillator strengths were then determined by intensity measurements, using a scanning technique. The O II results compared very well with previous work employing a high-current arc. Furthermore, for all measured oscillator strengths, theoretical values were obtained from the Coulomb approximation. The relative values from theory and experiment were found to be in satisfactory agreement. Absolute O III oscillator strengths could not be given with certainty due mainly to the rapid time characteristics of the source which made the establishment of an equilibrium population in the second ionization stage of oxygen uncertain.

The crystallography of some M^{2+} borates, S. Block, A. Perloff, and C. E. Weir, *Acta Cryst.* **17** *Pt. 3, 314–315 (Mar. 1964).*
Crystallographic information is presented for $BaO{\cdot}2B_2O_3$, $SrO{\cdot}2B_2O_3$, $PbO{\cdot}2B_2O_3$, $SrO{\cdot}B_2O_3$ and $BaO{\cdot}B_2O_3$. All constants are presented. A short discussion of the structures of $BaO{\cdot}2B_2O_3$ and $SrO{\cdot}2B_2O_3$ is also given. The powder patterns of $SrO{\cdot}2B_2O_3$ and $PbO{\cdot}2B_2O$ are given.

Theory of the electronic susceptibilities of stoichiometric rutile (TiO_2), A. R. Ruffa, *Phys. Rev.* **133,** *No. 5A, 1418–1426 (Mar. 2, 1964).*
A theoretical analysis of the symmetry properties of crystalline rutile is made leading to the conclusion that the isotropic solution of the local field equations for this material is correct. It is shown that this conclusion is supported by the experimentally determined isotropic nature of the magnetic susceptibility of rutile. The isotropic solution of the local field equations yields a value for the electronic polarizability of the titanium ion in rutile of $\alpha_T = 2.7$ A^3, an order of magnitude greater than the free ion values usually assigned to the Ti^{+4} ion.
This result is supported by a correlation of the ionic sizes as obtained from an electron density map of rutile determined by x-ray analysis with the polarizabilities in a manner described previously. Moreover, this conclusion is in reasonably good quantitative agreement with a theoretical prediction made previously of the effect of the crystalline potential on the cation polarizability.
The results of this study give a specific example of a conclusion arrived at in an earlier work to the effect that a cation polarizability in a crystal may be many times its free ion value. Moreover, it demonstrates the unreliability of the usually accepted additivity rule for the ionic radii.

The electrolysis of formamides, acetamides and propionamides, D. E. Couch, *Electrochem. Acta* **9,** *No. 4, 327–336 (Apr. 1964).*
Solid products were produced by the electrolysis of *N*-methyl amides, and *N, N*-dimethylamides. The products are of two general classes, i.e., bis-amides of methane ($C_nH_{2n}M_2O_2$) or bis-amides of methyl ether ($C_nH_{2n}N_2O_3$). These products show that it is the groups or atoms attached to the nitrogen that enter into the electrolytic reaction, and that the methyl groups are more susceptible to electrolytic change than is hydrogen when both are attached to the same nitrogen atom.

A review of photodetachment and related negative ion processes relevant to aeronomy. L. M. Branscomb, *Ann. Geophys.* **20,** *88–102 (Jan.–Mar. 1964).*
Taking the interpretation of the mechanism for Polar Cap Absorption as an illustration of the importance of negative ion reactions in aeronomy, processes for negative ion formation, destruction and rearrangement (other than recombination with positive ions) are reviewed. When possible cross sections, rate coefficients and binding energies are given. The models used in the interpretation of negative ion-effects

in PCA and Auroral Absorption events are criticized and several possible mechanisms are discussed.

Microwave studies of butadiene derivatives. II. Isoprene, D. R. Lide, Jr., and M. Jen, *J. Chem. Phys.* **40,** *No. 1, 252–253 (Jan. 1, 1964).*

The microwave spectrum of fluoroprene, $H_2C=CH\ CF=CH_2$ has been previously studied in this laboratory. The isoprene molecule, in which the fluorine atom is replaced by a CH_3 group, shows a very similar spectrum except for uniformly lower intensities. A number of b-type transitions in the 20–30 kmc region have been measured and assigned to the ground vibrational state of isoprene. The observed and calculated rigid-rotor frequencies are listed in Table I. No attempt was made to obtain a systematic assignment of vibrational satellite lines because of the weakness of the spectrum. As in the case of fluoroprene, no evidence for another isomer was found.

Effects of tensile stress on the domain structure in grain-oriented 3.25% silicon, J. J. Gniewek, *J. Appl. Phys.* **34,** *No. 12, 3618–3622 (Dec. 1963).*

A Kerr magneto-optic apparatus has been used to observe the effects of an electrical current and tensile stress on the domain structure in commercial, 3.25% silicon steel. Photographs are presented showing that it is possible, under certain conditions, for an electrical current to have a significant effect on the domain structure. This should be considered in elastoresistance and low field magnetoresistance experiments. Upon application of a tensile stress of only 0.57 KG/mm², a domain pattern resembling the 'lozenge' pattern is shown to occur in certain grains. The corresponding strain-free pattern is identified here as a 'chevron' pattern. From observations on the type of domain structure changes resulting from stress, it is concluded that in grains where the [001] direction tilts out of the surface plane by 4 to 8 degrees, the wall energy of the reverse domains and the surface pole energy combined make a significant contribution to the total crystal energy in .012" thick material.

Other NBS Publications

J. Res. NBS 68B (Math. and Math. Phys.), No. 3 (July–Sept. 1964), 75 cents.

Generation and composition of functions. A. J. Goldman.
Thermodynamics of perfect elastic fluids. B. Bernstein, E. A. Kearsley, and L. J. Zapas. (See above abstracts.)
Zeros of polynomials in several variables and fractional order differences of their coefficients. B. Mond and O. Shisha.
Theory of radiation from sources immersed in anisotropic media. J. R. Wait. (See above abstracts.)

J. Res. NBS 68C (Eng. and Instr.), No. 3 (July–Sept. 1964), 75 cents.

Response of highly precise balances to thermal gradients L. B. Macurdy. (See above abstracts.)
A direct-reading two-knife 50-pound balance of high precision suitable for State weights and measures laboratories. H. E. Almer, H. A. Bowman, M. W. Jensen, L. B. Macurdy, H. S. Peiser, and B. Wasko.
Wave front shearing prism interferometer. J. B. Saunders.
A new high resolution small-angle x-ray camera. H. Brumberger and R. Deslattes. (See above abstracts.)
Experimental determination of air drag on a textile yarn struck tranversely by a high-velocity projectile. J. C. Smith, C. A. Fenstermaker, and P. J. Shouse.

Radio Sci. J. Res. NBS/USNC–URSI, 68D, No. 8, (Sept. 1964) $1.00.

Extension of cosmic noise absorption measurements to lower frequencies, using polorized antennas. C. G. Little, G. M. Lerfald, and R. Parthasarathy.
Broadband radio-star scintillations, part I. Observations. D. G. Singleton.
F region irregularities studied by scintillation of signals from satellites. K. C. Yeh and G. W. Swenson, Jr.
Angels, insects, and weather. A. H. LaGrone, A. P. Deam, and G. B. Walker.
Measurement of the attenuation of radio signals by jungles. Jack W. Herbstreit and W. Q. Crichlow.
Influence of a circular ionospheric depression of VLF propagation. J. R. Wait.
An experimental study of mixed-path groundwave propagation. S. W. Maley and H. Ottesen.

Radio Sci. J. Res. NBS/USNC–URSI, 68D, No. 9 (Sept. 1964), $1.00.

Symposium on Signal Statistics, Seattle, Washington, U.S.A., December 6–7, 1963:
Signal statistics, yesterday and today. F. L. H. M. Stumpers.
Rayleigh distribution and its generalizations. P. Beckmann.
Some nonlinear problems arising in the study of random processes. M. Rosenblatt.
An approach to empirical time series analysis. E. Parzen.
Effect of linear and nonlinear signal processing on signal statistics. A. V. Balakrishnan.
Random volume scattering. H. Bremmer.
Phase fluctuation statistics. J. B. Smyth.
Current topics in the stochastic theory of radiation. F. J. Zucker.
On the intensity distribution

$$\frac{2R}{\sqrt{\alpha\beta}}\exp\left[-\frac{R^2}{2}\left(\frac{1}{\alpha}+\frac{1}{\beta}\right)\right]I_0\left(\frac{R^2}{2}\left[\frac{1}{\beta}-\frac{1}{\alpha}\right]\right)$$

and its application to signal statistics. M. Nakagami.
Statistical inference for Rayleigh distributions. M. M. Siddiqui.
A probabilistic approach to the problem of large antenna arrays. Y. T. Lo.
Influence of data processing on the design and communication of experiments. S. W. Golomb.
Spectral measurement techniques in planetary radar. G. Pettengill.
Quantum statistics and lasers. J. P. Gordon.
Statistics of random surfaces. I. Kay and P. Swerling.
Modified gaussian distributions for slightly nonlinear variables. M. S. Longuet-Higgins.

Radio Sci. J. Res. NBS/USNC–URSI, 68D, No. 10 (Oct. 1964).

Theoretical heights and durations of echoes from large meteors. L. A. Manning.
Experimental determination of meteoric line densities and attachment rates. L. A. Manning.
Broadband radio-star scintillations, II. Interpretation. D. G. Singleton.
Electron collision frequency in the ionospheric *D* region. R. F. Benson.
A discussion of the theory of ionospheric cross modulation. R. F. Benson.
Theory of a slotted-sphere antenna immersed in a compressible plasma. Part I. J. R. Wait.
Theory of a slotted-sphere antenna immersed in a compressible plasma. Part II. J. R. Wait.
Electromagnetic scattering coefficients for concentric spheres and the problem of interference free enclosures. R. A. Eldred, H. A. Lasitter, and J. Roberts.
Ionospheric sounding using coded pulse signals. D. C. Coll and J. R. Storey.
Measurement of the complex time-frequency channel correlation function. P. A. Bello.

The NBS standard hygrometer, A. Wexler and R. W. Hyland, NBS Mono. 73 (May 1, 1964), 30 cents.
Microstructure of ceramic materials, Proceedings of an American Ceramic Society Symposium, Pittsburgh, Pa., April 27–28, 1963, NBS Misc. Publ. 257 (Apr. 6, 1964), $1.75.
Physical aspects of irradiation, Recommendations of the International Commission on Radiological Units and Measurements, NBS Handb. 85 (Mar. 31, 1964), 70 cents. (Supersedes parts of H78. Handbooks 84 through 89 extend and largely replace H78.)

Vinyl-coated glass fiber insect screening and louver cloth, NBS CS248–64 (Feb. 17, 1964), 10 cents.

Shoeboard, CS260–63 (Sept. 10, 1963), 10 cents.

Structural insulating board (wood or cane fiber), NBS R179–63 (Dec. 23, 1963), 10 cents. (Supersedes R179–56.)

Correction factor tables for four-point resistivity measurements on thin, circular semiconductor samples, L. J. Swartzendruber, NBS Tech. Note 199 (Apr. 15, 1964), 30 cents.

The normal phase variations of the 18 kc/s signals from NBA observed at Maui, Hawaii, A. H. Brady, A. C. Murphy, and D. D. Crombie, NBS Tech. Note 206–2 (Mar. 19, 1964), 25 cents.

The normal phase variations of the 18 kc/s signals from NBA observed at Boulder, Colorado, U.S.A., A. H. Brady, A. C. Murphy and D. D. Crombie, NBS Tech. Note 206–3 (Apr. 10, 1964), 25 cents.

Quantum field theoretic techniques and the electromagnetic properties of a uniformly magnetized electron gas, L. A. Steinert, NBS Tech. Note 207 (Apr. 6, 1964), $1.50.

A portable rubidium-vapor frequency standard, R. J. Carpenter, NBS Tech. Note. 235 (Apr. 6, 1964), 25 cents.

Research on crystal growth and characterization at the National Bureau of Standards, July to December 1963, ed. H. S. Peiser, NBS Tech. Note 236 (Apr. 6, 1964), 40 cents.

Disclosures on various subjects: A frequency meter, a phase shifter, a double-tuned transformer, and a ram-controlled system, NBS Tech. Note 237 (Apr. 10, 1964), 15 cents.

Miscellaneous studies in probability and statistics: distribution theory, small-sample problems, and occasional tables, The Statistical Engineering Laboratory, NBS Tech. Note 238 (Apr. 24, 1964), 20 cents.

Average power dissipated in a diode swept along its reverse characteristic, H. A. Schafft, NBS Tech. Note 240 (Apr. 30, 1964), 20 cents.

Conference on non-linear processes in the ionosphere December 16–17, 1963, Ed. D. H. Menzel and E. K. Smith, Jr., NBS Tech. Note 211, Vol. 2 (Apr. 17, 1964); Vol. 3 (Apr. 19, 1964); Vol. 4 (Apr. 22, 1964); Vol. 5 (Apr. 24, 1964); and Vol. 6 (Apr. 24, 1964), 45 cents each.

Bolometric microwave power calibration techniques at the National Bureau of Standards, R. F. Desch and R. E. Larson, IEEE Trans. Instr. Meas. **IM–12,** No. 1, 29–33 (June 1963).

Potential distribution method in equilibrium statistical mechanics, J. L. Jackson and L. S. Klein, Phys. Fluids **7,** No. 2, 228–231 (Feb. 1964).

Gage blocks of superior stability. II. Fully hardened steels, M. R. Meyerson and W. A. Pennington, Am. Soc. Metals Trans. Quart. **57,** No. 1, 3–25 (Mar. 1964).

The U.S. basis of electromagnetic measurements, J. M. Richardson and J. F. Brockman, IEEE Spectrum **1,** No. 1, 129–138 (Jan. 1964).

An "air-core" primary radio frequency permeameter for reversible permeability measurements, C. A. Hoer and R. D. Harrington, Proc. IEEE **51,** No. 12, 1795–1796 (Dec. 1963).

Comparative rate measurements with a single-pulse shock tube, W. Tsang, J. Chem. Phys. **40,** No. 4, 1171–1172 (Feb. 15, 1964).

Radio propagation by reflection from meteor trails, G. R. Sugar, Proc. IEEE **52,** No. 2, 116–136 (Feb. 1964).

Fabry-Perot dilatometer, V. E. Bottom, Rev. Sci. Instr. **35,** No. 3, 374–376 (Mar. 1964).

Data processing system for the automatic transformation of observed plasma intensities into their radial distribution, D. R. Paquette and W. L. Wiese, Appl. Opt. **3,** No. 2, 291–295 (Feb. 1964).

Observation on dislocation loops in deformed copper, A. W. Ruff, Jr. and L. M. Kushner, Proc. Conf. Relation Between the Structure and Mechanical Properties of Metals, National Physical Lab., Teddington, Middlesex, England 1, 146–156 (1963).

Estimation of weighting factors in linear regression and analysis of variance, J. Mandel, Technometrics **6,** No. 1, 1–25 (Feb. 1964).

Gage blocks of superior stability. III. The attainment of ultrastability, M. R. Meyerson and M. S. Sola, Am. Soc. Metals Trans. Quart. **57,** No. 1, 164–185 (Mar. 1964).

Precession equation of a spinning particle in nonuniform fields, U. Fano, Phys. Rev. **133,** No. 3B, B828–B830 (Feb. 10, 1964).

Magnetic tape recording and reproducing of atmospheric noise with a wide dynamic range, E. C. Bolton, Rev. Sci. Instr. **35,** No. 3, 377–380 (Mar. 1964).

Classical model for the study of isotope effects in energy exchange and particle exchange reactions, R. J. Rubin, J. Chem. Phys. **40,** No. 4, 1069–1077 (Feb. 15, 1964).

Condensation model producing crystalline or amorphous tetrahedral networks, F. Ordway, Science **143,** No. 3608, 800–801 (Feb. 21, 1964).

Standards and contact lenses, A. G. McNish, Contacto **7,** No. 9, 4–5 (Nov.–Dec. 1963).

On the anomalous NMR linewidth in lithium and sodium, D. Zamir, R. C. Wayne, and R. M. Cotts, Phys. Rev. Letters **12,** No. 12, 327 (Mar. 23, 1964).

Linewidths in the 2–0 band of carbon monoxide broadened by nitrogen and hydrogen, T. C. James and E. K. Plyler, J. Chem. Phys. **40,** No. 1, 221–223 (Jan. 1, 1964).

Developments in polymer evaluation procedures, G. M. Kline, Mod. Plastics 41, No. 5, 182 (Jan. 1964).

Intensity of the quadrupole fundamental of molecular hydrogen. Rotation-vibration interaction correction, T. C. James and W. Klemperer, J. Chem. Phys. **40,** No. 3, 914–915 (Feb. 1, 1964).

Observatory reports, C. E. Moore and L. M. Branscomb, Astron. J. **68,** No. 9, 657–659 (Nov. 1963).

Absorption spectrum of the "pink" afterglow of nitrogen in the vacuum ultraviolet, A. M. Bass, J. Chem. Phys. **40,** No. 3, 695–700 (Feb. 1, 1964).

Spherical mirror Fabry-Perot resonators, R. W. Zimmerer, IEEE Trans. Microwave Theory Tech. **MTT–11,** No. 5, 371–379 (Sept. 1963).

Excitation by local electric fields in the aurora and airglow, L. R. Megill and N. P. Carleton, J. Geophys. Res. **69,** No. 1, 101–122 (Jan. 1, 1964).

Local curvature of wavefronts in an optical system, J. A. Kneisly II., J. Opt. Soc. Am. **54,** No. 2, 229–235 (Feb. 1964).

The γ-absorption cross section of holmium in the dynamic collective theory, M. Danos and W. Greiner, Phys. Letters **8,** No. 2, 113–115 (Jan. 15, 1964).

Electrical properties of elastomers and related polymers, A. T. McPherson, Rubber Chem. Technol. **36,** No. 5, 1230–1302 (Dec. 1963).

Relationships between different kinds of network parameters, not assuming reciprocity or equality of the waveguide or transmission line characteristic impedances. R. W. Beatty and D. M. Kerns, Proc. IEEE **52,** No. 1, 84 (Jan. 1964).

Determination of error rates for narrow-band communication of binary-coded messages in atmospheric radio noise, A. D. Spaulding, Proc. IEEE **52,** No. 2, 220–221 (Feb. 1964).

Examples relating to the simplex method, A. J. Goldman and D. Kleinman, Operations Res. **12,** No. 1, 159–161 (Jan.–Feb. 1964).

The ultraviolet realm of spectroscopy, C. E. Moore, J. Wash. Acad. Sci. **54,** 58–62 (1964).

Rate dependence in a solarizing commercial X-ray emulsion: Sensitometric properties, number, and structure of developed grains, M. Ehrlich, Wm. L. McLaughlin, and E. Zeitler, J. Opt. Soc. Am. **54,** No. 2, 176–183 (Feb. 1964).

The 1963 Symposium on Humidity and Moisture, 20–23 May 1963, Washington, D.C., A. Wexler, Intern. J. Heat Mass Transfer **7,** 275–277 (1964).

Hydride and proton transfer reactions involving sec-propyl ions, R. P. Borkowski and P. Ausloos, J. Chem. Phys. **40,** No. 4, 1128–1132 (Feb. 15, 1964).

Cation-exchange between molten salts and a special porcelain of high sodium content, R. J. Labrie, J. Electrochem Soc. **111,** No. 4, 473–476 (Apr. 1964).

On the height distribution of the ratio of negative ion and electron densities in the lowest ionosphere, G. C. Reid, D. K. Bailey, and H. Leinbach, J. Atmospheric and Terrest. Phys. **26,** 1451–47 (1964).

The following are chapters in the book, Modern Electroplating (1963):

Electroless plating, A. Brenner, pp. 698–713.
Iron, V. A. Lamb and C. T. Thomas, pp. 228–241.
Methods of testing, F. Ogburn, pp. 661–697.

New methods for constructing EPR cavities, A. R. Cook, L. M. Matarrese, and J. S. Wells, Rev. Sci. Instr. **35,** 114–115 (Jan. 1964).

Electron density profile analysis of topside sounder ionograms, A. K. Paul and J. W. Wright, J. Geophys. Res. **69,** 1431–1435 (Apr. 1964).

On phase changes in very-low-frequency propagation induced by an ionospheric depression of finite extent, J. R. Wait, J. Geophys. Res. **69,** No. 3, 441–445 (Feb. 1964).

Electronic transport in strontium titanate, H. P. R. Frederikse, W. R. Thurber, and W. R. Hosler, Phys. Rev. **134,** No. 2A, A442–A445 (Apr. 20, 1964).

Hydrogen reaction with carbon and nickel evaporated films, V. R. Deitz and E. F. McFarlane, Carbon **1,** 117–125 (1964).

Discussion of spin-spin relaxation formulae and experiments, R. L. Peterson, Phys. Letters **8,** No. 3, 158–159 (Feb. 1, 1964).

Soft X-ray microscopy of paper, S. B. Newman and D. Fletcher, Tappi **47,** No. 4, 177–180 (Apr. 1964).

The transmission of Rayleigh waves across an ocean floor with two surface layers, U. W. Hochstrasser and R. Stoneley, Geophys. J. (Jeffreys Jubilee Number) **4,** 197–201 (1961).

Thermal decomposition of some tert-butyl compounds at elevated temperatures, W. Tsang, J. Chem. Phys. **40,** No. 6, 1498–1505 (Mar. 15, 1964).

Vacuum ultraviolet absorption spectra of oxygen in liquid and crystalline argon and nitrogen, A. M. Bass and H. P. Broida, J. Mol. Spectry. **12,** No. 3, 221–230 (Mar. 1964).

The electron paramagnetic resonance spectrum of some tris-complexes of copper (II), H. C. Allen, Jr., G. F. Kokoszka, and R. G. Inskeep, J. Am. Chem. Soc. **86,** 1023–1025 (1964).

The structure and physics of the upper atmosphere, T. E. Van Zandt and R. W. Knecht, Book, Space Physics, pp. 166–225 (John Wiley & Sons, Inc., New York, N.Y., 1964).

An implication for lasers of an aspect of interference at high field strengths, J. A. White, Nature **201,** No. 4922, 911–912 (Feb. 29, 1964).

Weierstrass points of $\Gamma_0(n)$, J. Lehner and M. Newman, Ann. Math. **79,** No. 2, 360–368 (Mar. 1964).

A two-parameter family of hyper-Poisson distributions, G. E. Bardwell and E. L. Crow, J. Am. Stat. Assoc. **59,** 133–141 (Mar. 1964).

Accumulation of calibration errors and their optimum distribution, E. L. Crow, Trans. 18th Midwest Quality Control Conf., Am. Soc. Quality Control, Tulsa, Okla., pp. 86–100 (Oct. 10–12, 1963).

On the geomagnetic effect of the Starfish high-altitude nuclear explosion, H. Maeda, A. J. Shirgaokar, M. Yasuhara, and S. Matsushita, J. Geophys. Res. **69,** 917–945 (Mar. 1964).

Phase variations in V.L.F. propagation, C. J. Chilton, D. D. Crombie, and A. G. Jean, AGARDograph **74,** Propagation of Radio Waves at Frequencies below 300 Kilocycles, ch. 19, pp. 257-290 (Pergamon Press Inc., New York, N.Y., 1964).

Note on "interferometric measurement of vibration amplitudes," K. D. Mielenz, Appl. Opt. **3,** 542 (Apr. 1964).

Weights and measures and aerosols, M. W. Jensen, Scale J. **50,** No. 6, 2 (Mar. 1964).

Radiative tail in elastic electron scattering, L. C. Maximon and D. B. Isabelle, Phys. Rev. **133,** No. 5B, B1344–B1350 (Mar. 9, 1964).

Error rate in a multiple-frequency-shift system and the output signal/noise ratio in a frequency-modulation and a pulse-code-modulation/frequency-shift system, H. Akima, Proc. Inst. Elec. Engrs. **111,** No. 3, 547–555 (Mar. 1964).

Polymer compression: visual observations on stressed biaxially oriented nylon 66, J. Powers and A. Van Valkenberg, J. Polymer Sci. Polymer Letters, Pt. B, **2,** No. 5, 533–536 (May 1964).

Further observations of synchrotron radiation decay, G. R. Ochs, J. Geophys. Res. **69,** No. 3, 399–405 (Feb. 1964).

Gloss standards and glossmeter standardization, H. K. Hammond, III, Am. Paint J. pp. 360–364 (Apr. 1964).

Audiofrequency compliances of prestressed quartz, fused silica, and aluminum, M. Greenspan and C. E. Tschiegg, J. Acoust. Soc. Am. **36,** No. 3, 450–457 (Mar. 1964).

A note on the attenuation function for propagation over a flat layered ground, L. E. Vogler, IEEE Trans. Ant. Prop. **AP–12,** 240–242 (Mar. 1964).

Solubility of helium in liquid hydrogen, R. J. Corruccini, J. Chem. Phys. **40,** 2039–2040 (Apr. 1964).

Allotrophy in some rare-earth metals at high pressures, G. J. Piermarini and C. E. Weir, Science **144,** No. 3614, 69–71 (Apr. 3, 1964).

Pointwise bounds in the first biharmonic boundary value problem, J. H. Bramble and L. E. Payne, J. Math. Phys. **42,** No. 4, 278–286 (Dec. 1963).

Four-terminal-pair networks as precision admittance and impedance standards, R. D. Cutkosky, IEEE Trans. Commun. Elec. **CE–70,** 19–22 (Jan. 1964).

A differential microwave phase shifter, R. W. Beatty, IEEE Trans. Microwave Theory Tech. **MTT–12,** 250–251 (Mar. 1964).

An explanation for the apparent polarization of some geomagnetic micropulsations (pearls), J. H. Pope, IEEE Spectrum **1,** 129–138 (Jan. 1964).

Fluctuations in a laser beam over 9- and 90-mile paths, W. R. Hinchman and A. L. Buck, Proc. IEEE **52,** 305–306 (Mar. 1964).

Solvent participation in the anionic polymerization of styrene, L. J. Fetters, Polymer Letters **2,** 425–428 (1964).

Conductance of potassium chloride in highly purified *n*-methylpropionamide from 20 to 40°, T. B. Hoover, J. Phys. Chem. **68,** 876–879 (1964).

Tapered inlets for pipe culverts, J. L. French, J. Hydraulics Div., ASCE **90,** No. HY2, 255–299 (Mar. 1964).

Field trial of the 1959 supplementary standard observer proposal, I. Nimeroff, J. Opt. Soc. Am. **54,** No. 5, 696–704 (May 1964).

The relation between VLF propagation and *D*-layer characteristics, J. R. Wait, IEEE Trans. Ant. Prop. **AP–12,** 239–240 (Mar. 1964).

Analog simulation of zone melting, H. L. Mason, Instr. Control Systems **37,** No. 1, 121–123 (Jan. 1964).

Correlation between observed wavelength shifts produced in electrodeless discharge tubes and predicted Stark-effect shifts in the spectrum of neutral germanium (Ge I), L. Minnhagen, J. Opt. Soc. Am. **54,** No. 3, 320–322 (Mar. 1964).

Determination of *p*H, theory and practice, R. G. Bates, Book, 450 pages (John Wiley & Sons, Inc., New York, N.Y., Feb. 1964).

Disproportionation—combination reactions of alkyl radicals and hydrogen atoms at low temperatures, R. Klein, M.D. Scheer, and R. Kelley, J. Phys. Chem. **68,** 598 (1964).

Correlation of the phase of microwave signals on the same line-of-sight path at different frequencies, H. B. Janes, IEEE Trans. Ant. Prop. **AP–11,** 716–717 (Nov. 1963).

The theory of an antenna over an inhomogeneous ground plane, J. R. Wait, Book, Electromagnetic Theory and Antennas, Ed. E. C. Jordan, Pt. 2, pp. 1079–1098 (Pergamon Press, Oxford, England, 1963).

Mass-spectrometric investigation of the nickel-bromine surface reaction, J. D. McKinley, J. Chem. Phys. **40,** No. 2, 576–581 (Jan. 15, 1964).

Some observations of short-duration cosmic noise absorption events in nearly conjugate regions at high magnetic latitude, K. W. Eriksen, C. S. Gillmor, and J. K. Hargreaves, J. Atmospheric Terrest. Phys. **26,** 77–90 (1964).

The effect of Coulomb collisions on incoherent scattering of radio waves by a plasma, D. T. Farley, Jr., J. Geophys. Res. **69,** 197–200 (Jan. 1964).

Mass-spectrometric investigation of the high-temperature reaction between nickel and chlorine, J. D. McKinley, J. Chem. Phys. **40,** No. 1, 120–125 (Jan. 1, 1964).

Ferromagnetic resonance relaxation, wide spin-wave coverage by ellipsoids, A. S. Risley and H. E. Bussey, J. Appl. Phys. **35,** No. 3, 896–897 (Mar. 1964).

**Publications for which a price is indicated are available by purchase from the Superintendent of Documents, U.S. Government Printing Office, Washington, D.C., 20402 (foreign postage, one-fourth additional). Reprints from outside journals and the NBS Journal of Research may often be obtained directly from the authors.*

U.S. GOVERNMENT PRINTING OFFICE:1964

UNIVERSITY MICROFILMS
313 NORTH FIRST STREET
ANN ARBOR, MICHIGAN
SJR-A-OCT

PENALTY FOR PRIVATE USE TO AVOID
PAYMENT OF POSTAGE, $300
GPO

DIVISION OF PUBLIC DOCUMENTS
WASHINGTON, D.C. 20402

OFFICIAL BUSINESS

JOURNAL OF RESEARCH of the National Bureau of Standards Vol. 68A, No. 5 September–October 1964
A. Physics and Chemistry

Contents

	Page
Relaxation modes of trapped crystal point defects: the three-neighbor shells model in NaCl. A. D. Franklin, A. Shorb, and J. B. Wachtman, Jr.	425
Viscosity of a standard soda-lime-silica glass. Albert Napolitano and Earl G. Hawkins.	439
Hydrothermal preparation of a gehlenite hydrate. Elmer T. Carlson.	449
Action of water on calcium aluminoferrites. Elmer T. Carlson.	453
Infrared spectra of the crystalline inorganic borates. C. E. Weir and R. A. Schroeder.	465
Effect of pressure and temperature upon the optical dispersion of benzene, carbon tetrachloride, and water. R. M. Waxler, C. E. Weir, and H. W. Schamp, Jr.	489
Some changes in double-bond structure during the vulcanization of natural rubber. Frederic J. Linnig, Edwin J. Parks, and James E. Stewart.	499
Dislocations in polymer crystals. H. D. Keith and Elio Passaglia.	513
Dependence of mechanical relaxation on morphology in isotactic polypropylene. Elio Passaglia and Gordon M. Martin.	519
Precision density measurement of silicon. Ivars Henins.	529
Franck-Condon factors to high vibrational quantum numbers IV: NO band systems. R. W. Nicholls.	535
Publications of the National Bureau of Standards.	541

Library of Congress Catalog Card Number: 62–37059
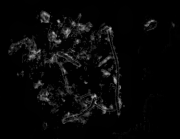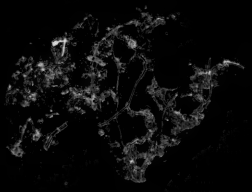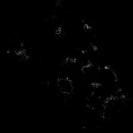
For sale by the Superintendent of Documents, U.S. Government Printing Office, Washington, D.C., 20402. Price 70 cents (single copy)
Subscription price: $4 a year; 75 cents additional for foreign mailing.
UNITED STATES GOVERNMENT PRINTING OFFICE, WASHINGTON : 1964